Intra-arterial Treatment of Primary and Metastatic Liver Tumors

Intra-arteriële Behandeling van Primaire Leverkanker en Lever Metastasen

(met een samenvatting in het Nederlands)

Proefschrift

ter verkrijging van de graad van doctor aan de Universiteit Utrecht
op gezag van de rector magnificus, prof.dr. J.C. Stoof, ingevolge
het besluit van het college voor promoties
in het openbaar te verdedigen op
woensdag 10 juni des middags

te 1.40 uur
door Manon Antal Myrthe Buijs
geboren op 15 november 1982
te Brunssum

te 2.30 uur
door Josephina Anna Vossen
geboren op 28 december 1981
te ‘s-Hertogenbosch

Promotoren:	Prof.dr. P.J. van Diest
	Prof.dr. E. van der Wall
	Prof.dr. J.-F.H. Geschwind
Co-promotor:	Dr. M. Vali

Intra-arterial treatment of primary and metastatic liver tumors
Thesis University of Utrecht, The Netherlands, 2009

ISBN:
Print: www.proefschriftmaken.nl
Design and Layout: www.proefschriftmaken.nl
Cover illustration:

CONTENTS

Chapters 2, 4, 7, 12 and the addendum will be defended by M.A.M. Buijs and chapters, 3, 6, 8, 10 and 11 by J.A. Vossen. The remaining chapters will be defended by both authors.

CHAPTER 1

GENERAL INTRODUCTION

The aims of this thesis are, first, to investigate the toxicities associated with transarterial chemoembolization of liver tumors and to evaluate the use of MR imaging in characterizing tumor response after this locoregional therapy, second, to further develop intra-arterial therapy of liver tumors with 3-bromopyruvate (3-BrPA), a novel anti-cancer agent, and finally, to assess the value of new MR imaging techniques in the characterization of liver lesions.

Hepatocellular carcinoma (HCC) is the most common type of primary liver cancer and is associated with more than 600,000 cases diagnosed worldwide each year (1). The incidence in the United States continues to increase, mainly due to the concomitant increase in hepatitis C virus infections (2). Other histologic types of primary liver cancer, including intrahepatic cholangiocarcinoma, while less common than HCC, are also experiencing a rise in incidence (3).

Metastatic disease is the most common malignancy of the liver in the Western world. The liver is the most common site for developing metastases, accounting for more than one half of cases of advanced cancer (4). Although primary tumors originating from gastrointestinal sites are more likely than others to develop hepatic metastases, many tumors arising in others locations, including those of the breast and eye, also commonly develop hepatic metastases (5-7).

Surgical resection and liver transplantation are considered to be the only curative treatment for patients with hepatic malignancies. Unfortunately, tumors in most patients are found to be unresectable at the time of presentation, leaving palliative therapy as the only option. This has resulted in increased utilization of minimally invasive strategies as therapeutic options for both primary and metastatic hepatic malignancies (8, 9). These locoregional therapies include ablative techniques and catheter-based approaches. Ablation can be applied either chemically (percutaneous ethanol injection) or thermally (radiofrequency ablation, microwave ablation and laser ablation). Catheter-based approaches include transarterial chemoembolization (TACE) and transarterial radioembolization.

During TACE, intra-arterial chemotherapy and arterial embolization are believed to act in a synergistic manner. A key theoretic advantage of TACE over systemic chemotherapy is that the chemotherapeutic agents used are not intravenously infused throughout the systemic circulation; rather, they are administered locally through the hepatic artery (10, 11). Thus, the

subjectively reported side effects of TACE are mild compared with those caused by systemic chemotherapy. However, current studies on TACE focus on survival benefits rather than TACE-induced systemic toxicities.

Therefore, in *Chapter 2*, we determine the toxicity profile of TACE at 6 months and 1 year after treatment in patients with HCC using a standardized oncology protocol (CTCAE, version 3.0) so that TACE can be compared with the use of the systemic chemotherapeutic agents most commonly used for liver cancer (ie, doxorubicin, cisplatin, and 5-fluorouracil).

Assessment of tumor response after locoregional therapy is an increasingly important task in oncologic imaging. New imaging modalities play a critical role in determining treatment success and in guiding future therapy (12). Various imaging modalities, including Doppler ultrasonography, angiography, computed tomography (CT) and MR imaging have been used to evaluate treatment response (13). In *Chapter 3*, we summarize the current available literature on the role of MR imaging in assessing treatment response after various locoregional therapies that are commonly used to treat patients with hepatic malignancies.

Unfortunately, conventional MR imaging techniques may be limited in providing clinically satisfactory information about the extent of tumor necrosis, which is the main indicator of tumor cell death (14). A novel imaging technique for assessment of tumor response is diffusion-weighted MR imaging. This imaging technique is used to detect the motion of water molecules, which is mapped by the Apparent Diffusion Coefficient (ADC). Viable tumors are high in cellularity and these cells have intact cell membranes, which restrict the mobility of the water molecules, thus causing a relatively low ADC value. Conversely, cellular necrosis causes increased membranous permeability, which allows water molecules to move freely, resulting in a high ADC value.

In the subsequent chapters of Part I we assess the value of functional MR imaging in the evaluation of early tumor response after TACE. Furthermore, we compare tumor response based on functional MR imaging versus traditional imaging assessment based on iodized oil deposition, tumor size, and tumor enhancement. *Chapter 4* focuses on breast cancer liver metastases, which are mainly hypovascular in nature. In *Chapter 5* we analyze liver metastases derived from neuroendocrine primaries, which are mainly hypervascular in nature. In the following chapters, we aim to

confirm these data in metastatic leiomyosarcoma (*Chapter 6*) and metastatic ocular melanoma (*Chapter 7*).

In Part II, we focus on the development of a new therapeutic strategy for liver cancer. In recent years, the development of new cancer medicines has shifted away from conventional cytotoxic drugs towards targeted therapies. These targeted agents promise to be a more effective form of anticancer therapy and are ideal candidates for intra-arterial administration. 3-BrPA, a synthetic brominated derivate of pyruvic acid, acts as an irreversible glycolytic inhibitor and is, therefore, a highly promising candidate for this targeted strategy for treating liver cancer (15).

Cancer cells depend on large quantities of energy to maintain elevated rates of proliferation. Specific adaptations in energy-yielding pathways are observed, including activation of glycolysis and down regulation of oxidative phosphorylation, known as the "Warburg effect" (16). Glycolysis is critical to cancer growth and is clearly validated as a target for cancer treatment (17). In line with this, 3-BrPA has been shown to have antitumor effects when injected intra-arterially in the hepatic artery of rabbits with VX2 liver tumors (18). In *Chapter 8*, we aim to develop a suitable animal model of liver cancer in order to compare the influence of partial hepatectomy, intra-arterial treatment with 3-BrPA and TACE on regional and distant metastases.

In order to thoroughly understand the in vivo effects of 3-BrPA and thus predict the toxicity and efficacy profiles, the aim of *Chapter 9* is to determine the biodistribution and tumor targeting ability of ^{14}C-labeled 3-BrPA ((^{14}C) 3-BrPA) after intra-arterial and intravenous delivery in the VX2 rabbit model. In addition, we evaluate the effects of (^{14}C) 3-BrPA on tumor and healthy tissue glucose metabolism by determining ^{18}F-deoxyglucose (FDG) uptake. Last, we determine the survival benefit of intra-arterial administered 3-BrPA.

In a subsequent study (Addendum) we evaluate the anti-glycolytic effects of 3-BrPA on rats bearing RMT mammary tumors, by determining FDG uptake after intravenous administration of the therapeutic dose.

Diagnostic imaging is crucial in determining treatment strategies in patients with liver cancer. Size, number and locations of tumors; anatomy and patency of relevant arteries and veins; evidence of organ obstruction; alterations due to surgery or stenting; and critical adjacent structures, are all

considered when formulating a treatment plan and judging its risks and benefits (19). In Part III we discuss advances in imaging of liver lesions.

Overlap between different lesions on conventional MR imaging may exist, therefore distinguishing liver cancer from other hypervascular liver lesions may be difficult. Diffusion-weighted MR imaging has been used previously in tissue characterization and may be of value in such cases (20, 21). In *Chapter 10*, we assess the accuracy of diffusion-weighted MR imaging in differentiating between hemangiomas and other relatively common hypervascular liver lesions, including focal nodular hyperplasia (FNH), HCC, and hypervascular liver metastases.

Another approach to tumor characterization and treatment evaluation is the use of tissue-specific contrast media. Normally, dynamic contrast-enhanced MRI is performed with the traditional extracellular gadolinium-based contrast agents. Gadolinium-ethoxybenzyl-diethylenetriamine-pentaacetic-acid (Gd-EOB-DTPA) is a third generation gadolinium-based MR contrast agent with the unique ability to combine MR perfusion imaging with hepatocyte specific uptake (22). In *Chapter 11* we report on the role of diffusion-weighted MR imaging in determining tumor necrosis and contrast-enhanced MR imaging using Gd-EOB-DTPA. Maximum tumor size measurement and tumor delineation are determined and compared to gold standard histologic measurements in the rabbit VX2 liver tumor model.

Finally, Proton MR spectroscopy (1H MRS) is an imaging technique that may be utilized to quantify biochemical metabolite concentrations. 1H MRS provides assessment of the concentration of several metabolites and is useful as a noninvasive means of studying the biochemistry of a lesion relative to normal tissue (23). In *Chapter 12* we compare these metabolic (absolute quantification of tumor choline concentration) MR imaging findings to percent necrosis at pathology in rabbits bearing VX2 liver tumors.

REFERENCES

1) Parkin, D.M., et al., Global cancer statistics, 2002. CA Cancer J Clin, 2005. 55(2): p. 74-108.
2) El-Serag, H.B. and A.C. Mason, Rising incidence of hepatocellular carcinoma in the United States. N Engl J Med, 1999. 340(10): p. 745-50.
3) DeOliveira, M.L., et al., Cholangiocarcinoma: thirty-one-year experience with 564 patients at a single institution. Ann Surg, 2007. 245(5): p. 755-62.
4) Dirisamer, A., et al., Dual-time-point FDG-PET/CT for the detection of hepatic metastases. Mol Imaging Biol, 2008. 10(6): p. 335-40.
5) Jemal, A., et al., Cancer statistics, 2007. CA Cancer J Clin, 2007. 57(1): p. 43-66.
6) Pentheroudakis, G., et al., Metastatic breast cancer with liver metastases: a registry analysis of clinicopathologic, management and outcome characteristics of 500 women. Breast Cancer Res Treat, 2006. 97(3): p. 237-44.
7) Singh, A.D., L. Bergman, and S. Seregard, Uveal melanoma: epidemiologic aspects. Ophthalmol Clin North Am, 2005. 18(1): p. 75-84, viii.
8) Dodd, G.D., 3rd, et al., Minimally invasive treatment of malignant hepatic tumors: at the threshold of a major breakthrough. Radiographics, 2000. 20(1): p. 9-27.
9) Goldberg, S.N. and M. Ahmed, Minimally invasive image-guided therapies for hepatocellular carcinoma. J Clin Gastroenterol, 2002. 35(5 Suppl 2): p. S115-29.
10) Cagol, P.P., E. Pasqual, and S. Bacchetti, Potential advantages of loco-regional intra-arterial chemotherapy. In Vivo, 2006. 20(6A): p. 777-9.
11) Collins, J.M., Pharmacologic rationale for regional drug delivery. J Clin Oncol, 1984. 2(5): p. 498-504.
12) Assumpcao, L., et al., Functional MR imaging as a new paradigm for image guidance. Abdom Imaging, 2008.
13) Bartolozzi, C., et al., Hepatocellular carcinoma: CT and MR features after transcatheter arterial embolization and percutaneous ethanol injection. Radiology, 1994. 191(1): p. 123-8.
14) Kamel, I.R., et al., The role of functional MR imaging in the assessment of tumor response after chemoembolization in patients with hepatocellular carcinoma. J Vasc Interv Radiol, 2006. 17(3): p. 505-12.
15) Geschwind, J.F., et al., Novel therapy for liver cancer: direct intraarterial injection of a potent inhibitor of ATP production. Cancer Res, 2002. 62(14): p. 3909-13.

16) Warburg, O., On the origin of cancer cells. Science, 1956. 123(3191): p. 309-14.
17) Gatenby, R.A. and R.J. Gillies, Glycolysis in cancer: a potential target for therapy. Int J Biochem Cell Biol, 2007. 39(7-8): p. 1358-66.
18) Vali, M., et al., Intraarterial therapy with a new potent inhibitor of tumor metabolism (3-bromopyruvate): identification of therapeutic dose and method of injection in an animal model of liver cancer. J Vasc Interv Radiol, 2007. 18(1 Pt 1): p. 95-101.
19) Heiken, J.P., Distinguishing benign from malignant liver tumours. Cancer Imaging, 2007. 7 Spec No A: p. S1-14.
20) Moody, A.R. and S.R. Wilson, Atypical hepatic hemangioma: a suggestive sonographic morphology. Radiology, 1993. 188(2): p. 413-7.
21) Burkholz, K.J. and A.C. Silva, AJR teaching file: hypervascular metastasis or hepatic hemangioma? AJR Am J Roentgenol, 2008. 190(6 Suppl): p. S53-6.
22) Gadoxate disodium: gadolinium EOB DTPA, gadoxetic acid, Gd-EOB-DTPA. Drugs R D, 2004. 5(4): p. 227-30.
23) Law, M., et al., Differentiating surgical from non-surgical lesions using perfusion MR imaging and proton MR spectroscopic imaging. Technol Cancer Res Treat, 2004. 3(6): p. 557-65.

PART I:
TRANSARTERIAL CHEMOEMBOLIZATION: TOXICITY AND MR IMAGING

CHAPTER 2

NONRESECTABLE HEPATOCELLULAR CARCINOMA:

LONG-TERM TOXICITY IN PATIENTS TREATED WITH TRANSARTERIAL CHEMOEMBOLIZATION – SINGLE-CENTRE EXPERIENCE

Buijs M, Vossen JA, Frangakis C, Hong K, Georgiades CS, Chen Y, Liapi E, Geschwind JF

Radiology 2008 Oct; 249(1): 346-54.

ABSTRACT

PURPOSE:
To determine the toxicity profile of transarterial chemoembolization (TACE) at 6 months and 1 year after treatment in patients with hepatocellular carcinoma (HCC) in a standardized oncology protocol so that TACE could be compared with systemic chemotherapeutic regimens for liver cancer.

MATERIALS AND METHODS:
The study was authorized by the institutional review board. Between January 2002 and January 2007, 190 patients (155 men, 35 women; median age, 65 years; age range, 18–84 years) with HCC who underwent TACE treatment were identified from a prospectively collected database. Clinical records of complete blood cell counts and chemical profiles at baseline and at 6 and 12 months after treatment were studied retrospectively. Toxicity was graded according to the common terminology criteria for adverse events (CTCAE). A transition (survival) analysis perspective was used to estimate the distribution of toxicity grades. Patient survival from the first TACE session was calculated with Kaplan-Meier analysis.

RESULTS:
Grade 3 or 4 toxicity 6 and 12 months, respectively, after treatment included leukocytopenia (7% and 19%); anemia (9% and 19%); thromobocytopenia (13% and 23%); prolonged activated partial thromboplastin time (8% and 18%); elevated aspartate aminotransferase (15% and 18%), alanine aminotransferase (10% and 18%), and alkaline phosphatase (8% and 18%) levels; hypoalbuminemia (10% and 19%); hyperbilirubinemia (10% and 22%); and alopecia (18%). The cumulative survival rate was 58% at 1 year, 39% at 2 years, and 29% at 3 years. These toxicity rates were considerably lower than those reported after treatment with currently used systemic chemotherapeutic agents.

CONCLUSION:
Study results show that TACE has a favorable long-term toxicity profile in patients with HCC. Data clearly support the role of TACE in the treatment of patients with nonresectable HCC.

INTRODUCTION

Hepatocellular carcinoma (HCC) is the fifth most common cancer in the world (1). The incidence of and mortality rate with HCC continue to rise steadily in North America and Europe, mainly owing to the concomitant increase in hepatitis C viral infections (2, 3).

Surgical treatments, including hepatic resection, liver transplantation, and percutaneous ablation, are considered the only curative treatments for patients with early-stage HCC and yield 5-year survival rates of 50%–70% (4). However, fewer than 20% of patients with HCC can be treated surgically, and given the lack of a survival benefit from systemic chemotherapy, locoregional therapeutic options such as transarterial chemoembolization (TACE) have become the mainstay of therapy.

A key theoretic advantage of chemoembolization over systemic chemotherapy is that the chemotherapeutic agents used (doxorubicin, cisplatin, and others) are not intravenously infused throughout the systemic circulation; rather, they are administered locally through the hepatic artery. This is especially important in patients with HCC, who also have underlying liver dysfunction. One of the main concerns regarding systemic chemotherapy is the fact that patients who receive this form of treatment may experience side effects that include pain, nausea, vomiting, myelosuppresion, and alopecia and/or serious adverse events such as cardiac toxicity. These side effects are well described in the Common Terminology Criteria for Adverse Events (CTCAE), version 3.0 (5), and represent one of the major disadvantages of using systemically delivered chemotherapy. Moreover, rates of response to single or combination chemotherapy are still very low—typically less than 20% (6).

The subjectively reported side effects of TACE are mild compared with those caused by systemic chemotherapy. These side effects are in large part attributed to postembolization syndrome and include nausea, vomiting, abdominal pain, fever, and loss of appetite (7, 8). Because the focus of most studies is patient survival rather than toxicities caused by TACE, precise analysis of potential TACE-induced systemic toxicities is lacking (9, 10). Yet the potential lack of severe systemic toxicities after TACE compared with those after systemic chemotherapy is one of the most important advantages of using this locoregional therapeutic approach. Therefore, the goal of our study was to determine the toxicity profile of TACE at 6 months

and 1 year after treatment in patients with HCC in a standardized oncology protocol (CTCAE, version 3.0) so that TACE could be compared with the use of the systemic chemotherapeutic agents most commonly used for liver cancer (ie, doxorubicin, cisplatin, and 5-fluorouracil).

MATERIALS AND METHODS

Patient Selection

The study was authorized by the institutional review board of Johns Hopkins Hospital. We retrospectively analyzed prospectively collected data on all patients with HCC who were evaluated at Johns Hopkins Hospital Liver Clinic for possible TACE between January 1, 2002, and January 1, 2007. For all of these patients, the diagnosis of HCC was based on either the findings in histologic specimens obtained with needle biopsy or the finding of a hypervascular lesion on cross-sectional magnetic resonance (MR) images in addition to an alpha-fetoprotein level higher than 400 U/L (400 μg/L). Only those patients who were not suitable for curative therapies such as resection, liver transplantation, or percutaneous intervention were considered for TACE. Patients were required to be at least 18 years old, have preserved liver function (Child-Pugh class A or B) without substantial liver decompensation, and have an Eastern Cooperative Oncology Group performance status score of 0–2. Encephalopathy, severe variceal bleeding, and/or either ascites, marked thrombocytopenia, prolonged impaired renal function, acute renal failure, or severe liver failure was considered an absolute contraindication to TACE. All patients provided written informed consent before undergoing any study-specific procedures. Only those patients whose baseline evaluation was performed at our institution were included. Baseline evaluation included complete blood cell count, a biochemical profile, and dynamic MR imaging.

Chemoembolization Technique

All chemoembolizations were performed by a single experienced interventional radiologist (J.F.H.G., K.H., C.S.G.) and by using the same technique. An 18-gauge single-wall needle was used with the Seldinger technique to access the right common femoral artery. A 5-F vascular sheath was placed in the right common femoral artery over a 0.035-inch guidewire (Terumo Medical, Somerset, NJ). With fluoroscopic guidance, a 5-F glide Simmons-1 catheter (Cordis, Miami, Fla) was advanced into the aortic arch

and then used to select the celiac axis. The catheter was advanced over the guidewire and into the desired hepatic artery branch, depending on the tumor location. Selective catheterization was performed to achieve lobar or segmental embolization based on the targeted lesions. A solution containing 100 mg of cisplatin (Platinol; Bristol-Myers Squibb, Princeton, NJ), 50 mg of doxorubicin (Adriamycin; Pharmacia-Upjohn, Kalamazoo, Mich), and 10 mg of mitomycin C (Mutamycin C; Bedford Laboratories, Bedford, Ohio) in a 1:1 mixture with iodized oil was infused and followed by the infusion of either polyvinyl alcohol particles or gelatin-coated trisacryl microspheres (Embosphere particles; Biosphere Medical, Rockland, Mass) until stasis was achieved.

Collected Data and Follow-up

According to the protocol, patients underwent contrast material–enhanced and diffusion MR imaging 4–6 weeks after TACE for assessment of tumor response. Complete blood cell counts and biochemistry profiles were acquired to assess toxicity. Patients with nearly complete tumor necrosis were followed up with MR imaging, complete blood cell counts and biochemistry profiles every 6–8 weeks. Patients with residual enhancement and a maintained clinical performance status underwent additional TACE treatment(s). Toxicity was assessed and graded according to the CTCAE, version 3.0, for toxicities. The CTCAE, version 3.0, are used to define grade 1–5 toxicities, with unique clinical descriptions of the severity for each adverse event (AE) based on the following general guidelines: Grade 1 indicates mild AE; grade 2, moderate AE; grade 3, severe AE; grade 4, life-threatening or disabling AE; and grade 5, death related to AE. At the time of analysis, the survival statuses of all patients were obtained from the Social Security Death Index. A decision was also made to exclude from the analysis any measurements that had been obtained within 3 weeks after TACE. This decision was based on the fact that transient transaminase elevation is a normal response to TACE (without clinical consequences) that is seen in nearly all patients who undergo this treatment. Typically, up to three separate TACE treatments are performed in a treatment cycle, similar to systemic chemotherapy cycles. The decision to repeat treatment was based on residual enhancement seen at MR imaging. We chose two time points at which to analyze the data: 6 months after the first TACE for evaluation of short-term toxicity after a complete TACE cycle and 1 year after TACE for assessment of the long-term effect of TACE on systemic and liver-specific toxicities. These time points also allowed us

to compare our results with those obtained with other liver chemotherapy regimens.

Statistical Analyses

The goal of our analysis was to estimate the distribution of toxicity grades at 6-month and 1-year follow-up after the first TACE. In the following paragraph, we discuss the methods that we used to estimate the toxicity distributions for one value at the 6 month follow-up, as these distributions are analogous for all toxicity substances and both follow-up times.

For the patients in whom toxicity measurements were obtained both before and after 6 months, the closest measurements were used to obtain interpolated grades of toxicity at 6 months. For patients who were alive but in whom measurements had stopped before 6 months had passed, interpolation was not possible. To estimate the goal under reasonable assumptions, we viewed the problem from a transition—that is, survival analysis—perspective. From this perspective, for each patient, *i,* there are six transition times—$T_{0,i}$, $T_{1,i}$, $T_{2,i}$, $T_{3,i}$, $T_{4,i}$, and $T_{\text{death},i}$—that start from the first TACE and end at the time (closest to 6 months) at which the patient transitions to toxicity grade 0, to grade 1, to grade 2, to grade 3, to grade 4, and to death, respectively. From this perspective, the early stopping of measurements before 6 months is expressed as a censoring of some transition times. For example, if the last toxicity measurement in a patient was obtained at 4 months and was grade 3, then times $T_{4,i}$ and $T_{\text{death},i}$ are censored at 4 months, whereas the times $T_{3,i}$, $T_{2,i}$, $T_{1,i}$, and $T_{0,i}$ are uncensored and can be determined by tracing back the patient's measurements.

Details of the procedure used to transform the original data to such censored transition data are given in the Appendix. For each grade *g,* we estimated the fraction of patients (Pr) for whom the transition time to grade *g, ($T_{g,i}$),* was longer than 6 months, $\Pr(T_{g,i} > 6\text{ m})$, by using survival analysis methods that account for censoring (see below). Finally, assuming that for the unobserved toxicity grades within a period close to 6 months or 1 year toxicity does not decrease, our goal—to determine the fraction of patients who were at a particular toxicity grade at 6 months, $\Pr(g_{6\text{m}})$—could be achieved by using our estimates of $\Pr(T_{g,i} > 6\text{ m})$ according to the following formula:

$$\Pr(g_{6m})$$
$$= \Pr(T_{g,i} > 6\text{ m}) - \Pr(T_{g+1,i} \leq 6\text{ m})$$
$$= [1 - \Pr(T_{g,i} > 6\text{ m})] - [1 - \Pr(T_{g+1,i} \leq 6\text{ m})]$$

In other words, patients who were at toxicity grade *g* at 6 months are those patients who had transitioned to grade *g* on or before the sixth month ($T_{g,i} \leq 6$ m) but had not transitioned to grade *g* + 1 on or before the sixth month ($T_{g+1,i} \leq 6$ m). Because the baseline toxicity grade can be predictive of both the transition times and the censoring rates, we first estimated $\Pr(T_{g,i} > 6$ m) within strata of baseline grades by using the within-strata Kaplan-Meier estimator (11). Then we reweighted these estimators according to the baseline grade distribution. We estimated baseline distributions of toxicity grades, transition distributions (see equation) within strata of baseline grades for 6 months and 1 year, and overall transition distributions.

RESULTS

Patient Characteristics

At analysis of the information in our database, we identified a total of 190 patients. The diagnosis of HCC was confirmed at histologic examination in 126 (66%) patients. The diagnosis of HCC in the remaining 64 patients was based on cross-sectional MR imaging findings and elevated serum alpha-fetoprotein levels. Patient characteristics are shown in Table 2.1. There were 155 male and 35 female patients (mean age, 65 years; age range, 18–84 years), and most of them (72%) were white. Forty patients had chronic hepatitis B, and 76 had chronic hepatitis C. The majority of patients (66%) had Child-Pugh class A cirrhosis. One hundred forty-one patients had multiple liver tumors. The average number of TACE sessions performed per patient was 2.4 (range, 1–3).

Hematologic Toxicity

The hematologic values observed in the 190 patients at baseline and 1 year after TACE were graded according to the CTCAE, version 3.0, and are presented in Figure 2.1. Leukocytopenia, anemia, thrombocytopenia, and

prolonged activated partial thromboplastin time were the most common hematologic toxic effects. For most patients, the observed toxicity was mild (grade 1 or 2). Grade 3 and grade 4 leukocytopenia was detected in 6% and 1% of the patients, respectively, after 6 months and in 6% and 13% of the patients, respectively, after 1 year. Grade 3 and grade 4 anemia was detected in 6% and 3% of the patients, respectively, after 6 months and in 4% and 15% of the patients, respectively, after 1 year. Grade 3 and grade 4 thrombocytopenia was detected in 10% and 3% of the patients, respectively, after 6 months and in 8% and 15% of the patients, respectively, after 1 year. Grade 3 prolonged activated partial thromboplastin time was detected in 8% of the patients after 6 months and in 18% of the patients after 1 year.

To assess the assumption that within a period close to 6 months or 1 year after TACE toxicity generally does not decrease, for each toxicity type we assessed the data for all patients with measurements obtained both before and after 6 months—or before and after 1 year—and thus in whom the assumption could be tested. Among these patients, the percentages of patients with measurements that were monotonic around 6 months ranged from 87% (glucose) to 99% (creatinine); these proportions ranged from 83% (alanine aminotransferase) to 100% (creatinine) around 12 months, indicating that our assumption was predominantly valid for the data with which it could be assessed.

Nonhematologic Toxicity

Postembolization syndrome consisting of abdominal pain, fever, loss of appetite, and nausea developed in most patients. However, these symptoms were generally mild and transient. Alopecia developed in 34 (18%) patients. Elevated aspartate aminotransferase, alanine aminotransferase, and alkaline phosphatase levels; hypoalbuminemia; and hyperbilirubinemia were frequent nonhematologic adverse effects (Fig 2.2). Grade 3 or 4 toxicity manifested as elevated aspartate aminotransferase levels in 15% of the patients after 6 months and in 18% after 1 year. Grade 3 or 4 alanine aminotransferase level elevations were detected in 10% of the patients after 6 months and in 18% after 1 year. Grade 3 alkaline phosphatase level elevations were detected in 8% of the patients after 6 months and in 18% after 1 year. Grade 3 hypoalbuminemia was detected in 10% of the patients after 6 months and in 19% after 1 year. Grade 3 or 4 total bilirubin level elevation was detected in 10% of the patients after 6 months and in 22% after 1 year.

In our patient group, severe complications were rare. Acute liver failure occurred in five (2.6%) patients and led to death in three of them. One patient died of variceal bleeding within 1 month after TACE. An intrahepatic abscess that developed in one patient 4 weeks after TACE was managed with drainage. One patient had a myocardial infarction 2 days after TACE and was treated with coronary artery bypass graft surgery.

Survival

The data of all patients were included in the survival analysis. Mean and median survival times after diagnosis were 27 and 16 months, respectively. Cumulative survival rates were 58% at 1 year, 39% at 2 years, and 29% at 3 years (Fig 2.3). Survival analysis of data for the 126 patients with Child-Pugh class A cirrhosis revealed cumulative survival rates of 68% at 1 year, 44% at 2 years, and 31% at 3 years.

DISCUSSION

HCC is one of the most common fatal cancers in the world. The incidence of HCC in the United States is on the rise owing to increased exposure to the hepatitis C virus (12). The prognosis is invariably poor, with a mean survival time of 6 months (13). Unfortunately, only a selected percentage of patients (10%–15%) are candidates for curative therapies because of the advanced stage of their disease at the time of diagnosis or the presence of comorbidity (14). TACE has become the mainstay of treatment for patients with nonresectable HCC. The aim in performing TACE is to deliver a high concentration of chemotherapeutic agents followed by an embolic agent to the tumor. This embolization blocks the arterial inflow and thus limits the washout of drugs and reduces the systemic side effects (15). Although this is a widely accepted notion, to our knowledge, there are no studies in the literature to date in which the systemic toxicities after TACE have been fully described. Therefore, our aim was to determine the toxicity profile of TACE in patients at 6 months and 1 year after treatment for HCC.

The results of several nonrandomized trials have demonstrated the positive effect of TACE in terms of increased tumor necrosis, as well as the improvements in patient survivals (16, 17). However, few controlled randomized studies have been published. Early randomized clinical trials revealed no survival benefit for patients with HCC who were treated with

TACE (18, 19). This can be explained by the fact that in these early trials, either the enrolled patients or the methods used for TACE were heterogeneous. The two most recent prospective randomized trials, however, revealed markedly longer survivals after chemoembolization (9, 10).

HCC is especially difficult to treat with systemic chemotherapy, and although multiple clinical trials have been performed to test many single- and combined-agent chemotherapies, to our knowledge, no regimen has facilitated a substantial tumor response or survival benefit. Furthermore, systemic toxicity is a well known disadvantage of chemotherapy. In fact, systemic toxicity is the limiting factor in establishing the dose of systemic chemotherapy, and in patients with HCC, who are already compromised owing to underlying liver disease, such toxicity can be extremely dangerous (20, 21). Sorafenib, an oral multikinase inhibitor, has induced partial tumor response; however, clinical trials are still underway and an extensive toxicity profile has yet to be determined (22). We believe that locoregional therapy, such as TACE, is unique because it delivers highly concentrated doses of chemotherapy to the tumor in a specific manner while preserving the nontumorous healthy liver tissue. In theory, this should prevent the occurrence of major systemic side effects.

The single chemotherapeutic agents that have facilitated a consistent tumor response rate of more than 10% are doxorubicin, 5-fluorouracil, and cisplatin. These agents reportedly have induced hematologic toxicities in as high as 22% of patients (grade 3 or 4 anemia), 28% of patients (grade 3 or 4 thrombocytopenia), and 67% of patients (grade 3 or 4 leukocytopenia) (23). In comparison, our results confirm the advantage of using locoregional treatment: Grade 3 or 4 hematologic toxicity manifesting as anemia, thrombocytopenia, or leukocytopenia was detected in only 9%, 13%, and 7% of the patients 6 months after TACE, respectively. The reported median survival time after systemic chemotherapy for HCC is less than 6 months (range, 6–20 weeks) (23). Our results indicate a median survival time of 16 months, and hematologic toxicities manifesting as leukocytopenia, anemia, thrombocytopenia, and prolonged activated partial thromboplastin time were detected in only 18%–23% of the patients after 1 year. Such results are even more remarkable given that all of these patients also had evidence of cirrhosis and thus were even more susceptible to the harmful effects from chemotherapy. In the patients with hematologic toxicities, we found no treatment-related mortalities, whereas treatment-related death rates as high as 25% have been reported in patients treated with doxorubicin (24).

Alopecia is considered to be one of the most distressing side effects of cancer therapy (25). This common side effect of systemic chemotherapy usually occurs 2–3 weeks after the first cycle of treatment. The likelihood of alopecia is related to the type of drugs used and the schedule of administration (26). Single-drug treatment with systemically administered anthracyclines leads to total alopecia in approximately 90% of treated patients (27). In our study, however, alopecia occurred in only 18% of the patients treated with TACE. This suggests that a substantial portion of the locally delivered chemotherapeutic agent in TACE stays in the tumor region. At the very least, it appears that TACE causes markedly lower rates of this traumatic side effect than does systemic chemotherapy.

Rarely, TACE induces hepatic failure that results in increased serum levels of aminotransferases and bilirubin, ascites, or hepatic encephalopathy (28). These adverse effects usually are transient, with liver function returning to baseline levels within 3 weeks after TACE—even in patients with advanced HCC (but with Child-Pugh class A or B cirrhosis). These effects are reportedly independent of patient age, embolization site, and number of treatments (29). In our patient population, grade 3 or 4 toxicities manifested as elevated aminotransferase and bilirubin serum levels in 18%–22% of the patients after 1 year. However, we cannot state conclusively whether this was a result of TACE or a part of the natural progression of liver disease. Acute liver failure occurred within 1 month after TACE in 2.6% of the patients and led to death in 1.6% of them.

Reported survival rates after TACE in patients with HCC vary between 60% and 88% at 1 year, between 30% and 60% at 2 years, and between 18% and 50% at 3 years, depending on several risk factors, such as Child-Pugh class, alpha-fetoprotein level, and presence or absence of portal vein thrombosis (30–32). In the present study, survival rates were 58% at 1 year, 39% at 2 years, and 29% at 3 years; however, we did not stratify the patients for potential risk factors. Portal vein thrombosis traditionally has been considered one of the main contraindications to performing TACE (33). However, we previously reported that TACE can be performed safely in patients with this condition (34). Therefore, patients with portal vein thrombosis were not excluded from this study. Moreover, 64 patients had baseline Child-Pugh class B cirrhosis. The relative risk factors for Child-Pugh class B cirrhosis (compared with Child-Pugh class A disease) and portal vein thrombosis are reported to be 1.72 and 1.58, respectively, and therefore may influence survival rates (35). The survival analysis of data for

the patients with Child-Pugh class A cirrhosis in our study revealed cumulative survival rates of 68% at 1 year, 44% at 2 years, and 31% at 3 years.

This study had several limitations: First, the study design was retrospective and not controlled. The uncontrolled nature of the study limited our ability to compare our study outcomes with those of other studies. However, our endpoints were objective and were obtained from a standardized source. Second, for obvious ethical reasons, not all patients underwent biopsy to confirm the diagnosis of HCC. We believe that the use of imaging features combined with elevated alpha-fetoprotein levels is a well-established alternative for confirming the diagnosis. Last, because it is difficult to differentiate procedural toxicity from progressive cirrhosis, our results represent findings in the worst-case scenario.

In conclusion, our results show that TACE has a favorable toxicity profile in patients with HCC, with minimal long-term toxicities. These data clearly support the role of TACE in the treatment of patients with nonresectable HCC. Our results give clinicians a good overview of the toxicities that can be expected after TACE and thereby will be helpful for optimizing treatment strategies.

TABLES & FIGURES

Characteristic	Value	
No. of patients	190	
Patient age (y)*	65 ± 14	
Male patients	155	(82)
Female patients	35	(18)
Race		
White	136	(72)
African-American	28	(15)
Asian	26	(14)
Child-Pugh class		
A	126	(66)
B	64	(34)
C	0	
Hepatitis B	40	(21)
Hepatitis C	76	(40)
Diagnosis method		
Histology	126	(66)
AFP level and MR imaging findings	64	(34)
Multiple lesions	141	(74)
One lesion	49	(26)

Table 2.1 Patient Characteristics, general information for all 190 patients evaluated. Note.—All except age data are numbers of patients, with percentages in parentheses. AFP = alpha-fetoprotein. * Mean age ± standard deviation.

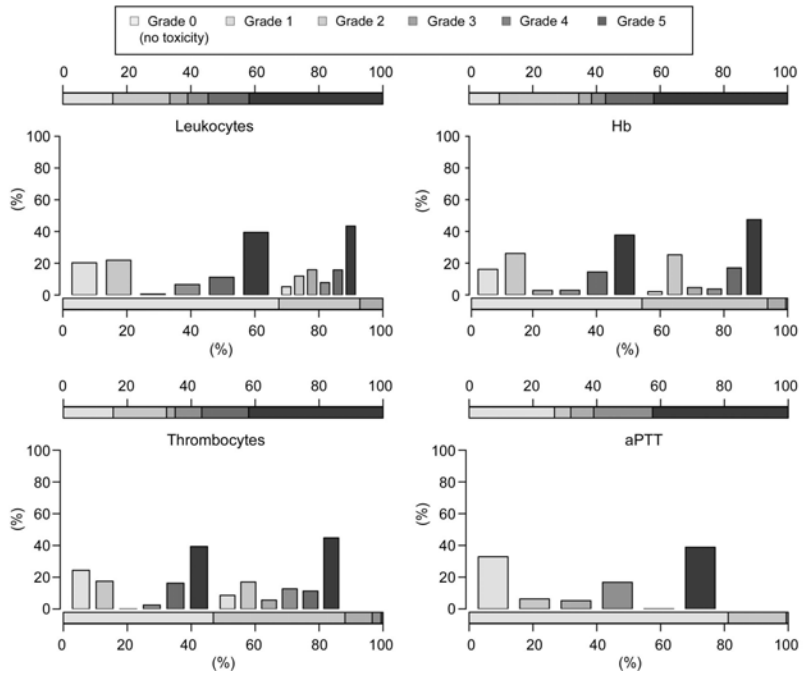

Figure 2.1 Hematologic toxicities. Histograms show estimated distributions at baseline and at 1 year after first TACE in all 190 patients. Horizontal bar scales convey the distributions of toxicity grades at baseline (bottom scale) and at 1 year (top scale). Vertical bars convey the possible associations between toxicity grades across the two time points. *aPTT* = activated partial thromboplastin time, *Hb* = hemoglobin.

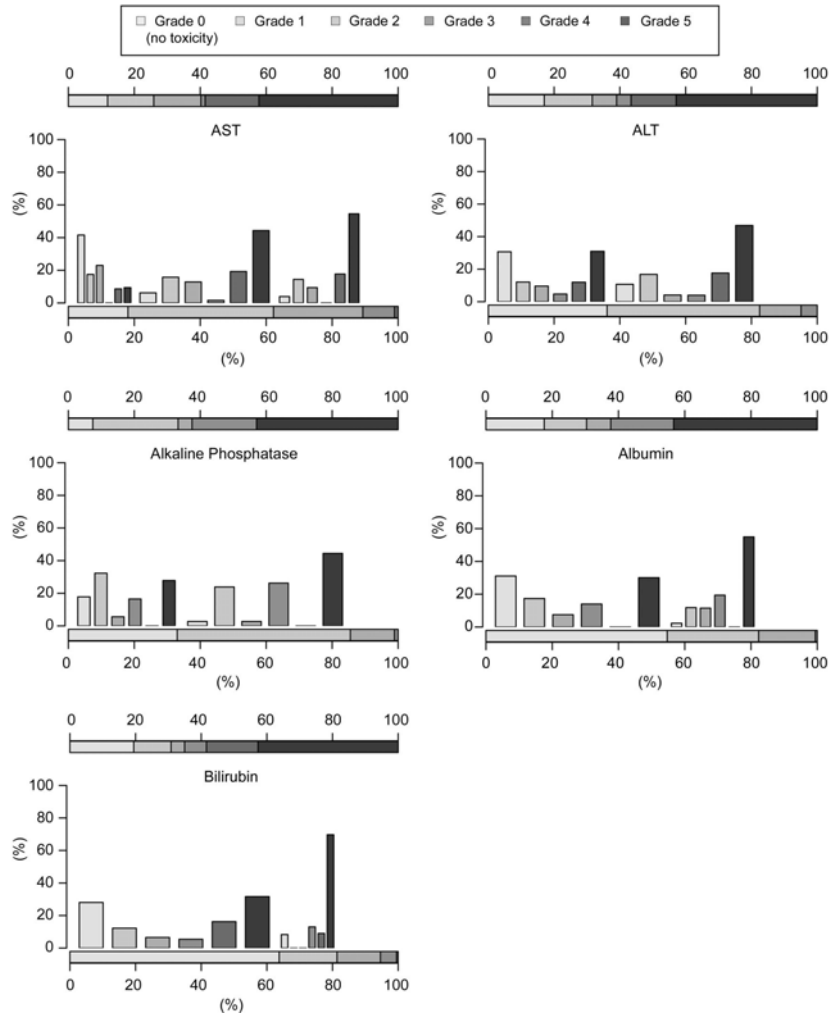

Figure 2.2 Nonhematologic toxicities. Histograms show estimated distributions at baseline and at 1 year after first TACE in all 190 patients. Horizontal bar scales convey the distributions of toxicity grades at baseline (bottom scale) and at 1 year (top scale). Vertical bars convey possible associations between toxicity grades across the two time points. *ALT* = alanine aminotransferase, *AST* = aspartate aminotransferase.

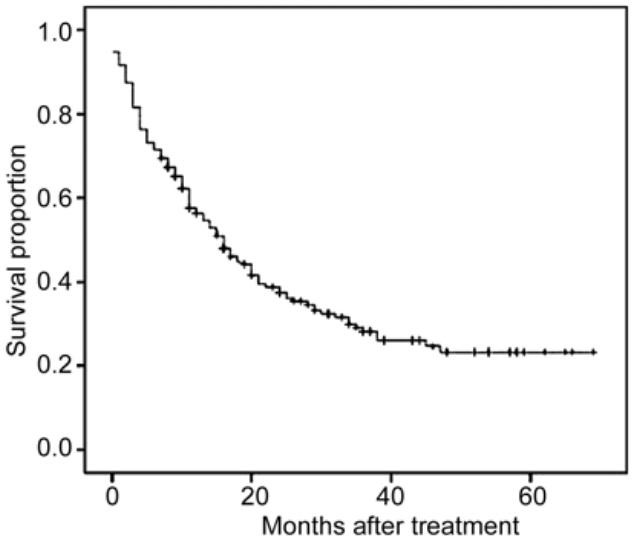

Figure 2.3 Overall survival curve for all 190 patients with nonresectable HCC who were treated with TACE.

APPENDIX

Below we describe in detail the procedure used to transform the original data to censored transition data. We describe the procedure used to obtain the transition data relevant for estimating the proportion of patients whose toxicity grade at D months is larger than grade g, $\Pr(T_{g,i} > D)$. There are two main cases:

Case 1

In case 1, the patient has measurements obtained both before and after the date D. In this case, we define the measurement grade on the left or right of the interval, which includes date D as level.left or level.right. Accordingly, time.left and time.right are defined as the times when these measurements are made. There are two subcases. In subcase 1, the toxicity grade, g, increases around date D: *(a)* If level.right is less than g, then the transition data for the time to cross toxicity grade g (ie, time of follow-up and observation status) are defined as (date D + 1, 0). *(b)* If level.left is less than g and level.right is greater than or equal to g, then the transition data for the time to cross toxicity grade g are defined as (crossing time, 1), where crossing time is the interpolated time between time.left and time.right for

crossing *g*. *(c)* If both level.left and level.right are greater than or equal to *g,* then the transition data for the time to cross toxicity grade *g* are defined as (track back, 1), where track back is the first time the grade crossed *g*.

In subcase 2, the toxicity grade either decreases or does not change around date *D: (a)* If that grade is less than *g,* then the transition data for the time to cross toxicity grade *g* are (date *D* + 1, 0). *(b)* Otherwise, the transition data for the time to cross toxicity grade *g* are (track back, 1).

Case 2

In case 2, there is no measurement after date *D*. In this case, level.left denotes the second to the last measurement and level.right denotes the last measurement. Accordingly, time.left and time.right are defined. There are three conditions: *(a)* If level.right is less than *g,* then the transition data are (time.right, 0). *(b)* If level.left is less than *g* and level.right is greater than or equal to *g,* then the transition data are (crossing time, 1). *(c)* If both level.left and level.right are greater than or equal to *g,* then the transition data are (track back, 1).

We provide an example: A patient had a measurement of glucose toxicity of grade 0 at 153 days, and the next measurement was obtained at grade 2 at 226 days. This patient is predicted to have crossed grade 2 at day 202; thus, this patient's contribution to estimating the proportion of patients whose toxicity grade at 180 days has crossed grade 2, $\Pr(T_{2,i} > 180 \text{ days})$, belongs in category 1(1)*b* (case 1, subcase 1, condition *b*) and the transition data are (202, 1).

REFERENCES

1) Parkin DM, Bray F, Ferlay J, Pisani P. Estimating the world cancer burden: Globocan 2000. Int J Cancer 2001;94:153–156.
2) El-Serag HB, Mason AC. Rising incidence of hepatocellular carcinoma in the United States. N Engl J Med 1999;340:745–750.
3) McGlynn KA, Tarone RE, El-Serag HB. A comparison of trends in the incidence of hepatocellular carcinoma and intrahepatic cholangiocarcinoma in the United States. Cancer Epidemiol Biomarkers Prev 2006;15:1198–1203.
4) Bruix J, Llovet JM. Prognostic prediction and treatment strategy in hepatocellular carcinoma. Hepatology 2002;35:519–524.
5) Trotti A, Colevas AD, Setser A, et al. CTCAE v3.0: development of a comprehensive grading system for the adverse effects of cancer treatment. Semin Radiat Oncol 2003;13:176–181.
6) Carr BI. Hepatocellular carcinoma: current management and future trends. Gastroenterology 2004;127(5 suppl 1):S218–S224.
7) Chung JW, Park JH, Han JK, et al. Hepatic tumors: predisposing factors for complications of transcatheter oily chemoembolization. Radiology 1996;198:33–40.
8) Xia J, Ren Z, Ye S, et al. Study of severe and rare complications of transarterial chemoembolization (TACE) for liver cancer. Eur J Radiol 2006;59:407–412.
9) Llovet JM, Real MI, Montana X, et al. Arterial embolisation or chemoembolisation versus symptomatic treatment in patients with unresectable hepatocellular carcinoma: a randomised controlled trial. Lancet 2002;359:1734–1739.
10) Lo CM, Ngan H, Tso WK, et al. Randomized controlled trial of transarterial lipiodol chemoembolization for unresectable hepatocellular carcinoma. Hepatology 2002;35:1164–1171.
11) Kaplan EL, Meier P. Nonparametric estimation from incomplete observations. J Am Stat Assoc 1958;53:457–481.
12) El-Serag HB. Epidemiology of hepatocellular carcinoma in USA. Hepatol Res 2007;37(suppl 2):S88–S94.
13) Capocaccia R, Sant M, Berrino F, Simonetti A, Santi V, Trevisani F. Hepatocellular carcinoma: trends of incidence and survival in Europe and the United States at the end of the 20th century. Am J Gastroenterol 2007;102:1661–1670.

14) Stuart KE, Anand AJ, Jenkins RL. Hepatocellular carcinoma in the United States: prognostic features, treatment outcome, and survival. Cancer 1996;77:2217–2222.
15) Breedis C, Young G. The blood supply of neoplasms in the liver. Am J Pathol 1954;30:969–977.
16) Barone M, Ettorre GC, Ladisa R, et al. Transcatheter arterial chemoembolization (TACE) in treatment of hepatocellular carcinoma. Hepatogastroenterology 2003;50:183–187.
17) Bronowicki JP, Vetter D, Dumas F, et al. Transcatheter oily chemoembolization for hepatocellular carcinoma: a 4-year study of 127 French patients. Cancer 1994;74:16–24.
18) Pelletier G, Roche A, Ink O, et al. A randomized trial of hepatic arterial chemoembolization in patients with unresectable hepatocellular carcinoma. J Hepatol 1990;11:181–184.
19) Bruix J, Llovet JM, Castells A, et al. Transarterial embolization versus symptomatic treatment in patients with advanced hepatocellular carcinoma: results of a randomized, controlled trial in a single institution. Hepatology 1998;27:1578–1583.
20) Aguayo A, Patt YZ. Nonsurgical treatment of hepatocellular carcinoma. Semin Oncol 2001;28:503–513.
21) Di Maio M, De Maio E, Perrone F, Pignata S, Daniele B. Hepatocellular carcinoma: systemic treatments. J Clin Gastroenterol 2002;35(5 suppl 2):S109–S114.
22) Abou-Alfa GK, Schwartz L, Ricci S, et al. Phase II study of sorafenib in patients with advanced hepatocellular carcinoma. J Clin Oncol 2006;24:4293–4300.
23) Simonetti RG, Liberati A, Angiolini C, Pagliaro L. Treatment of hepatocellular carcinoma: a systematic review of randomized controlled trials. Ann Oncol 1997;8:117–136.
24) Lai CL, Wu PC, Chan GC, Lok AS, Lin HJ. Doxorubicin versus no antitumor therapy in inoperable hepatocellular carcinoma: a prospective randomized trial. Cancer 1988;62:479–483.
25) Gunnars B, Nygren P, Glimelius B. Assessment of quality of life during chemotherapy. Acta Oncol 2001;40:175–184.
26) Ridderheim M, Bjurberg M, Gustavsson A. Scalp hypothermia to prevent chemotherapy-induced alopecia is effective and safe: a pilot study of a new digitized scalp-cooling system used in 74 patients. Support Care Cancer 2003;11:371–377.
27) Fischer DS, Knobf MT, Durivage HJ. The cancer chemotherapy handbook. 4th ed. St. Louis, Mo: Mosby, 1993.

28) Kiely JM, Rilling WS, Touzios JG, et al. Chemoembolization in patients at high risk: results and complications. J Vasc Interv Radiol 2006;17:47–53.
29) Caturelli E, Siena DA, Fusilli S, et al. Transcatheter arterial chemoembolization for hepatocellular carcinoma in patients with cirrhosis: evaluation of damage to nontumorous liver tissue—long-term prospective study. Radiology 2000;215:123–128.
30) Geschwind JF, Ramsey DE, Choti MA, Thuluvath PJ, Huncharek MS. Chemoembolization of hepatocellular carcinoma: results of a metaanalysis. Am J Clin Oncol 2003;26:344–349.
31) Ikeda M, Okada S, Yamamoto S, et al. Prognostic factors in patients with hepatocellular carcinoma treated by transcatheter arterial embolization. Jpn J Clin Oncol 2002;32:455–460.
32) Llado L, Virgili J, Figueras J, et al. A prognostic index of the survival of patients with unresectable hepatocellular carcinoma after transcatheter arterial chemoembolization. Cancer 2000;88:50–57.
33) Camma C, Schepis F, Orlando A, et al. Transarterial chemoembolization for unresectable hepatocellular carcinoma: meta-analysis of randomized controlled trials. Radiology 2002;224:47–54.
34) Georgiades CS, Hong K, D'Angelo M, Geschwind JF. Safety and efficacy of transarterial chemoembolization in patients with unresectable hepatocellular carcinoma and portal vein thrombosis. J Vasc Interv Radiol 2005;16:1653–1659.
35) A new prognostic system for hepatocellular carcinoma: a retrospective study of 435 patients: the Cancer of the Liver Italian Program (CLIP) investigators. Hepatology 1998;28:751–755.

CHAPTER 3

ASSESSMENT OF TUMOR RESPONSE ON MR IMAGING AFTER LOCOREGIONAL THERAPY

Vossen JA, Buijs M, Kamel IR

Tech Vasc Interv Radiol 2006 Sep;9(3):125-32.

ABSTRACT

Assessment of tumor response after locoregional therapies is important in determining treatment success and in guiding future therapy. Magnetic resonance imaging plays an important role in evaluating treatment response to new therapies directed toward hepatic lesion treatment. The traditional and accepted criteria to determine tumor response in oncology, namely the Response Evaluation Criteria in Solid Tumors (RECIST) and the European Association for the Study of the Liver (EASL) criteria, use decrease in tumor size and lesion enhancement as an indicator of successful therapy. A more recent evaluation method is the Apparent Diffusion Coefficient (ADC) measured by diffusion-weighted MR imaging. Diffusion-weighted MR imaging and ADC values map the thermally induced motion of water molecules in tissues and thereby are able to provide insight into tumor microstructure. In this article we discuss the role of MR imaging in assessing treatment response after various locoregional therapies. We describe the role of tumor size and lesion enhancement as well as ADC mapping. We also discuss the magnetic resonance imaging findings after radiofrequency ablation (RFA), transarterial chemoembolization (TACE) and radioembolization.

INTRODUCTION

Although liver resection continues to be the standard for curative care in patients with hepatic malignancies, most patients are not candidates for surgical therapy. Therefore, minimally invasive strategies have gained increased attention as therapeutic options for both primary and metastatic hepatic malignancies (1, 2). These locoregional therapies include tissue ablation and embolization procedures, such as transarterial chemoembolization and transarterial radioembolization. Locoregional therapies can be applied intraoperatively, percutaneously, or intra-arterially with the use of imaging or angiographic guidance. The aim of these treatments is to induce cellular necrosis and achieve cytoreduction. Possible benefits of minimally invasive therapies over surgery are reduction in morbidity and mortality, decrease in duration of hospital stay and extension of patient selection by including nonsurgical candidates.

Assessment of tumor response after locoregional therapies is important in determining treatment success and in guiding future therapy. Several monitors of tumor response have been used, including histology, tumor markers, and imaging. However, histologic evaluation using tissue biopsy can only be conclusive when it shows viable malignancy. Therefore, repeated negative biopsies do not exclude the presence of residual tumor. Tumor markers solely are of limited use in assessing tumor response. Various imaging modalities, including Doppler ultrasonography, angiography, computed tomography (CT), and magnetic resonance imaging (MRI) have been used to evaluate treatment response (3, 4). In this article we discuss the role of MRI in assessing treatment response after various locoregional therapies that are commonly used at our institution.

Role of Imaging in Assessing Treatment Response

Standardized criteria for measuring therapeutic response have been established in 1981 by the World Health Organization (WHO) (5). However, several problems were encountered when using these WHO criteria. These include wide variations between observers in estimating the position of the lesion boundary and the number of lesions that may be used to assess for response. Furthermore, the use of relatively new imaging modalities such as CT and MRI caused confusion about the use of 3-dimensional measurements. In 2000 the Response Evaluation Criteria in Solid Tumors (RECIST) was introduced to unify response assessment

criteria (6). These criteria included important changes such as unidimensional tumor measurement, selection of target lesions with a minimum size, details concerning imaging modalities, and a new threshold for assignment of objective progression (7). RECIST, however, still relies on size change of lesions to assess response. For this reason the validity of RECIST has recently been questioned in view of the emergence of new anticancer therapies, because these therapies are based on stabilizing disease rather than causing tumor disappearance (8). Therefore, the early effects of these therapies would not be detected by RECIST and occasionally patients may not be considered to have exhibited a response despite the presence of tumor necrosis.

This realization that anatomy may not change after locoregional therapies moved the focus toward new evaluation methods. These include assessment of tumor vascular and cellular integrity, motion of water molecules, and biochemical concentration. Vascular integrity is measured by the degree of extracellular contrast enhancement. The European Association for the Study of the Liver (EASL) has officially recommended the use of lesion enhancement on contrast-enhanced CT as the standard modality to determine treatment response of HCC after locoregional therapy (9). This change was also reflected in the national practice guideline released by the American Association for the Study of Liver Disease on the management of HCC in 2005 (10). Areas of tumor enhancement were considered viable whereas nonenhancing regions reflected tissue necrosis. The EASL also stated that tumor size measurements might not be accurate because these measurements would not take into account the true extent of tumor necrosis.

Cellular integrity and motion of water molecules are represented by the apparent diffusion coefficient (ADC) that is measured by diffusion-weighted MRI. Diffusion-weighted MRI and ADC values map the thermally induced motion of water molecules in tissues and thereby are able to provide insight into tumor microstructure (11). Viable tumors are high in cellularity. These cells have an intact cell membrane that restrict the mobility of water molecules and causes a low ADC value. Conversely, cellular necrosis causes increased membranous permeability, which allows water molecules to move freely and thus causes a marked increase in the ADC value.

Biochemical concentration can be evaluated by the use of MR spectroscopy (1H MRS). 1H MRS has been used successfully in the

diagnosis of tumors in the brain and breast and in the evaluation of chemotherapy (12-14). In the liver, 1H MRS has been proven useful in evaluating diffuse hepatic disease such as hepatic steatosis, chronic hepatitis, and cirrhosis (15). The role of 1H MRS in evaluating tumor response after locoregional therapies still has to be established. However, preliminary studies are promising, and show that hepatic choline levels may allow monitoring of therapeutic responses of HCC to TACE (16).

MRI Technique

Our current MRI protocol uses a 1.5-T MRI scanner (CV/i; GE Healthcare, Milwaukee, WI) and a phased-array torso coil. The technique consists of T2-weighted fast spin-echo images (matrix, 256 × 256; slice thickness, 8 mm; interslice gap, 2 mm; repetition time [TR]/ echo time [TE], 5000/100 msec; receiver bandwidth, 32 kHz) and breath-hold diffusion-weighted echoplanar images (matrix, 128 × 128; slice thickness, 8 mm; interslice gap, 2 mm; b value, 500 mm^2/sec; TR/TE, 5000-6500/110 msec; receiver bandwidth, 64 kHz).

The initial applications of diffusion-weighted MRI have been in brain imaging, mainly for the evaluation of acute ischemic stroke, intracranial tumors, and demyelinating disease (17, 18). In the brain diffusion gradients are measured multidirectional because the fiber tracks have different directionality of flow (19-22). The liver, however, has an isotropic diffusion pattern, probably because of its randomly organized structures. Therefore, the ADC is measured only in one direction (23). Higher b-values can reduce the effect of perfusion on the calculated ADC value. However, lower b-values can lead to the underestimation of ADC values (24). In prior studies preformed for brain imaging high b-values of 1000 sec/mm^2 were used. However, in our experience a b-value of 500 sec/mm^2 had better signal-to-noise compared with higher b-values. Therefore, in our institution a b-value of 500 sec/mm^2 is used.

The final component of our imaging protocol is breath-hold unenhanced and contrast-enhanced (0.1 mmol/kg intravenous gadodiamide [Omniscan; GE Healthcare, Princeton, NJ]) T1-weighted three-dimensional fat-suppressed spoiled gradient-echo images (field of view, 320-400 mm; matrix, 192 × 160; slice thickness, 4-6 mm TR/TE, 5.1/1.2 msec; receiver bandwidth, 64 kHz; flip angle, 15º). The contrast-enhanced images are

obtained in the arterial phase (20 seconds) and portal venous phase (60 seconds).

MRI after Tissue Ablation

Tissue ablation can be performed by several techniques, either chemical (eg, ethanol ablation), thermal [eg, radiofrequency (RF), microwave and laser ablation], or cooling effect (eg, cryotherapy). These therapies require imaging for adequate targeting, monitoring the ablation process and for follow-up. Ultrasonography (US) is most often used as the primary guidance technique. CT and MRI are more commonly used to assess treatment response (25, 26). We will discuss the role of MRI in evaluating therapeutic response to the most widely accepted method of tissue ablation; radiofrequency ablation (RFA).

RFA induces thermally mediated coagulation necrosis, resulting in cellular death, using heat and low-voltage alternating electrical current that is delivered to the tumor by means of an electrode. RFA can be applied percutaneously, laparoscopically, or at open surgery. Previous models of electrodes had several technological limitations that did not allow ablation in tumors larger than 3 cm. Modifications in these original designs, including hooked electrodes, internally cooled electrodes, pulsed techniques, multiple probes, multiple insertions, and more powerful generators have led to improved results (27, 28). It is critical for physicians to select the appropriate patient population, to improve results. It is generally accepted that the patient inclusion criteria for RFA are few (< 5), small (< 3 cm) lesions with no extrahepatic disease and near normal liver function (29, 30).

After RFA, imaging is commonly used to assess for treatment response. In our institution, MRI is the modality of choice for follow-up of these lesions. There are several factors influencing treatment response, such as treatment approach, tumor size, tumor location, histologic type, and presence of confounding liver disease. Smaller lesions (< 3 cm) have better necrosis and have a lower recurrence rate than larger lesions. Metastases have a higher recurrence rate, presumably because of the presence of occult disease at the time of initial ablation. Underlying cirrhosis in patients with HCC causes larger ablations than would be expected in metastatic disease, because the cirrhotic liver functions as a thermal insulator promoting better thermal coagulation (31).

Adequately treated lesions are uniformly hypointense on T2-weighted images, probably because of dehydration and coagulative necrosis induced by tissue heating. Occasionally hyperintense foci may be seen on T2-weighted images corresponding to an area of tissue loss filled by fibrin or hemorrhage. A tumor that has been completely treated no longer enhances on gadolinium-enhanced MRI. However, an enhancing rim may appear immediately after treatment, most likely because of reactive hyperemia representing an inflammation reaction to the thermal injury (32, 33). Most lesions demonstrate markedly heterogeneous signal intensity on T1-weighted images caused by an uneven evolution of necrosis over time (34). Arteriovenous shunting caused by needle puncture or thermal damage may result in wedge-shaped enhancement on the arterial phase within the liver parenchyma in close proximity to the treated lesion (Fig 3.1). However, it is expected that perfusional abnormalities vanish by 30 days after the procedure. Ideally, on MRI, the size of the treated lesion exceeds the size of the lesion before treatment, indicating complete ablation of the tumor margin, including a safety margin. On subsequent follow-up, the lesion shows an involution of the coagulation site. Small necrotic areas may disappear completely.

Residual or recurrent tumor manifests as a lesion with irregular and nondelineated contours and demonstrate moderately high signal on T2-weighted images, with the same characteristics as on preinterventional imaging. Residual or recurrent tumor is often located within or at the periphery of the ablated lesion (35). This focus may not enhance in the first 2 months after treatment. However, enhancement usually occurs on subsequent MRI.

MRI after TACE

Transarterial chemoembolization is the major transcatheter therapy for liver tumors. The technique of TACE consists of delivering high concentrations of chemotherapeutic agents emulsified in an oil-based medium directly to the tumor bed followed by some form of embolization. The purpose of the embolization is to reduce arterial inflow to prevent washout of the chemotherapeutic agents from the aqueous phase of the emulsion, as well as to increase contact time between tumor cells and the delivered chemotherapeutic agents. In addition, because arterial inflow is slowed down, high extraction of the chemotherapeutic agents by tumor cells occurs. These factors resolved in significantly reduced systemic toxicity that may result from treatment. Currently, various combinations of drugs have

been reported, with most agents coming from doxorubicin or cisplatin chemotherapy families.

Assessment of tumor response after TACE on imaging is generally based on iodized oil deposition on unenhanced CT and tumor enhancement and tumor size on contrast enhanced CT or MRI. Unenhanced CT can demonstrate the presence of hyperattenuating iodized oil within the tumor. Good iodized oil retention is associated with prolonged median survival but does not indicate complete necrosis. Hyperattenuating iodized oil impairs the assessment of residual tumor enhancement on contrast enhanced CT. In contrast to CT, the high concentration of iodized oil after chemoembolization does not affect MR signal intensity. Contrast-enhanced MRI determines areas of tumor enhancement by using an extracellular contrast agent. Enhancing portions of the tumor are presumed to be viable, whereas nonenhancing portions are presumed to be necrotic. The disadvantage of contrast-enhanced MRI is the incapability to distinguish viable cells from reactive granulation tissue. Contrast-enhancement in granulation tissue is believed to be caused by increased capillary permeability and marked increase in the passive distribution of gadolinium (36). After TACE an enhancing rim can appear on contrast-enhanced MRI. This rim can correlate to either viable tumor as well as to reactive tissue.

A recent imaging technique for assessment of tumor response is diffusion-weighted MRI (37). This imaging technique is used to detect the motion of water molecules. Initially diffusion-weighted MRI has been limited to the brain. With the advent of the ultrafast singleshot echoplanar imaging technique, diffusion-weighted MRI of the abdomen has become possible.

We will discuss the MRI features of different tumors after TACE, including primary and metastatic liver tumors. The primary tumors we will discuss are HCC and cholangiocarcinoma. The metastatic tumors we will discuss are divided into hypovascular (metastatic breast cancer) and hypervascular (metastatic neuroendocrine cancer) metastases.

HCC

Hepatocellular carcinoma (HCC) is the fifth most common cancer in the world and represents more than 5% of all cancers (38). The majority of HCC patients (approx 75%) are not candidates for curative treatments either

because of poor liver function or the presence of advanced disease. These patients may be eligible for treatment with TACE. TACE achieves partial response in 15 to 55% of patients and significantly delays tumor progression and vascular invasion (39-42). Because of its impact on survival, it has become essential to accurately determine tumor response after therapy (37).

For patients with HCC treated with TACE signal intensity on T1 and T2 weighted images varies. Hypointensity on T2 weighted images represents necrosis. Conversely, hyperintensity on T2 weighted images corresponds to residual tumor. However, this hyperintensity can also represent hemorrhage, liquefied necrosis or inflammatory infiltration. HCC is hypervascular and enhances rapidly at dynamic early phase scanning, and declines at the late phase. After TACE, on the arterial phase images, residual viable tumor is rapidly enhancing, either homogeneous or heterogeneous, whereas necrotic tumor is nonenhancing (43, 44). On portal venous phase images both viable tumor and inflammatory infiltration can cause persistent enhancement (Fig 3.2). After successful TACE diffusion-weighted MRI shows an increase in ADC value, representing tumor necrosis. In prior studies we have demonstrated that mean tumor ADC increased after TACE by 20% ($p = 0.026$), whereas the ADC remained unchanged in nontumorous liver, spleen, and muscle (37).

Cholangiocarcinoma

Cholangiocarcinoma is a rare hepatic malignancy with an incidence of 1 to 2 per 100,000 persons in the United States. Only approximately 30% of patients with cholangiocarcinoma are eligible for resection because of the advanced nature of the disease at the time of diagnosis. A previous study at our institution showed that TACE provided an effective therapeutic option for patients with unresectable intrahepatic cholangiocarcinoma, with a median survival of 23 months (45). Cholangiocarcinomas are commonly described as hypovascular tumors. After TACE, necrosis is represented as dark on T1 with a central-area void of contrast enhancement on gadolinium-enhanced perfusion MRI and increased signal on diffusion MR sequences reflecting cell death.

Hypovascular Liver Metastases: Metastatic Breast Cancer

In the Western World breast cancer is the most common cancer in women and in this group it is the second leading cause of cancer death (46). The liver is the most common site of intra-abdominal metastatic disease,

with metastases to the liver occurring in up to 20% of the patients (47). Metastatic breast cancer is essentially incurable and TACE has become more commonly used as a treatment (48). Before TACE most lesions are hypointense on T1 and after TACE they generally remain hypointense. According to preliminary data from our group, on gadolinium-enhanced MRI, overall tumor enhancement in the arterial and portal venous phases decreases significantly after TACE by 32% and 39%, respectively ($p < 0.0001$) (Fig 3.3). Diffusion MRI is also useful in monitoring response after treatment. Mean tumor ADC increases by 27% ($p < 0.0001$) after successful TACE, whereas the ADC remains unchanged in nontumorous liver, spleen, and muscle.

Hypervascular Liver Metastases: Metastatic Neuroendocrine Tumors

Neuroendocrine tumors (NET) are rare neoplasms with an incidence of 1 to 4 cases per 100,000 people per year (49). These heterogeneous tumors may originate from the pancreas (pancreatic endocrine tumors) or the gastrointestinal tract (carcinoids) (50). Hepatic metastases in patients with NET are frequent (25-90%) and despite their slow growth, their presence influences prognosis significantly (51, 52). Surgery is considered the first line therapy for patients with liver metastases from NET, but potential curative resection is possible for only 10% of patients, because of the diffuse pattern of hepatic metastases at the time of diagnosis (53). Moreover, systemic chemotherapy in patients with diffuse and/or progressive liver metastases yields disappointing results especially in patients with metastases from midgut origin.

Treatment of hepatic metastases of NETs with TACE seems to be an attractive palliative option, because of their slowly growing and localized hypervascular pattern. Multiple studies have demonstrated the effectiveness of TACE for hepatic metastases of NETs in achieving hormone symptoms control and reduction of tumor growth (54-57). In most previous reports, tumor response to treatment has been measured by contrast enhanced CT or MRI (55, 57). In a study of 66 lesions in 26 patients with hepatic metastases from NET we have reported the functional MRI findings after TACE. Mean tumor diameter before treatment was 5.5 cm and decreased to 4.5 cm after treatment. Even though the decrease in tumor size was statistically significant ($p < 0.0001$), the size change was small (18%), and did not fulfill the RECIST criteria for partial response. We have also reported significant decrease in tumor arterial and venous enhancement after TACE. This is particularly important because these tumors are hypervascular and TACE

results in occlusion of the blood flow to the tumor vasculature. Mean pretreatment tumor enhancement in the arterial phase was 61% and decreased to 31% after treatment ($p < 0.0001$). Mean pretreatment tumor enhancement in the portal venous phase was 82% and decreased to 43% after treatment ($p < 0.0001$). We have also reported a significant increase in tumor ADC value from 1.5×10^{-3} mm^2/sec before treatment to 1.8×10^{-3} mm^2/sec after treatment ($p < 0.0001$), indicating marked cellular necrosis in response to therapy.

MRI after Radioembolization with Yttrium-90 Microspheres

The use of whole-liver external beam radiotherapy has limited applicability, because the liver parenchyma is radiation-sensitive and therefore there is a high risk of radiation induced liver disease, a clinical syndrome of anicteric hepatomegaly, ascites, and increased liver enzymes occurring weeks to months after therapy. Radioembolization delivers internal radiation to liver lesions via catheter directed intra-arterial administration of Yttrium-90 embedded microspheres (58). The intention is to deliver a higher dose of radiation selectively to the tumor, thereby sparing normal liver parenchyma (59, 60). Lobar, segmental and subsegmental treatment can be performed. A lung scan using technetium-99m macroaggregated albumin is performed before treatment, to determine the pulmonary shunting. A shunt of 20% or less is usually acceptable (61).

Assessment of tumor response after treatment with Yttrium-90 microspheres is necessary in determining future therapeutic strategies. Change in tumor size and enhancement on CT and MRI according to RECIST and EASL are the accepted criteria for assessing tumor response. These criteria may also be useful in the evaluation of locoregional treatment with theraspheres. Some studies suggested that decrease in tumor enhancement is associated with a favorable response to therapy with Yttrium-90 microspheres (62). Preliminary data from our group showed a mean decrease in arterial enhancement of 22% ($P = 0.013$) and a mean decrease in venous enhancement of 25% ($p = 0.012$) in patients with HCC treated with Yttrium-90 microspheres (Fig 3.4).

Diffusion MRI has been successfully utilized to assess early tumor response after chemotherapy and radiation therapy. So far only one report suggested diffusion-weighted MRI is a promising technique for evaluating early tumor response after radioembolization, with a significantly increased

ADC of 65% (p = 0.004) after therapy (62). Preliminary data from our group showed an increase in ADC value of 13% (p = 0.02).

SUMMARY

MRI plays an important role in the follow-up of patients after locoregional therapy for hepatic neoplasms. We discussed the use of RECIST and EASL in the assessment of treatment response. We also presented the MRI findings after RFA, TACE, and radioembolization, including ADC mapping.

TABLES & FIGURES

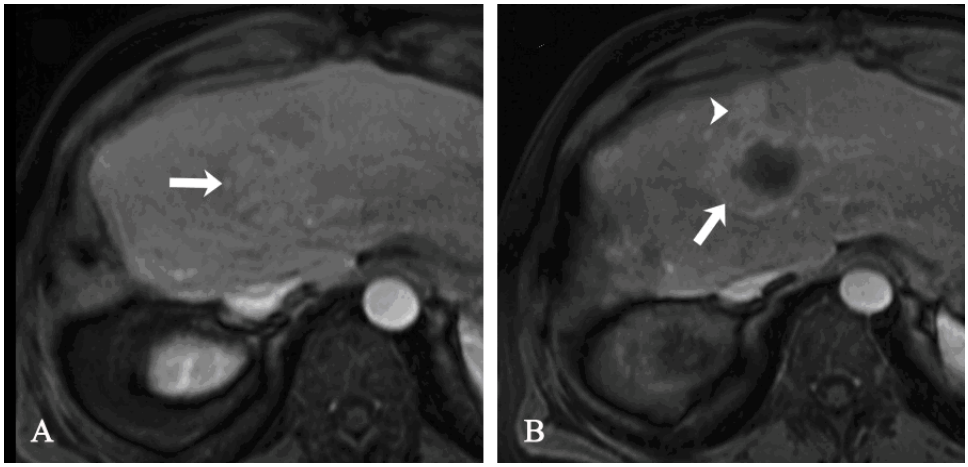

Figure 3.1 Changes on MR imaging after RF ablation of HCC.
(A) Gadolinium-enhanced image (TR/TE, 5.1/1.2 msec) shows a mass in the left lobe of the liver (arrow). Notice that the lesion has near 100% enhancement.
(B) Gadolinium-enhanced image (TR/TE, 5.1/1.2 msec) after RF shows significant decrease (75%) in enhancement. Minimal residual enhancement persists in the periphery (arrow) suggesting residual tumor. Notice wedge-shaped enhancement in close proximity to the treated lesion (arrowhead) due to needle puncture.

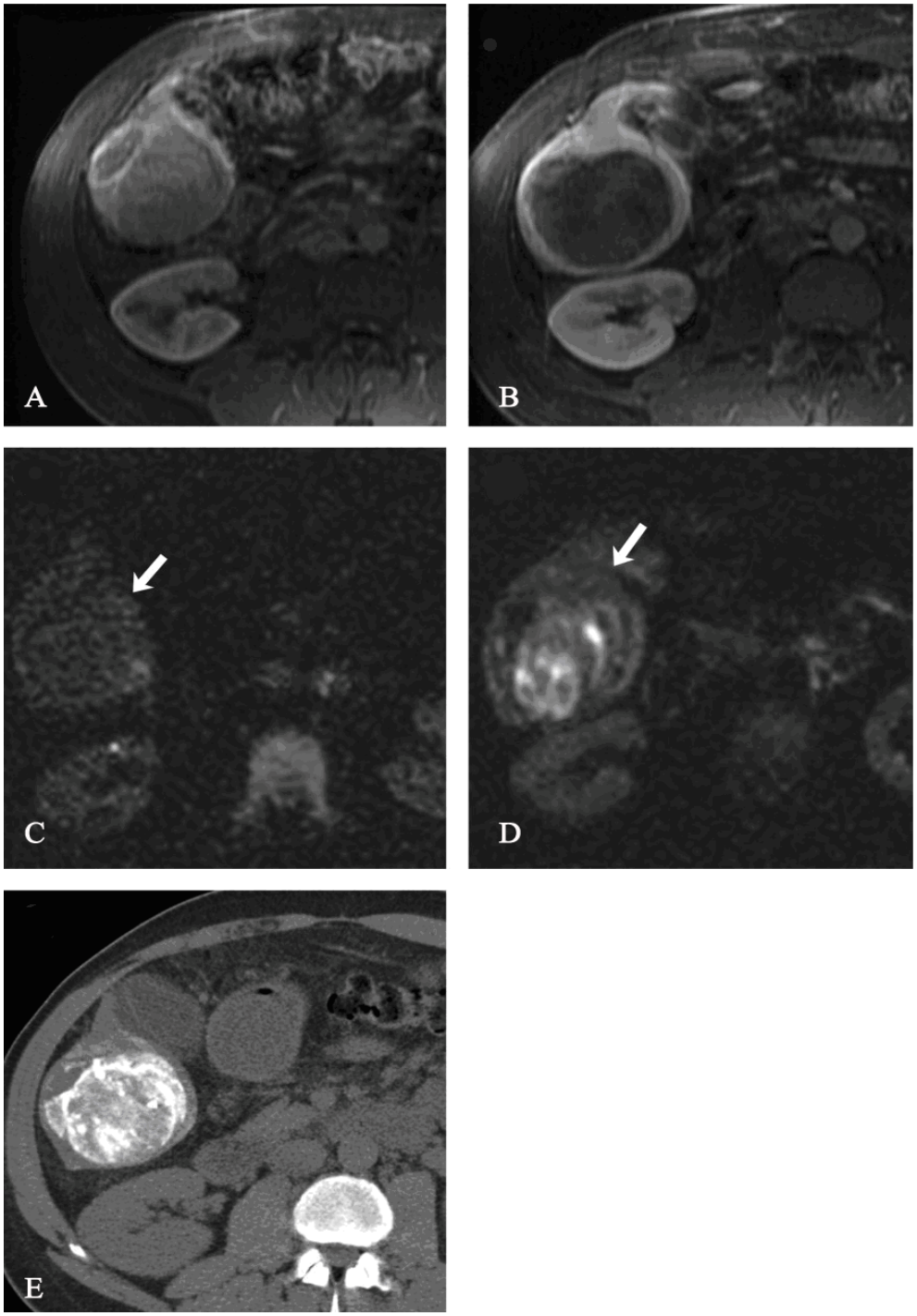

Figure 3.2 Changes on MR imaging after TACE of HCC.

(A) Gadolinium-enhanced image (TR/TE, 5.1/1.2 msec) shows a large enhancing mass in the right lobe of the liver. (B) Gadolinium-enhanced image (TR/TE, 5.1/1.2 msec) after TACE shows that the mass is almost completely avascular. Minimal residual enhancement persists in the periphery. Notice that the mass did not decrease in size.
(C) Diffusion-weighted image (TR/TE, 6500/110 msec) before TACE shows the mass to be slightly hyperintense (arrow), with low ADC value. (D) Diffusion-weighted image (TR/TE, 6500/110 msec) after TACE shows continued increase in signal intensity of the mass (arrow). The ADC value increased, confirming increasing cellular necrosis.
(E) Unenhanced CT of the abdomen following TACE of the right lobe. Notice intense deposition of iodized oil within the targeted mass.

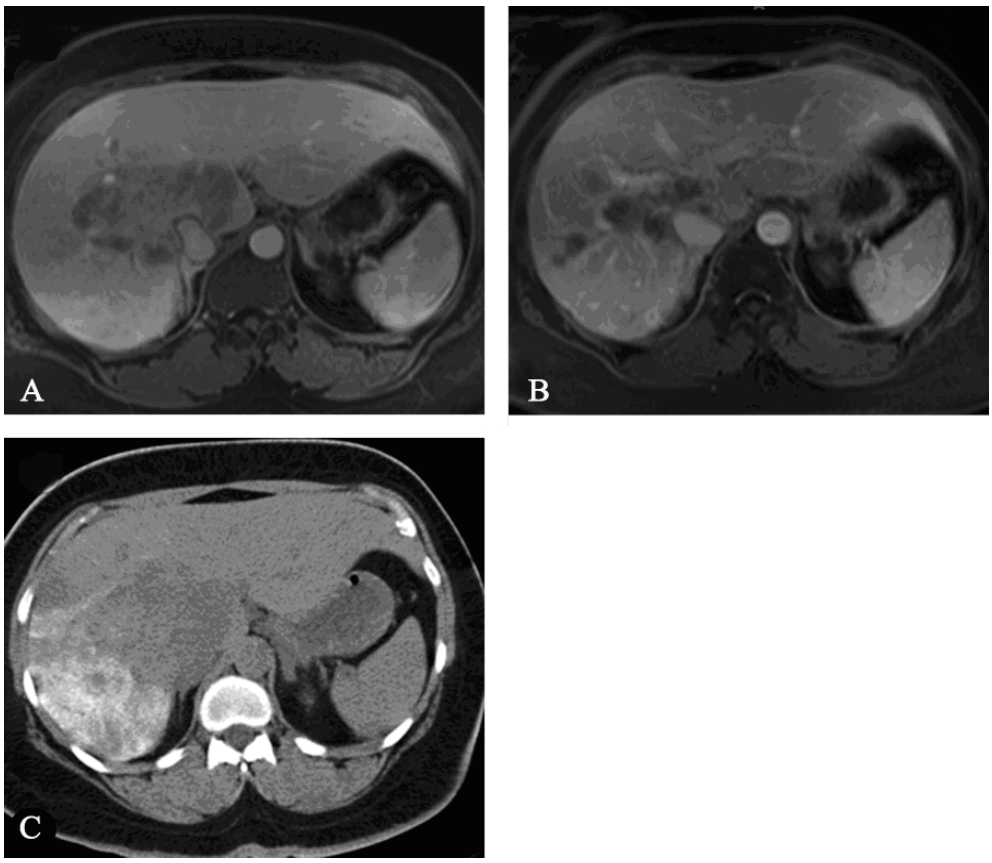

Figure 3.3 Changes on MR imaging after TACE of breast cancer metastases.
(A) Gadolinium-enhanced image (TR/TE, 5.1 msec/1.2 msec) shows a large central enhancing hepatic mass.
(B) Gadolinium-enhanced image (TR/TE, 5.1/1.2 msec) after TACE shows moderate (50%) decrease in enhancement. Notice that the mass has slightly decreased in size.
(C) Unenhanced CT of the abdomen following TACE. Notice intense deposition of iodized oil around the mass, with minimal iodized oil within it.

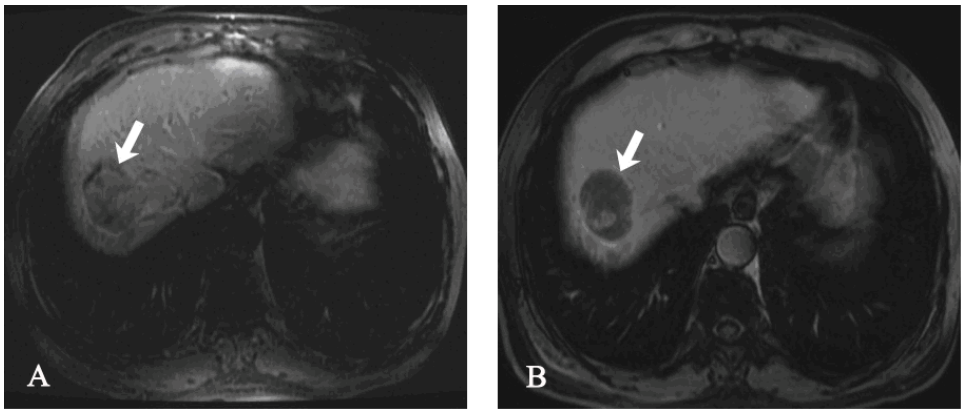

Figure 3.4 Changes on MR imaging after Yttrium-90 microspheres of HCC.
(A) Gadolinium-enhanced image (TR/TE, 5.1 msec/1.2 msec) shows a large enhancing mass in the dome of the liver (arrow).
(B) Gadolinium-enhanced image (TR/TE, 5.1/1.2 msec) after Yttrium-90 microspheres shows significant decrease in enhancement. Notice that the mass did not change in size.

REFERENCES

1) G.D. Dodd 3rd, M.C. Soulen and R.A. Kane *et al.*, Minimally invasive treatment of malignant hepatic tumors: At the threshold of a major breakthrough, *Radiographics* 20 (2000), pp. 9–27.
2) S.N. Goldberg and M. Ahmed, Minimally invasive image-guided therapies for hepatocellular carcinoma, *J Clin Gastroenterol* 35 (suppl 2) (2002), pp. S115–S129.
3) C. Bartolozzi, R. Lencioni and D. Caramella *et al.*, Hepatocellular carcinoma: CT and MR features after transcatheter arterial embolization and percutaneous ethanol injection, *Radiology* 191 (1994), pp. 123–128.
4) R. Lencioni, D. Caramella and C. Bartolozzi, Hepatocellular carcinoma: Use of color Doppler US to evaluate response to treatment with percutaneous ethanol injection, *Radiology* 194 (1995), pp. 113–118.
5) A.B. Miller, B. Hoogstraten and M. Staquet *et al.*, Reporting results of cancer treatment, *Cancer* 47 (1981), pp. 207–214.
6) P. Therasse, S.G. Arbuck, E.A. Eisenhauer *et al.*, European Organization for Research and Treatment of Cancer and National Cancer Institute of the United States and National Cancer Institute of Canada, New guidelines to evaluate the response to treatment in solid tumors, *J Natl Cancer Inst* 92 (2000), pp. 205–216.
7) C.C. Jaffe, Measures of response: RECIST, WHO, and new alternatives, *J Clin Oncol* 24 (2006), pp. 3245–3251.
8) I.R. Kamel and D.A. Bluemke, Magnetic resonance imaging of the liver: Assessing response to treatment, *Top Magn Reson Imaging* 13 (2002), pp. 191–200.
9) J. Bruix, M. Sherman, J.M. Llovet *et al.* and European Association for the Study of the Liver, Clinical management of hepatocellular carcinoma Conclusions of the Barcelona-2000 EASL conference, *J Hepatol* 35 (2001), pp. 421–430.
10) J. Bruix and M. Sherman, Management of hepatocellular carcinoma, *Hepatology* 42 (2005), pp. 1208–1236.
11) K. Nasu, Y. Kuroki and S. Nawano *et al.*, Hepatic metastases: Diffusion-weighted sensitivity-encoding versus SPIO-enhanced MR imaging, *Radiology* 239 (2006), pp. 122–130.
12) M. Law, S. Yang and H. Wang *et al.*, Glioma grading: Sensitivity, specificity, and predictive values of perfusion MR imaging and proton MR spectroscopic imaging compared with conventional MR imaging, *AJNR Am J Neuroradiol* 24 (2003), pp. 1989–1998.

13) D.K. Yeung, H.S. Cheung and G.M. Tse, Human breast lesions: Characterization with contrast-enhanced in vivo proton MR spectroscopy—initial results, *Radiology* 220 (2001), pp. 40–46.
14) N.R. Jagannathan, M. Kumar and V. Seenu *et al.*, Evaluation of total choline from in-vivo volume localized proton MR spectroscopy and its response to neoadjuvant chemotherapy in locally advanced breast cancer, *Br J Cancer* 84 (2001), pp. 1016–1022.
15) R. Longo, C. Ricci and F. Masutti *et al.*, Fatty infiltration of the liver Quantification by 1H localized magnetic resonance spectroscopy and comparison with computed tomography, *Invest Radiol* 28 (1993), pp. 297–302.
16) C.Y. Chen, C.W. Li and Y.T. Kuo *et al.*, Early response of hepatocellular carcinoma to transcatheter arterial chemoembolization: Choline levels and MR diffusion constants—initial experience, *Radiology* 239 (2006), pp. 448–456.
17) P.W. Schaefer, P.E. Grant and R.G. Gonzalez, Diffusion-weighted MR imaging of the brain, *Radiology* 217 (2000), pp. 331–345.
18) M. Elton, [Forensic psychiatrists must be more in agreement on the evaluation of juvenile delinquents], *Lakartidningen* 88 (1991), p. 2668.
19) B.A. Moffat, T.L. Chenevert and T.S. Lawrence *et al.*, Functional diffusion map: A noninvasive MRI biomarker for early stratification of clinical brain tumor response, *Proc Natl Acad Sci U S A* 102 (2005), pp. 5524–5529.
20) B.A. Moffat, T.L. Chenevert and C.R. Meyer *et al.*, The functional diffusion map: An imaging biomarker for the early prediction of cancer treatment outcome, *Neoplasia* 8 (2006), pp. 259–267.
21) H. Ni, V. Kavcic and T. Zhu *et al.*, Effects of number of diffusion gradient directions on derived diffusion tensor imaging indices in human brain, *AJNR Am J Neuroradiol* 27 (2006), pp. 1776–1781.
22) M.E. Moseley, Y. Cohen and J. Kucharczyk *et al.*, Diffusion-weighted MR imaging of anisotropic water diffusion in cat central nervous system, *Radiology* 176 (1990), pp. 439–445.
23) B. Taouli, V. Vilgrain and E. Dumont *et al.*, Evaluation of liver diffusion isotropy and characterization of focal hepatic lesions with two single-shot echo-planar MR imaging sequences: Prospective study in 66 patients, *Radiology* 226 (2003), pp. 71–78.
24) I. Yamada, W. Aung and Y. Himeno *et al.*, Diffusion coefficients in abdominal organs and hepatic lesions: Evaluation with intravoxel incoherent motion echo-planar MR imaging, *Radiology* 210 (1999), pp. 617–623.

25) R. Lencioni, D. Cioni and C. Bartolozzi, Percutaneous radiofrequency thermal ablation of liver malignancies: Techniques, indications, imaging findings, and clinical results, *Abdom Imaging* 26 (2001), pp. 345–360.
26) S. Sironi, T. Livraghi and F. Meloni *et al.*, Small hepatocellular carcinoma treated with percutaneous RF ablation: MR imaging follow-up, *AJR Am J Roentgenol* 173 (1999), pp. 1225–1229.
27) S.N. Goldberg, G.S. Gazelle and S.L. Dawson *et al.*, Tissue ablation with radiofrequency using multiprobe arrays, *Acad Radiol* 2 (1995), pp. 670–674.
28) S.N. Goldberg, P.F. Hahn and K.K. Tanabe *et al.*, Percutaneous radiofrequency tissue ablation: Does perfusion-mediated tissue cooling limit coagulation necrosis?, *J Vasc Interv Radiol* 9 (Pt 1) (1998), pp. 101–111.
29) S.A. Curley, P. Marra and K. Beaty *et al.*, Early and late complications after radiofrequency ablation of malignant liver tumors in 608 patients, *Ann Surg* 239 (2004), pp. 450–458.
30) C. Horkan, M. Ahmed and Z. Liu *et al.*, Radiofrequency ablation: Effect of pharmacologic modulation of hepatic and renal blood flow on coagulation diameter in a VX2 tumor model, *J Vasc Interv Radiol* 15 (2004), pp. 269–274.
31) T. Livraghi, S.N. Goldberg and S. Lazzaroni *et al.*, Small hepatocellular carcinoma: Treatment with radio-frequency ablation versus ethanol injection, *Radiology* 210 (1999), pp. 655–661.
32) C. Bartolozzi, L. Crocetti and D. Cioni *et al.*, Assessment of therapeutic effect of liver tumor ablation procedures, *Hepatogastroenterology* 48 (2001), pp. 352–358.
33) S. Rossi, E. Buscarini and F. Garbagnati *et al.*, Percutaneous treatment of small hepatic tumors by an expandable RF needle electrode, *AJR Am J Roentgenol* 170 (1998), pp. 1015–1022.
34) T. Shibata, Y. Iimuro and Y. Yamamoto *et al.*, Small hepatocellular carcinoma: Comparison of radio-frequency ablation and percutaneous microwave coagulation therapy, *Radiology* 223 (2002), pp. 331–337.
35) S.A. Curley, F. Izzo and P. Delrio *et al.*, Radiofrequency ablation of unresectable primary and metastatic hepatic malignancies: Results in 123 patients, *Ann Surg* 230 (1999), pp. 1–8.
36) C.Y. Lou, Y.M. Feng and A.R. Qian *et al.*, Establishment and characterization of human hepatocellular carcinoma cell line FHCC-98, *World J Gastroenterol* 10 (2004), pp. 1462–1465.
37) I.R. Kamel, D.A. Bluemke and J. Eng *et al.*, The role of functional MR imaging in the assessment of tumor response after chemoembolization in

patients with hepatocellular carcinoma, *J Vasc Interv Radiol* 17 (2006), pp. 505–512.
38) D.M. Parkin, F. Bray and J. Ferlay *et al.*, Estimating the world cancer burden: Globocan 2000, *Int J Cancer* 94 (2001), pp. 153–156.
39) D.Y. Lin, Y.F. Liaw and T.Y. Lee *et al.*, Hepatic arterial embolization in patients with unresectable hepatocellular carcinoma: A randomized controlled trial, *Gastroenterology* 94 (1988), pp. 453–456.
40) G. Pelletier, A. Roche and O. Ink *et al.*, A randomized trial of hepatic arterial chemoembolization in patients with unresectable hepatocellular carcinoma, *J Hepatol* 11 (1990), pp. 181–184.
41) Groupe d'Etude et de Traitement du Carcinome Hepatocellulaire, A comparison of lipiodol chemoembolization and conservative treatment for unresectable hepatocellular carcinoma, *N Engl J Med* 332 (1995), pp. 1256–1261.
42) J. Bruix, J.M. Llovet and A. Castells *et al.*, Transarterial embolization versus symptomatic treatment in patients with advanced hepatocellular carcinoma: Results of a randomized, controlled trial in a single institution, *Hepatology* 27 (1998), pp. 1578–1583.
43) M. De Santis, S. Alborino and P.L. Tartoni *et al.*, Effects of lipiodol retention on MRI signal intensity from hepatocellular carcinoma and surrounding liver treated by chemoembolization, *Eur Radiol* 7 (1997), pp. 10–16.
44) K. Ito, K. Honjo and T. Fujita *et al.*, Therapeutic efficacy of transcatheter arterial chemoembolization for hepatocellular carcinoma: MRI and pathology, *J Comput Assist Tomogr* 19 (1995), pp. 198–203.
45) I. Burger, K. Hong and R. Schulick *et al.*, Transcatheter arterial chemoembolization in unresectable cholangiocarcinoma: Initial experience in a single institution, *J Vasc Interv Radiol* 16 (2005), pp. 353–361.
46) A. Jemal, R. Siegel and E. Ward *et al.*, Cancer statistics, 2006, *CA Cancer J Clin* 56 (2006), pp. 106–130.
47) N.J. Carty, A. Foggitt and C.R. Hamilton *et al.*, Patterns of clinical metastasis in breast cancer: An analysis of 100 patients, *Eur J Surg Oncol* 21 (1995), pp. 607–608.
48) X.P. Li, Z.Q. Meng and W.J. Guo *et al.*, Treatment for liver metastases from breast cancer: Results and prognostic factors, *World J Gastroenterol* 11 (2005), pp. 3782–3787.
49) C. Lepage, A.M. Bouvier and J.M. Phelip *et al.*, Incidence and management of malignant digestive endocrine tumours in a well defined French population, *Gut* 53 (2004), pp. 549–553.

50) M.T. Barakat, K. Meeran and S.R. Bloom, Neuroendocrine tumours, *Endocr Relat Cancer* 11 (2004), pp. 1–18.
51) J.A. Norton, Surgical treatment of neuroendocrine metastases, *Best Practice Res Clin Gastroenterol* 19 (2005), pp. 577–583.
52) P. Tomassetti, D. Campana and L. Piscitelli *et al.*, Endocrine pancreatic tumors: Factors correlated with survival, *Ann Oncol* 16 (2005), pp. 1806–1810.
53) G.P. McEntee, D.M. Nagorney and L.K. Kvols *et al.*, Cytoreductive hepatic surgery for neuroendocrine tumors, *Surgery* 108 (1990), pp. 1091–1096.
54) S. Gupta, J.C. Yao and K. Ahrar *et al.*, Hepatic artery embolization and chemoembolization for treatment of patients with metastatic carcinoid tumors: The M.D. Anderson experience, *Cancer J* 9 (2003), pp. 261–267.
55) A. Roche, B. Girish and T. de BaÃŕe *et al.*, Trans-catheter arterial chemoembolization as first-line treatment for hepatic metastases from endocrine tumors, *Eur Radiol* 13 (2003), pp. 136–140.
56) B.K. Eriksson, E.G. Larsson and B.M. Skogseid *et al.*, Liver embolizations of patients with malignant neuroendocrine gastrointestinal tumors, *Cancer* 83 (1998), pp. 2293–2301.
57) S. Gupta, M.M. Johnson and R. Murthy *et al.*, Hepatic arterial embolization and chemoembolization for the treatment of patients with metastatic neuroendocrine tumors: Variables affecting response rates and survival, *Cancer* 104 (2005), pp. 1590–1602.
58) J.F. Geschwind, R. Salem and B.I. Carr *et al.*, Yttrium-90 microspheres for the treatment of hepatocellular carcinoma, *Gastroenterology* 127 (suppl 1) (2004), pp. S194–S205.
59) J.C. Andrews, S.C. Walker and R.J. Ackermann *et al.*, Hepatic radioembolization with yttrium-90 containing glass microspheres: Preliminary results and clinical follow-up, *J Nucl Med* 35 (1994), pp. 1637–1644.
60) M. Sarfaraz, A.S. Kennedy and Z.J. Cao *et al.*, Physical aspects of yttrium-90 microsphere therapy for nonresectable hepatic tumors, *Med Phys* 30 (2003), pp. 199–203.
61) J.R. Buscombe and A. Padhy, Treatment of hepatocellular carcinoma: A pivotal role for nuclear medicine?, *Nucl Med Commun* 22 (2001), pp. 119–120.
62) J. Deng, F.H. Miller and T.K. Rhee *et al.*, Diffusion-weighted MR imaging for determination of hepatocellular carcinoma response to yttrium-90 radioembolization, *J Vasc Interv Radiol* 17 (2006), pp. 1195–1200.

CHAPTER 4

ASSESSMENT OF METASTATIC BREAST CANCER RESPONSE TO CHEMOEMBOLIZATION WITH CONTRAST AGENT ENHANCED AND DIFFUSION-WEIGHTED MR IMAGING

Buijs M, Kamel IR, Vossen JA, Georgiades CS, Hong K, Geschwind JF

J Vasc Interv Radiol 2007 Aug;18(8):957-63.

ABSTRACT

PURPOSE:
To assess the value of functional magnetic resonance (MR) imaging in the evaluation of early tumor response after transarterial chemoembolization (TACE) for metastatic breast cancer and to compare tumor response based on functional MR imaging versus traditional assessment based on iodized oil deposition, tumor size, and tumor enhancement.

MATERIALS AND METHODS:
For 14 patients with metastatic breast cancer, MR imaging studies before and after TACE were evaluated. Diffusion and contrast medium–enhanced MR imaging was performed on a 1.5-T unit. Parameters evaluated included change in tumor size, enhancement, and apparent diffusion coefficient (ADC) values. Median survival was also calculated in the entire cohort.

RESULTS:
A total number of 27 lesions were evaluated, with a mean diameter of 5.5 cm. Although mean tumor size decreased by 18% after treatment, no tumors met the Response Evaluation Criteria In Solid Tumors (RECIST) for complete response (ie, complete disappearance of target lesions) and only seven of 27 met RECIST for partial response (ie, >30% decrease in target lesion size). After treatment, decrease of tumor enhancement in the arterial (32%) and portal venous (39%) phases was statistically significant ($p < 0.0001$). Mean tumor ADC increased by 27% ($p < 0.0001$) after TACE, whereas ADC remained unchanged in nontumorous liver, spleen, and kidney. Median survival was 25 months for the entire cohort.

CONCLUSION:
In patients with breast cancer and liver metastases who were treated with TACE, although changes in tumor size were small, significant early changes in the treated lesions occurred on contrast medium–enhanced and functional MR imaging. These include decrease in tumor enhancement and increase in tumor ADC value, which suggest increasing tumor necrosis and cell death.

INTRODUCTION

In the Western world, breast cancer is the most common cancer in women, and in this group it is the second leading cause of cancer death (after lung cancer) (1). Every year one to two women in every 1000 will be newly diagnosed with breast cancer. In 2006, 212,920 new cases of invasive breast cancer (stages I–IV) were estimated to have occurred among women in the United States (1). The mortality rate from breast cancer decreased approximately 2.3% per year from 1990 through 2001, in large part because of increased awareness, earlier detection, and more effective treatments (2). Nonetheless, it was estimated that 40,970 women in the US would die of breast cancer in 2006 (1).

The majority of breast cancer–related deaths are a result of complications from recurrent or metastatic disease. Approximately 50% of all patients develop metastatic disease (3). Metastatic breast cancer is uncommon at initial presentation, occurring in only approximately 6% of newly diagnosed cases (4). The liver is the most common site of intraabdominal metastatic disease, with metastases to the liver occurring in as many as 20% of patients (5, 6). Median survival time after the occurrence of liver metastases is poor, and ranges between 1 and 20 months (7, 8).

Metastatic breast cancer remains essentially incurable, and current goals of therapy are to ameliorate symptoms, delay tumor proliferation, improve or at least maintain quality of life, and increase overall survival (9). Various treatment options for metastatic breast cancer exist, including chemotherapy, hormone therapy, biologic therapy, and surgery. Metastatic breast cancer is generally considered to be a disseminated disease that requires systemic rather than local therapy. Nevertheless, a substantial number of patients have unresectable disease confined to the liver (10). As a result, transarterial chemoembolization (TACE) has become more commonly used as a treatment for liver metastases in metastatic breast cancer (11).

Several imaging procedures including ultrasonography, computed tomography (CT), and magnetic resonance (MR) imaging are commonly used to follow the size of breast cancer metastases over time and to determine the degree of response. Recently, some studies suggested that [^{18}F] fluorodeoxyglucose positron emission tomography can be useful in the quantitative assessment of the response to therapy of breast cancer

metastases (12-15). However, in our institution, MR imaging is the modality that is routinely used to assess treatment response of metastatic breast cancer after TACE.

Monitoring the effectiveness of TACE by imaging is important in determining treatment success and in guiding future therapy. Unenhanced CT can be used to confirm the technical success of chemoembolization by demonstrating the presence of hyperattenuating iodized oil (Lipiodol; Savage Laboratories, Melville, NY) within the tumor. However, to date, imaging modalities and imaging response criteria have been limited in their ability to provide clinically satisfactory information about the extent of tumor necrosis. The traditional and accepted criteria to determine tumor response in oncology, namely the World Health Organization criteria and Response Evaluation Criteria in Solid Tumors (RECIST), use decrease in tumor size as an indicator of successful therapy (16). However, tumor size may not change after locoregional therapy. More recently, the European Association for the Study of the Liver (EASL) has officially recommended the use of lesion enhancement as the standard modality to determine treatment response of hepatocellular carcinoma after locoregional therapy (17).

In recent years, the apparent diffusion coefficient (ADC), as measured by diffusion MR imaging, has become a promising surrogate marker of tumor response to therapy. ADC measures the mobility of water in tissues. Viable tumor cells restrict the mobility of water, whereas necrotic tumor cells allow increased diffusion of water molecules as a result of decreased cellularity and compromised cell membrane integrity. Diffusion MR imaging has been used to assess tumor response after chemotherapy and radiation therapy (18-21). Based on these studies, we hypothesized that contrast medium–enhanced and diffusion MR imaging could determine cellular necrosis and may therefore be more appropriate than the application of RECIST in providing information about early tumor response after TACE. Hence, the purposes of our study were (i) to assess the value of functional MR imaging in the evaluation of early tumor response after TACE for metastatic breast cancer and (ii) to compare tumor response based on functional MR imaging versus traditional imaging assessment with RECIST, which is based on tumor size, and EASL, which is based on tumor enhancement.

MATERIALS AND METHODS

Patients

Between January 1, 2002, and March 31, 2006, the care of 16 patients with metastatic breast cancer who received one or more cycles of TACE was discussed in the liver tumor board at our institution. Criteria for performing TACE included confirmed diagnosis of unresectable metastatic breast cancer in patients with or without minimally impaired liver function. Patients excluded from receiving TACE were those with an Eastern Cooperative Oncology Group performance status greater than 2, encephalopathy, severe variceal bleeding and/or severe ascites, significant thrombocytopenia, prolonged impaired renal function, acute renal failure (ie, an abrupt increase in serum creatinine level of ≥50% with respect to the baseline level or an absolute increase in the serum creatinine concentration of ≥ 0.5 mg/dL to a level > 1.5 mg/dL), or severe liver failure (ie, advanced Child-Pugh class C). Our study group included all patients treated with chemoembolization who had contrast medium–enhanced and diffusion-weighted MR imaging before and after treatment. Review of our database identified 16 patients, of whom 14 fulfilled our criteria. The two remaining patients did not have MR imaging after TACE and were excluded. Diagnosis of metastatic breast cancer was confirmed by biopsy of liver metastases in all patients. Data were collected prospectively and the study was authorized by the institutional review board.

Chemoembolization Technique

All chemoembolization procedures were performed by a single experienced interventional radiologist according to the same technique. An 18-gauge, single-wall needle was used to access the right common femoral artery with the Seldinger technique. A 5-F vascular sheath was placed into the right common femoral artery over a 0.035-inch Glidewire (Terumo Medical, Somerset, NJ) under fluoroscopic guidance and a 5-F Glide Simmons-1 catheter (Cordis, Miami, FL) was advanced into the aortic arch, formed, and then used to select the celiac axis. Over the guide wire, the catheter was advanced into the desired hepatic artery branch, depending on the tumor location. Selective catheterization was performed to achieve lobar or segmental embolization based on the targeted lesions. A solution containing 100 mg of cisplatin (Platinol; Bristol-Myers Squibb, Princeton, NJ), 50 mg of doxorubicin (Adriamycin; Pharmacia Upjohn, Kalamazoo,

MI), and 10 mg of mitomycin C (Mutamycin C; Bedford Laboratories, Bedford, OH) in a 1:1 mixture with iodized oil was injected, followed by infusion of Embosphere particles (Biosphere Medical, Rockland, MA) until stasis was achieved.

CT Technique

Within 1 day after chemoembolization, all patients underwent unenhanced helical CT imaging with use of a Sensation 16 scanner (Siemens Medical Solutions, Malvern, PA). Scanning parameters were 120 kVp, 210 mA, 5-mm section collimation, and 5-mm image reconstruction. Technical success of the procedure was demonstrated by the focal deposition of iodized oil in the targeted segment or lobe of the liver.

MRI Technique

Patients underwent imaging with use of a 1.5-T MRI scanner (CV/i; GE Healthcare, Milwaukee, WI) and a phased-array torso coil. Imaging protocol included T2-weighted fast spin-echo images (matrix, 256 × 256; slice thickness, 8 mm; interslice gap, 2 mm; repetition time [TR]/ echo time [TE], 5000/100 msec; receiver bandwidth, 32 kHz), breath-hold diffusion-weighted echoplanar images (matrix, 128 × 128; slice thickness, 8 mm; interslice gap, 2 mm; b value, 500 mm^2/sec; TR/TE, 5000-6500/110 msec; receiver bandwidth, 32 kHz), and breath-hold unenhanced and contrast-enhanced (0.1 mmol/kg intravenous gadodiamide [Omniscan; GE Healthcare, Princeton, NJ]) T1-weighted three-dimensional fat-suppressed spoiled gradient-echo images (field of view, 320-400 mm; matrix, 192 × 160; slice thickness, 4-6 mm TR/TE, 5.1/1.2 msec; receiver bandwidth, 64 kHz; flip angle, 15º) in the arterial phase (20 seconds) and portal venous phase (60 seconds).

Follow-up

According to protocol, patients received contrast medium–enhanced and diffusion MR imaging 4–6 weeks after TACE to assess tumor response. Patients with near-complete tumor necrosis were followed up by imaging every 6–8 weeks. Patients with residual enhancement and maintained clinical performance status received additional TACE treatment(s).

Image Analysis

MR image processing and ADC maps were generated with use of a commercially available workstation (Advantage; GE Healthcare, Milwaukee, WI). Images were interpreted by consensus of two experienced MR radiologists. Parameters evaluated included change in tumor size, enhancement, and ADC values as measured on axial planes. For patients with more than one TACE cycle, the MR study performed after the last cycle was used for comparison. All target lesions of 2 cm or larger on the largest axial diameter were evaluated, with a maximum of three lesions per patient to ensure independent sampling. The maximum diameter of the targeted lesions was measured by electronic calipers as proposed by RECIST. Areas of tumor enhancement were considered viable and areas of nonenhancement were considered necrotic, as suggested by the European Association for the Study of the Liver (EASL) (17). Percent enhancement was based on enhancement seen on the axial portal venous phase image with the largest tumor size. ADC maps were generated from the diffusion-weighted images, and values were recorded by placing a region of interest over the entire treated mass as seen on the image with the largest lesion size. ADC maps of normal-appearing liver (in the nonembolized parenchyma), spleen, and muscle were generated. Percentage of iodized oil deposition on CT was also recorded. In patients who had received multiple iodized oil treatments, the maximum iodized oil retention in the target lesions was recorded.

Statistical Analysis

Statistical analysis was performed with Stata software package (Version 8; Stata, College Station, TX). A paired t test was used to compare parameters used to assess tumor response before and after TACE. These included tumor size, enhancement, and ADC before and after TACE. A paired t test was also used to compare ADC values of the liver, spleen, and muscle before and after treatment. Median survival was calculated in the entire cohort from the date of presentation with liver metastases until death from any cause, and surviving patients were censored at the date of analysis. A Kaplan-Meier survival curve was generated. P values < 0.05 were considered to indicate statistical significance.

RESULTS

Demographic Information

General information for all 14 patients evaluated is shown in Table 4.1. The average number of chemoembolization procedures per patient was two (range, 1–3). The average duration between pre- and postprocedural MR imaging was 60 days ± 32 (SD). MR imaging was performed within 4 days ± 5 before TACE. Mean duration between the last TACE treatment and follow up MR imaging was 54 days ± 33.

A total of 27 lesions were evaluated. The mean evaluated number of lesions per patient was two (range, 1–3). Mean maximum iodized oil retention on CT was 36% (range, 0%–100%); most of the oil was deposited around the lesions.

Assessment of Change in MR Imaging Parameters after TACE

On gadolinium-enhanced MR imaging, overall tumor enhancement in the arterial and portal venous phases decreased significantly after TACE (Table 4.2, Table 4.3).

Arterial enhancement decreased after TACE by 32%, and the decrease was statistically significant ($p < 0.0001$). Similarly, venous enhancement decreased by 39%, which was also significant ($p < 0.0001$). Diffusion MR imaging was also useful in monitoring response after treatment. Mean tumor ADC increased after TACE by 27% ($p < 0.0001$), whereas the ADC remained unchanged in nontumorous liver, spleen, and muscle (Table 4.2; Fig 4.1).

Although mean tumor size decreased from 5.5 cm to 4.5 cm (18%) after TACE, it did not meet RECIST for complete response (ie, disappearance of all measurable disease). Seven of the 27 lesions had a decrease of more than 30% in tumor size, which meets the RECIST of partial response. Based on these results according to RECIST, on a lesion-by-lesion basis, 26% of the reviewed lesions were considered to have shown a partial response to TACE; however, on a patient by patient basis, all patients in our cohort were considered nonresponders to TACE because the total tumor burden did not decrease by 30% in any given patient.

Patient Survival

Median survival was 25 months for the entire cohort. Survival rates at 1, 2, and 3 years were 79%, 52%, and 35%, respectively. These survival times are significantly longer than those previously reported for patients treated with systemic chemotherapy, which range between 14 and 16 months (6, 22).

DISCUSSION

Metastatic breast cancer is generally considered a widespread disease with a poor prognosis. Locoregional therapy, particularly TACE in carefully selected patients, may result in improved patient survival. Although the impact on survival is difficult to evaluate because of the absence of randomized trials, retrospective studies of TACE for metastatic breast cancer are promising (11, 23).

In the clinical setting, it is critical to assess tumor response, especially shortly after treatment, because early favorable response generally indicates effectiveness of therapy (18). The objective of the present study was to compare traditional imaging assessments (which are based on iodized oil deposition, tumor enhancement, and tumor size) with diffusion MR imaging in the evaluation of early tumor response after TACE for metastatic breast cancer. Our results suggest that diffusion and contrast medium–enhanced MR imaging may be used to detect early tumor necrosis before reduction in tumor size occurs.

Intense accumulation of iodized oil within tumors after TACE has been reported to correlate well with complete tumor necrosis and survival in patients with hepatocellular carcinoma. In contrast, inhomogeneous or poor retention of iodized oil has been shown to indicate persistent tumor viability (24-26). The question remains whether this correlation also exists in patients with metastatic breast cancer. In this study, tumors had very poor retention of oil, likely because they were hypovascular. Most of the oil was deposited around the lesions and not within them. It has been suggested that patients with hepatocellular carcinoma who exhibited persistent iodized oil retention for at least 6 months within the tumor had a higher probability of survival than patients who exhibited a lower rate of iodized oil retention (27, 28). In our experience, the main use of noncontrast CT was to determine the technical success of TACE by verifying adequate tumor targeting. In the

current study, the mean maximum iodized oil deposition was only 36% immediately after TACE, which had a poor correlation with diffusion and ADC (R = 0.233). Therefore, the amount of iodized oil deposition alone could not be used as a consistent predictor of tumor response after treatment.

Contrast agent–enhanced MR imaging determines areas of tumor enhancement with the use of extracellular contrast agents (29-31). Enhancing portions of the tumor are presumed to be viable, whereas nonenhancing portions are presumed to be necrotic. The disadvantage of contrast medium–enhanced MR imaging is the incapability to distinguish viable cells from reactive granulation tissue. Contrast medium enhancement in granulation tissue is believed to be caused by increased capillary permeability and marked increase in the passive distribution of gadolinium (32). TACE does not typically cause an intense reaction at the tumor periphery, but enhancing granulation tissue remains a potential confounding factor. In our study, we found a significant decrease in enhancement after TACE, which suggests that early enhancement can be used as a predictor of tumor response.

Standardized criteria for the measurement of therapeutic response were established in 1981 by the World Health Organization and have been modified several times. In 2000, RECIST was introduced to unify response assessment criteria (16). However, RECIST still relies on size change of lesions to assess response. For this reason, the validity of RECIST has recently been questioned in view of the emergence of new anticancer therapies, as these therapies are based on stabilizing disease rather than causing tumor disappearance (18). Therefore, the early effects of these therapies would not be detected by RECIST and patients would not be considered to have exhibited a response. In some institutions, metabolic monitoring of cancer chemotherapy is applied with the use of sequential quantitative positron emission tomographic scans of tumor glucose metabolism with the glucose analogue [^{18}F] fluorodeoxyglucose (12-15). This imaging technique has been useful in evaluating tumor response in patients with metastatic breast cancer. However, we use MR imaging at our institution, and therefore the aim of the present study was to explore new MR techniques to assess tumor response.

Similar observations to those in the literature were made in the current study after TACE. According to RECIST, only seven of the 27 lesions

treated with TACE exhibited partial response despite an 18% decrease in tumor size during the follow-up period of this study. These results point out the disconnect that exists between lack of contrast enhancement, increase in ADC value, and decrease in tumor size. To emphasize the importance of measuring response adequately, the EASL has officially recommended the use of lesion enhancement on contrast medium–enhanced CT as the standard modality to determine treatment response after locoregional therapy (17). Areas of tumor enhancement were considered viable whereas nonenhancing regions reflected tissue necrosis (33, 34). The EASL also stated that tumor size measurements might not be accurate because these measurements would not take into account the true extent of tumor necrosis. Our results are in line with these recommendations.

Diffusion-weighted MR imaging and ADC values map the mobility of water molecules in tissues and thereby are able to provide insight into tumor microstructure. Viable tumors consist of a high amount of cells with an intact cell membrane. These cell membranes restrict the mobility of water molecules, which causes a low ADC value. Conversely, cellular necrosis causes increased membranous permeability, which allows water molecules to move freely and thereby causes a marked increase in the ADC value. Because of these characteristics, the imaging techniques described herein are able to detect early cellular necrosis and apoptosis before size regression (35, 36). Diffusion-weighted MR imaging has been successfully used to assess response to radiation or systemic chemotherapy in patients with brain and breast cancers (36, 37). These results reinforce the notion that diffusion-weighted MR imaging is useful in the assessment of tumor response. In addition, ADC values add a quantifiable measure of tumor cell death by directly reporting the state of water diffusion within the tumor, which is especially valuable because of the wide spectrum of histopathologic findings after TACE, ranging from total viability to complete necrosis (38-40).

In our patient group, Kaplan-Meier analysis revealed a median patient survival time of 25 months for the entire cohort. This is significantly longer than that for untreated patients and for patients treated with only systemic chemotherapy, in whom the reported median survival times are less than 6 months and 14–16 months, respectively (6, 22). Our results suggest that tumor response by imaging is a valid positive prognostic indicator of survival. Early response imaging may also influence toxicities caused by treatment because early response shown on imaging may restrict the number

of treatments. This results in preservation of functioning healthy liver tissue, which may contribute to prolonged survival.

This study has several limitations. First, our patient population was relatively small, so further studies with a larger sample size are needed to confirm our conclusions. A second limitation includes possible selection bias, as only patients with MR imaging before and after treatment were included in our study. Another limitation is the lack of histopathologic correlation of the lesions after chemoembolization. We could not obtain histologic correlation in this study for obvious ethical reasons. The mean follow-up interval in this study was 60 days. It is possible that, with more extended follow-up, tumors treated with TACE may be seen to decrease in size to a degree that would satisfy RECIST. However, the aim of this study was to show an early response, which is more useful in the clinical setting. This is essential to establish the need for repeat treatment.

In conclusion, contrast medium–enhanced and diffusion-weighted MR imaging could potentially be used to predict the degree of tumor necrosis after TACE. The functional information provided by the ADC maps and contrast medium enhancement may improve response evaluation, which currently is based only on size change. In addition, these MR imaging techniques are quantitative and may be subject to statistical testing individually and in combination to ascertain their utility in the assessment of tumor necrosis. Accurate assessment of early treatment response is necessary to guide future therapy and is likely to have survival benefit in patients who exhibit a favorable response to therapy.

TABLES & FIGURES

Characteristic	Value
No. of patients	14
Mean age, y (range)	57 (41-81)
Sex (M/F)	0/14
Child-Pugh class	
A	12
B	2
C	0
Other metastatic sites	7
Chemotherapy before TACE	13
Type of previous chemotherapy	
Taxanes	2
Anthracyclines	2
Both	5
Other	4
Number of lesions	
< 10	3
10-50	5
> 50	6
Mean size of targeted lesion, mm (range)	5.5 (1.9-16.6)

Table 4.1 Patient Characteristics, general information for all 14 patients evaluated.

Features	Before TACE	After TACE	Change (%)	*P* Value*
Size of mass (cm)	5.5 ± 3.6	4.5 ± 3.3	18	0.002
Enhancement of mass (%)				
Arterial	42 ± 34	10 ± 16	32	<0.0001
Venous	60 ± 33	21 ± 26	39	<0.0001
ADC (x 10^{-3} mm^2/sec)				
Mass	1.81 ± 0.52	2.29 ± 0.61	27	<0.0001
Liver	1.89 ± 0.43	1.82 ± 0.39	4	0.388
Spleen	1.08 ± 0.26	1.21 ± 0.32	12	0.073
Muscle	1.53 ± 0.51	1.77 ± 0.024	16	0.072

Table 4.2 Changes in tumor size, enhancement, and ADC value after TACE.
Note.— Values presented as means ± SD unless specified otherwise.
* Paired *t* test.

Tumor Feature	Findings in Current Study	RECIST	EASL
Size	Small decrease (18%)	Requires 30% decrease for responders	NA
Arterial enhancement	Decreased (32%)	NA	NA
Venous enhancement	Decreased (39%)	NA	Unspecified decrease in enhancement
ADC value	Increased (27%)	NA	NA

Table 4.3 Comparison of study results with currently accepted criteria
Note.— NA = not applicable.

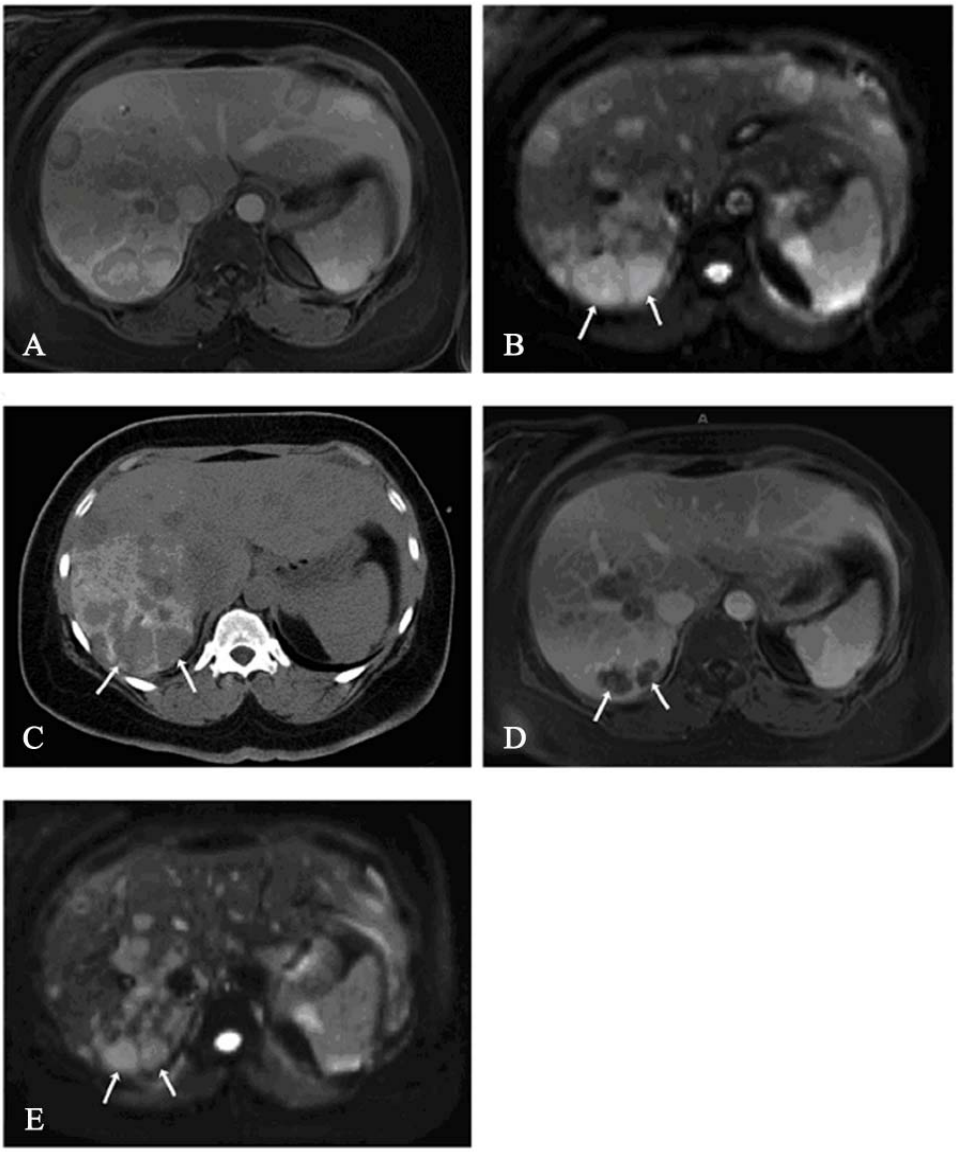

Figure 4.1 Changes in enhancement and ADC value after TACE.
(A) Gadolinium-enhanced image (TR/TE, 5.1/1.2 msec) shows multiple liver metastases. Notice that most lesions have near 100% enhancement.
(B) Diffusion-weighted image (TR/TE, 6500/110 msec) shows multiple hyperintense masses (arrow). The ADC values were 1.29×10^{-3} and 1.33×10^{-3} mm^2/sec for the two lesions in the right lobe (arrows).
(C) Nonenhanced CT of the abdomen after TACE of the right lobe. Notice intense deposition of iodized oil around the two right-lobe lesions (arrows) with minimal iodized oil within the lesions.

(D) Gadolinium-enhanced image (TR/TE, 5.1/1.2 msec) after TACE shows significant decrease (75%) in enhancement. Minimal residual enhancement persists in the periphery (arrows). Notice that the lesions have only minimally decreased in size.

(E) Diffusion-weighted image (TR/TE, 6,500/110 msec) after TACE shows continued increase in signal intensity of the lesions (arrows). The ADC values were 1.81×10^{-3} and 1.83×10^{-3} mm^2/sec for the two lesions in the right lobe, confirming increasing cellular necrosis.

REFERENCES

1) Jemal A, Siegel R, Ward E, et al.Cancer statistics, 2006. CA Cancer J Clin. 2006;56:106–130.
2) Berry DA, Cronin KA, Plevritis SK, et al.Effect of screening and adjuvant therapy on mortality from breast cancer. N Engl J Med. 2005;353:1784–1792.
3) Patanaphan V, Salazar OM, Risco R. Breast cancer: metastatic patterns and their prognosis. South Med J. 1988;81:1109–1112.
4) Kamby C, Dirksen H, Vejborg I, et al.Incidence and methodologic aspects of the occurrence of liver metastases in recurrent breast cancer. Cancer. 1987;59:1524–1529.
5) Carty NJ, Foggitt A, Hamilton CR, Royle GT, Taylor I. Patterns of clinical metastasis in breast cancer: an analysis of 100 patients. Eur J Surg Oncol. 1995;21:607–608.
6) Zinser JW, Hortobagyi GN, Buzdar AU, Smith TL, Fraschini G. Clinical course of breast cancer patients with liver metastases. J Clin Oncol. 1987;5:773–782.
7) Hoe AL, Royle GT, Taylor I. Breast liver metastases–incidence, diagnosis and outcome. J R Soc Med. 1991;84:714–716.
8) Wyld L, Gutteridge E, Pinder SE, et al.Prognostic factors for patients with hepatic metastases from breast cancer. Br J Cancer. 2003;89:284–290.
9) Rubens RD. Management of advanced breast cancer. Int J Clin Pract. 2001;55:676–679.
10) Elias D, Lasser PH, Montrucolli D, Bonvallot S, Spielmann M. Hepatectomy for liver metastases from breast cancer. Eur J Surg Oncol. 1995;21:510–513.
11) Li XP, Meng ZQ, Guo WJ, Li J. Treatment for liver metastases from breast cancer: results and prognostic factors. World J Gastroenterol. 2005;11:3782–3787.
12) Benard F, Turcotte E. Imaging in breast cancer: single-photon computed tomography and positron-emission tomography. Breast Cancer Res. 2005;7:153–162.
13) Cachin F, Prince HM, Hogg A, Ware RE, Hicks RJ. Powerful prognostic stratification by (18F)fluorodeoxyglucose positron emission tomography in patients with metastatic breast cancer treated with high-dose chemotherapy. J Clin Oncol. 2006;24:3026–3031.

14) Dose Schwarz J, Bader M, Jenicke L, Hemminger G, Janicke F, Avril N. Early prediction of response to chemotherapy in metastatic breast cancer using sequential 18F-FDG PET. J Nucl Med. 2005;46:1144–1150.
15) Jansson T, Westlin JE, Ahlstrom H, Lilja A, Langstrom B, Bergh J. Positron emission tomography studies in patients with locally advanced and/or metastatic breast cancer: a method for early therapy evaluation?. J Clin Oncol. 1995;13:1470–1477.
16) Therasse P, Arbuck SG, Eisenhauer EA, et al.European Organization for Research and Treatment of CancerNational Cancer Institute of the United StatesNational Cancer Institute of CanadaNew guidelines to evaluate the response to treatment in solid tumors. J Natl Cancer Inst. 2000;92:205–216.
17) Bruix J, Sherman M, Llovet JM, et al.European Association for the Study of the LiverClinical management of hepatocellular carcinoma (Conclusions of the Barcelona-2000 EASL conference). J Hepatol. 2001;35:421–430.
18) Kamel IR, Bluemke DA, Eng J, et al.The role of functional MR imaging in the assessment of tumor response after chemoembolization in patients with hepatocellular carcinoma. J Vasc Interv Radiol. 2006;17:505–512.
19) Geschwind JF, Artemov D, Abraham S, et al.Chemoembolization of liver tumor in a rabbit model: assessment of tumor cell death with diffusion-weighted MR imaging and histologic analysis. J Vasc Interv Radiol. 2000;11:1245–1255.
20) Deng J, Miller FH, Rhee TK, et al.Diffusion-weighted MR imaging for determination of hepatocellular carcinoma response to yttrium-90 radioembolization. J Vasc Interv Radiol. 2006;17:1195–1200.
21) Kamel IR, Reyes DK, Liapi E, Bluemke DA, Geschwind JF. Functional MR imaging assessment of tumor response after 90Y microsphere treatment in patients with unresectable hepatocellular carcinoma. J Vasc Interv Radiol. 2007;18:49–56.
22) Pentheroudakis G, Fountzilas G, Bafaloukos D, et al.Metastatic breast cancer with liver metastases: a registry analysis of clinicopathologic, management and outcome characteristics of 500 women. Breast Cancer Res Treat. 2006;97:237–244.
23) Gofuku J, Yayoi E, Ikeda N, Nishi T, Yagyu T, Kawasaki K. Long-term survivors with liver metastasis from breast cancer who were received intra-arterial chemotherapy. Gan To Kagaku Ryoho. 2004;31:1828–1831.

24) Lo CM, Ngan H, Tso WK, et al.Randomized controlled trial of transarterial Lipiodol chemoembolization for unresectable hepatocellular carcinoma. Hepatology. 2002;35:1164–1171.
25) Choi BI, Kim HC, Han JK, et al.Therapeutic effect of transcatheter oily chemoembolization therapy for encapsulated nodular hepatocellular carcinoma: CT and pathologic findings. Radiology. 1992;182:709–713.
26) Nakamura H, Hashimoto T, Oi H, Sawada S. Transcatheter oily chemoembolization of hepatocellular carcinoma. Radiology. 1989;170:783–786.
27) Lee HS, Kim KM, Yoon JH, et al.Therapeutic efficacy of transcatheter arterial chemoembolization as compared with hepatic resection in hepatocellular carcinoma patients with compensated liver function in a hepatitis B virus-endemic area: a prospective cohort study. J Clin Oncol. 2002;20:4459–4465.
28) Stefanini GF, Amorati P, Biselli M, et al.Efficacy of transarterial targeted treatments on survival of patients with hepatocellular carcinoma (An Italian experience). Cancer. 1995;75:2427–2434.
29) Murakami T, Nakamura H, Hori S, et al.Detection of viable tumor cells in hepatocellular carcinoma following transcatheter arterial chemoembolization with iodized oil (Pathologic correlation with dynamic turbo-FLASH MR imaging with Gd-DTPA). Acta Radiol. 1993;34:399–403.
30) Castrucci M, Sironi S, De Cobelli F, Salvioni M, Del Maschio A. Plain and gadolinium-DTPA-enhanced MR imaging of hepatocellular carcinoma treated with transarterial chemoembolization. Abdom Imaging. 1996;21:488–494.
31) Bartolozzi C, Lencioni R, Caramella D, Mazzeo S, Ciancia EM. Treatment of hepatocellular carcinoma with percutaneous ethanol injection: evaluation with contrast-enhanced MR imaging. AJR Am J Roentgenol. 1994;162:827–831.
32) Yuen MF, Chan AO, Wong BC, et al.Transarterial chemoembolization for inoperable, early stage hepatocellular carcinoma in patients with Child-Pugh grade A and B: results of a comparative study in 96 Chinese patients. Am J Gastroenterol. 2003;98:1181–1185.
33) Takayasu K, Arii S, Matsuo N, et al.Comparison of CT findings with resected specimens after chemoembolization with iodized oil for hepatocellular carcinoma. AJR Am J Roentgenol. 2000;175:699–704.
34) Lim HK, Han JK. Hepatocellular carcinoma: evaluation of therapeutic response to interventional procedures. Abdom Imaging. 2002;27:168–179.

35) Ross BD, Chenevert TL, Rehemtulla A. Magnetic resonance imaging in cancer research. Eur J Cancer. 2002;38:2147–2156.
36) Hall DE, Moffat BA, Stojanovska J, et al.Therapeutic efficacy of DTI-015 using diffusion magnetic resonance imaging as an early surrogate marker. Clin Cancer Res. 2004;10:7852–7859.
37) Mardor Y, Pfeffer R, Spiegelmann R, et al.Early detection of response to radiation therapy in patients with brain malignancies using conventional and high b-value diffusion-weighted magnetic resonance imaging. J Clin Oncol. 2003;21:1094–1100.
38) Sakurai M, Okamura J, Kuroda C. Transcatheter chemo-embolization effective for treating hepatocellular carcinoma: a histopathologic study. Cancer. 1984;54:387–392.
39) Di Carlo V, Ferrari G, Castoldi R, et al. Pre-operative chemoembolization of hepatocellular carcinoma in cirrhotic patients. Hepatogastroenterology. 1998;45:1950–1954.
40) Paye F, Jagot P, Vilgrain V, Farges O, Borie D, Belghiti J. Preoperative chemoembolization of hepatocellular carcinoma: a comparative study. Arch Surg. 1998;133:767–772.

CHAPTER 5

FUNCTIONAL MRI EVALUATION OF TUMOR RESPONSE IN PATIENTS WITH NEUROENDOCRINE HEPATIC METASTASES TREATED WITH TRANSCATHETER ARTERIAL CHEMOEMBOLIZATION

Liapi E, Geschwind JF, Vossen JA, Buijs M, Georgiades CS, Bluemke DA, Kamel IR.

AJR Am J Roentgenol 2008 Jan;190(1):67-73.

ABSTRACT

OBJECTIVE:

The purpose of this study was to evaluate contrast-enhanced and diffusion-weighted MRI changes in neuroendocrine tumors treated with transcatheter arterial chemoembolization (TACE).

MATERIALS AND METHODS:

Sixty-six targeted lesions in 26 patients (18 men, eight women; mean age, 57 years) with hepatic metastasis of neuroendocrine tumors treated with TACE were retrospectively analyzed. MRI studies were performed before and after TACE. Imaging features included tumor size, percentage of enhancement in the arterial and portal venous phases, and diffusion-weighted imaging apparent diffusion coefficients (ADCs) of the tumor, liver, and spleen. Tumor response to treatment was recorded according to World Health Organization criteria and Response Evaluation Criteria in Solid Tumors. Liver function tests were performed, and clinical performance was assessed before and after treatment. Statistical analysis included paired Student's t tests and Kaplan-Meier survival curves.

RESULTS:

Mean tumor size and percentage enhancement in the arterial and portal venous phases decreased significantly after treatment ($p < 0.0001$). The tumor ADC increased from 1.51 x 10^{-3} mm^2/sec before treatment to 1.79 x 10^{-3} mm^2/sec after treatment ($p < 0.0001$), but the ADCs for the liver and spleen remained unchanged. Despite the change in tumor size, no patient in this cohort achieved complete response according to World Health Organization criteria and Response Evaluation Criteria in Solid Tumors. Partial response was achieved in only 27% and 23% of the patients according to the respective criteria. Results of liver function tests and performance status also remained unchanged. The mean survival period for all patients was 78 months.

CONCLUSION:

Contrast-enhanced and diffusion-weighted imaging showed significant changes after TACE of neuroendocrine tumors and can be used to assess response of targeted tumors.

INTRODUCTION

Neuroendocrine tumors (NETs) are a heterogeneous group of rare neoplasms with a typically indolent natural history (1, 2). Hepatic metastasis is frequent (25-90% of cases) in patients with NET, and despite the slow growth of the lesions, their presence substantially influences prognosis (3, 4). Surgical resection is considered the first-line treatment of patients with hepatic metastasis of NET. However, resection for cure is possible in only 10% of patients because of the diffuse pattern of distribution of hepatic metastatic lesions at diagnosis (5, 6). Systemic chemotherapy in patients with diffuse or progressive hepatic metastasis yields disappointing results, especially in patients with metastasis of midgut origin. Hormonal therapy has been used as a first- or second-line option, especially in combination with cytoreductive surgery. In patients with carcinoid syndrome, however, the efficacy of somatostatin analogues decreases over time because of disease progression and development of tachyphylaxis (7). Among the various palliative options in the management of metastatic NET, transcatheter arterial chemoembolization (TACE) has been shown to be effective in controlling hormonal symptoms and tumor growth (8-11).

Response assessment in solid tumors is established with imaging for measurement of tumor size according to the modified World Health Organization (WHO) or the Response Evaluation Criteria in Solid Tumors (RECIST) guidelines (12, 13). TACE has been shown to decrease tumor size, but despite favorable clinical outcome, many responses do not qualify as complete according to the WHO and RECIST guidelines (14). Moreover, a cyst-like appearance of lesions after TACE, indicating response to treatment without alteration in size, is possible (15). Therefore, a decrease in functional tumor burden with TACE cannot be fully assessed with the current WHO and RECIST guidelines, which rely solely on anatomic changes. Functional contrast-enhanced and diffusion-weighted MRI (DWI) has been introduced as a new technique for assessing tumor response after TACE in patients with primary liver cancer (14, 16). This approach has been shown to help identify intracellular changes in tumor necrosis in patients with hepatocellular carcinoma treated with TACE and has led the way to the acquisition of important information about tumor burden and function. To our knowledge, this approach has not been used to assess the response of NET metastasis to TACE.

In this study, our aim was to evaluate multiparametric MRI anatomic and functional changes in NET hepatic metastatic lesions after sequential treatments with TACE. For the standard of reference, response evaluation was recorded according to the WHO and RECIST guidelines. In addition, overall imaging response was supported by results of liver function tests, patient performance status, and results of analysis of survival data.

MATERIALS AND METHODS

A prospective database of the records of patients who had undergone TACE for primary and metastatic liver disease at our institution was reviewed. The database was approved by the institutional review board and was compliant with the HIPAA. Inclusion criteria for the study were presence of a neuroendocrine hepatic metastatic lesion; treatment with TACE as a first- or second-line option; performance of unenhanced CT 1 day after TACE; and performance of contrast-enhanced DWI before and after chemoembolization. Electronic medical records and images were used to collect patient demographic, laboratory, and clinical data. Functional and non-functional pancreatic NETs were labeled as islet cell tumors. A total of 42 patients underwent TACE at our institution between December 1, 1999, and January 1, 2004. Sixteen patients were excluded from the study because of incomplete MRI before or after therapy. The remaining 26 patients with hepatic metastasis of NETs (12 with islet cell and 14 with carcinoid tumors) were included. These patients underwent TACE and baseline and follow-up DWI and were subsequently observed for survival until death or until March 1, 2007.

The location of the primary tumors in patients who had a histologic diagnosis of carcinoid included the small bowel in three patients, the large bowel in six patients, the stomach and duodenum in three patients, and other locations in two patients. Patients who had undergone chemotherapy or surgery were not excluded from the study. Targeted lesions close to the diaphragm were excluded because of breathing artifacts. Targeted lesions smaller than 1 cm also were excluded from the study because they were too small to be detected with DWI.

Chemoembolization Technique

According to our standard institutional protocol, experienced interventional radiologists performed all TACE procedures. For most

patients with bilateral liver disease, only one lobe of the liver was subjected to embolization during each treatment session. To prevent carcinoid crisis, somatostatin analogues were preoperatively administered to patients with active hormone hypersecretion. Chemoembolization was performed as previously described (14). Selective catheterization of the feeding artery was followed by infusion of a solution containing 100 mg of cisplatin (Platinol; Bristol-Myers Squibb, Princeton, NJ), 50 mg of doxorubicin (Adriamycin; Pharmacia Upjohn, Kalamazoo, MI), and 10 mg of mitomycin C (Mutamycin C; Bedford Laboratories, Bedford, OH) in a 1:1-2:1 mixture of iodized oil (Lipiodol, Guerbet). The infusion was followed by injection of either 150- to 250-µm polyvinyl alcohol particles (Ivalon, Interventional Therapeutic, Fremont, CA) or 300- to 500-µm trisacryl gelatin microspheres (Embospheres, Biosphere Medical, Rockland, MA) to slow arterial inflow and prevent washout of the chemotherapeutic agent.

CT Technique

Within 24 hours after TACE, all patients underwent unenhanced MDCT with a Volume Zoom scanner (Somatom Plus 4, Siemens Medical Solutions, Malvern, PA). Scanning parameters were 120 kVp, 210 mA, 5-mm section collimation, and 5-mm image reconstruction. Technical success of the procedure was shown by the presence of intratumoral iodized oil deposition and relative sparing of the nontumorous liver parenchyma.

MRI Technique and Imaging Features

All patients underwent baseline and follow-up MRI with a 1.5-T MRI scanner (CV/i; GE Healthcare, Milwaukee, WI) and a phased-array torso coil. Imaging protocol included T2-weighted fast spin-echo images (matrix, 256 × 256; slice thickness, 8 mm; interslice gap, 2 mm; repetition time [TR]/ echo time [TE], 5000/100 msec; receiver bandwidth, 32 kHz), breath-hold diffusion-weighted echoplanar images (matrix, 128 × 128; slice thickness, 8 mm; interslice gap, 2 mm; b value, 500 mm^2/sec; TR/TE, 5000-6500/110 msec; receiver bandwidth, 64 kHz), and breath-hold unenhanced and contrast-enhanced (0.1 mmol/kg intravenous gadodiamide [Omniscan; GE Healthcare, Princeton, NJ]) T1-weighted three-dimensional fat-suppressed spoiled gradient-echo images (field of view, 320-400 mm; matrix, 192 × 160; slice thickness, 4-6 mm TR/TE, 5.1/1.2 msec; receiver bandwidth, 64 kHz; flip angle, 15º) in the arterial (20 seconds after contrast administration) and portal venous (60 seconds after contrast administration) phases.

We compared imaging features on unenhanced MRI and post-TACE MRI. The features included tumor size, percentage of arterial and portal venous targeted tumor enhancement, patency of the portal vein, and ADCs of tumors, liver, and spleen.

Image Analysis

Images for each patient were obtained retrospectively with a workstation (Advantage; GE Healthcare, Milwaukee, WI) and were interpreted by consensus of two experienced MRI radiologists in the same reading session to ensure careful comparison of preprocedural and postprocedural MRI features. Image magnification and window and level settings were adjusted accordingly, and the relevant settings were recorded. Bidimensional targeted tumor measurements (maximal tumor diameter and largest perpendicular diameter), percentage of arterial and portal venous targeted tumor enhancement, and patency of the portal vein were recorded. For patients who underwent more than one TACE session, the MRI study performed after the last session was used for comparison. Percentage of enhancement was visually estimated as enhancement seen on the axial image with the largest tumor diameter and was quantified as follows: less than 25%, 25% to less than 50%, 50-75%, and greater than 75%. ADC maps were generated from the diffusion-weighted images, and values were recorded by placement of a region of interest over the entire treated mass, as seen on the image with the largest lesion size. Percentage of iodized oil deposition on CT was estimated with the same four quartiles used for percentage of tumor enhancement. For patients who had undergone multiple treatments, the cumulative iodized oil deposition in the targeted lesion was recorded.

Anatomic tumor response was recorded and classified according to the WHO and RECIST guidelines as complete response, partial response, stable disease, or progressive disease. Complete response was described as tumor disappearance confirmed 4 weeks after treatment. Partial response was defined as corresponding to a 50% decrease in the summation of the products of bidimensional measurements of tumor lesions according to the WHO criteria and to at least a 30% decrease in the sum of the longest diameter of targeted lesions according to the RECIST. Stable disease was defined as neither sufficient shrinkage to qualify for partial response nor sufficient increase to qualify for progressive disease. Progressive disease was defined as at least a 20% increase in the sum of the longest diameter of

target lesions according to the RECIST or an at least 25% increase in the summation of the products of bidimensional measurements of tumor lesions according to the WHO guidelines (12, 13). Tumor response determined as change in tumor size according to the WHO and RECIST guidelines was recorded.

Clinical Data

Laboratory data included results of liver function tests before and after treatment. Hormonal and tumor markers were not included in the analysis because they were primarily used for diagnostic purposes. The clinical status of each patient was assessed before and after treatment according to the Eastern Cooperative Oncology Group performance status scale (17).

Survival Data

Survival rates were calculated from the date of diagnosis of metastatic disease because in some cases there was no available information on the time of diagnosis of the primary lesion.

Statistical Analysis

Statistical analysis was performed with the SPSS 14.0 statistical software package. Paired Student's *t* tests and Wilcoxon's rank tests were used for comparisons of pretreatment and posttreatment values. Tumor size, enhancement, and ADC in patients with pancreatic NETs were compared with those in patients with nonpancreatic NETs. The same variables were compared for patients with first-line and those with second-line TACE therapy. Survival rates were calculated on the basis of the time of diagnosis of metastatic liver disease and analyzed with the Kaplan-Meier method. A value of $p < 0.05$ was considered statistically significant.

RESULTS

Demographic Data

Our retrospective analysis included 66 lesions in 26 patients with neuroendocrine hepatic metastasis who were treated with TACE at our institution between December 1, 1999, and January 1, 2004, and were observed for survival until death or until March 1, 2007, whichever occurred

first. Fifteen of the 26 patients (six with metastatic carcinoid and nine with metastatic islet cell lesions) underwent TACE as first-line therapy for metastatic disease. The other 11 patients (nine with metastatic carcinoid lesions and two with metastatic islet cell lesions) underwent TACE as a second-line treatment. All patients underwent an average of two (range, 1-6) consecutive TACE sessions per lesion. The average number of targeted lesions per patient was 2.5 (range, 1-4). To reduce selection bias, in patients with numerous lesions in the targeted lobe, the largest and up to four lesions were included in the study. A total of 37 metastatic carcinoid lesions and 29 metastatic islet cell lesions were reviewed. Detailed demographic data and treatment response according to the WHO and RECIST guidelines are included in Table 5.1. No complications related to TACE were encountered in our study population.

Imaging Data

The mean time between pretreatment and posttreatment MRI was 206 ± 201 (SD) days. The mean longest tumor diameter was 5.6 ± 3.1 cm before treatment and 4.6 ± 3.1 cm after treatment ($p < 0.0001$), as shown in Table 5.2. Mean tumor enhancement in the arterial phase was 60.8% ± 25.3% before treatment and 31.1% ± 30.8% after treatment ($p < 0.0001$). Mean tumor portal venous enhancement was 82.4% ± 20.7% before and 42.5% ± 36.1% after treatment ($p < 0.0001$) (Fig 5.1A-G). Mean tumor ADC increased from 1.51 ± 0.55 x 10^{-3} mm^2/sec before treatment to 1.79 ± 0.54 x 10^{-3} mm^2/sec after treatment ($p < 0.0001$). The ADCs for liver ($p = 0.17$) and spleen ($p = 0.58$) remained unchanged before and after treatment. A mean change of 26.4% ± 45.5% in tumor ADC was recorded for all targeted lesions. According to the WHO criteria, seven (27%) patients had a partial response, and the other 19 (73%) had stable disease. A mean change of 34.5% ± 22.9% in bidimensional tumor size was found for all patients. According to the RECIST, six (23%) of the patients had a partial response, 19 (73%) had stable disease, and one (4%) had progressive disease. A mean change of 16.3% ± 27.2% in unidimensional tumor size according to the RECIST was recorded. Tested correlation between the WHO and RECIST guidelines was significant ($p < 0.001$, $\rho = 0.8$). No significant correlation, however, was detected between the WHO criteria and mean tumor ADC ($p = 0.8$, $\rho = 0.025$) or the RECIST and mean tumor ADC ($p = 0.2$, $\rho = 0.2$) (Table 5.3).

Testing for possible correlation between tumor ADC after treatment, percentage of arterial and portal venous tumor enhancement after treatment, and percentage of iodized oil deposition for each targeted lesion showed no correlation between percentage of iodized oil deposition and tumor ADC after treatment ($p = 0.3$, $\rho = 0.13$) or between percentage of iodized oil deposition and percentage of tumor enhancement after treatment ($p = 0.5$, $\rho = 0.09$). A marginal value of $p = 0.06$ ($\rho = 0.24$) was observed in the test of correlation between percentage of tumor enhancement in the portal venous phase and iodized oil deposition. The tumor variables size, enhancement, and ADC in patients with pancreatic NETs were not significantly different from those in patients with nonpancreatic NETs. Similarly, the tumor variables in patients undergoing TACE as first-line treatment were not significantly different from those in patients undergoing TACE as a second-line treatment.

Clinical and Laboratory Data

No statistically significant change was found in any clinical or laboratory value tested before and after treatment.

Survival Data

The mean survival period for all patients was 78 months (Fig 5.2). There was no statistically significant difference between the survival rate of patients with metastatic carcinoid and that of patients with islet cell lesions (logrank $p = 0.65$). Moreover, there was no statistically significant difference between the survival rate of patients who underwent TACE as first-line treatment and that of those who underwent the procedure as second-line treatment (log-rank $p = 0.87$).

DISCUSSION

Hepatic metastasis from NETs is fairly common, encountered in 25-90% of patients with NETs (18). Hepatic metastatic lesions of NETs typically have an indolent course of progression and may be diagnosed at an advanced stage of disease. Curative surgical resection is possible in only 10-20% of cases. Therefore, a large portion of patients are candidates for palliation (1). Medical palliative treatments have been effective in controlling hormonal symptoms but not as successful in controlling tumor growth (19). Moreover, the rate and median duration of objective response to systemic chemotherapy have been disappointing, and the survival rate has

not substantially increased (20). TACE exploits the hypervascularity of NET metastatic lesions and the blood supply through the hepatic artery to deliver high concentrations of chemotherapeutic agents and embolic materials to the tumor bed. This treatment has been shown to be an effective palliative method of controlling hormonal symptoms and tumor growth in patients with hepatic metastasis of NETs (8, 10, 11, 21, 22).

Assessment of response to treatment is necessary for clinical management and is critical for the evaluation of clinical trials. Currently used tumor response criteria include the WHO and RECIST guidelines (12, 13). Both sets of guidelines rely on anatomic information on tumor status derived before and after treatment, measured as a change in tumor size. However, the validity of the criteria has been challenged with various types of tumors and treatments, mainly because of a need for additional information on functional tumor burden (23). New targeted cancer therapies may not result in changes in tumor size that qualify as complete or partial response. They may, however, lead to cellular necrosis, measured with functional imaging (PET, SPECT, and MRI). As a form of targeted therapy, TACE has been effective in reducing tumor burden in patients with NET hepatic metastasis, but despite the favorable clinical outcome, response to treatment often does not meet the criteria for complete response.

The need for functional assessment of tumor burden in NET hepatic metastasis was introduced in a study of treated NET metastases assessed with ^{111}In-pentetreotide SPECT (24). Not all tumors, however, exhibit uptake with this imaging technique. DWI is a functional technique based on motion of water molecules across cell membranes. DWI has been used to evaluate tumor cell death of primary unresectable hepatocellular carcinomas treated with TACE (14, 16). Viable highly cellular tumors have intact cell membranes that restrict the motion of water molecules, producing a low ADC. After TACE, cellular necrosis causes membrane disruption and increases membranous permeability, allowing free diffusion of water molecules and an increase in ADC (14, 16). Our results show that DWI can be used to assess response to treatment on a functional molecular level and to quantify tumor cell death by showing the state of water diffusion across tumor cell membranes on ADC maps. This observation may explain the lack of correlation between the WHO and RECIST guidelines and the DWI measurements. The first two refer to anatomic information, and the last offers information on a cellular level.

Another indicator of treatment effectiveness measured in our study is tumor vascularity, shown by percentage of enhancement of targeted lesions in the arterial and portal venous phases of imaging before and after treatment. Several studies have shown a decrease in tumor vascularity after successful treatment with TACE. It is difficult, however, to compare results of previous reports because of variability in the measurement methods of tumor vascularity (25). Contrast-enhanced perfusion imaging is a promising method of measuring tumor vascularity in a more reproducible manner (26, 27).

Our results showed lack of correlation between iodized oil deposition, tumor DWI measurements, and arterial and portal venous enhancement measurements. This lack of correlation may be due to the different physical properties measured. Contrast enhancement is determined by the amount of contrast material in the extracellular space, DWI is a measure of water motion across membranes, and iodized oil deposition refers to a possible biochemical tumor cell pump defect (28). Iodized oil deposition has been shown not to correlate well with tissue necrosis (29). In our experience, the main use of unenhanced CT has been to determine the technical success of TACE by verifying adequate tumor targeting. Moreover, iodized oil deposition and arterial and portal venous tumor enhancement are based on visual estimates, whereas ADC is a computed value and can be objectively reproduced.

Patients with untreated hepatic metastasis historically have a 5-year survival rate of 35% with a median survival period of 2-4 years (30, 31). Comparison of survival data with findings in other studies shows that our mean survival period of 78 months is in accordance with other reported survival times (8, 11). Eriksson et al. (10) reported a median survival period of 80 months in a group of 41 patients with NET metastasis, but all of those patients had previously undergone other medical treatments. Other reports (8, 21, 32) have suggested that the natural history of metastatic NETs is unpredictable and that the median survival period among these patients after embolization treatment ranges from 13 to 80 months.

Our study had several limitations. Because of the rarity of the disorder, the number of subjects was small. Therefore, we were not able to detect trends between the carcinoid and the neuroendocrine groups or between the first-line TACE and second-line TACE groups. Future studies with a larger subset of patients are warranted to assess the correlation between tumor enhancement and ADC with an objective outcome, such as survival.

Moreover, patients who had incomplete imaging evaluations or had tumors less than 1 cm in diameter were excluded, leading to potential selection bias. NET hepatic metastasis is known for a long, variable, and indolent course, making it difficult to assess survival benefit. Histopathologic data were not obtained for any of the patients in the study. Therefore, tumor cell death was measured only with DWI. Previous reports (14, 16), however, have shown good correlation between the histopathologic percentage of necrosis and the ADC obtained with DWI.

The results of our analysis suggest that multiparametric DWI may effectively show treatment effect after TACE in patients with hepatic metastasis of NETs. The addition of DWI seems to provide important information about the functional tumor burden, whereas contrast-enhanced MRI depicts morphologic changes in NET hepatic metastasis after TACE. These preliminary results need to be further validated in a prospective randomized way that may strengthen the role of multiparametric functional MRI.

TABLES & FIGURES

Characteristic	Value
Sex	
Men	16
Women	10
Mean age (y)	57 ± 14 (SD)
Primary tumor (n)	
Carcinoid	14
Islet cell	12
Previous therapy (n)	
No	15
Yes	11
WHO response criteria (n)	
Complete response	0
Partial response	7
Stable response	19
Progressive disease	0
RECIST (n)	
Complete response	0
Partial response	6
Stable response	19
Progressive disease	1

Table 5.1 Demographic Data and Treatment Response According to World Health Organization (WHO) Criteria and Response Evaluation Criteria in Solid Tumors (RECIST) for All Patients with Neuroendocrine Tumors Treated with Transcatheter Arterial Chemoembolization (n = 26)

Feature	Before treatment	After treatment	p*
Size of mass (cm)			
Maximum diameter	5.6 ± 3.1	4.6 ± 3.1	<0.0001
Perpendicular diameter	4.5 ± 2.4	3.6 ± 2.3	<0.0001
Enhancement of mass (%)			
Arterial phase	60.8 ± 25.3	31.1 ± 30.8	<0.0001
Venous phase	82.4 ± 20.7	42.5 ± 36.1	<0.0001
ADC (x 10^{-3} mm^2/sec)			
Mass	1.51 ± 0.55	1.79 ± 0.54	<0.0001
Liver	1.81 ± 0.71	1.63 ± 0.58	0.17
Spleen	1.06 ± 0.33	1.10 ± 0.33	0.58

Table 5.2 Descriptive Data and Comparison of Imaging Variables Before and After Transcatheter Arterial Chemoembolization for all Patients with Metastatic Neuroendocrine Tumors. Note.— Values are mean ± SD. *Paired Student's *t* test.

Characteristic	WHO	RECIST	Diffusion-Weighted Imaging
Criterion	Size (summation of products of bidimensional measurements of targeted lesions)	Size (sum of longest diameters of targeted lesions)	Apparent diffusion coefficient
Percentage of change in criterion (mean ± SD)	34.5 ± 22.9	16.3 ± 27.2	26.4 ± 45.5
Information provided	Anatomic	Anatomic	Functional

Table 5.3 Comparison and Correlation Between World Health Organization (WHO) Criteria, Response Evaluation Criteria in Solid Tumors (RECIST), and Diffusion-Weighted Imaging Features for Neuroendocrine Tumor Response After Transcatheter Arterial Chemoembolization
Note.— Results of univariate analysis are as follows: WHO versus RECIST ($p < 0.001$, $\rho = 0.8$), RECIST versus diffusion-weighted imaging ($p = 0.2$; $\rho = 0.2$), WHO versus diffusion-weighted imaging ($p = 0.8$; $\rho = 0.025$).

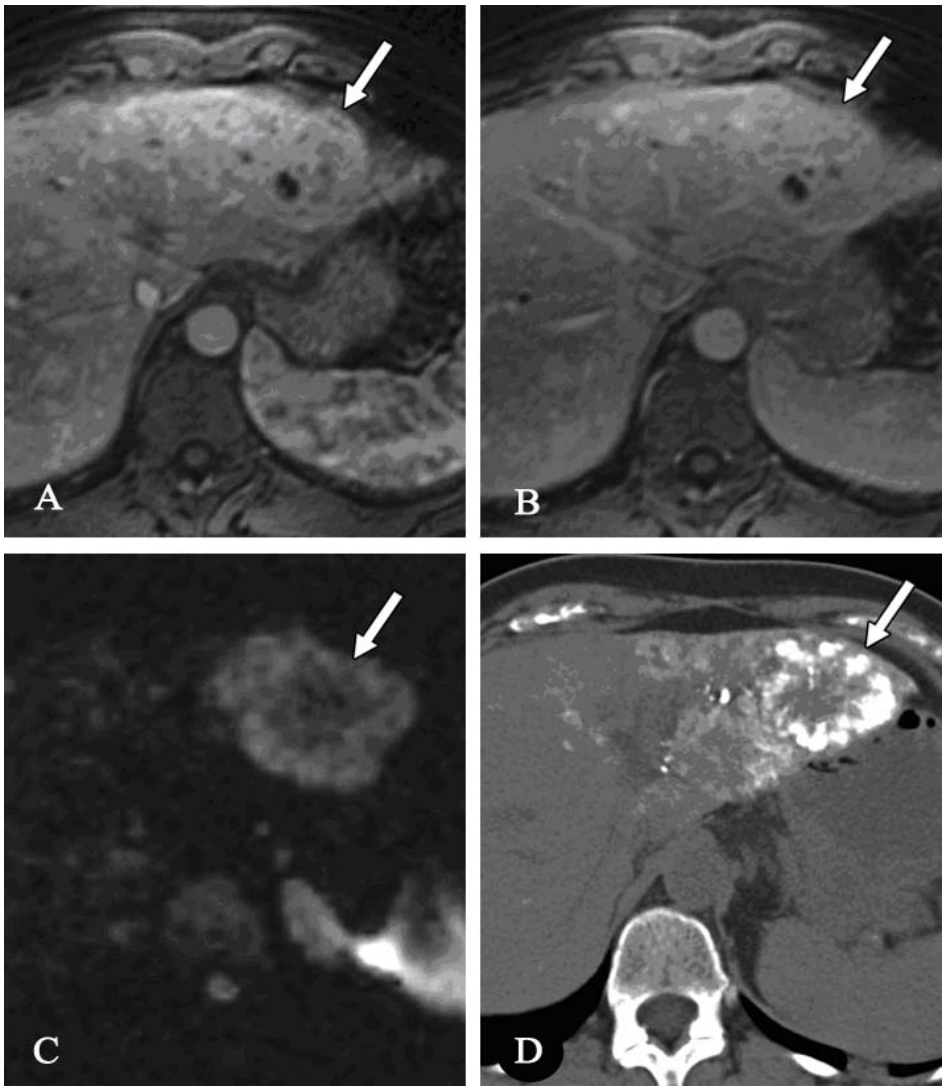

Figure 5.1 67-year-old woman with hepatic metastasis of neuroendocrine tumor. Changes were seen in contrast enhancement and apparent diffusion coefficient after transcatheter arterial embolization (TACE).
(A) MR image (5.1/1.2) in arterial phase of gadolinium enhancement shows 6-cm hypervascular mass (*arrow*) in left lobe.
(B) MR image (5.1/1.2) in portal venous phase of gadolinium enhancement shows almost complete enhancement of mass (*arrow*) in left lobe.
(C) Diffusion-weighted MR image (6,500/110) shows hyperintense mass (*arrow*). Apparent diffusion coefficient is 1.90×10^{-3} mm^2/sec.
(D) Unenhanced CT scan of abdomen shows intense deposition of iodized oil in periphery of mass (*arrow*) after TACE.

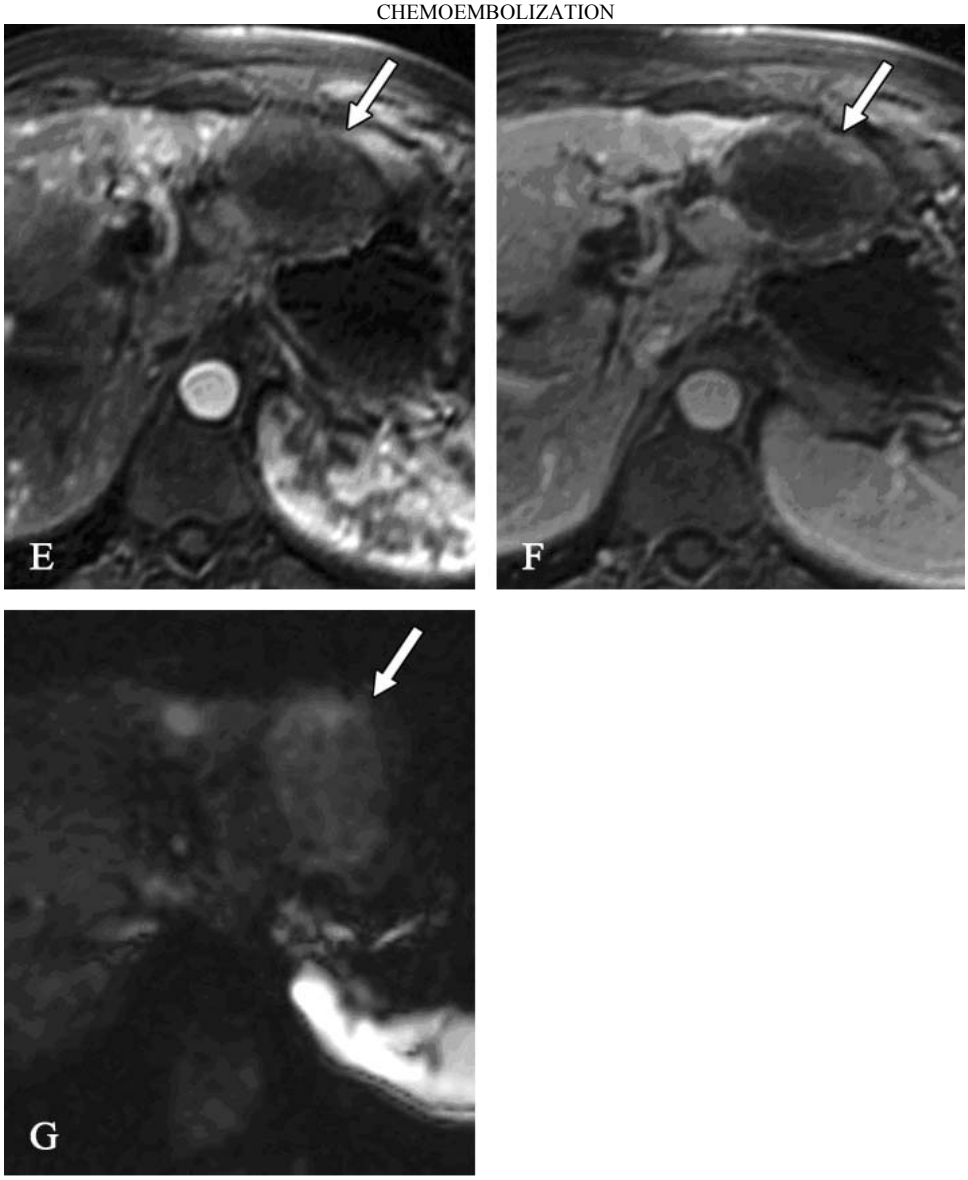

Figure 5.1 (continued) 67-year-old woman with hepatic metastasis of neuroendocrine tumor. Changes were seen in contrast enhancement and apparent diffusion coefficient after transcatheter arterial embolization (TACE).
(E) MR image (5.1/1.2) in arterial phase of gadolinium enhancement shows mass (*arrow*) as almost completely avascular after TACE.
(F) MR image (5.1/1.2) in portal venous phase of gadolinium enhancement shows minimal residual peripheral enhancement (< 10%) of mass (*arrow*) after TACE. Size of mass has only slightly decreased.
(G) Diffusion-weighted MR image (6,500/110) with apparent diffusion coefficient of 2.37 x 10^{-3} mm^2/sec confirms increasing cellular necrosis (*arrow*) after TACE.

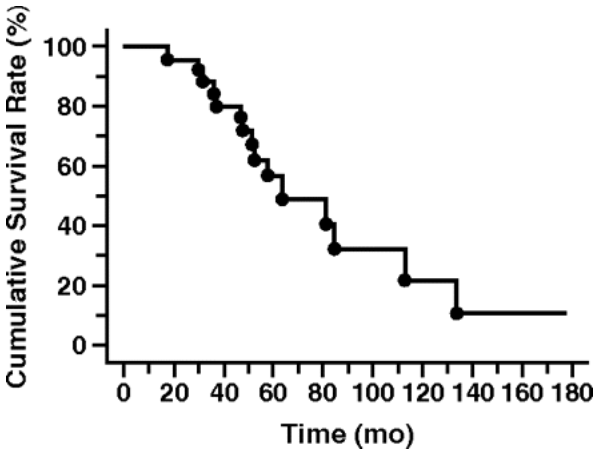

Figure 5.2 Graph shows Kaplan-Meier survival curve for patients with neuroendocrine tumors managed with transcatheter arterial embolization.

REFERENCES

1) Lepage C, Bouvier AM, Phelip JM, Hatem C, Vernet C, Faivre J. Incidence and management of malignant digestive endocrine tumours in a well defined French population. *Gut* 2004;53 : 549-553
2) Barakat MT, Meeran K, Bloom SR. Neuroendocrine tumours. *Endocr Relat Cancer* 2004;11 : 1-18
3) Norton JA. Endocrine tumours of the gastrointestinal tract: surgical treatment of neuroendocrine metastases. *Best Practice Res Clin Gastroenterol* 2005; 19:577 -583
4) Tomassetti P, Campana D, Piscitelli L, et al. Endocrine pancreatic tumors: factors correlated with survival. *Ann Oncol*2005; 16:1806 -1810
5) Chamberlain RS, Canes D, Brown KT, et al. Hepatic neuroendocrine metastases: does intervention alter outcomes? *J Am Coll Surg* 2000; 190:432 -445
6) McEntee GP, Nagorney DM, Kvols LK, Moertel CG, Grant CS. Cytoreductive hepatic surgery for neuroendocrine tumors. *Surgery* 1990; 108:1091 -1096
7) Oberg K, Kvols L, Caplin M, et al. Consensus report on the use of somatostatin analogs for the management of neuroendocrine tumors of the gastroenteropancreatic system. *Ann Oncol*2004; 15:966 -973
8) Gupta S, Yao JC, Ahrar K, et al. Hepatic artery embolization and chemoembolization for treatment of patients with metastatic carcinoid tumors: the MD Anderson experience. *Cancer J*2003; 9:261 -267
9) Roche A, Girish B, de Baère T, et al. Trans-catheter arterial chemoembolization as first-line treatment for hepatic metastases from endocrine tumors. *Eur Radiol* 2003;13 : 136-140
10) Eriksson BK, Larsson EG, Skogseid BM, Löfberg AM, Lörelius LE, Oberg KE. Liver embolizations of patients with malignant neuroendocrine gastrointestinal tumors. *Cancer*1998; 83:2293 -2301
11) Gupta S, Johnson MM, Murthy R, et al. Hepatic arterial embolization and chemoembolization for the treatment of patients with metastatic neuroendocrine tumors: variables affecting response rates and survival. *Cancer* 2005; 104:1590 -1602
12) Miller AB, Hoogstraten B, Staquet M, Winkler A. Reporting results of cancer treatment. *Cancer* 1981;47 : 207-214
13) Therasse P, Arbuck SG, Eisenhauer EA, et al. New guidelines to evaluate the response to treatment in solid tumors. *J Natl Cancer Inst* 2000; 92:205 -216

14) Kamel IR, Bluemke DA, Eng J, et al. The role of functional MR imaging in the assessment of tumor response after chemoembolization in patients with hepatocellular carcinoma. *J Vasc Interv Radiol* 2006; 17:505 -512
15) Lim HS, Jeong YY, Kang HK, Kim JK, Park JG. Imaging features of hepatocellular carcinoma after transcatheter arterial chemoembolization and radiofrequency ablation. *AJR* 2006;187 :945; [web]W341-W349
16) Kamel IR, Bluemke DA, Ramsey D, et al. Role of diffusion-weighted imaging in estimating tumor necrosis after chemoembolization of hepatocellular carcinoma. *AJR* 2003;181 : 708-710
17) Oken MM, Creech RH, Tormey DC, et al. Toxicity and response criteria of the Eastern Cooperative Oncology Group. *Am J Clin Oncol* 1982; 5:649 -655
18) Proye C. Natural history of liver metastasis of gastroenteropancreatic neuroendocrine tumors: place for chemoembolization. *World J Surg* 2001;25 : 685-688
19) Strosberg JR, Kvols LK. A review of the current clinical trials for gastroenteropancreatic neuroendocrine tumours. *Expert Opin Investig Drugs* 2007; 16:219 -224
20) Kouvaraki MA, Ajani JA, Hoff P, et al. Fluorouracil, doxorubicin, and streptozocin in the treatment of patients with locally advanced and metastatic pancreatic endocrine carcinomas. *J Clin Oncol* 2004; 22:4762 -71
21) Ajani JA, Carrasco CH, Charnsangavej C, Samaan NA, Levin B, Wallace S. Islet cell tumors metastatic to the liver: effective palliation by sequential hepatic artery embolization. *Ann Intern Med*1988; 108:340 - 344
22) Drougas JG, Anthony LB, Blair TK, et al. Hepatic artery chemoembolization for management of patients with advanced metastatic carcinoid tumors. *Am J Surg* 1998;175 : 408-412
23) Therasse P, Eisenhauer EA, Verweij J. RECIST revisited: a review of validation studies on tumour assessment. *Eur J Cancer*2006; 42:1031 - 1039
24) Gopinath G, Ahmed A, Buscombe JR, Dickson JC, Caplin ME, Hilson AJ. Prediction of clinical outcome in treated neuroendocrine tumours of carcinoid type using functional volumes on ^{111}In-pentetreotide SPECT imaging. *Nucl Med Commun* 2004;25 : 253-257
25) Semelka RC, Worawattanakul S, Mauro MA, Bernard SA, Cance WG. Malignant hepatic tumors: changes on MRI after hepatic arterial chemoembolization—preliminary findings. *J Magn Reson Imaging* 1998; 8:48 -56

26) Rosen MA, Schnall MD. Dynamic contrast-enhanced magnetic resonance imaging for assessing tumor vascularity and vascular effects of targeted therapies in renal cell carcinoma. *Clin Cancer Res*2007; 13:770s -776s
27) Morgan B, Utting JF, Higginson A, Thomas AL, Steward WP, Horsfield MA. A simple, reproducible method for monitoring the treatment of tumours using dynamic contrast-enhanced MR imaging. *Br J Cancer* 2006; 94:1420 -1427
28) Tancredi T, McCuskey PA, Kan Z, Wallace S. Changes in rat liver microcirculation after experimental hepatic arterial embolization: comparison of different embolic agents. *Radiology*1999; 211:177 -181
29) Takayasu K, Arii S, Matsuo N, et al. Comparison of CT findings with resected specimens after chemoembolization with iodized oil for hepatocellular carcinoma. *AJR* 2000;175 : 699-704
30) Chen H, Hardacre JM, Uzar A, Cameron JL, Choti MA. Isolated liver metastases from neuroendocrine tumors: does resection prolong survival? *J Am Coll Surg* 1998;187 : 88-92
31) Thompson GB, van Heerden JA, Grant CS, Carney JA, Ilstrup DM. Islet cell carcinomas of the pancreas: a twenty-year experience. *Surgery* 1988; 104:1011 -1017
32) Dominguez S, Denys A, Madeira I, et al. Hepatic arterial chemoembolization with streptozotocin in patients with metastatic digestive endocrine tumours. *Eur J Gastroenterol Hepatol*2000; 12:151 -157

CHAPTER 6

ROLE OF FUNCTIONAL MAGNETIC RESONANCE IMAGING IN ASSESSING METASTATIC LEIOMYOSARCOMA RESPONSE TO CHEMOEMBOLIZATION

Vossen JA, Kamel IR, Buijs M, Liapi E, Georgiades CS, Hong K, Geschwind JF

J Comput Assist Tomogr 2008 May-Jun;32(3):347-52.

ABSTRACT

PURPOSE:
To assess the value of functional magnetic resonance (MR) imaging in the evaluation of early tumor response after transarterial chemoembolization (TACE) for metastatic leiomyosarcoma and compare tumor response using functional MR imaging versus traditional imaging response assessment, which is based on tumor size.

MATERIALS AND METHODS:
We evaluated 31 lesions in 10 patients with liver metastases from leiomyosarcoma using MR imaging studies before and after TACE. Diffusion and contrast-enhanced MR imaging was performed on a 1.5-T unit. Imaging protocol consisted of T2-weighted fast spin-echo images, breath-hold diffusion-weighted echoplanar images, and breath-hold unenhanced and contrast-enhanced T1-weighted three-dimensional fat-suppressed spoiled gradient-echo images in the arterial phase (20 seconds) and portal venous phase (60 seconds). Parameters evaluated included change in tumor size, enhancement, and apparent diffusion coefficient (ADC) values. Median survival was also calculated for the entire cohort.

RESULTS:
The 31 lesions evaluated had a mean size of 4.8 cm before treatment. Tumor size decreased only 2% immediately after treatment. Decrease of tumor enhancement after treatment was significant ($p < 0.0001$) in the arterial phase (69%) as well as in the portal venous phase (64%). After TACE, mean tumor ADC increased by 20% ($p = 0.0015$), whereas mean nontreated liver, spleen, and muscle ADC values did not change significantly ($p = 0.44$, $p = 0.287$, and $p = 0.098$, respectively). Patient survival from time of first TACE was 21 months for the entire cohort.

CONCLUSION:
In patients with leiomyosarcoma and liver metastases who were treated with TACE, significant early changes in the treated lesions occurred on functional MR imaging. These include decrease in tumor enhancement and increase in tumor ADC value, suggesting increasing tumor necrosis and cell death. Changes in tumor size were small and inadequate to assess treatment response, suggesting limitation of the current response criteria in the early assessment of tumor response.

INTRODUCTION

Approximately 12% of all soft tissue sarcomas are leiomyosarcomas, arising from smooth muscle (1). Estimated new cases and deaths from soft tissue sarcoma in the United States in 2006 are 9530 and 3500, respectively (2). Leiomyosarcoma can occur anywhere in the body, but the most frequent primary tumor sites are visceral and retroperitoneal. The liver is a common site for metastases from visceral and retroperitoneal leiomyosarcomas (3).

Surgical resection has been proven to increase survival, with reported median survival of 32 months (4, 5). Unfortunately, most patients with liver metastases appear to be unresectable at the time of diagnosis. Without treatment, the reported survival rate for patients with nonresectable hepatic metastases from the time of diagnosis is 14 months (6). The most common treatment of nonresectable liver metastases is chemotherapy. Unfortunately, reported tumor response rates are low. Better results have been obtained by using transarterial chemoembolization (TACE), with a reported median survival of 18 months (7).

The goal of TACE is to deliver high concentrations of chemotherapeutic agents through the feeding artery directly into the tumor mass, with minimal systemic toxicity (8). Embolic particles are used to reduce arterial inflow and drug washout and maximize contact time between the drugs and the tumor cells (9, 10). Extensive data have shown evidence that TACE causes significant tumor necrosis (11).

Assessing tumor response after TACE is not only essential for evaluating treatment success, but it also influences therapy strategies. Traditional imaging modalities and imaging response criteria are constrained by the lack of capability to reliably assess the extent of tumor necrosis. Unenhanced computed tomography (CT) can demonstrate the presence of hyperattenuating iodized oil within the tumor, but iodized oil impairs assessment of residual tumor enhancement on contrast-enhanced CT (12). Enhanced areas on gadolinium-enhanced magnetic resonance (MR) images can be used to evaluate tumor necrosis but can also represent posttreatment granulation tissue (13, 14). Presently, no standardized response criteria exist to evaluate lesions treated with TACE. The traditional and accepted criteria to determine tumor response in oncology, namely, the World Health Organization criteria and Response Evaluation Criteria in

Solid Tumors (RECIST), use decrease in tumor size as an indicator of successful therapy (15).

A novel imaging technique is diffusion MR imaging, which generates the apparent diffusion coefficient (ADC) maps. Apparent diffusion coefficient maps the mobility of water in tissues. Because of reduced cellularity and diminished cell membrane integrity in necrotic tumor cells, water mobility is increased, whereas viable tumor cells restrict diffusion of water molecules. Diffusion MR imaging has been successfully used to assess tumor response after chemotherapy and radiation therapy, as well as after TACE (16-18, 19, 20).

Based on these studies, we hypothesized that diffusion MR imaging could determine cellular necrosis and may therefore be useful in providing additional information about early tumor response after TACE. Hence, the purpose of our study was to assess the value of functional MR imaging in the evaluation of early tumor response after TACE in patients with metastatic leiomyosarcoma. In addition, we compared tumor response using functional MR imaging with traditional imaging assessment using tumor size.

MATERIALS AND METHODS

Patients

Between January 1, 2001, and December 31, 2005, the care of 12 patients with metastatic leiomyosarcoma who were to receive one or more cycles of TACE was discussed in the liver tumor board at our institution. Criteria for performing TACE included confirmed diagnosis of unresectable metastatic leiomyosarcoma in patients with or without minimally impaired liver function. Patients excluded from receiving TACE were those with an Eastern Cooperative Oncology Group performance status greater than 2, encephalopathy, severe variceal bleeding and/or severe ascites, significant thrombocytopenia, prolonged impaired renal function, acute renal failure (ie, an abrupt increase in serum creatinine level of $\geq$ 50% with respect to the baseline level or an absolute increase in the serum creatinine concentration of $\geq$ 0.5 to > 1.5 mg/dL), or severe liver failure (advanced Child-Pugh score C). Our study group included all patients treated with chemoembolization who had contrast-enhanced and diffusion-weighted MR imaging before and after chemoembolization. Review of our database identified 10 patients who

fulfilled these criteria; 2 patients were excluded for not having MR imaging after TACE. Diagnosis of metastatic leiomyosarcoma was confirmed by biopsy in all patients. The study was authorized by the institutional review board.

Chemoembolization Technique

An 18-gauge single-wall needle was used to access the right common femoral artery using the Seldinger technique. A 5-F vascular sheath was placed into the right common femoral artery over a 0.035-inch Glidewire (Terumo Medical, Somerset, NJ). Under fluoroscopic guidance, a 5-F glide Simmons-1 catheter (Cordis, Miami, FL) was advanced into the aortic arch, formed, and then used to select the celiac axis. Over the guidewire, the catheter was advanced into the desired hepatic artery branch, depending on the tumor location. A solution containing 100 mg of cisplatin (Platinol; Bristol-Myers Squibb, Princeton, NJ), 50 mg of doxorubicin (Adriamycin; Pharmacia Upjohn, Kalamazoo, MI), and 10 mg of mitomycin C (Mutamycin C; Bedford Laboratories, Bedford, OH) in a 1:1 mixture with iodized oil, followed by infusion of Embosphere particles (Biosphere Medical, Rockland, MA), was administered until stasis was achieved.

CT Technique

Within 1 day after chemoembolization, all patients underwent unenhanced helical CT imaging with use of a Siemens Somatom Volume Zoom scanner (Siemens Medical Systems, Iselin, NJ). Scanning parameters were 120 kVp, 210 mA, 5-mm section collimation, and 5-mm image reconstruction. Technical success of the procedure was demonstrated by the focal deposition of iodized oil in the tumor and relative sparing of the nontumorous liver parenchyma.

MRI Technique

Patients were scanned using a 1.5-T MRI scanner (CV/i; GE Healthcare, Milwaukee, WI) and a phased-array torso coil. Imaging protocol included T2-weighted fast spin-echo images (matrix, 256 × 256; slice thickness, 8 mm; interslice gap, 2 mm; repetition time [TR]/ echo time [TE], 5000/100 msec; receiver bandwidth, 32 kHz), breath-hold diffusion-weighted echoplanar images (matrix, 128 × 128; slice thickness, 8 mm; interslice gap, 2 mm; b value, 500 mm^2/sec; TR/TE, 5000-6500/110 msec; receiver bandwidth, 32 kHz), and breath-hold unenhanced and contrast-

enhanced (0.1 mmol/kg intravenous gadodiamide [Omniscan; GE Healthcare, Princeton, NJ]) T1-weighted three-dimensional fat-suppressed spoiled gradient-echo images (field of view, 320-400 mm; matrix, 192 × 160; slice thickness, 4-6 mm TR/TE, 5.1/1.2 msec; receiver bandwidth, 64 kHz; flip angle, 15º) in the arterial phase (20 seconds) and portal venous phase (60 seconds).

Follow-up

According to our protocol, patients received contrast-enhanced and diffusion MR 4 to 6 weeks after TACE to assess tumor response. Patients with near-complete tumor necrosis were followed by imaging every 6 to 8 weeks. All patients had follow-up for at least 6 weeks to assess morbidity and mortality after TACE.

Image Analysis

Magnetic resonance image processing and ADC maps were generated using a commercially available Advantage Windows workstation (General Electric Medical Systems). Images were interpreted by consensus of 2 experienced MR radiologists. Parameters evaluated included change in tumor size, enhancement, and ADC values. All target lesions of 2 cm or larger were evaluated, with a maximum of 5 lesions per patient. The maximum diameter of the targeted lesions was measured by electronic calipers as proposed by RECIST. Areas of tumor enhancement were considered viable, and areas of nonenhancement were considered necrotic. The percentage of enhancement was based on enhancement seen on the axial image with the largest tumor size. Apparent diffusion coefficient maps were generated from the diffusion-weighted images, and values were recorded by placing a region of interest over the entire treated mass, as seen on the image with the largest lesion size. Apparent diffusion coefficient maps of untreated liver, spleen, and muscle were generated. The percentage of iodized oil deposition on CT was also recorded. In patients who had received multiple iodized oil treatments, the maximum iodized oil retention in the targeted lesion was recorded.

Statistical Analysis

Statistical analysis was performed with use of Stata software package (Version 8; Stata, College Station, TX). Paired *t* test was used to compare parameters used to assess tumor response before and after TACE. These

included tumor size, enhancement, and ADC before and after TACE. Paired *t* test was also used to compare ADC values of the liver, spleen, and muscle before and after treatment. Median survival was calculated in the entire cohort from the date of presentation with liver metastases until death from any cause, or until October 1, 2006, and surviving patients were censored at the date of analysis. A Kaplan-Meier survival curve was generated. P values < 0.05 were considered to indicate statistical significance.

RESULTS

Demographic Information

General patient information is shown in Table 6.1. A total of 31 lesions were evaluated in 10 patients. Each lesion received a single TACE treatment, except for 1 lesion that received 2 cycles of TACE. The average duration between preprocedural and postprocedural MR imaging was 57 ± 22 days. Magnetic resonance imaging was performed within 9 ± 18 days before TACE. Mean duration between the last TACE treatment and follow-up MR imaging was 48 ± 24 days. Mean duration between last TACE treatment and second follow-up MR for size evaluation was 141 ± 67 days. Mean maximum iodized oil retention within the tumor as seen on CT was 42%.

Assessment of Change in MR Imaging Parameters After TACE

On gadolinium-enhanced MR imaging, overall tumor enhancement in the arterial and portal venous phases decreased significantly after TACE (Tables 6.2, 6.3). Arterial enhancement decreased after TACE by 35%, and the decrease was statistically significant ($p < 0.0001$). Similarly, venous enhancement decreased by 49%, which was also statistically significant ($p < 0.0001$). Diffusion MR imaging was also useful in monitoring response after treatment. Mean tumor ADC increased after TACE by 20% ($p = 0.0015$), whereas the ADC remained unchanged in nontumorous liver, spleen, and muscle (Table 6.2) (Fig 6.1). Mean tumor size did not change immediately after TACE, and therefore, it did not meet RECIST for partial or complete response. For 17 lesions in 5 patients, we were able to evaluate size on the second follow-up MR after a mean duration of 141 days. Mean tumor size decreased from 4.1 to 3.4 cm (17%) in these 5 patients. Based on these results, all patients in our cohort were considered nonresponders to TACE, even with more extended follow-up measurements of tumor size.

Patient Survival

Median survival from time of liver metastases was 34 months for the entire cohort. Survival rate at 1, 2, and 3 years was 100%, 70%, and 47%, respectively. Median survival from time of first TACE was 21 months for the entire cohort. Survival rate at 1, 2, and 3 years from first TACE was 100%, 38%, and 13%, respectively. This is significantly higher than the previous reported survival rate for untreated patients from the time of diagnosis, which was 14 months (6).

Morbidity and Mortality

None of the patients in our cohort died within the first 30 days after TACE. One patient developed a liver abscess 1 month after TACE, which was managed by percutaneous drainage.

DISCUSSION

Leiomyosarcoma metastatic to the liver is an uncommon neoplasm. Traditionally, chemotherapy has been used for these patients as the standard treatment modality, although chemotherapy generally does not provide a survival benefit. Locoregional therapy is a promising treatment modality that has already been proven to improve survival in patients with other hepatic malignancies (21, 22).

Without treatment, the reported survival rate for patients with unresectable hepatic metastases from the time of diagnosis is 14 months (6) In our cohort, median survival was 21 months from the time of first TACE, whereas reported survival rate in the literature for patients that undergo incomplete resection ranges from 8 to 21 months (4, 5). Our morbidity and mortality rates were significantly lower than the rates reported after resection. Our results suggest that TACE is a safe treatment modality that could potentially improve survival in patients with unresectable metastatic leiomyosarcoma. In addition, early response may restrict the number of treatments, resulting in preservation of functioning healthy liver tissue, which likely contributes to prolonged survival.

It is essential for physicians to assess response to treatment, especially shortly after treatment, because response influences treatment strategies. Therefore, we compared traditional imaging assessments (which are based on iodized oil deposition, enhancement, and change in tumor size) with

diffusion and contrast-enhanced MR imaging in the evaluation of early tumor response after TACE for metastatic leiomyosarcoma. Our results indicate that early tumor necrosis may be seen with diffusion and contrast-enhanced MR imaging, before significant decrease in tumor size occurs.

It has been suggested that accumulation of iodized oil within tumors after TACE correlates well with tumor necrosis and survival in patients with hepatocellular carcinoma (23-25). In our study, however, mean maximum lipiodol deposition was only 42% immediately after TACE, which had a poor correlation with ADC ($R = 0.07$). In our experience, the amount of iodized oil deposition alone could not be used as a consistent predictor of tumor response after treatment.

Extracellular contrast agents are used in contrast-enhanced MR imaging to determine areas of tumor viability (26-28). Enhancement is believed to be caused by viable tumor, whereas necrotic tumor is nonenhancing. Enhanced areas can also represent posttreatment reactive granulation tissue, caused by increased capillary permeability and marked increase in the passive distribution of gadolinium (29). In our study, we found a decrease in enhancement of 35% in the arterial phase and 49% in the venous phase, which indicates that reduction in enhancement can be used as a predictor of tumor response.

Currently, the accepted methods to measure treatment response are based on changes in tumor size. In our study, tumor size did not change after treatment, whereas contrast enhancement and ADC value changed significantly, suggesting favorable tumor response. These results point out the disconnect that exists among lack of contrast enhancement, increase in ADC value, and decrease in tumor size. Our results are in line with recommendations of the European Association for the Study of Liver Disease, which recommend the use of lesion enhancement on contrast-enhanced CT as the standard modality to determine treatment response after locoregional therapy, instead of relying on tumor size only (30).

The mobility of water molecules in tissues is represented by diffusion MR imaging and ADC values. This provides insight into tumor microstructure. Viable tumors contain cells with an intact cell membrane, restricting water mobility, thereby causing low ADC values. Conversely, cellular necrosis causes increased membranous permeability, which leads to an increase in the ADC value. These characteristics are used to detect early cellular necrosis, before size regression occurs (31, 32).

This study has several limitations. First, our study had a small sample size. However, because metastatic leiomyosarcoma is a rare disease, it is unlikely to acquire a large sample size from a single institution. To confirm our conclusions, further studies including a larger sample size are needed. Second, we were only able to include patients with MR imaging before and after treatment, which can cause a possible selection bias. For obvious ethical reasons, we could not obtain histopathology after TACE; therefore, this study lacks histologic correlation. The mean follow-up interval in this study was 57 days. Even the more extended second follow-up period, which was 141 days, showed no decrease in size to a degree that would satisfy current treatment response criteria. Unfortunately, the second follow-up MR was not available for all patients. The aim of this study, however, was to show an early response, which is more useful in the clinical setting. At our institution, follow-up MR studies are performed at 4 to 6 weeks after TACE, and it is not clear whether this is the ideal follow-up time to evaluate enhancement, diffusion, and ADC values.

In conclusion, contrast-enhanced and diffusion-weighted MR imaging could potentially be used to predict the degree of tumor necrosis after TACE. The functional information provided by the ADC maps and contrast-enhanced changes on MR imaging may improve response evaluation, which currently is based only on size change. In addition, these MR imaging techniques are quantitative and may be subject to statistical testing individually and in combination to ascertain their utility in the assessment of tumor necrosis. Accurate assessment of early treatment response is necessary to guide future therapy and is likely to have survival benefit in patients who show a response to therapy.

TABLES & FIGURES

Characteristic	Value
Age (yrs), mean (range)	56 (44-68)
Sex (male/female)	3/7
Location primary (uterus/retroperitoneum/ lower extremity/kidney/unknown)	3/4/1/1/1
Pre-TACE chemotherapy (yes/no)	6/4
Pre-TACE liver resection (yes/no)	3/7
No. lesions (<10, 10-20, >20)	5/4/1
% of liver involvement, mean (range)	17 (5-30)
No. targeted lesions per patient, mean (range)	3.1 (1-5)
Size of targeted lesions, mean (range)	4.8 (1.3-15.2)

Table 6.1 Patient demographics.

Features	Pretreatment (SD)	Posttreatment (SD)	% Change	p*
Size of mass (cm)	4.8 (3.5)	4.7 (3.3)	2	0.31
% Enhancement of mass				
Arterial	51 (36)	16 (27)	35	<0.0001
Venous	76 (31)	27 (33)	49	<0.0001
ADC (x 10^{-3} mm^2/sec)				
Mass	1.77 (0.47)	2.13 (0.44)	20	0.0015
Liver	1.79 (0.41)	1.81 (0.43)	1	0.44
Spleen	1.16 (0.15)	1.11 (0.33)	4	0.287
Muscle	1.87 (0.36)	1.83 (0.48)	2	0.098

Table 6.2 Mean changes in tumor size, enhancement and ADC value after TACE.
* Paired t-test

Tumor Feature	Findings in Current Study	RECIST	EASL
Size	Small decrease (2%)	Requires 30% decrease for responders	NA
Arterial enhancement	Decreased (35%)	NA	NA
Venous enhancement	Decreased (49%)	NA	Unspecified decrease in enhancement
ADC value	Increased (20%)	NA	NA

Table 6.3 Comparison of our criteria with currently accepted criteria
EASL indicates European Association for the Study of Liver Disease; NA, not analyzed.

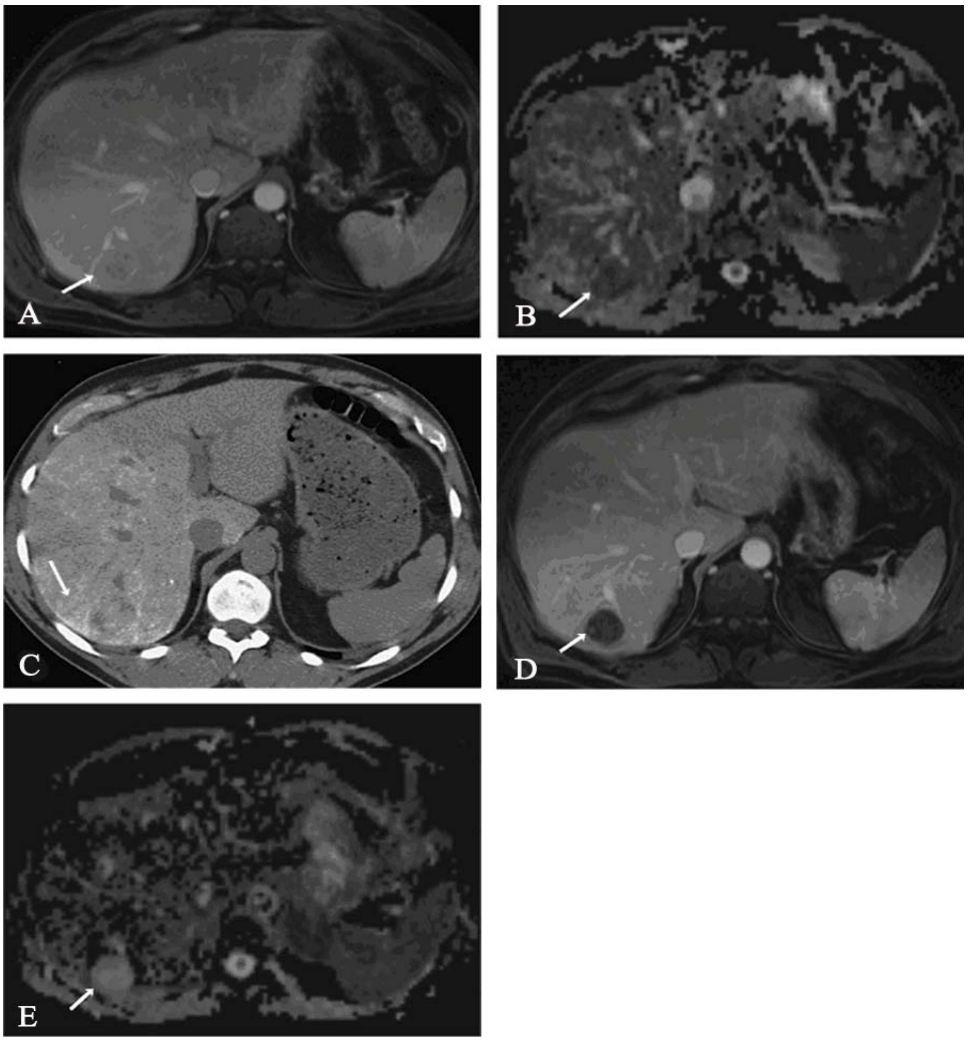

Figure 6.1 Changes in enhancement and ADC value after TACE.
(A) Gadolinium-enhanced image (TR/TE, 5.1 milliseconds/1.2 milliseconds) shows a 2.2-cm mass (arrow) in the right lobe posteriorly, with almost complete (100%) enhancement.
(B) Diffusion-weighted image (TR/TE, 6500/110 milliseconds) shows a hypointense mass (arrow). The ADC value was 1.27×10^{-3} mm^2/sec.
(C) Unenhanced CT of the abdomen after TACE shows low (<50%) deposition of iodized oil in the mass. Most lipiodol was deposited in the surrounding liver parenchyma (arrow).
(D) Gadolinium-enhanced image (TR/TE, 5.1/1.2 milliseconds) after TACE shows significant decrease (greater than 90%) in enhancement. Minimal residual enhancement persists in the periphery (arrow). Notice that the mass is unchanged in size.
(E) Diffusion-weighted image (TR/TE, 6500/110 milliseconds) after TACE shows significant increase in signal intensity of the mass (arrow). The ADC value was 2.75×10^{-3} mm^2/sec, confirming increasing cellular necrosis.

REFERENCES

1) Coindre JM, Terrier P, Guillou L, et al. Predictive value of grade for metastasis development in the main histologic types of adult soft tissue sarcomas: a study of 1240 patients from the French Federation of Cancer Centers Sarcoma Group. *Cancer*. 2001;91:1914-1926.
2) Jemal A, Siegel R, Ward E, et al. Cancer statistics, 2006. *CA Cancer J Clin*. 2006;56:106-130.
3) Jaques DP, Coit DG, Casper ES, et al. Hepatic metastases from soft-tissue sarcoma. *Ann Surg*. 1995;221:392-397.
4) DeMatteo RP, Shah A, Fong Y, et al. Results of hepatic resection for sarcoma metastatic to liver. *Ann Surg*. 2001;234:540-547. discussion 547-578.
5) Lang H, Nussbaum KT, Kaudel P, et al. Hepatic metastases from leiomyosarcoma: a single-center experience with 34 liver resections during a 15-year period. *Ann Surg*. 2000;231:500-505.
6) Ng EH, Pollock RE, Romsdahl MM. Prognostic implications of patterns of failure for gastrointestinal leiomyosarcomas. *Cancer*. 1992;69: 1334-1341.
7) Mavligit GM, Zukwiski AA, Ellis LM, et al. Gastrointestinal leiomyosarcoma metastatic to the liver. Durable tumor regression by hepatic chemoembolization infusion with cisplatin and vinblastine. *Cancer*. 1995;75:2083-2088.
8) Trevisani F, De Notariis S, Rossi C, et al. Randomized control trials on chemoembolization for hepatocellular carcinoma: is there room for new studies? *J Clin Gastroenterol*. 2001;32:383-389.
9) Johnson PJ, Kalayci C, Dobbs N, et al. Pharmacokinetics and toxicity of intraarterial adriamycin for hepatocellular carcinoma: effect of coadministration of lipiodol. *J Hepatol*. 1991;13:120-127.
10) Raoul JL, Heresbach D, Bretagne JF, et al. Chemoembolization of hepatocellular carcinomas. A study of the biodistribution and pharmacokinetics of doxorubicin. *Cancer*. 1992;70:585-590.
11) Ramsey DE, Geschwind JF. Chemoembolization of hepatocellular carcinoma-what to tell the skeptics: review and meta-analysis. *Tech Vasc Interv Radiol*. 2002;5:122-126.
12) Imaeda T, Yamawaki Y, Seki M, et al. Lipiodol retention and massive necrosis after lipiodol-chemoembolization of hepatocellular carcinoma: correlation between computed tomography and histopathology. *Cardiovasc Intervent Radiol*. 1993;16:209-213.

13) De Santis M, Alborino S, Tartoni PL, et al. Effects of lipiodol retention on MRI signal intensity from hepatocellular carcinoma and surrounding liver treated by chemoembolization. *Eur Radiol*. 1997;7:10-16.
14) Kuszyk BS, Boitnott JK, Choti MA, et al. Local tumor recurrence following hepatic cryoablation: radiologic-histopathologic correlation in a rabbit model. *Radiology*. 2000;217:477-486.
15) Therasse P, Arbuck SG, Eisenhauer EA, et al. New guidelines to evaluate the response to treatment in solid tumors. European Organization for Research and Treatment of Cancer, National Cancer Institute of the United States, National Cancer Institute of Canada. *J Natl Cancer Inst*. 2000;92:205-216.
16) Galons JP, Altbach MI, Paine-Murrieta GD, et al. Early increases in breast tumor xenograft water mobility in response to paclitaxel therapy detected by non-invasive diffusion magnetic resonance imaging. *Neoplasia*. 1999;1:113-117.
17) Geschwind JF, Artemov D, Abraham S, et al. Chemoembolization of liver tumor in a rabbit model: assessment of tumor cell death with diffusion-weighted MR imaging and histologic analysis. *J Vasc Interv Radiol*. 2000;11:1245-1255.
18) Mardor Y, Pfeffer R, Spiegelmann R, et al. Early detection of response to radiation therapy in patients with brain malignancies using conventional and high b-value diffusion-weighted magnetic resonance imaging. *J Clin Oncol*. 2003;21:1094-1100.
19) Kamel IR, Bluemke DA, Ramsey D, et al. Role of diffusion-weighted imaging in estimating tumor necrosis after chemoembolization of hepatocellular carcinoma. *AJR Am J Roentgenol*. 2003;181:708-710.
20) Kamel IR, Bluemke DA, Eng J, et al. The role of functional MR imaging in the assessment of tumor response after chemoembolization in patients with hepatocellular carcinoma. *J Vasc Interv Radiol*. 2006;17: 505-512.
21) Llovet JM, Real MI, Montana X, et al. Arterial embolisation or chemoembolisation versus symptomatic treatment in patients with unresectable hepatocellular carcinoma: a randomised controlled trial. *Lancet*. 2002;359:1734-1739.
22) Li XP, Meng ZQ, Guo WJ, et al. Treatment for liver metastases from breast cancer: results and prognostic factors. *World J Gastroenterol*. 2005;11:3782-3787.
23) Lo CM, Ngan H, Tso WK, et al. Randomized controlled trial of transarterial lipiodol chemoembolization for unresectable hepatocellular carcinoma. *Hepatology*. 2002;35:1164-1171.

24) Choi BI, Kim HC, Han JK, et al. Therapeutic effect of transcatheter oily chemoembolization therapy for encapsulated nodular hepatocellular carcinoma: CT and pathologic findings. *Radiology*. 1992;182:709-713.
25) Nakamura H, Hashimoto T, Oi H, et al. Transcatheter oily chemoembolization of hepatocellular carcinoma. *Radiology*. 1989;170(pt 1):783-786.
26) Murakami T, Nakamura H, Hori S, et al. Detection of viable tumor cells in hepatocellular carcinoma following transcatheter arterial chemoembolization with iodized oil. Pathologic correlation with dynamic turbo-FLASH MR imaging with Gd-DTPA. *Acta Radiol*. 1993;34:399-403.
27) Castrucci M, Sironi S, De Cobelli F, et al. Plain and gadolinium-DTPA-enhanced MR imaging of hepatocellular carcinoma treated with transarterial chemoembolization. *Abdom Imaging*. 1996;21:488-494.
28) Bartolozzi C, Lencioni R, Caramella D, et al. Treatment of hepatocellular carcinoma with percutaneous ethanol injection: evaluation with contrast-enhanced MR imaging. *AJR Am J Roentgenol*. 1994;162:827-831.
29) Yuen MF, Chan AO, Wong BC, et al. Transarterial chemoembolization for inoperable, early stage hepatocellular carcinoma in patients with Child-Pugh grade A and B: results of a comparative study in 96 Chinese patients. *Am J Gastroenterol*. 2003;98:1181-1185.
30) Bruix J, Sherman M, Llovet JM, et al. Clinical management of hepatocellular carcinoma. Conclusions of the Barcelona-2000 EASL conference. European Association for the Study of the Liver. *J Hepatol*. 2001;35:421-430.
31) Ross BD, Chenevert TL, Rehemtulla A. Magnetic resonance imaging in cancer research. *Eur J Cancer*. 2002;38:2147-2156.
32) Hall DE, Moffat BA, Stojanovska J, et al. Therapeutic efficacy of DTI-015 using diffusion magnetic resonance imaging as an early surrogate marker. *Clin Cancer Res*. 2004;10:7852-7859.

CHAPTER 7

CHEMOEMBOLIZATION OF HEPATIC METASTASES FROM OCULAR MELANOMA: ASSESSMENT OF RESPONSE WITH CONTRAST-ENHANCED AND DIFFUSION-WEIGHTED MRI

Buijs M, Vossen JA, Hong K, Georgiades CS,
Geschwind JF, Kamel IR

AJR Am J Roentgenol 2008 Jul;191(1):285-9.

ABSTRACT

OBJECTIVE:

The purpose of this study was to assess the utility of assessment of tumor size and enhancement with diffusion-weighted and conventional MRI in the evaluation of response to transarterial chemoembolization therapy for metastatic ocular melanoma.

CONCLUSION:

In patients with ocular melanoma and liver metastasis treated with transarterial chemoembolization, functional MRI showed significant changes in the lesions. These changes included a decrease in tumor enhancement and an increase in the apparent diffusion coefficient of the tumor, suggesting increasing tumor necrosis and cell death.

INTRODUCTION

Ocular melanoma arising from melanocytes in the uvea (uveal melanoma) is the most common primary malignant tumor of the eye. The incidence in the United States is 4.3 cases per million persons per year. Uveal melanoma constitutes 85–95% of ocular melanomas. The reported 5-year survival rate for ocular melanoma ranges from 31% to 80% (1, 2). The liver is the most common site of metastatic disease, with liver metastasis occurring in as many as 50% of patients (3, 4). The prognosis of metastatic ocular melanoma is poor with median survival periods of 2 months without treatment and 5–9 months with treatment (5, 6).

Various treatment techniques exist for patients with metastatic ocular melanoma, including surgical resection, systemic chemotherapy, and locoregional therapy (7, 8). Monitoring the effectiveness of transarterial chemoembolization (TACE), a locoregional therapy, with imaging is important in determining treatment success and in guiding future therapy. However, imaging techniques and imaging response criteria have been limited in giving clinically satisfactory information about the extent of tumor necrosis.

The apparent diffusion coefficient (ADC) calculated in diffusion-weighted MRI has become a promising biomarker of tumor response to therapy (9). The ADC is a measure of the mobility of water in tissues. Viable tumors are high in cellularity, and the cells have an intact cell membrane that restricts the mobility of water molecules and results in a relatively low ADC. Conversely, cellular necrosis increases membrane permeability, allowing water molecules to move freely and causing a relative increase in ADC. Diffusion-weighted MRI has been used to assess tumor response after chemotherapy and radiation therapy.

The primary application of diffusion-weighted MRI has been in brain imaging (10–12). In the liver, diffusion-weighted imaging has been used to characterize focal hepatic lesions and to assess tumor response to locoregional therapy (13, 14). We hypothesize that diffusion-weighted MRI can be added to contrast-enhanced MRI to determine the presence of cellular necrosis and therefore be useful in obtaining information about tumor response to TACE. To our knowledge, the use of diffusion-weighted imaging in the follow-up of metastatic ocular melanoma has not been described. The purpose of our study was to assess the value of diffusion-

weighted MRI in the evaluation of tumor response to TACE for metastatic ocular melanoma.

MATERIALS AND METHODS

Patients

This study was a retrospective analysis of a prospectively collected database. The study population consisted of six patients with metastatic ocular melanoma who underwent TACE. The criterion for TACE was confirmed diagnosis of unresectable metastatic ocular melanoma in patients with or without minimally impaired liver function. Patients excluded from TACE were those with Eastern Cooperative Oncology Group performance status greater than grade 2, encephalopathy, severe variceal bleeding or severe ascites, clinically significant thrombocytopenia (platelet count < 50,000/mL), impaired renal function (creatinine concentration > 2 mg/dL), or severe liver failure (advanced Child-Pugh class C or serum bilirubin concentration > 2 mg/dL). The study group included all patients treated with chemoembolization who underwent contrast-enhanced and diffusion-weighted MRI before and after treatment. Between January 1, 2003, and December 31, 2006, the care of eight patients with metastatic ocular melanoma who underwent one or more cycles of TACE was discussed by the liver tumor board at our institution, and six of the patients fulfilled the inclusion criteria. The other two patients did not undergo MRI after TACE and were excluded. The diagnosis of metastatic ocular melanoma was confirmed by biopsy of liver metastatic lesions in all patients. Data were collected prospectively, and the study was authorized by the institutional review board.

Chemoembolization Technique

All chemoembolization procedures were performed by one experienced interventional radiologist using the same technique in all procedures. A 5-F micropuncture introducer set was used to access the right common femoral artery with the Seldinger technique. After a 0.035-inch Bentson guidewire was advanced into the abdominal aorta, the needle was exchanged for a 5-F vascular sheath, which was placed into the right common femoral artery under fluoroscopic guidance. Through the sheath, a 5-F catheter (Glidecath Simmons-1; Terumo Medical, Somerset, NJ) was advanced into the aorta and reformed in the aortic arch. Selective

angiography of the celiac axis was performed. The catheter was advanced into the hepatic artery branch indicated by the tumor location. If selective catheterization was necessary, a 3-F catheter (Renegade Hi-Flow, Boston Scientific, Natick, MA) was used.

Once the appropriate catheter (5-F Simmons-1, 3-F microcatheter, or other selected catheter) was in position, TACE was performed through the catheter to achieve lobar or segmental embolization according to the target lesions. A solution containing 100 mg of cisplatin (Platinol; Bristol-Myers Squibb, Princeton, NJ), 50 mg of doxorubicin (Adriamycin; Pharmacia Upjohn, Kalamazoo, MI), and 10 mg of mitomycin C (Mutamycin C; Bedford Laboratories, Bedford, OH) in a 1:1 mixture with iodized oil followed by infusion of 300- to 500-µm embolic microspheres (Embosphere, Biosphere Medical, Rockland, MA) was administered until stasis was achieved.

CT Technique

Within 1 day after chemoembolization, all patients underwent unenhanced helical CT (Sensation 16 scanner; Siemens Medical Solutions, Malvern, PA). The scanning parameters were 120 kVp, 210 mA, 5-mm section collimation, and 5-mm image reconstruction. Technical success of the procedure was confirmed with focal deposition of iodized oil in the targeted segment or lobe of the liver.

MRI Technique

A 1.5-T MRI scanner (CV/i; GE Healthcare, Milwaukee, WI) and a phased-array torso coil. Imaging protocol included T2-weighted fast spin-echo images (matrix, 256 × 256; slice thickness, 8 mm; interslice gap, 2 mm; repetition time [TR]/ echo time [TE], 5000/100 msec; receiver bandwidth, 32 kHz), breath-hold diffusion-weighted echoplanar images (matrix, 128 × 128; slice thickness, 8 mm; interslice gap, 2 mm; b value, 500 mm^2/sec; TR/TE, 5000-6500/110 msec; receiver bandwidth, 32 kHz) along the section-select gradient (*z*-axis), and breath-hold unenhanced and contrast-enhanced (0.1 mmol/kg intravenous gadodiamide [Omniscan; GE Healthcare, Princeton, NJ]) T1-weighted three-dimensional fat-suppressed spoiled gradient-echo images (field of view, 320-400 mm; matrix, 192 × 160; slice thickness, 4-6 mm TR/TE, 5.1/1.2 msec; receiver bandwidth, 64 kHz; flip angle, 15º) in the arterial phase (20 seconds) and portal venous

phase (60 seconds). Typical acquisition time was a single breath-hold of 30 seconds to cover the entire liver.

Follow-Up

According to protocol, patients underwent contrast-enhanced and diffusion-weighted MRI 4–6 weeks after TACE for assessment of tumor response. Patients with near complete tumor necrosis determined by lack of enhancement on MRI and an increase in ADC of the lesion did not undergo additional treatments and underwent follow-up imaging every 6–8 weeks. Patients with residual enhancement whose clinical performance status was maintained underwent additional TACE treatments.

Image Analysis

MR image processing and ADC maps were generated with a commercially available workstation (Advantage; GE Healthcare, Milwaukee, WI). Images were interpreted by consensus of two experienced MRI radiologists in the same session. Parameters evaluated included change in tumor size, enhancement, and ADC. For patients who underwent more than one TACE cycle, the MR images obtained after the last cycle were used for comparison.

All target lesions 2 cm or larger in the treated lobe were evaluated; a maximum of four lesions per patient were used to ensure independent sampling. The target lesions were selected by consensus of two radiologists. Target lesions in the treated lobe of the liver were selected. The maximum diameter of the targeted lesions was measured with electronic calipers as proposed in the Response Evaluation Criteria in Solid Tumors (RECIST). Areas of tumor enhancement were considered viable, and areas without enhancement were considered necrotic, as suggested by the European Association for the Study of the Liver (15). Percentage enhancement was based on enhancement seen on the axial arterial and portal venous phase MR images with the largest tumor size. Complete absence of enhancement was reported as 0%. Enhancement was reported as 25% if there was 25% or less enhancement, 50% if more than 25% and up to 50% enhancement, 75% if more than 50% and up to 75% enhancement, and 100% if greater than 75% enhancement was present.

In cases of lesions that had higher signal intensity than the surrounding liver parenchyma on unenhanced T1-weighted images, subtraction was

performed to assess for enhancement. ADC maps were generated from the diffusion-weighted images side by side with the gadolinium-enhanced images, and mean values were recorded by placement of a region of interest (ROI) over the entire treated mass seen on the image with the largest lesion size. ROIs placed on the diffusion-weighted images were automatically generated in the same location on the images with ADC maps. ADC maps of normal-appearing liver, spleen, and paraspinal muscle were generated. Percentage iodized oil deposition on CT was recorded and reported as 25% if 25% or less of the tumor exhibited iodized oil uptake, 50% if more than 25% and up to 50% of the tumor exhibited uptake, 75% if more than 50% and up to 75% of the tumor exhibited uptake, and 100% if 75% or more of the tumor exhibited uptake. For patients who had undergone multiple iodized oil treatments, the mean maximum iodized oil retention in the targeted lesion was recorded.

Statistical Analysis

Statistical analysis was performed with the Stata software package (Version 8; Stata, College Station, TX). A paired Student's *t* test was used to compare tumor sizes, degrees of enhancement, and ADCs before and after TACE to evaluate tumor response. A paired Student's *t* test also was used to compare ADCs of liver, spleen, and muscle before and after treatment. A value of $p < 0.05$ was considered to indicate statistical significance.

RESULTS

Demographic Information and Tumor Features

A total of 21 lesions were evaluated in six patients (two men, four women; mean age, 70 years). All lesions were located in the right lobe of the liver. Eleven lesions received a single TACE treatment, seven lesions received two cycles of TACE, and three lesions received three cycles of TACE. The average duration between preprocedural and postprocedural MRI was 79 days (range, 32–161 days). MRI was performed within 16 days (range, 1–45 days) before TACE. The mean interval between the last TACE treatment and follow-up MRI was 33 days (range, 21–45 days). On T1-weighted MRI before TACE, 17 lesions were hypointense, three lesions were isointense, and one lesion was hyperintense compared with the surrounding liver parenchyma. After TACE, 15 lesions were hypointense, one lesion was isointense, and six lesions were hyperintense on T1-weighted

MRI. On T2-weighted MRI before treatment, 19 lesions were hyperintense and two lesions were isointense compared with the surrounding liver parenchyma. After TACE, 20 lesions were hyperintense and one lesion was isointense on T2-weighted MRI. Mean iodized oil retention within the tumor on CT was 45%.

Assessment of Change in MRI Parameters after TACE

On gadolinium-enhanced MRI, overall tumor enhancement on a lesion-by-lesion basis in the arterial and portal venous phases decreased significantly after TACE (Table 7.1). Arterial phase enhancement decreased 41% after TACE, and the decrease was statistically significant ($p = 0.0002$). Venous phase enhancement decreased 56%, also statistically significant ($p < 0.0001$). Diffusion-weighted MRI was useful in monitoring response after treatment. The mean tumor ADC increased 48% after TACE ($p = 0.0003$), whereas the ADC remained unchanged in nontumorous liver, spleen, and muscle (Fig 7.1A-G, Table 7.1). Figure 7.2 shows changes in ADC after treatment. Although mean tumor size decreased 16% from 4.9 to 4.1 cm after TACE, none of the lesions met the RECIST for complete response (disappearance of all measurable disease), and only eight lesions were considered partial responders (> 30% decrease in size).

DISCUSSION

The overall prognosis among patients with primary ocular melanoma is good. However, liver metastasis develops in 40–50% of the patients and is related to a poor median survival time of 2–9 months (5, 6). Among these patients TACE can result in clinically significant regression of hepatic metastasis and lengthen overall survival (7). In this setting it is critical to assess tumor response. Studies have shown that diffusion-weighted MRI can be used to identify and characterize hepatic lesions and assess tumor response after locoregional therapy (16). The objective of our study was to use the criteria of iodized oil deposition, tumor size, and tumor enhancement to assess the utility of diffusion-weighted and conventional MRI in the evaluation of tumor response after TACE for metastatic ocular melanoma. Our results indicate that diffusion-weighted and contrast-enhanced MRI can be used to detect tumor necrosis before reduction in tumor size occurs.

Several imaging techniques are used in traditional assessment of tumor response. One of the RECIST is change in tumor size on CT or MRI. Patients who have complete disappearance of all disease are considered

responders. Partial response requires a greater than 30% decrease in tumor size. After TACE, however, many lesions do not initially decrease in size. To address this issue, the European Association for the Study of the Liver has officially recommended the use of lesion enhancement on contrast-enhanced CT as the standard factor for determining treatment response after locoregional therapy (15). Enhanced portions of the tumor are presumed to be viable, whereas unenhanced portions are presumed necrotic. However, accumulation of iodized oil after TACE limits the use of enhancement on contrast-enhanced CT. At our institution we therefore use contrast-enhanced MRI to evaluate enhancement after TACE.

Our data showed that none of the treated lesions was considered a complete responder on the basis of RECIST. Therefore, our results suggest that the RECIST are not useful in determining early tumor response after TACE. Contrast-enhanced MRI depicts areas of tumor enhancement with extracellular contrast agents. Hepatic metastatic lesions of ocular melanoma, however, are already hyperintense on T1-weighted images, and this factor may interfere with accurate determination of contrast enhancement on nonsubtracted images. In this study we saw a significant decrease in enhancement after TACE, indicating that tumor enhancement can be used as a predictor of tumor response.

The mobility of water molecules in tissues is represented by the ADC on diffusion-weighted MRI. This value provides insight into tumor microstructure. Viable tumors contain cells with an intact cell membrane that restricts water mobility and causes low ADCs. Conversely, cellular necrosis increases membrane permeability, which increases the ADC. These characteristics are used to detect cellular necrosis before size regression occurs (17). Our study showed a significant increase in ADCs of the lesions after treatment, indicating marked cellular necrosis in response to therapy. The ADCs of normal liver tissue, spleen, and muscle showed no significant changes after treatment.

This study had several limitations. First, the patient population was relatively small, so further studies with a larger sample size are needed to confirm our conclusions and to stratify patients into responders and nonresponders. The objective would be to establish a cutoff value between the two groups. A second limitation was possible selection bias, because only patients who underwent MRI before and after treatment were included in the study. Another limitation was the lack of histopathologic correlation of the lesions after chemoembolization. For ethical reasons, we did not

obtain histologic correlation in this study. In addition, we could not confirm that the changes in ADC were due only to cellular necrosis and not to oil deposition within the tumor. Our results, however, are in line with those of a previous evaluation of the use of diffusion-weighted imaging after ^{90}Y-microsphere treatment without oil deposition (18). Changes in ADC occurred only in the targeted tumors, whereas the nontargeted tumors in the contralateral lobe of the liver had no change in ADCs. Therefore, we believe that these changes are due to cellular necrosis resulting from the targeted therapy. Last, we did not perform a reproducibility analysis of our imaging sequence because it was not one of the study objectives. However, our results are in line with those of a previous work (19) that showed an increase in ADC values after locoregional therapy.

Our results indicate that diffusion-weighted MRI can be useful for assessing tumor response after TACE in patients with metastatic ocular melanoma.

TABLES & FIGURES

Feature	Before Treatment	After Treatment	Percentage Change	p*
Size of mass (cm)	4.90 (3.2)	4.10 (3.3)	16	0.003
Percentage enhancement of mass				
Arterial phase	64 (31)	23 (25)	41	0.0002
Venous phase	93 (12)	37 (34)	56	< 0.0001
ADC (x 10^{-3} mm^2/sec)				
Mass	1.57 (0.62)	2.32 (0.86)	48	0.0003
Liver	1.88 (0.33)	1.79 (0.26)	5	0.13
Spleen	1.21 (0.34)	1.33 (0.30)	10	0.21
Muscle	1.78 (0.29)	1.72 (0.26)	3	0.33

Table 7.1 Mean changes in tumor size, enhancement, and ADC value after TACE
Note—Values in parentheses are SD. ADC = apparent diffusion coefficient, TACE = transarterial chemoembolization.
* Paired Student's *t* test.

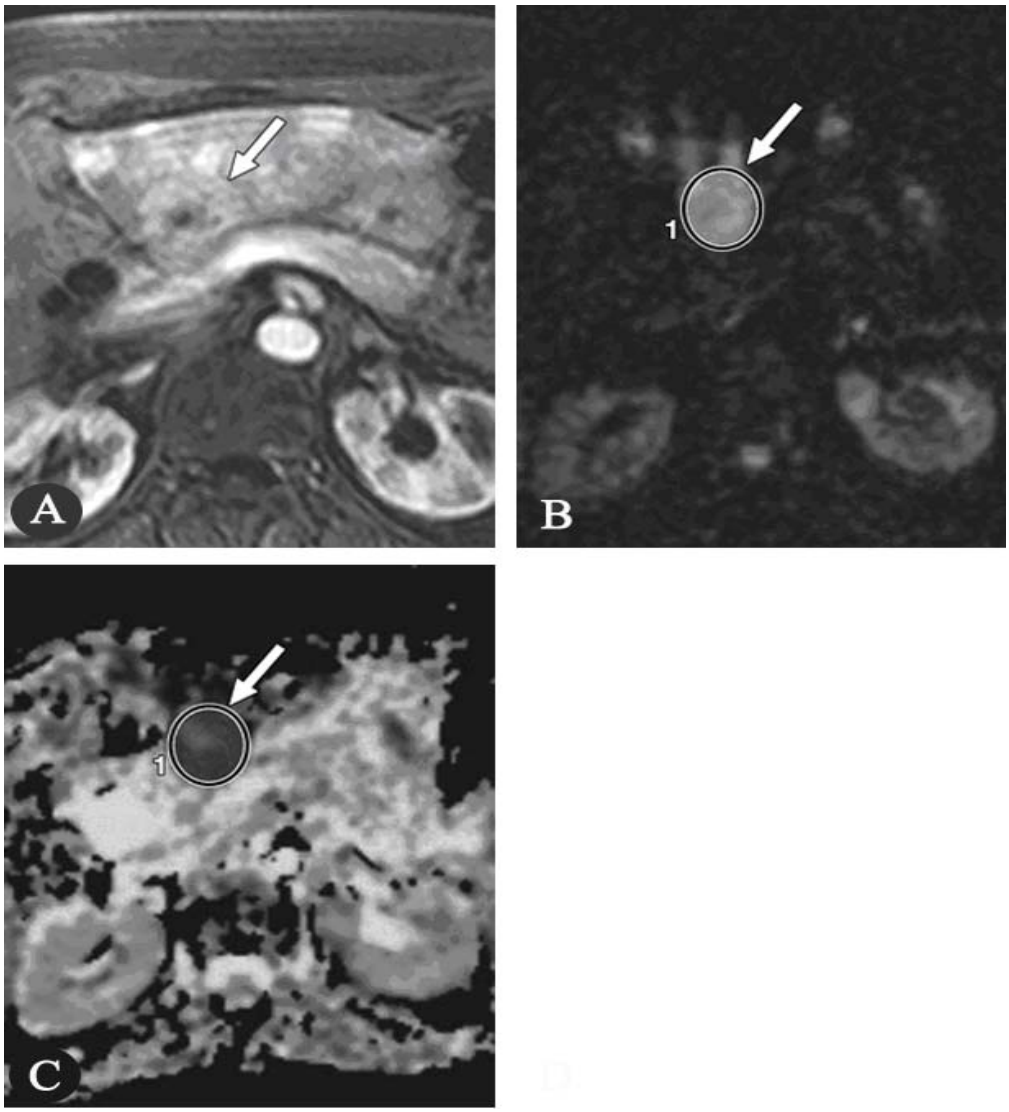

Figure 7.1 60-year-old woman with hepatic metastases from ocular melanoma. Changes in enhancement and apparent diffusion coefficient after transarterial chemoembolization.
(A)Gadolinium-enhanced arterial phase MR image (TR/TE, 5.1/1.2) shows 3.1-cm mass (*arrow*) in left lobe with almost complete (100%) enhancement.
(B) Diffusion-weighted MR image (6,500/110) shows hyperintense mass (*arrow*).
(C) After placement of region of interest on entire mass (*arrow*), apparent diffusion coefficient is 0.00138 mm^2/sec.

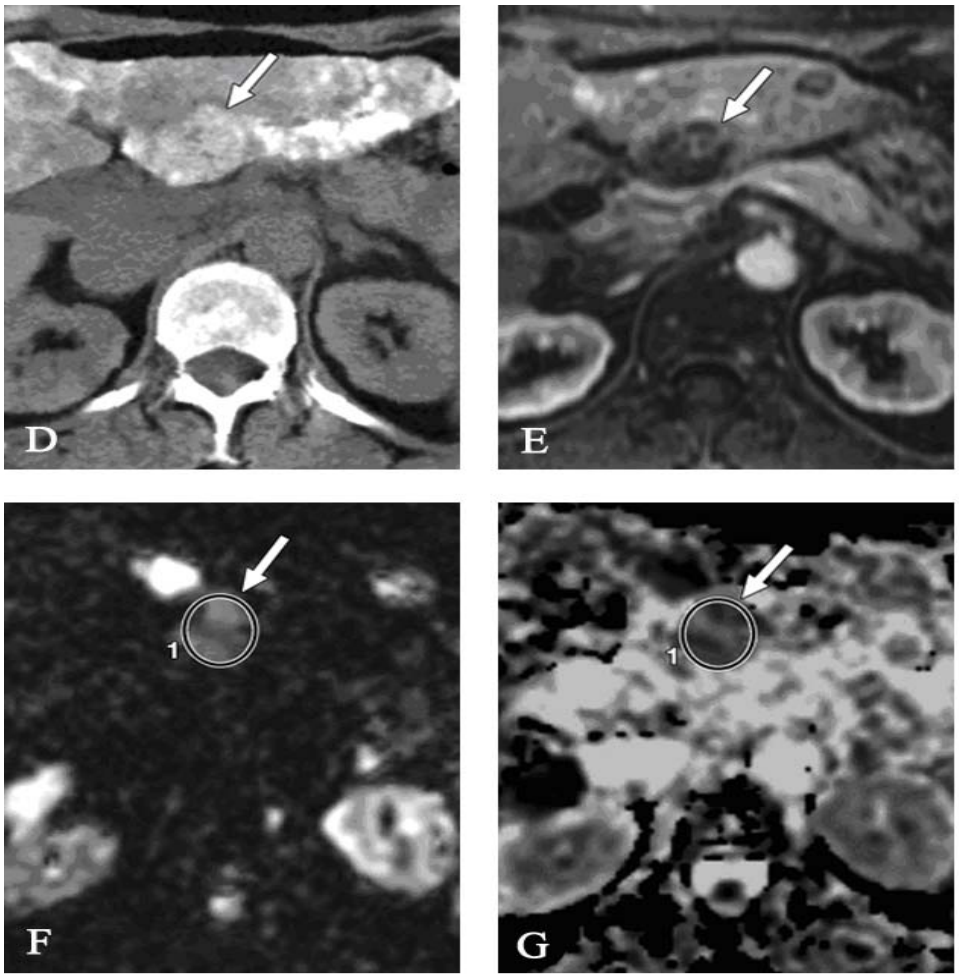

Figure 7.1 (continued) 60-year-old woman with hepatic metastases from ocular melanoma. Changes in enhancement and apparent diffusion coefficient after transarterial chemoembolization.
(D) Unenhanced CT scan of abdomen shows intense deposition of iodized oil in mass (*arrow*) after transarterial chemoembolization.
(E) Gadolinium-enhanced arterial phase MR image (TR/TE, 5.1/1.2) after transarterial chemoembolization shows significant decrease in enhancement of mass (*arrow*), now less than 10%. Size of mass decreased slightly to 2.9 cm.
(F) Diffusion-weighted MR image (6,500/110) after transarterial chemoembolization.
(G) After placement of region of interest on entire mass (*arrow*), apparent diffusion coefficient is 0.00229 mm^2/sec, confirming increasing cellular necrosis.

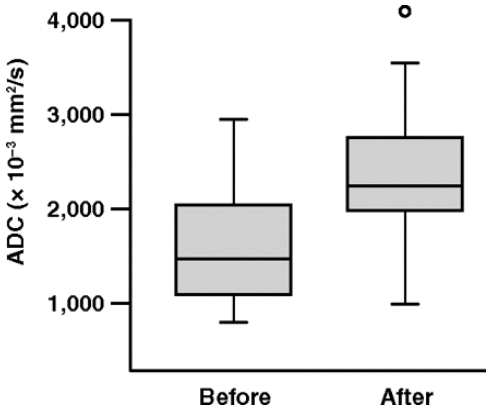

Figure 7.2 Graph shows changes in apparent diffusion coefficient after treatment. ADC = apparent diffusion coefficient.

REFERENCES

1) Kujala E, Makitie T, Kivela T. Very long-term prognosis of patients with malignant uveal melanoma. *Invest Ophthalmol Vis Sci* 2003; 44:4651 –4659
2) Singh AD, Topham A. Incidence of uveal melanoma in the United States: 1973–1997. *Ophthalmology*2003; 110:956 –961
3) Becker JC, Terheyden P, Kampgen E, et al. Treatment of disseminated ocular melanoma with sequential fotemustine, interferon alpha, and interleukin 2. *Br J Cancer* 2002;87 : 840–845
4) Patel JK, Didolkar MS, Pickren JW, Moore RH. Metastatic pattern of malignant melanoma: a study of 216 autopsy cases. *Am J Surg* 1978; 135:807 –810
5) Feldman ED, Pingpank JF, Alexander HR Jr. Regional treatment options for patients with ocular melanoma metastatic to the liver. *Ann Surg Oncol* 2004;11 : 290–297
6) Gragoudas ES, Egan KM, Seddon JM, et al. Survival of patients with metastases from uveal melanoma. *Ophthalmology*1991; 98:383 –389
7) Leyvraz S, Spataro V, Bauer J, et al. Treatment of ocular melanoma metastatic to the liver by hepatic arterial chemotherapy. *J Clin Oncol* 1997; 15:2589 –2595
8) Pawlik TM, Zorzi D, Abdalla EK, et al. Hepatic resection for metastatic melanoma: distinct patterns of recurrence and prognosis for ocular versus cutaneous disease. *Ann Surg Oncol*2006; 13:712 –720
9) Vossen JA, Buijs M, Kamel IR. Assessment of tumor response on MR imaging after locoregional therapy. *Tech Vasc Interv Radiol* 2006; 9:125 –132
10) Schaefer PW, Grant PE, Gonzalez RG. Diffusion-weighted MR imaging of the brain. *Radiology* 2000;217 : 331–345
11) Moffat BA, Chenevert TL, Lawrence TS, et al. Functional diffusion map: a noninvasive MRI biomarker for early stratification of clinical brain tumor response. *Proc Natl Acad Sci U S A*2005; 102:5524 –5529
12) Law M, Yang S, Wang H, et al. Glioma grading: sensitivity, specificity, and predictive values of perfusion MR imaging and proton MR spectroscopic imaging compared with conventional MR imaging. *Am J Neuroradiol* 2003; 24:1989 –1998
13) Deng J, Miller FH, Rhee TK, et al. Diffusion-weighted MR imaging for determination of hepatocellular carcinoma response to yttrium-90 radioembolization. *J Vasc Interv Radiol*2006; 17:1195 –1200

14) Chen CY, Li CW, Kuo YT, et al. Early response of hepatocellular carcinoma to transcatheter arterial chemoembolization: choline levels and MR diffusion constants—initial experience. *Radiology* 2006;239 : 448–456
15) Bruix J, Sherman M, Llovet JM, et al.; EASL Panel of Experts on HCC. Clinical management of hepatocellular carcinoma: conclusions of the Barcelona-2000 EASL conference—European Association for the Study of the Liver. *J Hepatol* 2001;35 : 421–430
16) Koh DM, Collins DJ. Diffusion-weighted MRI in the body: applications and challenges in oncology. *AJR*2007; 188:1622 –1635
17) Kamel IR, Bluemke DA, Eng J, et al. The role of functional MR imaging in the assessment of tumor response after chemoembolization in patients with hepatocellular carcinoma. *J Vasc Interv Radiol* 2006; 17:505 –512
18) Kamel IR, Reyes DK, Liapi E, Bluemke DA, Geschwind JF. Functional MR imaging assessment of tumor response after ^{90}Y microsphere treatment in patients with unresectable hepatocellular carcinoma. *J Vasc Interv Radiol* 2007; 18:49 –56
19) Buijs M, Kamel IR, Vossen JA, Georgiades CS, Hong K, Geschwind JF. Assessment of metastatic breast cancer response to chemoembolization with contrast agent enhanced and diffusion-weighted MR imaging. *J Vasc Interv Radiol* 2007; 18:957 –963

PART II:
INTRA-ARTERIAL TREATMENT WITH 3-BROMOPYRUVATE

CHAPTER 8

DEVELOPMENT OF A NEW ORTHOTOPIC ANIMAL MODEL OF METASTATIC LIVER CANCER IN THE RABBIT VX2 MODEL: EFFECT ON METASTASES AFTER PARTIAL HEPATECTOMY, INTRA-ARTERIAL TREATMENT WITH 3-BROMOPYRUVATE AND CHEMOEMBOLIZATION

Vossen JA, Buijs M, Syed L, Kutiyanwala F,
Kutiyanwala M, Geschwind JF, Vali M

Clin Exp Metastasis 2008;25(7):811-7.

ABSTRACT

PURPOSE:

The aim of our study was to compare the influence of partial hepatectomy, intra-arterial treatment with 3-BrPA and TACE on regional and distant metastases. In order to achieve our objective, we tested the feasibility of both resection, intra-arterial therapy with 3-BrPA and TACE of VX2 liver cancer in New Zealand white rabbits.

MATERIALS AND METHODS:

VX2 tumors were implanted in the left lateral lobe of the liver of 20 rabbits. Tumors were allowed to grow for 14 days. Rabbits were divided in four groups. Group 1 (n = 2) was sacrificed 14 days post implantation. Group 2, 3 and 4 (n = 6 per group) underwent left lateral hepatectomy, a 1 h intra-arterial infusion with 3-BrPA and TACE respectively. Animals in groups 2, 3 and 4 were further subdivided into three groups of two animals each corresponding to the time-point of sacrifice after the procedure (7, 14 and 21 days respectively). After sacrifice, organs were harvested, fixed and analyzed.

RESULTS:

Pathologic examination showed lung metastases in all 20 rabbits. Abdominal cavity dissemination was seen in five rabbits in Group 2, two rabbits in Group 3 and all rabbits in Group 4. Kidney metastases were seen in two rabbits treated with TACE (Group 4).

CONCLUSION:

The VX2 rabbit model of liver cancer is a suitable model to compare the influence of partial hepatectomy, intra-arterial treatment with 3-BrPA and TACE on tumor recurrence in the form of regional and distant metastases. Our results indicate that intra-arterial delivery of 3-BrPA may result in a favorable metastatic profile when compared to both liver resection and TACE.

INTRODUCTION

Hepatocellular carcinoma (HCC) is the fifth most common cause of mortality from cancer worldwide and is responsible for about one million deaths yearly (1, 2). The number of cases of HCC will rise dramatically over the next 10–15 years in North America because of the high prevalence of chronic hepatitis infections (3). Liver resection and transplantation are currently considered the only two potentially curative treatments for this cancer (4, 5).

For the treatment of unresectable HCC or intrahepatic recurrences, several effective therapeutic modalities (such as transcatheter arterial chemoembolization [TACE] and radiofrequency ablation) are widely employed (6). Currently, however, TACE is not utilized in patients with resectable disease confined to the liver. From an oncology point of view, evaluating the therapeutic efficacy of TACE for patients with resectable disease requires a comparison with resection in a randomized controlled study. However, such an approach would raise critical ethical concerns. Therefore, a suitable animal model, to compare these two treatment modalities is of high importance. This animal model should allow direct access to the tumor feeding artery, in order to provide a route for intra-arterial infusion. The VX2 liver tumor model in the rabbit is currently the most suitable animal model that allows access to the tumor feeding hepatic artery, which is necessary to study intra-arterial therapies. Unfortunately, human HCC does not grow in a rabbit liver, due to the rabbit's intact immune system.

With the recent progress in diagnostic modalities, pre- and postoperative treatment, and operative techniques, the results of resection and TACE for patients with HCC have been improving steadily (7, 8). However, the long-term prognosis remains poor in most series, with 5-year overall survival rates of 33–69% and 5-year recurrence rates approaching 70% after resection (9-12). Tumor recurrence may present in the form of metastatic foci in distant organs, such as the lungs, brain, and bone (13). Therefore it is important to identify new aggressive agents for patients with HCC. One such novel agent, 3-bromopyruvate (3-BrPA), a known inhibitor of glycolysis, has proven to be effective in the treatment of VX2 liver cancer in rabbits, when administered intra-arterially (14).

The aim of our study was to compare the influence of partial hepatectomy, intra-arterial treatment with 3-BrPA and TACE on tumor recurrence in the form of regional and distant metastases. In order to achieve our objective, we tested the feasibility of both resection, intra-arterial therapy with 3-BrPA and TACE of VX2 liver cancer in New Zealand white rabbits.

MATERIALS AND METHODS

All animals received human care and all the experimental procedures were performed according to our Institutional Guidelines.

Tumor Implantation

Adult New Zealand white rabbits weighing 8–9 lbs (n = 20; Myrtle's Rabbitry, Thompson's Station, TN) were used for this study. For successful implantation of the VX2 tumor into the liver, the tumor was first grown for 2 weeks in the hind leg of a carrier rabbit. Before tumor implantation all rabbits were anesthetized with a mixture of acepromazine (2.5 mg/kg Phoenix, St Joseph, MO) and ketamine hydrochloride (44 mg/kg, Phoenix) administered i.m.; i.v. access was gained via a marginal ear vein and sodium pentobarbital (Abbott Laboratories, Abbott Park, IL) was given to maintain anesthesia. The abdomen was shaved and prepped in a sterile fashion. A midline subxyphoid incision was made. The left lateral lobe of the liver was exposed and the VX2 tumor excised from a carrier rabbit was minced and implanted into the left lobe of the liver using the outer cannula of a 21-gauge angiocatheter. The abdomen was closed in 2 layers.

Experimental Design

All rabbits underwent ultrasound examination to confirm the presence of a liver tumor 14 days after implantation. Rabbits were divided in four groups. Group 1 (n = 2) was sacrificed 14 days post implantation to assess for the presence of metastases. Rabbits in group 2 (n = 6) underwent left lateral hepatectomy 14 days post implantation, and were sacrificed 7, 14 and 21 days respectively, after the procedure. Rabbits in group 3 (n = 6) underwent a 1 h intra-arterial infusion with 3-BrPA 14 days post implantation, and were sacrificed 7, 14 and 21 days respectively, after the procedure. Rabbits in group 4 (n = 6) underwent TACE 14 days post

implantation, and were sacrificed 7, 14 and 21 days respectively, after the procedure.

Partial Hepatectomy

Fourteen days after tumor implantation a laparotomy was performed in six animals under general anesthesia and with aseptic operative techniques. Heart and respiration rates, were continuously monitored throughout the procedure. The animal was prepped and draped in a sterile fashion. A midline incision from xyphoid to umbilicus was made. The falciform and left triangular ligaments were divided to help free the right and left lateral lobe of the liver. The inferior surface of the liver was completely isolated from the stomach and the gut by means of gauzes. The circulation in the left lateral liver lobe was interrupted by ligation of the hilar vessels with a 2–0 silk tie. Subsequently the ligated lobe was resected about 5 mm distal to the ligature. Blood which drained from the excised liver was sponged from the abdominal cavity and the ligated pedicles inspected for complete hemostasis. The incision was closed in two layers.

Intra-arterial Delivery Protocol

Fourteen days after tumor implantation a laparotomy was performed under general anesthesia and with aseptic operative techniques. Transcatheter hepatic artery infusion of 3-BrPA was performed under fluoroscopic guidance. The animals were brought to the angiography suite and incubated by using a 3.0-mm endotracheal tube (Mallinkrodt Medical, St Louis, MO) but not ventilated. Surgical cutdown was performed to gain access into the right common femoral artery, after which a 3-F sheath (Cook, Bloomington, Ind) was inserted. A 2-F JB1 catheter (Cook) was manipulated into the celiac axis, after which a celiac arteriogram was obtained to delineate the blood supply to the liver and confirm the location of the tumor. The tumor could readily be visualized as a region of hypervascular blush located on the left side of the liver near the gastric fundus. The left hepatic artery, which provides most of the blood flow to the tumor, was selectively catheterized via the common hepatic artery by using a Transcend guide wire (Boston Scientific, Natick, Mass.).

Intra-arterial Infusion with 3-BrPA

After the catheter was adequately positioned within the left hepatic artery, a syringe containing 25 ml of 1.75 mM 3-BrPA was connected to the

end of the JB1 catheter and carefully placed and adjusted on an infusion syringe pump (Harvard Apparatus model 11 infuse/withdraw single syringe pump; Instech Solomon, Plymouth Meeting, Pa). The infusion rate was set to 25 ml per h. During the infusion, maintenance of appropriate positioning of the catheter in the hepatic artery was monitored with fluoroscopy. After completion of the infusion the catheter was removed and the common femoral artery was ligated. All rabbits were monitored during and after the procedure and given analgesics when they showed signs of physical distress.

TACE

After the catheter was adequately positioned within the left hepatic artery, a mixture of doxorubicin (Bedford Laboratories, Bedford, Ohio; 5 mg) and iodized oil (Ethiodol, 0.5 ml; Savage Laboratories, Melville, New York) was injected, followed by embolization with Embosphere particles (Biosphere Medical, Rockland, MA) until flow reduction was observed. After completion of the TACE the catheter was removed and the common femoral artery was ligated. All rabbits were monitored during and after the procedure and given analgesics when they showed signs of physical distress.

Pathology

After partial hepatectomy, the resected lobe was macroscopically inspected and multiple specimens from the resection margin, healthy liver and tumor were fixed in formalin, embedded in paraffin, stained with hematoxylin–eosin and evaluated with a light microscope.

After euthanization, the abdomen of all rabbits was opened and inspected for metastases. The primary tumor (if present), lungs, heart, liver, spleen and kidneys were removed and weighed. The number of macroscopic metastases was determined per organ. Multiple biopsy specimens from the primary tumor (if present) lungs, heart, liver, spleen and kidneys, were fixed in formalin, embedded in paraffin, stained with hematoxylin–eosin (H&E) and evaluated with a light microscope.

RESULTS

In all 20 rabbits a solid liver tumor was seen on ultrasound examination 14 days after implantation (Fig 8.1).

Partial Hepatectomy

All six partial hepatectomies were successful in removing the tumor completely. No complications occurred during the procedure or during the follow-up period (Fig 8.2). Blood loss during the procedure was minimal. Mean procedure time was 20 min. At macroscopic examination a resection margin of at least 1 cm was observed in all animals.

Intra-arterial Infusion with 3-BrPA

In all six rabbits catheterization of the left hepatic artery was successful. The 1 h infusion with 25 ml of 1.75 mM 3-BrPA was tolerated well. All animals recovered without complications.

TACE

In all six rabbits catheterization of the left hepatic artery was successful. The TACE procedure was tolerated well. All animals recovered without complications.

Pathology

Results of pathologic examination of the two rabbits that were sacrificed 14 days after tumor implantation are shown in Table 8.1. Pathologic analysis showed the presence of lung metastases in one rabbit. None of the rabbits had abdominal cavity, kidney or brain metastases.

Results of pathologic examination of the rabbits that underwent partial hepatectomy are shown in Table 8.2. Pathologic analysis showed the presence of lung metastases in six of the six rabbits (Fig 8.3). Abdominal cavity dissemination was seen in one of the rabbits that were sacrificed 7 days after partial hepatectomy and in all rabbits that were sacrificed 14 and 21 days after partial hepatectomy. Local recurrence near the resection margin was seen in one rabbit that was sacrificed 7 days after partial hepatectomy. None of the rabbits had kidney or brain metastases.

Results of pathologic examination of the rabbits that underwent intra-arterial infusion with 3-BrPA are shown in Table 8.3. Pathologic analysis showed the presence of lung metastases in six of the six rabbits (Fig 8.4). Abdominal cavity dissemination was seen in none of the rabbits that were

sacrificed 7 days after the infusion and in one rabbit that was sacrificed 14 days after infusion and in one rabbit that was sacrificed 21 days after infusion. None of the rabbits had kidney or brain metastases. Pathologic analysis of the liver tumor showed that their primary liver tumors had not grown from baseline, were mostly necrotic and surrounded by a capsule (Fig 8.5).

Results of pathologic examination of the rabbits that underwent TACE are shown in Table 8.4. Pathologic analysis showed the presence of lung metastases in six of the six rabbits (Fig 8.6). Abdominal cavity dissemination was seen in all rabbits. Kidney metastases were present in two of the six rabbits. None of the rabbits had brain metastases. Pathologic analysis of the primary liver tumor showed only partial necrosis, with an increase in tumor size corresponding to the time-point of sacrifice (Fig 8.7).

DISCUSSION

The present study aimed to compare the impact of partial hepatectomy, intra-arterial treatment with 3-BrPA and TACE on tumor recurrence in the form of regional and distant metastases. The VX2 rabbit model of liver cancer has proven to be suitable for the study of intra-arterial approaches. In order to achieve our objective of comparing partial hepatectomy to two forms of intra-arterial therapies, we tested the feasibility of partial hepatectomy in rabbits bearing VX2 liver cancer.

The success of scientific research, as measured by the ability to correctly obtain the answers to important questions, is predominantly influenced by the quality and availability of appropriate models. In the case of medical research, this frequently involves selecting the best available animal model. Model selection is perhaps the most essential step in determining the success of a research venture. An ideal model should satisfy several criteria: it should be truly representative or a close approximation of the condition being studied; it should permit necessary tests or procedures to be performed.

The rabbit VX2 tumor model, an orthotopic model of liver cancer, was developed in 1940 from a papilloma virus-transformed keratinocyte (15). VX2 tumors have been shown to exhibit fast tumor growth and extensive metastases in a short time (16, 17). The main advantages of the

VX2 liver tumor model are a straightforward tumor-inoculation technique and a higher incidence of tumor metastases (18). Therefore, we further developed the VX2 model to be used in studies focusing on tumor therapy, especially on therapy of recurrent HCC after partial liver resection.

For in vivo experiments, rabbits readily allow surgical procedures and/or repeated, blood sampling and can carry a much greater tumor burden (particularly with orthotopic tumors) than small rodents, thereby increasing both the time available to study the tumor and the amount of tumor tissue obtainable. More importantly, rabbits allow direct access for intra-arterial delivery of anti-cancer treatments. Our study showed that partial hepatectomy was a straightforward and feasible procedure on rabbits. The techniques required for our model are simple and reproducible. All procedures can be carried out quickly. Our method was associated with no procedure related animal mortality and is favorable for a large scale application.

Although liver resection and liver transplant are the first choice of treatment for patients with HCC, recurrence is still a major setback of these approaches (11). TACE has proven to significantly improve survival in patients with unresectable HCC (19). However, it is unclear whether patients with surgically resectable HCC should always be treated with hepatectomy as opposed to TACE. Our results show that TACE caused only partial necrosis in the primary liver tumor. Furthermore, when compared to resection, more rabbits receiving TACE presented with abdominal and kidney metastases. One possible explanation for this finding is that in our study rabbits only received one TACE treatment, whereas in the clinical setting, TACE treatments typically are repeated until tumor response is achieved (19).

In previous studies we showed that 3-BrPA acts as an irreversible inhibitor of glycolytic enzymes (20). Many cancer types, including HCC, are associated with a high glycolytic rate and therefore are ideal targets for 3-BrPA (21). Moreover, we established intra-arterial delivery of 25 ml, 1.75 mM 3-BrPA over 1 h as the optimal method of delivery (14). In this study we compared this treatment regimen to resection and TACE. Our results indicate that rabbits treated with 3-BrPA exhibit less abdominal metastases than rabbits treated with either resection or TACE. Kidney and brain metastases after 3-BrPA treatment were absent which was comparable to resection and superior to TACE. Interestingly, all animals showed lung metastases. This finding suggests that metastatic spread in the VX2 liver

tumor model is a result of hematogenic rather than local seeding. Clinically, lung metastases are known to be an important metastatic pathway of HCC.

After successful surgical resection of the primary liver tumor, HCC may recur in various distant sites such as lungs, brain and abdominal cavity. Whenever metastases are present, patients are essentially incurable and current treatment strategies are unsatisfactory (22, 23). The described method of left lateral hepatectomy could be useful as an animal model to test new anti-cancer agents for this patient group. Our results indicate that this animal model reflects the recurrent metastatic features of HCC after liver resection. Furthermore, this model uses animals with tumor material implanted in orthotopic sites which offers better tumorigenicity and metastatic potential (24, 25).

This study has several limitations. First, our sample size was relatively small, so further studies with a larger sample size are needed to confirm our conclusions. However, our results are in line with previous studies on intra-arterial therapy with 3-BrPA (14, 26). Second, the VX2 tumor used in our study is of non-hepatic origin. However, it has proven to be convenient to study liver cancer in the animal because of the similarities in blood supply, genotype and metabolism to advanced human HCC.

CONCLUSION

The VX2 rabbit model of liver cancer is a suitable model to compare the influence of partial hepatectomy, intra-arterial treatment with 3-BrPA and TACE on tumor recurrence in the form of regional and distant metastases. Our results indicate that intra-arterial delivery of 3-BrPA may result in a favorable metastatic profile when compared to both liver resection and TACE.

TABLES & FIGURES

Animal ID	Days Post Implantation	Lung	Abdominal Cavity	Kidney / Brain	Liver Recurrence
1	14	Y	N	N	N/A
2	14	N	N	N	N/A

Table 8.1 Overview of metastases in control animals on pathologic examination.

Animal ID	Days Post Implantation	Lung	Abdominal Cavity	Kidney / Brain	Liver Recurrence
1	21	Y	Y	N	Y
2	21	Y	N	N	N
3	28	Y	Y	N	N
4	28	Y	Y	N	N
5	35	Y	Y	N	N
6	35	Y	Y	N	N

Table 8.2 Overview of metastases on pathologic examination in animals that underwent a partial hepatectomy.

Animal ID	Days Post Implantation	Lung	Abdominal Cavity	Kidney / Brain
1	21	Y	N	N
2	21	Y	N	N
3	28	Y	N	N
4	28	Y	Y	N
5	35	Y	N	N
6	35	Y	Y	N

Table 8.3 Overview of metastases on pathologic examination in animals that underwent an intra-arterial infusion with 25 ml of 1.75 mM 3-BrPA.

Animal ID	Days Post Implantation	Lung	Abdominal Cavity	Kidney	Brain
1	21	Y	Y	N	N
2	21	Y	Y	N	N
3	28	Y	Y	Y	N
4	28	Y	Y	N	N
5	35	Y	Y	N	N
6	35	Y	Y	Y	N

Table 8.4 Overview of metastases on pathologic examination in animals that underwent TACE

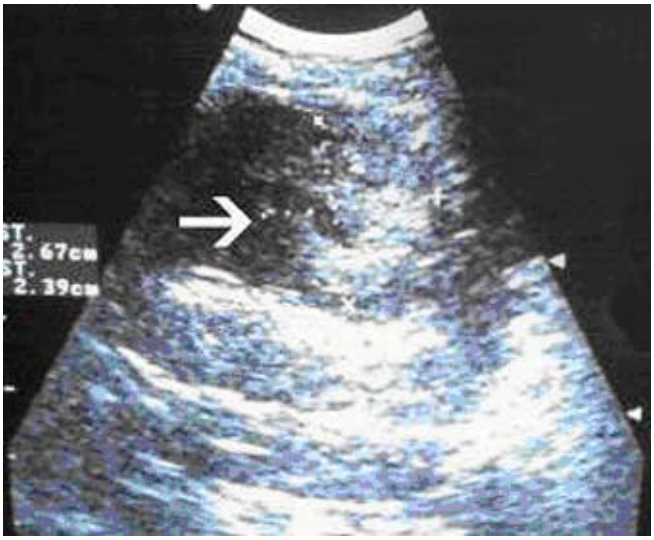

Figure 8.1 Ultrasound of liver tumor 14 days after implantation shows a 2.7 by 2.4 cm slightly hyperechoic hepatic VX2 tumor (arrow)

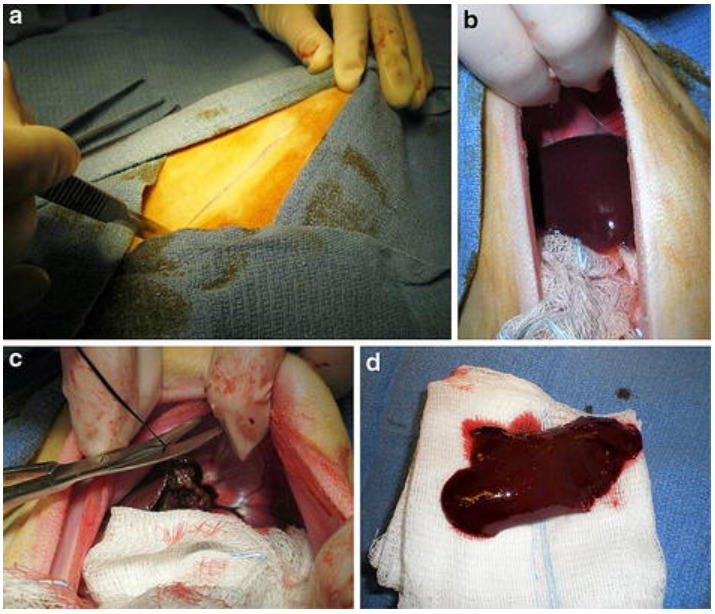

Figure 8.2 (A) Shows the midline incision from xyphoid to umbilicus. (B) Shows the isolation of the inferior surface of the liver from the stomach and the gut by means of gauzes. (C) Shows the ligation of the hilar vessels with a 2–0 silk tie in order to interrupt the circulation in the left lateral liver lobe. (D) Shows the resected left liver lobe.

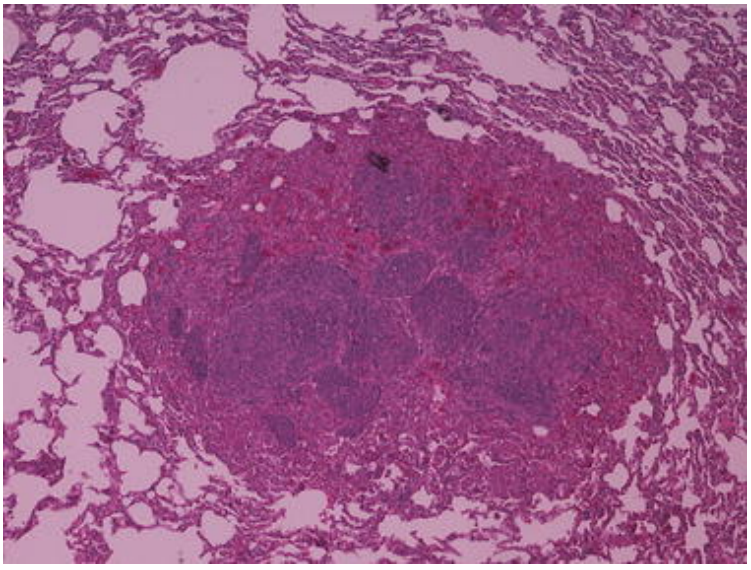

Figure 8.3 H&E stained slide of a typical lung metastasis after partial hepatectomy.

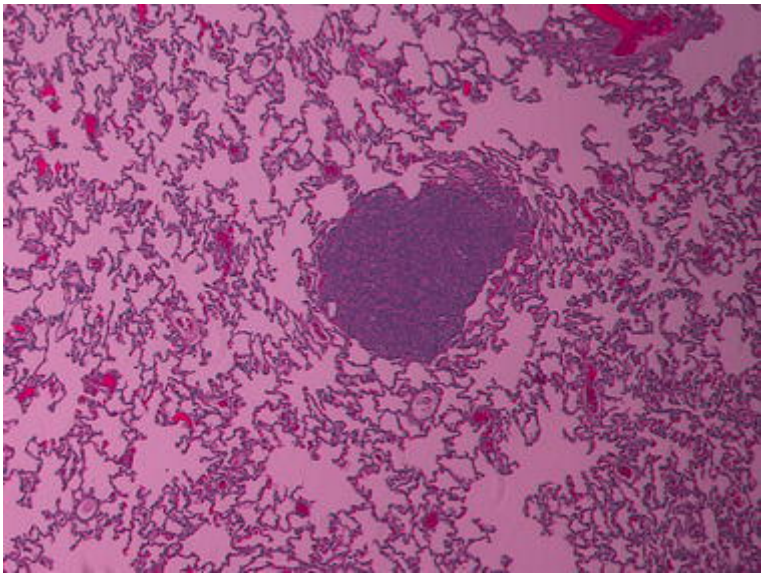

Figure 8.4 H&E stained slide of a typical lung metastasis after intra-arterial treatment with 3-BrPA.

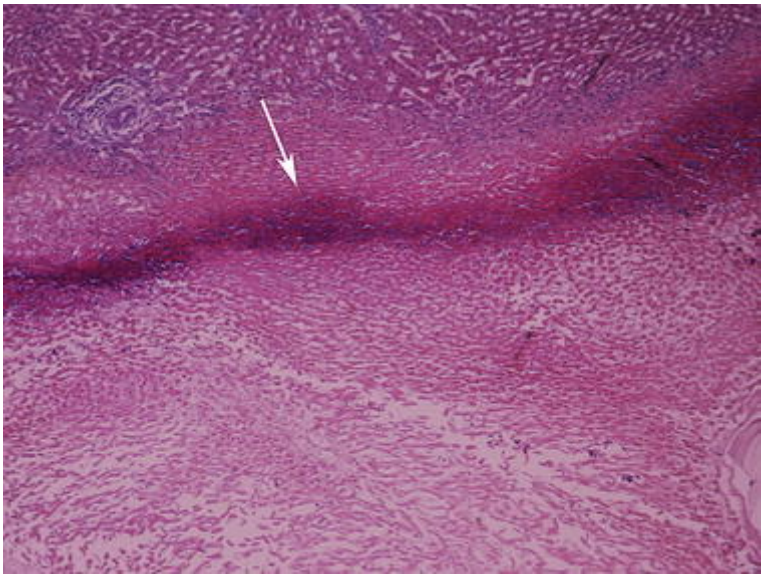

Figure 8.5 H&E stained slide of a VX2 liver tumor treated with 3-BrPA, consisting of necrotic cells surrounded by a capsule (arrow).

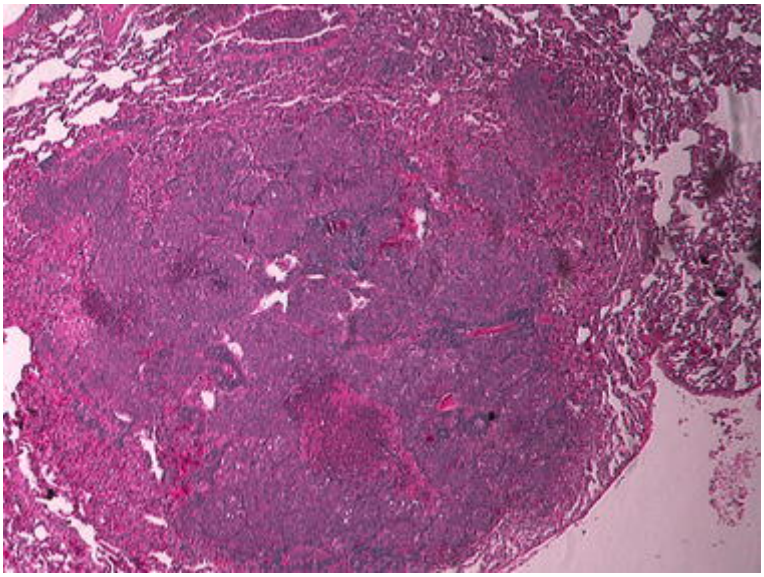

Figure 8.6 H&E stained slide of a typical lung metastasis after TACE.

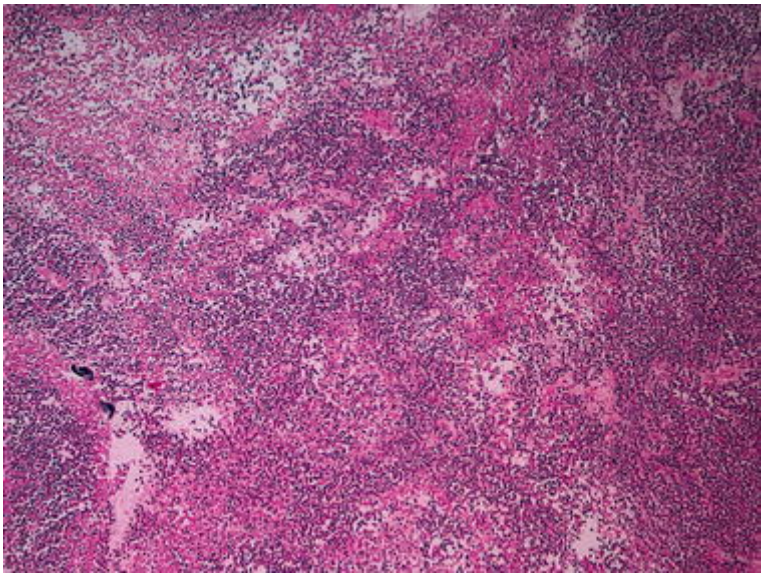

Figure 8.7 H&E stained slide of a VX2 liver tumor treated with TACE, consisting of both viable and necrotic areas.

REFERENCES

1) Motola-Kuba D, Zamora-Valdes D, Uribe M, Mendez-Sanchez N (2006) Hepatocellular carcinoma: an overview. Ann Hepatol 5:16–24
2) Jemal A, Siegel R, Ward E et al (2008) Cancer statistics, CA: a cancer. J Clin 58:71–96
3) Leong TY, Leong AS (2005) Epidemiology and carcinogenesis of hepatocellular carcinoma. HPB (Oxford) 7:5–15
4) Blum HE, Spangenberg HC (2007) Hepatocellular carcinoma: an update. Arch Iran Med 10:361–371
5) Forner A, Hessheimer AJ, Isabel Real M, Bruix J (2006) Treatment of hepatocellular carcinoma. Crit Rev Oncol/Hematol 60:89–98.
6) Poon RT, Fan ST, Lo CM, Liu CL, Wong J (1999) Intrahepatic recurrence after curative resection of hepatocellular carcinoma: long-term results of treatment and prognostic factors. Ann Surg 229:216–222.
7) Zimmerman MA, Ghobrial RM, Tong MJ et al (2008) Recurrence of hepatocellular carcinoma following liver transplantation: a review of preoperative and postoperative prognostic indicators. Arch Surg 143:182–188. Discussion 188.
8) Lo CM, Ngan H, Tso WK et al (2002) Randomized controlled trial of transarterial lipiodol chemoembolization for unresectable hepatocellular carcinoma. Hepatology 35:1164–1171
9) Llovet JM, Burroughs A, Bruix J (2003) Hepatocellular carcinoma. Lancet 362:1907–1917.
10) Befeler AS, Di Bisceglie AM (2002) Hepatocellular carcinoma: diagnosis and treatment. Gastroenterology 122:1609–1619.
11) Poon RT, Fan ST, O'Suilleabhain CB, Wong J (2002) Aggressive management of patients with extrahepatic and intrahepatic recurrences of hepatocellular carcinoma by combined resection and locoregional therapy. J Am Coll Surg 195:311–318.
12) Bruix J, Sherman M, Llovet JM et al (2001) Clinical management of hepatocellular carcinoma: conclusions of the Barcelona-2000 EASL conference: European Association for the Study of the Liver. J Hepatol 35:421–430.
13) Katyal S, Oliver JH 3rd, Peterson MS, Ferris JV, Carr BS, Baron RL (2000) Extrahepatic metastases of hepatocellular carcinoma. Radiology 216:698–703
14) Vali M, Liapi E, Kowalski J et al (2007) Intraarterial therapy with a new potent inhibitor of tumor metabolism (3-bromopyruvate): identification

of therapeutic dose and method of injection in an animal model of liver cancer. J Vasc Interv Radiol 18:95–101.
15) Rous P, Kidd JG, Smith WE (1952) Experiments on the cause of the rabbit carcinomas derived from virus-induced papillomas, II: loss by the Vx2 carcinoma of the power to immunize hosts against the papilloma virus. J Exp Med 96:159–174.
16) Ling R, Li Y, Yao Q et al (2005) Lymphatic chemotherapy induces apoptosis in lymph node metastases in a rabbit breast carcinoma model. J Drug Target 13:137–142.
17) Phillips PC, Than TT, Cork LC et al (1992) Intrathecal 4-hydroperoxycyclophosphamide: neurotoxicity, cerebrospinal fluid pharmacokinetics, and antitumor activity in a rabbit model of VX2 leptomeningeal carcinomatosis. Cancer Res 52:6168–6174
18) Chen JH, Lin YC, Huang YS, Chen TJ, Lin WY, Han KW (2004) Induction of VX2 carcinoma in rabbit liver: comparison of two inoculation methods. Lab Anim 38:79–84.
19) Georgiades CS, Hong K, Geschwind JF (2008) Radiofrequency ablation and chemoembolization for hepatocellular carcinoma. Cancer J (Sudbury, Mass.) 14:117–122.
20) Ko YH, Pedersen PL, Geschwind JF (2001) Glucose catabolism in the rabbit VX2 tumor model for liver cancer: characterization and targeting hexokinase. Cancer Lett 173:83–91.
21) Peng SY, Lai PL, Pan HW, Hsiao LP, Hsu HC (2008) Aberrant expression of the glycolytic enzymes aldolase B and type II hexokinase in hepatocellular carcinoma are predictive markers for advanced stage, early recurrence and poor prognosis. Oncol Rep 19:1045–1053
22) Yang Y, Nagano H, Ota H et al (2007) Patterns and clinicopathologic features of extrahepatic recurrence of hepatocellular carcinoma after curative resection. Surgery 141:196–202.
23) Zhu AX (2008) Development of sorafenib and other molecularly targeted agents in hepatocellular carcinoma. Cancer 112:250–259.
24) Fidler IJ (1995) Critical factors in the biology of human cancer metastasis. Am Surg 61:1065–1066
25) Khanna C, Hunter K (2005) Modeling metastasis in vivo. Carcinogenesis 26:513–523.
26) Vali M, Vossen J, Buijs M et al (2008) Targeting of VX2 rabbit liver tumor by selective delivery of 3-bromopyruvate: a biodistribution and survival study. J Pharmacol Exp Ther.

CHAPTER 8 – DEVELOPMENT OF A NEW ORTHOTOPIC ANIMAL MODEL OF METASTATIC LIVER CANCER IN THE RABBIT VX2 MODEL: EFFECT ON METASTASES AFTER PARTIAL HEPATECTOMY, INTRA-ARTERIAL TREATMENT WITH 3-BROMOPYRUVATE AND CHEMOEMBOLIZATION

CHAPTER 9

TARGETING OF VX2 RABBIT LIVER TUMOR BY SELECTIVE DELIVERY OF 3-BROMOPYRUVATE: A BIODISTRIBUTION AND SURVIVAL STUDY

Vali M, Vossen JA, Buijs M, Engles JM, Liapi E, Prieto Ventura V, Khwaja A, Acha-Ngwodo O, Shanmugasundaram G, Syed L, Wahl RL, Geschwind JF

J Pharmacol Exp Ther 2008 Oct;327(1):32-7.

ABSTRACT

PURPOSE:

The aim of this study was to determine the biodistribution and tumor targeting ability of ^{14}C-labeled 3-bromopyruvate ([^{14}C]3-BrPA) after i.a. and i.v. delivery in the VX2 rabbit model. In addition, we evaluated the effects of [^{14}C]3-BrPA on tumor and healthy tissue glucose metabolism by determining ^{18}F-deoxyglucose (FDG) uptake. Last, we determined the survival benefit of i.a. administered 3-BrPA.

MATERIALS AND METHODS:

In total, 60 rabbits with VX2 liver tumor received either 1.75 mM [^{14}C]3-BrPA via intra-arterial administration., 1.75 mM [^{14}C]3-BrPA via intravenous administration, 20 mM [^{14}C]3-BrPA via intravenous administration, or 25 ml of phosphate-buffered saline (PBS). All rabbits (with the exception of the 20 mM intravenous group) received FDG 1 h before sacrifice. Next, we compared survival of animals treated with intra-arterially administered 1.75 mM [^{14}C]3-BrPA in 25 ml of PBS (n = 22) with controls (n = 10).

RESULTS:

After intra-arterial infusion, tumor uptake of [^{14}C]3-BrPA was 1.8 ± 0.2% percentage of injected dose per gram of tissue (%ID/g), whereas other tissues showed minimal uptake. After intravenous infusion (1.75 mM), tumor uptake of [^{14}C]3-BrPA was 0.03 ± 0.01% ID/g. After intra-arterial administration of [^{14}C]3-BrPA, tumor uptake of FDG was 26 times lower than in controls. After intravenous administration of [^{14}C]3-BrPA, there was no significant difference in tumor FDG uptake. Survival analysis showed that rabbits treated with 1.75 mM 3-BrPA survived longer (55 days) than controls (18.6 days).

CONCLUSION:

Intra-arterially delivered 3-BrPA has a favorable biodistribution profile, combining a high tumor uptake resulting in blockage of FDG uptake with no effects on healthy tissue. The local control of the liver tumor by 3-BrPA resulted in a significant survival benefit.

INTRODUCTION

The knowledge that cancer cells rely on increased glycolysis rather than oxidative phosphorylation for survival is known as "The Warburg Hypothesis" (1). This concept constitutes the basis for using glycolysis and its associated enzymes as targets for the development of new anticancer therapeutic agents (2, 3). In our previous studies, we showed that 3-bromopyruvate (3-BrPA) acts as an irreversible inhibitor of metabolic enzyme(s) associated with glycolysis (4, 5). Furthermore, we established the therapeutic dose [1.75 mM in 25 ml of phosphate-buffered saline (PBS) and optimal method of delivery (continuous i.a. infusion for 1 h)] of 3-BrPA in a rabbit VX2 model of liver cancer based on pathology (6). However, the impact of this treatment strategy on animal survival remains unknown. This information is critical to further develop this approach to the clinic.

Transarterial therapy is one of the most frequently used locoregional treatment options in patients with hepatocellular carcinoma (7). The main advantage of transarterial delivery of anticancer agents over systemic chemotherapy is the fact that these agents are not infused i.v. throughout the systemic circulation but rather administered locally via the hepatic artery. Thereby, the concentration of the agent within the tumor tissue can be 10 to 100 times higher after i.a. delivery than after systemic delivery (8, 9). Because i.a. delivery of 3-BrPA is more complex than the more classic systemic administration, a thorough evaluation of the expected advantages should be made, thereby justifying a detailed pharmacokinetic and biodistribution analysis.

A recent study demonstrated that ^{18}F-deoxyglucose (FDG)-positron emission tomography (PET) can be a useful modality for the early evaluation of the antitumor effect of i.a. administration of 3-BrPA in VX2 liver tumor (10). The use of PET with the glucose analog FDG is based on the recognition that tumor cells have an increased glucose metabolism (11, 12). Increased FDG uptake is considered to be indicative of the presence of a metabolically active tumor, whereas lack of FDG uptake indicates tumor cell death.

The aim of this study was to determine and compare the biodistribution as well as tumor targeting ability of ^{14}C-labeled 3-BrPA ([^{14}C]3-BrPA) delivered either i.a. or i.v. delivery in the VX2 model of liver cancer. In addition, we evaluated the effects of [^{14}C]3-BrPA on tumor and

healthy tissue glucose metabolism by determining FDG uptake. Last, we determined the survival benefit of intra-arterially administered 3-BrPA in the rabbit VX2 model of liver cancer.

MATERIALS AND METHODS

Study Design

Two distinct experiments were carried out. The first experiment (n = 60) was designed to assess the biodistribution profile of [^{14}C]3-BrPA and to monitor its influence on FDG uptake. The second experiment (n = 32) was designed to document the survival benefit of 3-BrPA by comparing survival of animals treated with 3-BrPA (n = 22) to controls (n = 10).

Tumor Model

The study was approved by the Animal Care Committee of Johns Hopkins University (Baltimore, MD) and in compliance with institutional guidelines. Adult New Zealand white rabbits weighing 8 to 9 lbs (n = 92; Myrtle's Rabbitry, Thompson's Station, TN) were used for this study. For successful implantation of the VX2 tumor into the liver, the tumor was first grown for 2 weeks in the hind leg of a carrier rabbit. Each carrier rabbit was used for implantation into the left lobe of the liver of six rabbits. Before tumor implantation all rabbits were anesthetized with a mixture of acepromazine (2.5 mg/kg; Phoenix, St Joseph, MO) and ketamine hydrochloride (44 mg/kg; Phoenix) administered i.m.; intravenous access was gained via a marginal ear vein, and sodium pentobarbital (Abbott Laboratories, Abbott Park, IL) was given to maintain anesthesia. VX2 tumor excised from a carrier rabbit was minced and injected into the left lobe of the liver using a 21-gauge angiocatheter. The tumor was allowed to grow for 14 days in all rabbits before treatment was initiated.

Intra-Arterial Delivery Protocol

The induction and maintenance of anesthesia were carried out as described above. Transcatheter hepatic artery infusion of 3-BrPA was performed under fluoroscopic guidance. The animals were brought to the angiography suite and intubated by using a 3.0-mm endotracheal tube (Mallinckrodt Medical, St. Louis, MO) but not ventilated. Surgical cutdown was performed to gain access into the right common femoral artery, after

which a 3-F sheath (Cook, Bloomington, IN) was inserted. A 2-F JB1 catheter (Cook) was manipulated into the celiac axis, after which a celiac arteriogram was obtained to delineate the blood supply to the liver and confirm the location of the tumor. The tumor could readily be visualized as a region of hypervascular blush located on the left side of the liver near the gastric fundus. The left hepatic artery, which provides most of the blood flow to the tumor, was selectively catheterized via the common hepatic artery by using a Transcend guide wire (Boston Scientific, Natick, MA).

After the catheter was adequately positioned within the left hepatic artery, a syringe containing 3-BrPA was connected to the end of the JB1 catheter and carefully placed and adjusted on an infusion syringe pump (Harvard Apparatus model 11 infuse/withdraw single syringe pump; Instech Laboratories, Plymouth Meeting, PA). The infusion rate was set. During the infusion, maintenance of appropriate positioning of the catheter in the hepatic artery was monitored with fluoroscopy. After completion of the infusion the catheter was removed, and the common femoral artery was ligated. All rabbits were monitored during and after the procedure and given analgesics when they showed signs of physical distress.

Radiolabeling

After screening various radioactive markers, we selected carbon-14 as the radiotracer to label 3-BrPA because of its relative ease of synthesis and long half-life. The labeling process consisted of incorporating carbon-14 into pyruvate at the first carbon atom resulting in [1-^{14}C]pyruvate, which was then reacted with elemental bromine leading to the synthesis of [^{14}C]3-BrPA. The radiolabeled analog was purified using normal-phase high-performance liquid chromatography column. The radiochemical purity of the formulated product was determined using analytical high-performance liquid chromatography performing four separate infusions: 1) unlabeled 3-BrPA standard; 2) unlabeled 3-BrPA standard plus [^{14}C]3-BrPA, to demonstrate coelution; 3) [^{14}C]3-BrPA alone; and 4) unlabeled 3-BrPA standard to demonstrate that the retention time for the product has not changed. The chemical purity was >95%. [^{14}C]3-BrPA (15 mCi/mmol) was synthesized at PerkinElmer Life and Analytical Sciences (Waltham, MA). The chemical structure and the position of the ^{14}C label are shown in Figure 9.1.

In Vivo Biodistribution Studies

Biodistribution studies were performed in 60 rabbits, 14 days after tumor implantation. Fifty-four rabbits were divided into three groups of 18 animals each. Group 1 was treated i.a. with a 1.75 mM mixture of 100 μCi of [^{14}C]3-BrPA and 3-BrPA in 25 ml of PBS, group 2 received i.v. infusion with a 1.75 mM mixture of 100 μCi of [^{14}C]3-BrPA and 3-BrPA in 25 ml of PBS, and group 3 received i.v. infusion with a 20 mM mixture of 100 μCi of [^{14}C]3-BrPA and 3-BrPA in 25 ml of PBS. Each group was further subdivided into six groups of three rabbits each, corresponding to various time points of sacrifice (0, 30, 60, 120, and 240 min and 24 h after the end of the infusion). Intravenous infusions were given as a continuous infusion over 1 h through a marginal ear vein (infusion rate 25 ml/h). Intra-arterial infusions were given as a continuous infusion over 1 h directly in the left hepatic artery, using the technique described above (infusion rate 25 ml/h). Control rabbits (n = 6) received a 1-h i.v. (n = 3) or i.a. (n = 3) infusion of 25 ml of PBS.

All rabbits, except 18 rabbits in group 3, received 1 mCi of FDG (0.22 mCi/kg) via an ear vein 1 h before sacrifice. After sacrifice, blood, normal tissues (brain, heart, lung, liver, kidney, spleen, stomach, transverse colon, and skeletal muscle) and tumor samples were obtained from each rabbit. The tissue samples were weighed, and FDG uptake was evaluated using a gamma counter (LKB Wallac, Little Chalfont, Buckinghamshire, UK). To correct for radioactive decay and permit calculation of the concentration of radioactivity in each organ as a fraction of the administered dose, aliquots of the injected dose (ID) were counted simultaneously.

Subsequently, the samples were transferred to scintillation vials, dissolved in 1 ml of Solvable solution (PerkinElmer Life and Analytical Sciences), and color-treated with hydrogen peroxide. After adding scintillation fluid (10 ml) (Ultima Gold; PerkinElmer Life and Analytical Sciences), the sample cpm were counted using a liquid scintillation counter. The percentage of injected dose per gram of tissue (%ID/g) was calculated using the cpm.

Survival Study

Survival studies were performed in 32 animals. Rabbits were divided into three groups; study group 1 (n = 19) and a control group (n = 10), all treated 14 days after tumor implantation in the liver, and study group 2 (n =

3), treated 7 days after tumor implantation. Animals in the study groups (n = 22) were treated with a 1 h i.a. infusion of 1.75 mM 3-BrPA in 25 ml of PBS, whereas animals in the control group (n = 10) received a 1-h i.a. infusion of 25 ml of PBS. All rabbits were examined daily for appetite, bowel and bladder function, level of activity, and tumor growth. Ten months after treatment or when animals became moribund, failed to eat and drink for more than 3 days, had weight loss >20%, and displayed apathetic behavior, rabbits were sacrificed.

Histologic Analysis

All animals in the survival study were euthanized under deep anesthesia by slow injection of a lethal dose (100 mg/5 ml) of sodium pentobarbital i.v. Immediately after euthanasia, liver, lungs, heart, liver, spleen, and kidneys were removed and weighed. Multiple biopsy specimens from the tumor, lungs, heart, liver, spleen, and kidneys, were fixed in formalin, embedded in paraffin, stained with hematoxylin and eosin, and evaluated with a light microscope.

Statistical Analysis

Data were analyzed by use of SPSS for Windows, version 10.0 (SPSS Inc., Chicago, IL). Continuous parameters are reported as mean ± S.D. The data for the treatment groups (%ID/g) were compared. Differences between groups were tested with the two-sample *t* test. Median survival was calculated from the date of tumor implantation until death. A Kaplan-Meier curve was generated. A p value < 0.05 was considered statistically significant.

RESULTS

Biodistribution and Tumor Uptake

The detailed biodistribution data of [^{14}C]3-BrPA at 0 min, 30 min, 60 min, 120 min, 240 min, and 24 h after infusion in VX2 liver tumor-bearing rabbits are shown in Table 9.1 (i.a. infusion) and Table 9.2 (i.v. infusion of 1.75 mM). After i.a. infusion, tumor uptake of [^{14}C]3-BrPA was 1.8 ± 0.2, 0.7 ± 0.4, 0.5 ± 0.1, and 0.1 ± 0.03% ID/g at 0 min, 30 min, 120 min, and 24 h, showing tumor retention of the [^{14}C]3-BrPA. Radioactivity levels in the blood were 0.12 ± 0.01% ID/g at 0 min after infusion, followed by a rapid

clearance by the end of 240 min (0.03 ± 0.02% ID/g). Selective tumor targeting resulted in a tumor-to-blood ratio of 15.0 at the end of the infusion, which dropped to 3.4 120 min after infusion, but due to rapid blood clearance increased to 20.9 240 min after infusion. Uptake of [^{14}C]3-BrPA in the nontumorous liver was consistently low, ranging from 0.31 240 min after infusion to 0.09 24 h after infusion. Excluding the liver, only the kidneys displayed any appreciable retention of radioactivity. There was very little radioactive retention in the remaining tissues. Uptake of [^{14}C]3-BrPA in the brain was consistently low, with a maximum of 0.009 ± 0.006% ID/g 60 min after infusion.

After i.v. infusion (1.75 mM), tumor uptake of [^{14}C]3-BrPA was significantly lower than after i.a. infusion, measuring 0.03 ± 0.01, 0.04 ± 0.01, 0.05 ± 0.03, and 0.03 ± 0.02% ID/g at 0 min, 30 min, 120 min, and 24 h, respectively. Radioactivity levels in the blood were 0.05 ± 0.01% ID/g at 0 min after infusion, which remained stable over 24 h. Intravenous infusion resulted in a tumor-to-blood ratio of 0.6 at the end of the infusion, which increased to a peak value of 1.3 at 60 min after infusion, a value that is 16 times lower than the peak value after intra-arterial administration. Normal tissue uptake of [^{14}C]3-BrPA was highest in the kidneys, reaching a peak value of 0.16 ± 0.02 at 120 min after infusion.

Intravenous administration with the higher dose (20 mM) did not show any significant difference in biodistribution compared with the lower dose (1.75 mM). Tumor uptake of [^{14}C]3-BrPA was 0.05 ± 0.01, 0.03 ± 0.02, 0.07 ± 0.05, and 0.02 ± 0.01% ID/g at 0 min, 30 min, 120 min, and 24 h. Tumor uptake of [^{14}C]3-BrPA in all groups is shown in Figure 9.2.

Influence of intra-arterial and intravenous infusion of [^{14}C]3-BrPA on FDG tumor uptake compared with controls are shown in Figure 9.3. Immediately after i.a. administration of [^{14}C]3-BrPA tumor uptake of FDG was 26 times lower compared with tumor uptake of FDG in control animals. This ratio reached a peak of 33 at 30 min after infusion and slowly declined to 2 at 24 h after infusion. However, after i.v. administration of [^{14}C]3-BrPA, there was no significant difference in tumor uptake of FDG compared with control animals.

Survival

Rabbits treated with 1.75 mM i.a. 3-BrPA survived significantly longer than the animals in the control group (Fig 9.4). The mean survival

time in the control group was 18.6 days, whereas the mean survival time in the treatment group was 55.0 days, showing a statistically significant 296% increase in survival for the rabbits treated i.a. with 3-BrPA ($p < 0.001$).

Histopathologic analysis of the liver in treated animals showed, that their primary liver tumors had not grown from baseline and were mostly necrotic (Fig 9.5). Furthermore, the surrounding healthy liver tissue showed no signs of toxicity (Fig 9.6). In contrast, histopathologic analysis of the liver in control animals showed near complete replacement of liver parenchyma by tumor with direct extension into adjacent tissues such as the diaphragm and lungs. When examining the extent of tumor dissemination, we observed widespread metastases in the peritoneum, stomach, intestine, and lung in both control and treated animals, indicating that by the time of i.a. treatment the tumor had already spread to extrahepatic sites. The cause of death in the 3-BrPA-treated animals was attributed to the presence of extrahepatic disease, especially in the lungs.

To address this issue, a subgroup of three animals was treated earlier in their disease, i.e., 1 week after tumor implantation mimicking earlier stage liver cancer in humans. One of three animals showed no evidence of recurrence and was considered cured 10 months after treatment. When the liver was excised at the time of sacrifice, a small (less than 1 cm) calcified lesion was present at the site of the tumor, confirming complete tumor destruction. The other two animals did die approximately 80 days after implantation but as with the other animals with advanced liver cancer, they died of respiratory failure due to the presence of lung metastases.

DISCUSSION

Hepatic arterial therapies have become the mainstay of therapy for patients presenting with unresectable hepatocellular carcinoma (13, 14). The rationale for hepatic arterial chemotherapy is that the infusion of cytotoxic drugs directly into the artery feeding the tumor will maximize tumor concentration and minimize systemic toxicity. In a previous study, we showed that i.a. delivered 3-BrPA in a concentration of 1.75 mM resulted in complete tumor death (6). Because i.a. drug delivery is more complex than the classic systemic administration, a pharmacokinetic and biodistribution analysis was appropriate. Therefore, the first aim of our study was to evaluate the biodistribution of i.a. delivered [^{14}C]3-BrPA and to compare its profile with that obtained after i.v. administration.

For the success of an anticancer agent, a high tumor uptake and a high tumor to normal tissue ratio indicating selective targeting is desirable. The data collected in our study showed that i.a. delivery of [^{14}C]3-BrPA resulted in the highest tumor uptake, with a maximum of 1.8% ID/g. In contrast, i.v. administration of [^{14}C]3-BrPA resulted in significantly lower tumor uptake, with a maximum of 0.07% ID/g, even after a 10-fold increase of the dose. This convincingly shows the superiority of i.a. delivery over i.v. administration in achieving high concentrations of [^{14}C]3-BrPA within the tumor. As expected, uptake of [^{14}C]3-BrPA in the liver was higher after i.a. delivery, compared with i.v. delivery. However, liver uptake of i.a. administered [^{14}C]3-BrPA reached a maximum of only 0.3% ID/g. All remaining tissues showed minimal uptake of [^{14}C]3-BrPA after both i.a. and i.v. delivery, with the kidney showing the highest uptake of 0.23% ID/g. A major finding was the consistently low uptake of [^{14}C]3-BrPA in the high metabolic tissue of the brain, indicating that the drug did not cross the blood-brain barrier.

FDG is a glucose analog that accumulates in cells in a velocity that is dependent on the glycolytic rate of the cell (15, 16). In this study, we used FDG to monitor the effects of i.a. and i.v. delivered 3-BrPA on tumor and healthy tissue metabolism. Our study showed that neither i.a. nor i.v. administration of [^{14}C]3-BrPA influenced the glucose metabolism of healthy tissues. However, after i.a. administration, FDG uptake in the tumor was blocked during the first 2 h after administration followed by a slow increase of FDG uptake, comparable with control levels after 24 h. It is interesting to note that this observation may contradict the results of the histopathologic analysis in our survival study, which unequivocally showed that the primary liver tumors had not grown from baseline and were mostly necrotic. A possible explanation is that a few cancer cells remain viable after the treatment with 3-BrPA. These cells could have simply been stunned by the treatment but not killed. Note that this measurement of FDG activity as described in our study is much more sensitive than PET imaging. Isolated viable cells may therefore not be able to generate a signal that could be detected on PET imaging. Another explanation is that these "stunned" cells could indeed be on a way to a certain death but are still able to take up glucose for their energy needs. After i.v. administration, tumor uptake levels of FDG did not differ from uptake in controls. These results clearly indicate selective tumor metabolism targeting of i.a. delivered [^{14}C]3-BrPA, where healthy tissues are being spared and confirms the advantage of the i.a. delivery method.

The uniquely selective targeting properties of 3-BrPA are evident compared with those of other conventional chemotherapeutic agents. One report using ^{14}C-labeled doxorubicin in a mixture with lipiodol in the same VX2 rabbit model showed that almost all of the doxorubicin disappeared from the tumor immediately after infusion. Therefore, targeting of the tumor by doxorubicin could not be achieved (9).

One possible explanation for the lack of effect of i.v. administered [^{14}C]3-BrPA on FDG uptake in the tumor is the lower concentration at the tumor site (maximum 0.05% ID/g). To achieve concentrations of [^{14}C]3-BrPA in the tumor tissue that are similar to those obtained after i.a. administration, a significantly higher dose of i.v. [^{14}C]3-BrPA is required. However, administration of a higher dose may not show a comparably favorable biodistribution profile and result instead in unfavorable systemic side effects.

The second aim of our study was to evaluate the survival benefit of i.a. administered 3-BrPA in rabbits implanted with the VX2 liver tumor. Our experiments were conducted using the already established dose of 1.75 mM in 25 ml of PBS infused i.a. over 1 h. Treated rabbits had a significant increase in survival compared with the control group. This extension of life span by 36 days or 296% provides convincing evidence for 3-BrPA-mediated survival benefit.

Noteworthy is the absence of toxicity to the normal liver on histopathological analysis, which is in keeping with previous data from our laboratory (6). Because most liver cancers arise in the background of underlying liver disease (cirrhosis) and liver failure is a major risk of treatment-related morbidity and mortality in patients, this absence of toxicity is of great importance (17). These data further confirm the selective targeting of 3-BrPA, which is in line with the results of our biodistribution study.

Although the treatment with 3-BrPA was successful at killing the tumor cells, most animals were not cured by this approach. This may be attributed to the natural biology of the VX2 tumor, which is known to be extremely aggressive, fast growing, and rapidly metastasizes to other tissues and organs, especially the lungs (18-20). Histopathologic examination showed that the animals did not die from progression of their liver tumors, but rather from the presence of extrahepatic metastases especially in the

lungs. This suggests that the locoregional delivery of 3-BrPA was successful in selectively targeting the liver tumor without causing toxicity to the normal liver parenchyma, and controlling its growth within the liver. Unfortunately, it was not successful in preventing metastatic spread of the VX2 tumor outside the liver.

To minimize the risk of metastatic spread, we decided to treat a small number of rabbits (three animals) at an earlier stage of liver tumor development (7 days after implantation) and showed that earlier intervention leads to further improvement in survival. One of the three animals survived more than 10 months after treatment. When this animal was sacrificed, histopathology showed the tumor to be small (less than 1 cm in diameter), densely calcified, and nonviable. Here, despite evidence of success (one cure of three animals) and a clear attempt on our part to treat earlier in the disease process, our results suggest that this animal model is not appropriate to conduct survival studies because the two animals that died did so as a result of lung metastases. It is for this reason that we did not extend this survival study with a larger number of animals.

This survival study demonstrates the potency of 3-BrPA when given i.a. and its ability kill the liver tumor locally. Specifically, a single bolus infusion of 3-BrPA is not sufficient to kill the entire tumor. By administering 3-BrPA for a prolonged period (>1 h) to the tumor, as we demonstrated from the histopathologic standpoint in a previous report, we were able to achieve significant improvement in survival through complete local tumor control. These results therefore support our therapeutic approach.

In conclusion, we have shown that i.a. delivered 3-BrPA has a favorable biodistribution profile, combining a high tumor uptake resulting in direct blockage of FDG uptake with no effects on healthy tissue. Furthermore, i.a. infusion of 3-BrPA in VX2 implanted liver tumors proved to be beneficial because it resulted in significant survival benefit without any treatment related toxicity. These results argue strongly for the initiation of clinical studies to investigate the safety and efficacy of 3-BrPA as a human anticancer drug.

TABLES & FIGURES

	% ID (mean ± S.D.) of [^{14}C]3-BrPA in Organ Tissue Samples at Different Time Points after i.a. Administration (1.75 mM)											
	0 min		30 min		60 min		120 min		240 min		24 h	
Blood	0.117	0.013	0.055	0.040	0.066	0.014	0.131	0.087	0.025	0.021	0.016	0.003
Brain	0.006	0.003	0.008	0.002	0.009	0.006	0.007	0.001	0.007	0.004	0.006	0.003
Heart	0.029	0.012	0.044	0.016	0.041	0.028	0.041	0.036	0.030	0.015	0.025	0.024
Lung	0.043	0.006	0.069	0.012	0.053	0.013	0.056	0.018	0.076	0.021	0.026	0.018
Liver	0.115	0.071	0.143	0.072	0.229	0.238	0.290	0.146	0.305	0.230	0.088	0.057
Kidney	0.096	0.031	0.180	0.084	0.143	0.039	0.124	0.056	0.225	0.039	0.056	0.052
Spleen	0.037	0.018	0.045	0.012	0.062	0.028	0.040	0.004	0.055	0.029	0.046	0.045
Stomach	0.024	0.014	0.061	0.019	0.033	0.008	0.052	0.034	0.041	0.012	0.057	0.074
GI tract	0.021	0.003	0.039	0.008	0.041	0.015	0.049	0.033	0.053	0.029	0.022	0.017
Muscle	0.007	0.002	0.031	0.014	0.032	0.018	0.016	0.006	0.014	0.006	0.020	0.018
Tumor	1.781	0.222	0.744	0.391	0.274	0.354	0.452	0.099	0.523	0.405	0.099	0.029

Table 9.1 Biodistribution data in 18 animals at 0 min (n = 3), 30 min (n = 3), 60 min (n = 3), 120 min (n = 3), 240 min (n = 3), and 24 h (n = 3) after the end of a 1-h i.a. infusion with a 1.75 mM mixture of 100 µCi of [^{14}C]3-BrPA and 3-BrPA in 25 ml of PBS (infusion rate 25 ml/h).

	% ID (mean ± S.D.) of [^{14}C]3-BrPA in Organ Tissue Samples at Different Time Points after i.v. Administration (1.75 mM)											
	0 min		30 min		60 min		120 min		240 min		24 h	
Blood	0.048	0.011	0.089	0.009	0.026	0.001	0.058	0.005	0.062	0.012	0.038	0.001
Brain	0.034	0.041	0.010	0.006	0.002	0.000	0.002	0.001	0.003	0.000	0.003	0.001
Heart	0.046	0.007	0.042	0.006	0.025	0.003	0.025	0.003	0.022	0.004	0.018	0.006
Lung	0.055	0.011	0.059	0.009	0.046	0.008	0.038	0.003	0.037	0.008	0.025	0.005
Liver	0.073	0.017	0.080	0.003	0.070	0.012	0.059	0.049	0.048	0.022	0.054	0.026
Kidney	0.154	0.015	0.158	0.038	0.143	0.036	0.163	0.022	0.094	0.033	0.040	0.007
Spleen	0.051	0.004	0.045	0.010	0.058	0.035	0.043	0.008	0.034	0.006	0.026	0.006
Stomach	0.037	0.014	0.051	0.016	0.030	0.005	0.046	0.013	0.036	0.017	0.013	0.004
GI tract	0.064	0.062	0.045	0.011	0.024	0.001	0.028	0.006	0.020	0.004	0.018	0.002
Muscle	0.005	0.005	0.023	0.016	0.005	0.001	0.008	0.004	0.005	0.004	0.005	0.001
Tumor	0.029	0.008	0.038	0.008	0.033	0.010	0.045	0.028	0.033	0.005	0.026	0.016

Table 9.2 Biodistribution data in 18 animals at 0 min (n = 3), 30 min (n = 3), 60 min (n = 3), 120 min (n = 3), 240 min (n = 3), and 24 h (n = 3) after the end of a 1-h i.v. infusion with a 1.75 mM mixture of 100 µCi [^{14}C]3-BrPA and 3-BrPA in 25 ml of PBS (infusion rate 25 ml/h).

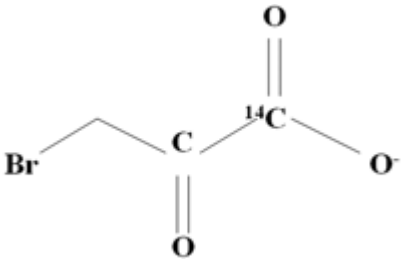

Figure 9.1 The chemical structure of [^{14}C]3-BrPA with the position of the ^{14}C label.

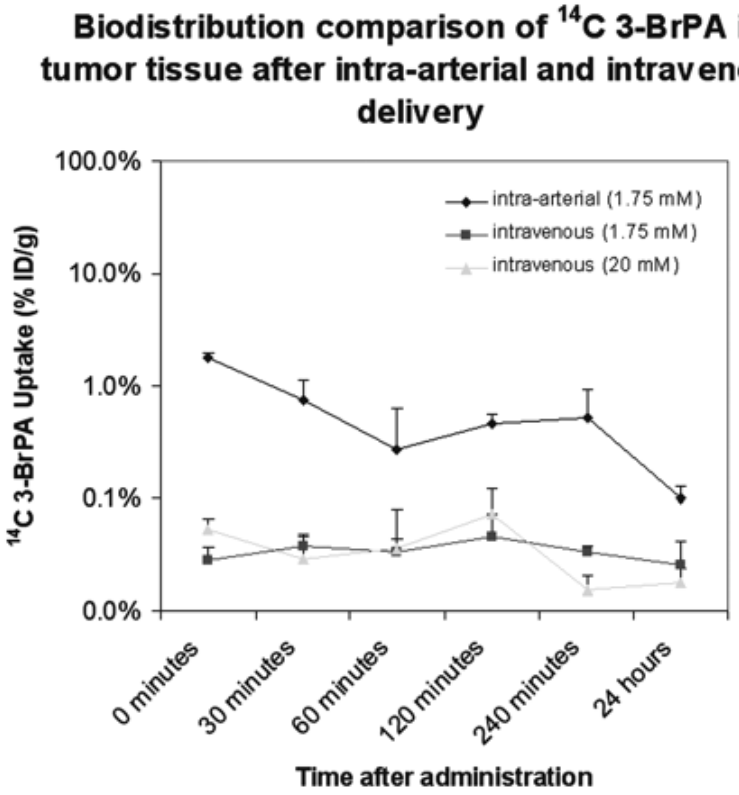

Figure 9.2 Comparison of [^{14}C]3-BrPA tumor uptake after the end of a 1-h i.a. infusion with a 1.75 mM mixture of 100 µCi of [^{14}C]3-BrPA and 3-BrPA in 25 ml of PBS (infusion rate 25 ml/h); after the end of a 1-h i.v. infusion with a 1.75 mM mixture of 100 µCi of [^{14}C]3-BrPA and 3-BrPA in 25 ml of PBS (infusion rate 25 ml/h); after the end of a 1-h i.v. infusion with a 20 mM mixture of 100 µCi of [^{14}C]3-BrPA and 3-BrPA in 25 ml of PBS (infusion rate 25 ml/h).

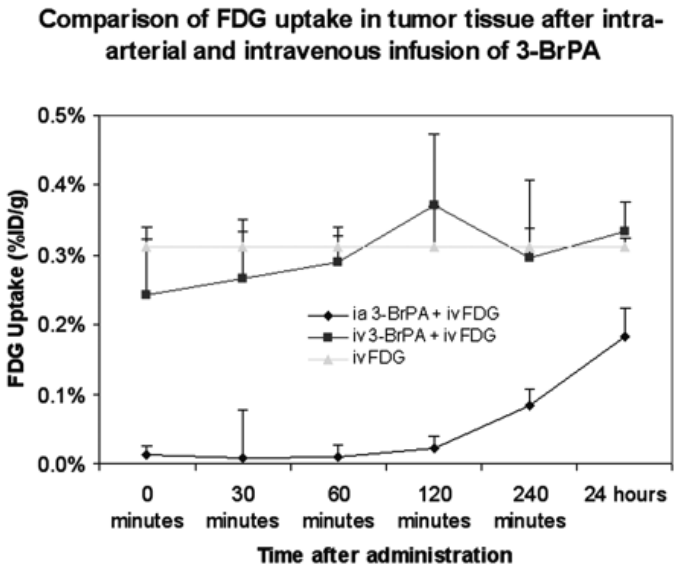

Figure 9.3 Comparison of FDG tumor uptake after the end of a 1-h i.a. (n = 18) or i.v. (n = 18) with a 1.75 mM mixture of 100 µCi of [^{14}C]3-BrPA and 3-BrPA in 25 ml of PBS (infusion rate 25 ml/h). Control rabbits (n = 6) received a 1-h i.v. (n = 3) or i.a. (n = 3) infusion of 25 ml of PBS. All rabbits received 1 mCi of FDG (0.22 mCi/kg) via an ear vein (i.v.) 1 h before sacrifice.

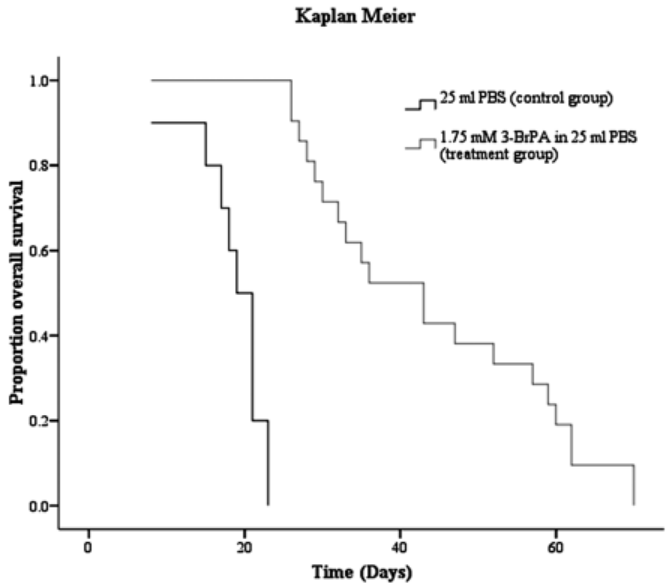

Figure 9.4 Kaplan-Meier survival curves, comparing animals treated with a 1-h i.a. infusion of 1.75 mM 3-BrPA in 25 ml of PBS (n = 22) to control animals treated with a 1-h i.a. infusion of 25 ml of PBS (n = 10).

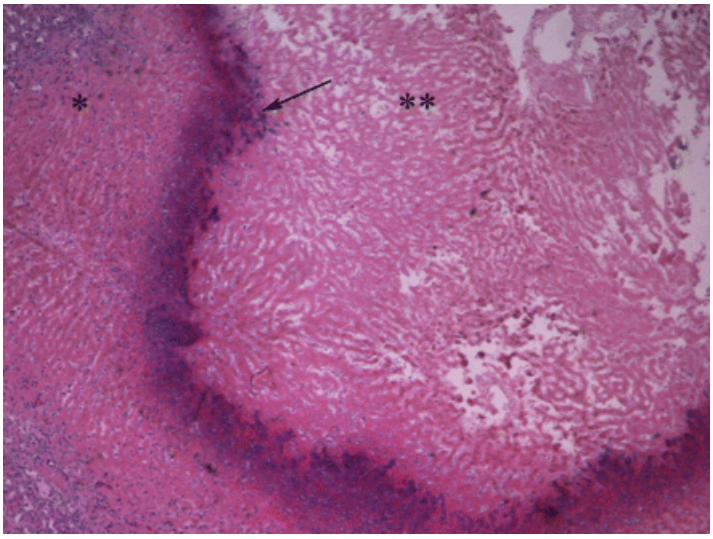

Figure 9.5 Hematoxylin and eosin slide of the tumor (**) and surrounding liver (*) in a rabbit treated with 1.75 mM of 3-BrPA. The tumor has not grown from baseline, is necrotic and encapsulated (arrow).

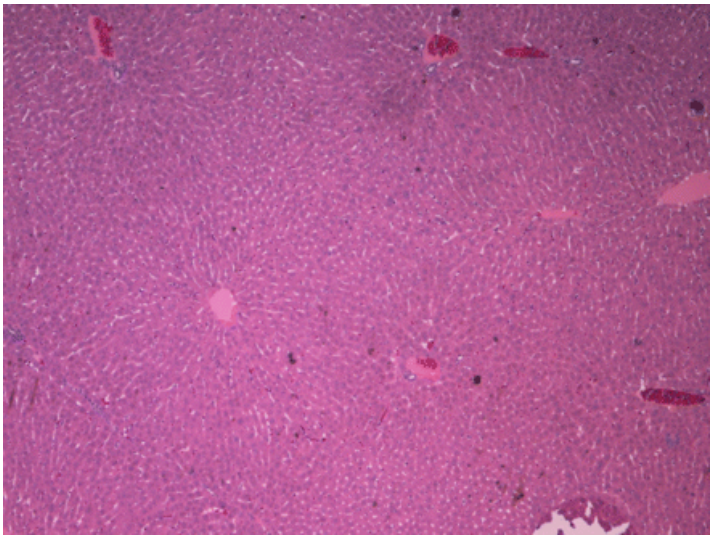

Figure 9.6 Hematoxylin and eosin slide of the liver tissue in a rabbit treated with 1.75 mM of 3-BrPA. The liver tissue shows no signs of toxicity.

REFERENCES

1) Warburg O (1956) On the origin of cancer cells. *Science* **123:** 309-314.
2) Shaw RJ (2006) Glucose metabolism and cancer. *Curr Opin Cell Biol* **18:** 598-608.
3) Gatenby RA and Gillies RJ (2007) Glycolysis in cancer: a potential target for therapy. *Int J Biochem Cell Biol* **39:** 1358-1366.
4) Ko YH, Pedersen PL, and Geschwind JF (2001) Glucose catabolism in the rabbit VX2 tumor model for liver cancer: characterization and targeting hexokinase. *Cancer Lett* **173:** 83-91.
5) Geschwind JF, Ko YH, Torbenson MS, Magee C, and Pedersen PL (2002) Novel therapy for liver cancer: direct intraarterial injection of a potent inhibitor of ATP production. *Cancer Res* **62:** 3909-3913.
6) Vali M, Liapi E, Kowalski J, Hong K, Khwaja A, Torbenson MS, Georgiades C, and Geschwind JF (2007) Intraarterial therapy with a new potent inhibitor of tumor metabolism (3-bromopyruvate): identification of therapeutic dose and method of injection in an animal model of liver cancer. *J Vasc Interv Radiol* **18:** 95-101.
7) Georgiades CS, Ramsey DE, Solomon S, and Geschwind JF (2001) New nonsurgical therapies in the treatment of hepatocellular carcinoma. *Tech Vasc Interv Radiol* **4:** 193-199.
8) Egawa H, Maki A, Mori K, Yamamoto Y, Mitsuhashi S, Bannai K, Asano K, and Ozawa K (1990) Effects of intra-arterial chemotherapy with a new lipophilic anticancer agent, estradiol-chlorambucil (KM2210), dissolved in lipiodol on experimental liver tumor in rats. *J Surg Oncol* **44:** 109-114.
9) Konno T (1990) Targeting cancer chemotherapeutic agents by use of lipiodol contrast medium. *Cancer* **66:** 1897-1903.
10) Park HS, Chung JW, Jae HJ, Kim YI, Son KR, Lee MJ, Park JH, Kang WJ, Yoon JH, Chung H, et al. (2007) FDG-PET for evaluating the antitumor effect of intraarterial 3-bromopyruvate administration in a rabbit VX2 liver tumor model. *Korean J Radiol* **8:** 216-224.
11) Wagner HN Jr (1993) Oncology: a new engine for PET/SPECT. Highlights of the Society of Nuclear Medicine annual meeting. *J Nucl Med* **34:** 13N-16N, 19N, 22N-29N.
12) Bomanji JB, Costa DC, and Ell PJ (2001) Clinical role of positron emission tomography in oncology. *Lancet Oncol* **2:** 157-164.
13) Bruix J and Sherman M (2005) Management of hepatocellular carcinoma. *Hepatology* **42:** 1208-1236.

14) Del Pozo AC and López P (2007) Management of hepatocellular carcinoma. *Clin Liver Dis* **11:** 305-321.
15) Gallagher BM, Fowler JS, Gutterson NI, MacGregor RR, Wan CN, and Wolf AP (1978) Metabolic trapping as a principle of oradiopharmaceutical design: some factors responsible for the biodistribution of [18F]2-deoxy-2-fluoro-D-glucose. *J Nucl Med* **19:** 1154-1161.
16) Kumar R, Nadig MR, and Chauhan A (2005) Positron emission tomography: clinical applications in oncology. Part 1. *Expert Rev Anticancer Ther* **5:** 1079-1094.
17) Fattovich G, Stroffolini T, Zagni I, and Donato F (2004) Hepatocellular carcinoma in cirrhosis: incidence and risk factors. *Gastroenterology* **127:** S35-S50.
18) Rous P, Kidd JG, and Smith WE (1952) Experiments on the cause of the rabbit carcinomas derived from virus-induced papillomas. II. Loss by the Vx2 carcinoma of the power to immunize hosts against the papilloma virus. *J Exp Med* **96:** 159-174.
19) Georges E, Breitburd F, Jibard N, and Orth G (1985) Two Shope papillomavirus-associated VX2 carcinoma cell lines with different levels of keratinocyte differentiation and transplantability. *J Virol* **55:** 246-250.
20) Nishizaki T, Matsumata T, Kanematsu T, Yasunaga C, and Sugimachi K (1990) Surgical manipulation of VX2 carcinoma in the rabbit liver evokes enhancement of metastasis. *J Surg Res* **49:** 92-97.

Addendum

SPECIFICITY OF THE ANTI-GLYCOLYTIC ACTIVITY OF 3-BROMOPYRUVATE CONFIRMED BY FDG UPTAKE IN A RAT MODEL OF BREAST CANCER

Buijs M, Vossen JA, Geschwind JF, Ishimori T, Engles JM, Acha-Ngwodo O, Wahl RL, Vali M.

Invest New Drugs 2009 Apr;27(2):120-3.

ABSTRACT

PURPOSE:
To evaluate the anti-glycolytic effects of 3-BrPA on rats bearing RMT mammary tumors, by determining FDG uptake after intravenous administration of the therapeutic dose.

MATERIALS AND METHODS:
Sixteen rats bearing RMT tumors were treated either with 15 mM 3-BrPA in 2.5 ml of PBS or with 2.5 ml of PBS. After treatment, all rats received FDG and were sacrificed 1 h later.

RESULTS:
3-BrPA treatment significantly decreased FDG uptake in tumors by 77% ($p = 0.002$). FDG uptake did not significantly decrease in normal tissues after treatment.

CONCLUSION:
Our study showed that 3-BrPA exhibits a strong anti-glycolytic effect on RMT cells implanted in rats.

INTRODUCTION

In the Western World breast cancer is the most common cancer in women and in this group it is the second leading cause of cancer death (after lung cancer) (1). Every year one or two women in every thousand will be newly diagnosed with breast cancer (2). Invasive ductal carcinoma accounts for 80% of these tumors, followed by lobular, tubular, medullary and other types (3). Approximately 50% of all patients develop metastatic breast cancer (4, 5). Once metastases have developed, conventional therapies, including surgery, radiation therapy and systemic chemotherapy have rather limited success in the treatment of human breast cancer, highlighting the need for the development of new therapeutics (6, 7).

Currently, breast cancer chemotherapeutics are administered predominantly through the systemic route. Although systemic administration is the most efficient route of delivery to cancers in many organs, it also frequently results in harmful side effects, by exposure of all healthy tissues to the delivered drugs (8). Therefore, to reduce systemic toxicity and increase survival, it is essential to establish new, selective treatment strategies for patients with breast cancer.

Wide spectrums of human cancers, such as breast cancer, fulfill the 'Warburg Hypothesis," which constitutes the basis for using glycolysis and its associated enzymes as targets for new anti-cancer agents (9, 10). 3-Bromopyruvate (3-BrPA) has shown to be a potent glycolytic inhibitor, both in vitro and in vivo (9, 11, 12). 3-BrPA abolishes ATP production and causes severe depletion of cellular ATP in hepatoma and leukemia cell lines (13, 14). We have previously shown that 3-BrPA has a significant therapeutic effect in the rabbit VX2 model of liver cancer (12, 15). The effects of 3-BrPA on breast cancer however, are still unknown.

The uptake of the glucose analogue ^{18}F-deoxyglucose (FDG) is clinically used in the oncology setting and based on the recognition that tumor cells have an increased glucose metabolism (16, 17). Increased FDG uptake is considered to be indicative of the presence of a metabolically active tumor, whereas lack of FDG uptake indicates tumor cell death.

The aim of this study was to evaluate the anti-glycolytic effects of 3-BrPA on rats bearing RMT mammary tumors, by determining FDG uptake after intravenous administration of the therapeutic dose.

MATERIALS AND METHODS

Animals

The study was approved by the Animal Care Committee of Johns Hopkins University and in compliance with institutional guidelines. 8–10 week old Lewis female rats (200–250 g) were kept in the animal housing facilities at least 1 week before the start of the experiments. Food and water were given ad libitum.

Dose–escalation Study

In order to determine the therapeutic dose of 3-BrPA for intravenous administration, a dose–escalation study was conducted in nontumor bearing rats (n = 21). Rats were divided into seven groups of three animals each and received incremental doses of 3-BrPA intravenously (5, 10, 15, 20, 25, 30 and 50 mM) in 2.5 ml of phosphate buffered saline (PBS). Drug induced toxicities were assessed daily by monitoring food intake, feces production and finally checking for signs of guarding or reluctance to move when touched. The weights of the rats were measured twice a week. Rats were euthanized 3 weeks after initiation of the treatment or when they became moribund or showed signs of distress (irregular behavior, lethargy, circling, or >20% weight loss).

After euthanization, all major organs were removed and weighed. The samples were fixed in 10% formalin, embedded in paraffin blocks, stained with hematoxylin–eosin and evaluated with a light microscope.

Tumor Model

Frozen rat mammary tumor (RMT) cells were thawed for implantation into 16 rats. These cells were provided by one of the authors (Wahl). The origin and in vitro and in vivo growth characteristics of these cells have been described previously (*18*). RMT cells (106 cells per rat) were implanted in the interscapular fat pad of the rats. The tumor was allowed to grow for 4 weeks in all rats before treatment was initiated.

3-BrPA Treatment and FDG Uptake Studies

All experiments were performed 8–10 days after tumor implantation. The rats were divided into two groups of eight animals each. Group 1 was treated intravenous with a concentration of 3-BrPA in 2.5 ml of PBS, which was 50% of the lethal dose based on the results of the dose escalation study; group 2 received an intravenous injection with 2.5 ml of PBS. 10 min after treatment, all rats received 200–300 μCi/200 μl of ^{18}F-Fluorodeoxyglucose (FDG) via the tail vein and were sacrificed 1 h after initiation of FDG administration. After sacrifice, blood, normal tissues (brain, heart, lung, liver, kidney, spleen, stomach, transverse colon and skeletal muscle) and tumor samples were obtained from each rat. The tissue samples were weighed and FDG uptake was evaluated using a gamma counter (LKB Wallac, Turku, Finland). To correct for radioactive decay and permit calculation of the concentration of radioactivity in each organ as a fraction of the administered dose, aliquots of the injected dose (ID) were counted simultaneously.

Subsequently the samples were transferred to scintillation vials, dissolved in 1 ml of Solvable solution (Perkin-Elmer, Inc., Wellesley, MA, USA), and color-treated with hydrogen peroxide. After adding scintillation fluid (10 ml; Ultima Gold, Perkin-Elmer, Inc., Wellesley, MA, USA), the samples were counted using a liquid scintillation counter. The results were expressed as the percentage of injected dose per gram of tissue (%ID/g).

Statistical Analysis

The data for the treatment group (%ID/g) were compared with the data for the control group (%ID/g) using the Mann–Whitney *U* Test. A p value < 0.05 was considered statistically significant.

RESULTS

Dose–escalation Study

Intravenous treatment with 3-BrPA was well tolerated in the groups receiving 5–20 mM. No deaths occurred in these groups and there was no evidence of clinical distress. Intravenous treatment of 25 mM 3-BrPA resulted in 25% weight loss in one of three animals. Analysis at necropsy confirmed the safety of the 5–25 mM doses, with all tissue samples

appearing healthy. Intravenous treatment of 30–50 mM 3-BrPA resulted in death within 15 min after administration in all animals. It was observed that all organs were normal at histopathologic analysis and that there was no evidence of corrosive effects of 3-BrPA even at that high dose. These results established 30 mM to be the lethal dose. Therefore, 15 mM was chosen as the dose for the 3-BrPA treatment and FDG uptake studies.

3-BrPA Treatment and FDG Uptake Studies

In all 16 rats a solid tumor developed within 28 days after implantation. The data on %ID/gram of tissue for both the treatment and control group are shown in Figure Add 1. The tumor tissue in the control group showed very high FDG uptake, the highest of all measured tissues. 3-BrPA treatment significantly decreased the FDG uptake in the tumor to 23% of the control value ($p = 0.002$). As expected, FDG uptake of all normal organs in the control group was highest in the brain, and did not show a statistically significant difference with the FDG uptake in the brain of 3-BrPA treated animals ($p = 0.28$). Animals receiving 3-BrPA treatment, exhibited a substantially higher uptake of FDG in both the liver and kidney when compared to the control group. The liver showed the highest difference, with FDG uptake being 126% higher in the treatment group ($p = 0.001$). FDG uptake in the kidney was 71% higher in the 3-BrPA treated animals, when compared to controls ($p = 0.01$). All other normal tissues did not show a statistically significant difference of FDG uptake between the two groups.

DISCUSSION

In the present study, we showed that 3-BrPA selectively targets tumor cells in the well established RMT rat model of breast cancer (19). Selective targeting was demonstrated by a significant lesser FDG uptake in the tumor tissue after 3-BrPA administration, when compared to uptake in the tumor tissue of control animals. All other healthy tissues did not show a significant decrease in FDG uptake, confirming the tumor specific targeting abilities of 3-BrPA.

To date, FDG is the most widely used tracer in oncologic PET (20). FDG is taken up into cells by glucose transporters and then phosphorylated by the enzyme hexokinase, the first enzyme of glycolysis. Tumor cells exhibit a high glycolytic rate, which explains the differential uptake of FDG

in different tumor tissues. Successful imaging has been reported in multiple human tumors such as cerebral gliomas, liver tumors, thyroid cancer and breast cancer (21, 22). Measurement of FDG uptake in tumors may not only assist in oncologic imaging, but can also be useful in the evaluation of the treatment effect of anti-glycolytic agents (23). Several studies showed that FDG may be used to study drug effects in vitro (24, 25). Our study further validated this principle in vivo, by showing lesser FDG uptake after 3-BrPA treatment, which was specific for tumor tissue.

3-BrPA, a synthetic brominated derivate of pyruvic acid acts as an irreversible inhibitor of metabolic enzymes associated with glycolysis. 3-BrPA has shown great promise in a number of cancer cell lines and preclinical studies (12, 26). When glycolysis is inhibited, the intact mitochondria in normal cells enable them to use alternative energy sources such as fatty acids and amino acids to produce metabolic intermediates channeled to the tricarboxylic acid (TCA) cycle for ATP production. Therefore, normal cells are expected to be less sensitive to 3-BrPA. Our study confirmed this relative sparing of healthy tissues, by showing no significant decrease in FDG uptake after treatment with 3-BrPA in all measured non tumorous tissues.

Interestingly, liver and kidney tissue showed a higher FDG uptake after administration of 3-BrPA when compared to control. A biodistribution study of [^{14}C]-labeled 3-BrPA from our group indicated an important role for the liver and kidney in the excretion of 3-BrPA (unpublished data). One possible explanation may be that clearance requires higher energy levels, thereby resulting in higher glucose demand and thus FDG uptake. It is important to note, however that administration of 3-BrPA did not result in a significant lower FDG uptake, confirming that 3-BrPA does not influence glucose metabolism of healthy tissues.

Our results are promising and may contribute to the translation of 3-BrPA towards the clinic. Before taking these important steps however, a number of additional factors, besides the inherent differences in tumor response between animals and humans, need to be considered. First, the survival benefits of 3-BrPA for breast cancer should be investigated in an appropriate animal model with a sufficient sample size. Second, since most breast cancer deaths are related to metastatic spread, further experiments should take this into account.

CONCLUSION

In conclusion, our study showed that 3-BrPA exhibits a strong anti-glycolytic effect on RMT cells implanted in rats. This effect was demonstrated by decrease in FDG uptake in tumor tissue after treatment with 3-BrPA. The absence of this decrease in healthy tissues confirmed the specific tumor targeting of 3-BrPA.

TABLES & FIGURES

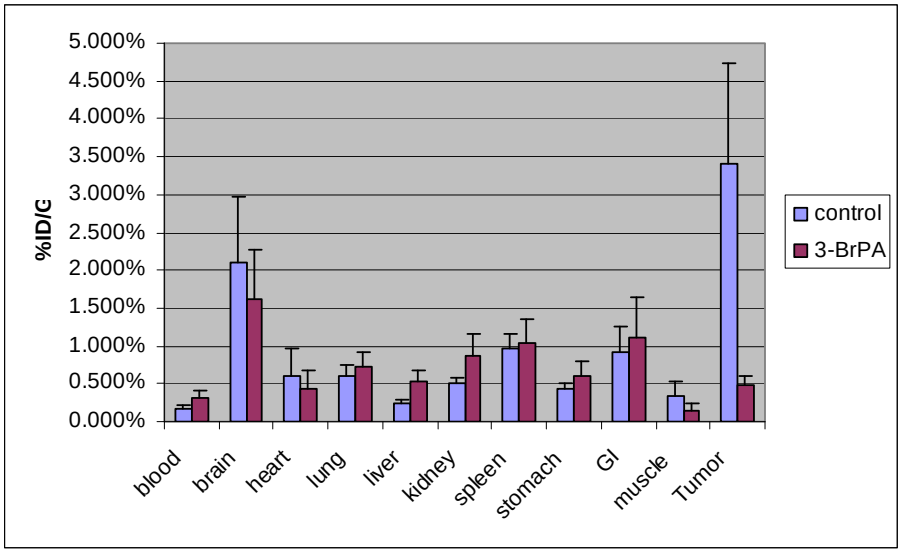

Figure Add 1 FDG uptake in rat tissues after i.v. administration of 2.5 ml PBS (control) or 15 mM 3-BrPA in 2.5 ml of PBS.

REFERENCES

1) Jemal A, Siegel R, Ward E et al (2008) Cancer statistics, 2008. CA Cancer J Clin 58:71–96
2) Dumitrescu RG, Cotarla I (2005) Understanding breast cancer risk—where do we stand in 2005? J Cell Mol Med 9:208–221
3) Louwman MW, Vriezen M, van Beek MW et al (2007) Uncommon breast tumors in perspective: incidence, treatment and survival in The Netherlands. Int J Cancer 121:127–135
4) Elias D, Pietroantonio DD (2006) Surgery for liver metastases from breast cancer. HPB Oxf 8:97–99
5) Perez EA (1999) Current management of metastatic breast cancer. Semin Oncol 26:1–10
6) Anderson DM, Rolnick SJ, Jackson J, Amundson J, Asche SE, Loes LM (2007) Impact of chemotherapy in women with metastatic breast cancer diagnosed 1990–2003. Clin Breast Cancer 7:801–803
7) Rabbani SA, Mazar AP (2007) Evaluating distant metastases in breast cancer: from biology to outcomes. Cancer Metastasis Rev 26:663–674
8) Trotti A, Colevas AD, Setser A et al (2003) CTCAE v3.0: development of a comprehensive grading system for the adverse effects of cancer treatment. Semin Radiat Oncol 13:176–181
9) Geschwind JF, Georgiades CS, Ko YH, Pedersen PL (2004) Recently elucidated energy catabolism pathways provide opportunities for novel treatments in hepatocellular carcinoma. Expert Rev Anticancer Ther 4:449–457
10) Isidoro A, Casado E, Redondo A et al (2005) Breast carcinomas fulfill the Warburg hypothesis and provide metabolic markers of cancer prognosis. Carcinogenesis 26:2095–2104
11) Shin SW, Han H, Choo SW et al (2006) Hepatic intra-arterial injection of 3-bromopyruvate in rabbit VX2 tumor. Acta Radiol 47:1036–1041
12) Vali M, Liapi E, Kowalski J et al (2007) Intraarterial therapy with a new potent inhibitor of tumor metabolism (3-bromopyruvate): identification of therapeutic dose and method of injection in an animal model of liver cancer. J Vasc Interv Radiol 18:95–101
13) Ko YH, Pedersen PL, Geschwind JF (2001) Glucose catabolism in the rabbit VX2 tumor model for liver cancer: characterization and targeting hexokinase. Cancer Lett 173:83–91
14) Xu RH, Pelicano H, Zhou Y et al (2005) Inhibition of glycolysis in cancer cells: a novel strategy to overcome drug resistance associated

with mitochondrial respiratory defect and hypoxia. Cancer Res 65:613–621
15) Kim W, Yoon JH, Jeong JM et al (2007) Apoptosis-inducing antitumor efficacy of hexokinase II inhibitor in hepatocellular carcinoma. Mol Cancer Ther 6:2554–2562
16) Tatsumi M, Cohade C, Mourtzikos KA, Fishman EK, Wahl RL (2006) Initial experience with FDG-PET/CT in the evaluation of breast cancer. Eur J Nucl Med Mol Imaging 33:254–262
17) Delbeke D (1999) Oncological applications of FDG PET imaging. J Nucl Med 40:1706–1715
18) Ethier SP, Cundiff KC (1987) Importance of extended growth potential and growth factor independence on in vivo neoplastic potential of primary rat mammary carcinoma cells. Cancer Res 47:5316–5322
19) Wahl RL, Henry CA, Ethier SP (1992) Serum glucose: effects on tumor and normal tissue accumulation of 2-[F-18]-fluoro-2-deoxy-D-glucose in rodents with mammary carcinoma. Radiology 183:643–647
20) Margolis DJ, Hoffman JM, Herfkens RJ, Jeffrey RB, Quon A, Gambhir SS (2007) Molecular imaging techniques in body imaging. Radiology 245:333–356
21) Avril N, Menzel M, Dose J et al (2001) Glucose metabolism of breast cancer assessed by 18F-FDG PET: histologic and immunohistochemical tissue analysis. J Nucl Med 42:9–16
22) Endo K, Oriuchi N, Higuchi T et al (2006) PET and PET/CT using 18F-FDG in the diagnosis and management of cancer patients. Int J Clin Oncol 11:286–296
23) Pantaleo MA, Nannini M, Maleddu A et al (2008) Conventional and novel PET tracers for imaging in oncology in the era of molecular therapy. Cancer Treat Rev 34:103–121
24) Minn H, Kangas L, Knuutila V, Paul R, Sipila H (1991) Determination of 2-fluoro-2-deoxy-D-glucose uptake and ATP level for evaluating drug effects in neoplastic cells. Res Exp Med (Berl) 191:27–35
25) Yamada K, Brink I, Bisse E, Epting T, Engelhardt R (2005) Factors influencing [F-18] 2-fluoro-2-deoxy-D-glucose (F-18 FDG) uptake in melanoma cells: the role of proliferation rate, viability, glucose transporter expression and hexokinase activity. J Dermatol 32:316–334
26) Geschwind JF, Ko YH, Torbenson MS, Magee C, Pedersen PL (2002) Novel therapy for liver cancer: direct intraarterial injection of a potent inhibitor of ATP production. Cancer Res 62:3909–3913

PART III:
ADVANCES IN IMAGING OF LIVER LESIONS

CHAPTER 10

RECEIVER OPERATING CHARACTERISTIC ANALYSIS OF DIFFUSION-WEIGHTED MAGNETIC RESONANCE IMAGING IN DIFFERENTIATING HEPATIC HEMANGIOMA FROM OTHER HYPERVASCULAR LIVER LESIONS

Vossen JA, Buijs M, Liapi E, Eng J, Bluemke DA, Kamel IR

J Comput Assist Tomogr 2008 Sep-Oct;32(5):750-6.

ABSTRACT

PURPOSE:
To evaluate the role of diffusion-weighted imaging in differentiating between hepatic hemangiomas, both typical and atypical, and other hypervascular liver lesions.

MATERIALS AND METHODS:
Retrospective review of 182 hypervascular liver lesions in 117 patients was performed. Diffusion and contrast-enhanced magnetic resonance imaging were performed using a 1.5-T unit. Imaging protocol consisted of T2-weighted fast spin-echo images, breath-hold diffusion-weighted echoplanar images, and breath-hold unenhanced and contrast-enhanced T1-weighted three-dimensional fat-suppressed spoiled gradient-echo images in the arterial phase (20 seconds) and portal venous phase (60 seconds). Signal intensity changes and apparent diffusion coefficient (ADC) values were evaluated for all lesions. Unpaired t test was used to compare the mean ADC values for different lesions, and statistical significance was set at $p < 0.01$. Receiver operating characteristic analysis was used to determine the accuracy of diffusion-weighted imaging in differentiating hemangiomas from other hypervascular liver lesions.

RESULTS:
Lesions included typical and atypical hemangioma (n = 38), hepatocellular carcinoma (HCC; n = 58), focal nodular hyperplasia (FNH; n = 22), and neuroendocrine tumor metastasis (NET; n = 64) with a mean tumor size of 5.3 cm. Mean ADC value for hemangioma, HCC, FNH, and NET was 2.29×10^{-3}, 1.55×10^{-3}, 1.65×10^{-3}, and 1.43×10^{-3} mm^2/sec, respectively. There was a statistically significant difference in the ADC value of hemangioma compared with that of FNH ($p < 0.001$), HCC ($p < 0.001$), and NET ($p < 0.001$), respectively. The area under the receiver operating characteristic curve was 0.91.

CONCLUSION:
Diffusion-weighted magnetic resonance imaging and ADC maps can provide rapid quantifiable information to differentiate typical and atypical hemangiomas from other hypervascular liver lesions.

INTRODUCTION

Diffusion-weighted (DW) magnetic resonance (MR) imaging and apparent diffusion coefficient (ADC) values map the thermally induced motion of water molecules in biologic tissues, known as Brownian motion, and are thereby able to provide insight into tumor microstructure (1, 2). The motion includes not only molecular diffusion of water but also microcirculation of blood (microperfusion). The primary application of diffusion-weighted imaging (DWI) has been in brain imaging (3-5). More recently, DWI has been used to characterize focal hepatic lesions (6-10). However, the accuracy of DWI in the differentiation between hepatic hemangioma and other hypervascular lesions remains unknown.

Hemangioma is the most common benign hepatic tumor, occurring in 5% to 20% of the population (11, 12). Typical hemangiomas are less than 3 cm in size and are usually spheroid or ovoid. On nonenhanced computed tomography (CT) images, hemangiomas typically appear as a low attenuating lesion (13, 14). On T1-weighted MR images, hemangiomas characteristically appear as hypointense lesions, and on T2-weighted MR images, they are extremely hyperintense. After administration of an intravenous contrast, CT and dynamic MR imaging demonstrate peripheral nodular enhancement in the early phase. Venous-phase imaging shows centripetal enhancement that progresses to uniform filling. This enhancement persists on delayed-phase images (15, 16).

Although atypical hemangiomas are less common, they are clinically important, because their differential diagnosis includes a large variety of liver tumors (17). Clinically relevant atypical hemangiomas include large heterogeneous hemangiomas, calcified hemangiomas, pedunculated hemangiomas, and hemangiomas developing in diffuse fatty liver (5, 18-20). On imaging, these atypical hemangiomas may resemble malignant liver lesions, such as hepatocellular carcinoma (HCC), hypervascular liver metastases, or occasionally, other benign lesions such as focal nodular hyperplasia (FNH).

It is essential for physicians to accurately differentiate between hemangiomas and other liver lesions to determine future therapy and prognosis. Presently, CT and MR imaging are the mainstay for detection and characterization of liver tumors (21-27). It has been reported that contrast-enhanced MR imaging is more sensitive in detecting and more

useful in characterizing focal hepatic lesions than CT (28-31). However, there is a growing interest in the role of DWI in characterizing hepatic lesions.

Therefore, the aim of this study was to perform receiver operating characteristic (ROC) analysis of the accuracy of DWI in the differentiation between hepatic hemangiomas and other hypervascular liver lesions more than 1 cm in size.

MATERIALS AND METHODS

Patients

Between January 2003 and January 2005, we reviewed all patients with MR imaging studies performed for the characterization of 1 or more liver lesions. The following patients were included in our study: (1) those who had 1 or more hypervascular liver lesions, including hemangioma, FNH, HCC, and hypervascular liver metastases; (2) those who had liver lesions with the size of more than 1 cm to be detected by DWI. The confirmation criteria for typical hemangioma were characteristic findings on dynamic-enhanced MR imaging (high signal intensity on T2-weighted images and marked and progressive nodular enhancement) with a minimum of 1 year of follow-up, showing stability in size and morphology. The confirmation criteria for atypical hemangioma were pathological proof or dynamic-enhanced MR imaging with a minimum of 2 years of follow-up, showing stability in size and morphology. The confirmation criteria for FNH were typical findings on MR imaging (ie, isointensity on T1- and T2-weighted images with a central scar, homogeneous enhancement in the hepatic arterial phase, and isointense to the liver in the portal venous phase). The confirmation criteria for FNH presenting without a central scar were stability in size and morphology (ie, isointensity on T1- and T2-weighted images, homogeneous enhancement in the hepatic arterial phase, and isointense to the liver in the portal venous phase) for more than 2 years or tissue biopsy. The diagnosis of HCC was based on either histology obtained by needle biopsy or a single hypervascular lesion on MR imaging in addition to an alpha-fetoprotein level greater than 400 in a cirrhotic patient. All hypervascular metastases were diagnosed by biopsy of a representative liver lesion. This retrospective review was approved by our institutional review board. One experienced MR radiologist not involved in the image analysis reviewed the clinical reports, collected demographic information,

histopathologic, and imaging findings, and identified 117 patients who met the inclusion criteria. Up to 5 lesions per patient were evaluated, resulting in a total of 182 lesions.

MRI Technique

Patients were scanned using a 1.5-T MRI scanner (CV/i; GE Healthcare, Milwaukee, WI) and a phased-array torso coil. Imaging protocol included T2-weighted fast spin-echo images (matrix, 256 × 256; slice thickness, 8 mm; interslice gap, 2 mm; repetition time [TR]/ echo time [TE], 5000/100 msec; receiver bandwidth, 32 kHz), breath-hold diffusion-weighted echoplanar images (matrix, 128 × 128; slice thickness, 8 mm; interslice gap, 2 mm; b value, 500 mm^2/sec; TR/TE, 5000-6500/110 msec; receiver bandwidth, 32 kHz), and breath-hold unenhanced and contrast-enhanced (0.1 mmol/kg intravenous gadodiamide [Omniscan; GE Healthcare, Princeton, NJ]) T1-weighted three-dimensional fat-suppressed spoiled gradient-echo images (field of view, 320-400 mm; matrix, 192 × 160; slice thickness, 4-6 mm TR/TE, 5.1/1.2 msec; receiver bandwidth, 64 kHz; flip angle, 15º) in the arterial (20 seconds) and portal venous (60 seconds) phases.

Image Analysis

Magnetic resonance image processing and ADC maps were generated using a commercially available Advantage Windows workstation (GE Healthcare, Milwaukee, WI). Images were interpreted by consensus of 2 experienced MR radiologists, who were blinded to the diagnosis at the time of evaluation of the DW images. The reviewers were not provided with the conventional images. Parameters evaluated included signal intensity changes and ADC values. For patients with more than 1 lesion, all lesions of 1 cm or larger were evaluated, up to a maximum of 5 lesions to ensure independent sampling. Apparent diffusion coefficient maps were generated from the DW images, and values were recorded by placing a region of interest over the entire lesion, as seen on the image with the largest lesion size.

Statistical Analysis

Statistical analysis was performed with the Stata software package (Version 8; Stata, College Station, TX). Mean ADC values of the 4 lesion types (hemangioma, HCC, FNH, neuroendocrine tumor metastasis [NET])

were compared with multinomial logistic regression using robust variance estimation to account for potential correlation of multiple lesions within the same patient. Mean ADC values of classic versus atypical hemangiomas were compared with an unpaired t test. $P < 0.01$ was considered statistically significant. An ROC curve was constructed to summarize the trade-off between sensitivity and specificity of different threshold ADC values that may be chosen to separate hemangiomas from the other lesion types. The nonparametric (trapezoidal rule) area under the ROC curve was calculated to represent the overall accuracy.

RESULTS

Demographic Information

General information for all 117 patients (68 men and 49 women) is shown in Table 10.1. A total of 182 hypervascular lesions were evaluated. The mean number of evaluated lesions per patient was 1.5 (range, 1-5). The lesions were diagnosed as either hemangioma (n = 38), HCC (n = 58), FNH (n = 22), or NET (n = 64). Mean tumor size on MR imaging was 5.3 cm (range, 1.0-17.8 cm).

Findings on MR Imaging

A total of 25 hemangiomas had characteristic findings on unenhanced (high signal intensity on T2-weighted images) and dynamic-enhanced (marked and progressive nodular enhancement) MR imaging (Fig 10.1) and remained stable in size and morphology at 1 year. The remaining 13 hemangiomas were classified as atypical, 7 were diagnosed as giant (>4cm) hemangiomas on MR imaging, and the remaining 6 hemangiomas had an atypical enhancement pattern. Four of 6atypical lesions did not fill on delayed images (Fig 10.2), and 2lesions showed complete filling in the arterial phase (flash filling) that persisted on delayed images (Fig 10.3). The diagnosis was confirmed histologically in 2 of 13 atypical lesions. The remaining 11 lesions remained stable on MR imaging at 2 years.

All NETs were hyperintense on T2-weighted images and were hypervascular in the arterial phase. All FNH lesions showed homogeneous enhancement in the arterial phase and became isointense to the liver in the portal venous phase. A central scar that was bright on T2 was present in 14 (64%) of 22 lesions. Thirty-seven (64%) of 58 HCCs were found in patients

with underlying cirrhosis. The remaining 21 lesions (36%) developed in noncirrhotic livers. In these patients, biopsy confirmed the diagnosis of HCC.

Findings on DW MR Imaging

On DW MR imaging, all 38 hemangiomas (100%) were markedly hyperintense compared to surrounding liver parenchyma. Most HCC lesions (n = 45; 78%) were slightly hyperintense relative to the surrounding liver parenchyma. The remaining lesions were either markedly hyperintense (10 lesions; 17%) or isointense (3 lesions; 5%) to surrounding liver parenchyma. Of 22 FNH lesions, 20 were slightly hyperintense, and 2 were isointense to surrounding liver parenchyma. All except for 1 of NETs were markedly hyperintense (Table 10.2).

After drawing a region of interest on the ADC maps, the mean ADC value for hemangioma, HCC, FNH, and NET was 2.29×10^{-3}, 1.55×10^{-3}, 1.65×10^{-3}, and 1.43×10^{-3} mm^2/sec, respectively (Table 10.3). Multinomial logistic regression demonstrated a statistically significant difference between ADC values for hemangiomas and all other hypervascular lesions (FNH, HCC, and NET) ($p < 0.001$). Statistical significance was maintained even when considering classic and atypical hemangiomas separately. No statistically significant difference was found between the ADC values of classic hemangiomas and of atypical ones ($p = 0.99$). No statistically significant difference was found between the ADC values of HCC in cirrhotic and those of noncirrhotic livers ($p = 0.38$).

Furthermore, ROC analysis demonstrated an area under the curve of 0.91, indicating that DW MR imaging is good at correctly classifying hemangiomas from the other hypervascular liver lesions (Fig 10.4). As in all tests summarized by an ROC curve, the optimum operating point (sensitivity-specificity pair) along the ROC curve will depend on the particular clinical circumstances and the utilities assigned to the possible clinical outcomes. Scatterplot of the ADC values of all lesions is shown in Figure 10.5. Apparent diffusion coefficient values were very accurate when a threshold value of 2.30×10^{-3} mm^2/sec was used, correctly categorizing 21 (55%) of 38 hemangiomas, and missing no other hypervascular liver lesions with a sensitivity of 55% (confidence interval [CI], 38%-71%), a specificity of 100% (CI, 97%-100%), a positive predictive value of 100% (CI, 81%-100%), and a negative predictive value of 89% (CI, 83%-94%). A threshold of 2.00×10^{-3} mm^2/sec included 29 of 38 hemangiomas, but misclassified 4

NET, 1 HCC, and 1 FNH, if only the ADC values were considered in the diagnosis, with a sensitivity of 76% (CI, 59%-88%), a specificity of 96% (CI, 91%-98%), a positive predictive value of 83% (CI, 66%-93%), and a negative predictive value of 94% (CI, 88%-97%). All lesions with an ADC value below 1.17×10^{-3} mm^2/sec were malignant.

DISCUSSION

Diffusion is the random microscopic translation motion of water molecules, known as Brownian motion. By applying 2 motion-probing gradients before and after the 180-degree pulse, MR imaging can be made sensitive to the diffusion of water molecules in tissue. The combined motion effects of both capillary perfusion and diffusion are quantified by means of the ADC value (32). The initial applications of DW MR imaging have been in brain imaging, mainly for the evaluation of acute ischemic stroke, intracranial tumors, and demyelinating disease (33,34). The ultrafast echoplanar imaging technique has broadened the clinical use of DW MR imaging to other organs, such as the liver. Several studies showed that DWI can be used to identify and characterize focal hepatic lesions (9, 10, 35, 36).

Because of the high prevalence of hemangiomas in the general population, differentiation between hemangiomas and other hypervascular liver lesions is of great clinical importance. Several techniques of image acquisition and analysis have been used to evaluate liver lesions. These techniques include dynamic contrast-enhanced imaging and moderately T2-weighted SE images, heavily T2-weighted SE images, moderately T2-weighted fast SE images, and dual-echo images, performed with conventional SE, half Fourier-acquired single-shot turbo SE (HASTE), and echoplanar imaging (26). In the evaluation of T2-weighted images, both quantitative and qualitative analyses may be used (37-40). However, the quantitative measurement of T2 relaxation times is significantly better than that of the subjective visual assessment, resulting in a more accurate differentiation between hepatic lesions. However, the value of DWI is not yet established.

Although most hemangiomas have typical imaging characteristics, atypical hemangiomas are clinically important, because they often resemble malignant liver lesions. Heterogeneous giant hemangiomas (>4 cm in diameter) have a differential diagnosis that includes all malignant liver lesions with a scar, such as FNH and HCC (18). Diffuse fatty infiltration of

the liver may alter the typical appearance of hepatic lesions including hemangioma (20). With progressive cirrhosis, hemangiomas are likely to decrease in size and become more fibrotic (41).

Focal nodular hyperplasia is the second most common benign hepatic tumor (11). On MR imaging, FNH is usually isointense on T1-weighted images and slightly hyperintense on T2-weighted images. A central scar, which is typical for FNH, can be seen on T1- and T2-weighted images. On contrast-enhanced MR imaging, because of their prominent vascularity, FNH lesions tend to enhance homogeneously with marked hyperintensity in the hepatic arterial phase and usually become isointense to liver parenchyma in the portal venous phase (42).

Hepatocellular carcinoma is the fifth most common cancer in the world and represents more than 5% of all cancers (43). On T1-weighted MR images, HCC is frequently observed as hypointense, but depending on fat content, copper deposition, and protein content, it can range from hypointense to hyperintense. On T2-weighted images, HCC is normally observed as hyperintense. After administration of a contrast, enhancement in the arterial phase and heterogeneous washout in the portal venous phase are typical findings for HCC (44). Hepatocellular carcinoma developing in a cirrhotic liver is commonly seen and easily recognized by radiologists. However, HCC occurring in a noncirrhotic liver may be difficult to distinguish from other hypervascular liver lesions and therefore, DW imaging may be of value in such cases (45, 46).

The aim of our study was to assess the usefulness of DW MR imaging in this serious matter. In our study, we tested the accuracy of DW MR imaging in differentiating between hemangiomas and other relatively common hypervascular liver lesions, including FNH, HCC, and hypervascular liver metastases. There are several advantages for using DW sequences over conventional acquisitions. These echoplanar acquisitions are obtained in a breath-hold, and the ADC values generated provide quantifiable information that can be statistically analyzed. Moreover, this information is independent on the dynamics of contrast enhancement, and therefore can be easily reproduced. Furthermore, DWI can be used in those patients where contrast images cannot be obtained. An important category of patients for whom the use of intravenous contrast is contraindicated are those patients with nephrogenic systemic fibrosis. In these patients, T2 images alone can prove difficult to interpret, and adding DW imaging would improve diagnostic success. Our results showed that the difference between

ADC values for hemangioma and for all other evaluated hypervascular lesions was statistically significant ($p < 0.001$). However, our results slightly differed from those found by Quan et al and Sun et al (10, 47). These differences might be explained by the fact that the generated ADC values are equipment-specific. Furthermore, the ROC analysis showed an area under the curve of 0.91 for differentiating hemangioma from all other observed hypervascular liver lesions, indicating that DW MR imaging can be of great value. On the basis of the ADC measurements, we can expect certain sensitivity and specificity in making the diagnosis of hemangioma. In our study, the ADC values were very accurate when a threshold value of 2.30×10^{-3} mm^2/sec was used, correctly categorizing 21 (55%) of 38 hemangiomas, and missing no other hypervascular liver lesions with a sensitivity of 55% (CI, 38%-71%), a specificity of 100% (CI, 97%-100%), a positive predictive value of 100%(CI, 81%-100%), and a negative predictive value of 89% (CI, 83%-94%). A threshold of 2.00×10^{-3} mm^2/sec included 29 of 38 hemangiomas, but misclassified 4 NET, 1 HCC, and 1 FNH, if only the ADC values were considered in the diagnosis, with a sensitivity of 76% (CI, 59%-88%), a specificity of 96% (CI, 91%-98%), a positive predictive value of 83% (CI, 66%-93%), and a negative predictive value of 94% (CI, 88%-97%). All lesions with an ADC value below 1.17×10^{-3} mm^2/sec were malignant (Fig 11.5).

In our study, we included both typical hemangiomas and atypical hemangiomas. Atypical hemangiomas mimic other malignant liver lesions and are therefore difficult to characterize. However, atypical hemangiomas were not statistically different from atypical hemangiomas in ADC values ($p = 0.99$). Our results are in line with previous studies, which concluded that DW MR imaging is useful in the diagnosis and differentiation of focal hepatic lesions, such as distinguishing cavernous hemangioma from hepatic cysts and hepatic abscess from cystic or necrotic tumor (10, 48-50). To our knowledge, however, this study was the first to use ROC analysis in assessing DW MR imaging.

This study has several limitations. First, it was a retrospective study. However, readers were blinded to the diagnosis, and there was extended follow-up (up to 2 years) to confirm the diagnosis. Second, not all lesions were histopathologically verified, because this is not usually clinically appropriate. In typical cases, histopathology is not needed to confirm the diagnosis of benign lesions. In HCC, typical imaging findings and a markedly raised alpha-fetoprotein level (>400) can be considered

diagnostic. Third, we did not include hepatic adenomas in our study; however, we feel that this is of less clinical importance, because they are very rare and they may contain fat and are associated with a history of oral contraceptives (51). In addition, we only included NET because they are typically hypervascular, and therefore may represent all other hypervascular liver metastases. Last, the ADC values generated in this study are equipment-specific and may not be applicable to different vendors and various b values that may be used. Additional studies are warranted to verify these findings using various b values and different MR units.

CONCLUSIONS

We conclude that DW MR imaging and ADC maps have a potential role in the differentiation of typical and atypical hemangiomas from other hypervascular liver lesions. They provide fast and quantifiable information, independent of contrast dynamics. This information can potentially be useful when overlap between different lesions on conventional MR imaging exists.

TABLES & FIGURES

Characteristics	Value
No. patients	117
Age, mean (range), yrs	55 (14-87)
Sex, male/female	68/49
No. lesions, mean (range)	1.5 (1-5)
Size of lesions, mean (range), cm	5.3 (1.0-17.8)
Hemangioma	3.4 (1.0-12.0)
HCC	6.7 (1.5-17.8)
FNH	4.2 (1.0-9.4)
NET	5.6 (2.0-17.0)

Table 10.1 Patient Demographics.

	Signal Intensity		
Diagnosis, No. Lesions	Very Hyperintense	Slightly Hyperintense	Isointense
Hemangioma, n = 38	38	0	0
HCC, n = 58	10	45	3
FNH, n = 22	0	20	2
NET, n = 64	63	0	1

Table 10.2 Signal Intensity of the Lesions Relative to the Surrounding Liver Parenchyma on Diffusion-Weighted MR Images (b = 500).

Diagnosis	Mean	SD	P (compared to Hemangioma)
Hemangioma	2.29×10^{-3}	5.1×10^{-4}	NA
Typical	2.29×10^{-3}	5.6×10^{-4}	
Atypical	2.29×10^{-3}	3.9×10^{-4}	
HCC	1.55×10^{-3}	2.2×10^{-4}	<0.001
Cirrhotic	1.55×10^{-3}	2.4×10^{-4}	<0.001
Noncirrhotic	1.57×10^{-3}	2.1×10^{-4}	<0.001
FNH	1.65×10^{-3}	2.6×10^{-4}	<0.001
NET	1.43×10^{-3}	3.9×10^{-4}	<0.001

Table 10.3 Apparent diffusion coefficient (ADC) values (mm^2/sec) of the lesions. NA indicates not applicable.

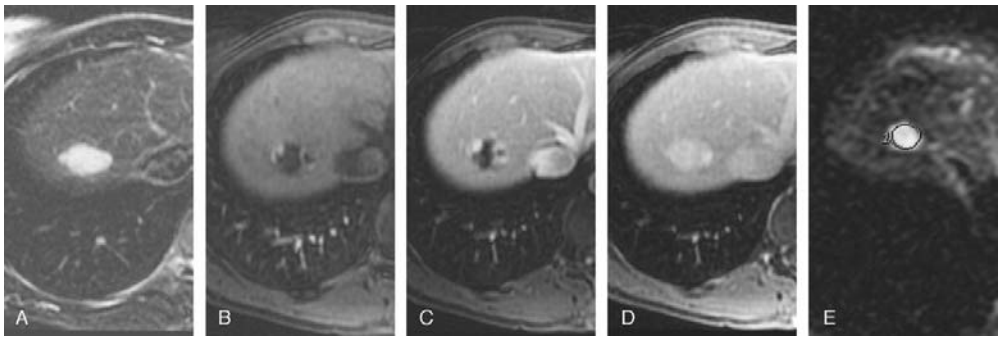

Figure 10.1 Typical hemangioma in a 41-year-old woman. T2-weighted image (T_R/T_E, 5000:100 milliseconds) with fat suppression shows a hyperintense lesion in the right lobe (A). Transverse dynamic fat-suppressed T1-weighted MR images (T_R/T_E, 5.1:1.2 milliseconds) of this lesion show peripheral nodular enhancement in the hepatic arterial phase (B), centripetal enhancement in the portal venous phase (C), progressing into complete uniform filling in the delayed phase (D). Diffusion-weighted image (b = 500; T_R/T_E, 6500:110 milliseconds) shows a bright lesion with an ADC value of 2.14×10^{-3} mm^2/sec (E).

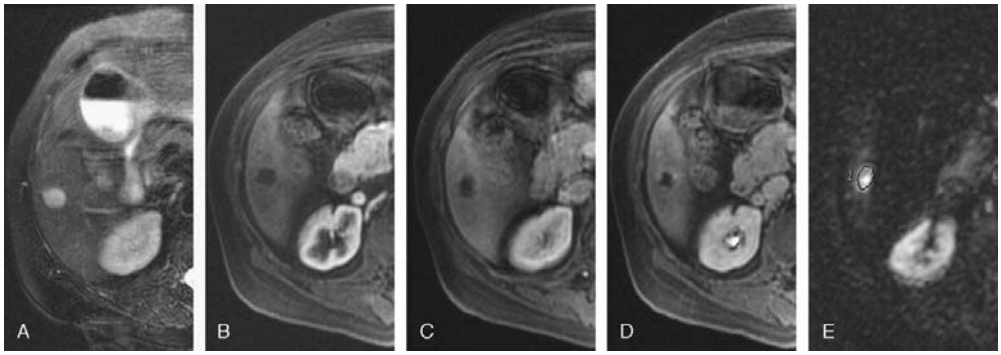

Figure 10.2 Atypical hemangioma in a 71-year-old man. T2-weighted images (T_R/T_E, 5000:100 milliseconds) with fat suppression show a hyperintense lesion in the right lobe (A). Transverse dynamic fat-suppressed T1-weighted MR images (T_R/T_E, 5.1:1.2 milliseconds) of this lesion after contrast administration show no enhancement in the arterial (B) and venous (C) phases and minimal peripheral nodular in the delayed phase (D). Diffusion-weighted MR image (b = 500; T_R/T_E, 6500:110 milliseconds) shows a bright lesion (E). The ADC value was 2.00×10^{-3} mm^2/sec for this lesion. The lesion remained stable for 2 years.

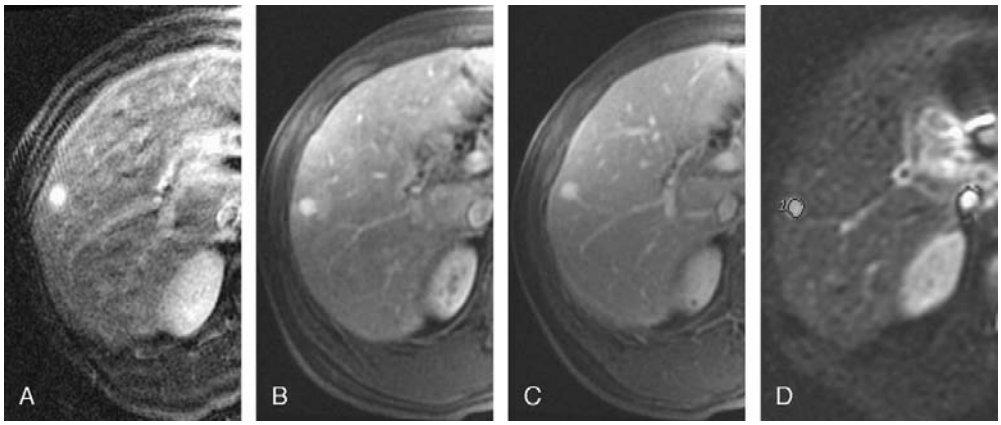

Figure 10.3 Atypical hemangioma in a 42-year-old man. T2-weighted images (T_R/T_E, 5000:100 milliseconds) with fat suppression show a hyperintense lesion in the right lobe (A). Transverse dynamic fat-suppressed T1-weighted MR image (T_R/T_E, 5.1:1.2 milliseconds) of this lesion shows flash filling in the arterial phase (B) and follows the blood pool in the portal venous phase (C). Diffusion-weighted MR image (b = 500; T_R/T_E, 6500:110 milliseconds) shows a bright lesion (D). The ADC value was 3.08×10^{-3} mm^2/sec for this hemangioma.

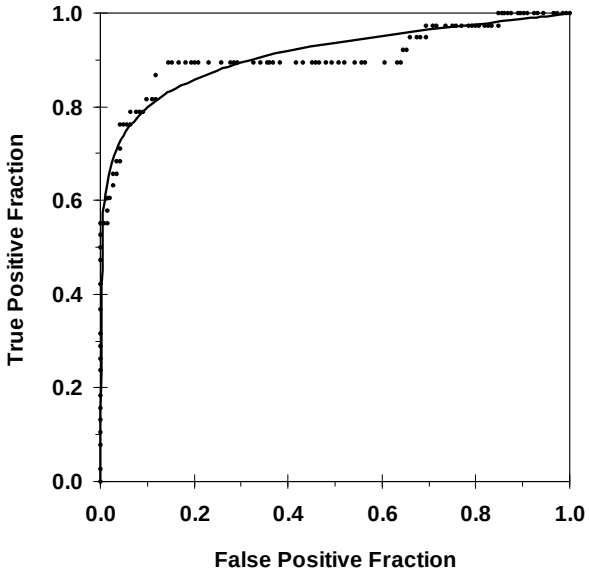

Figure 10.4 Receiver operating characteristic curve and fitted ROC curve with an area under the ROC curve of 0.91.

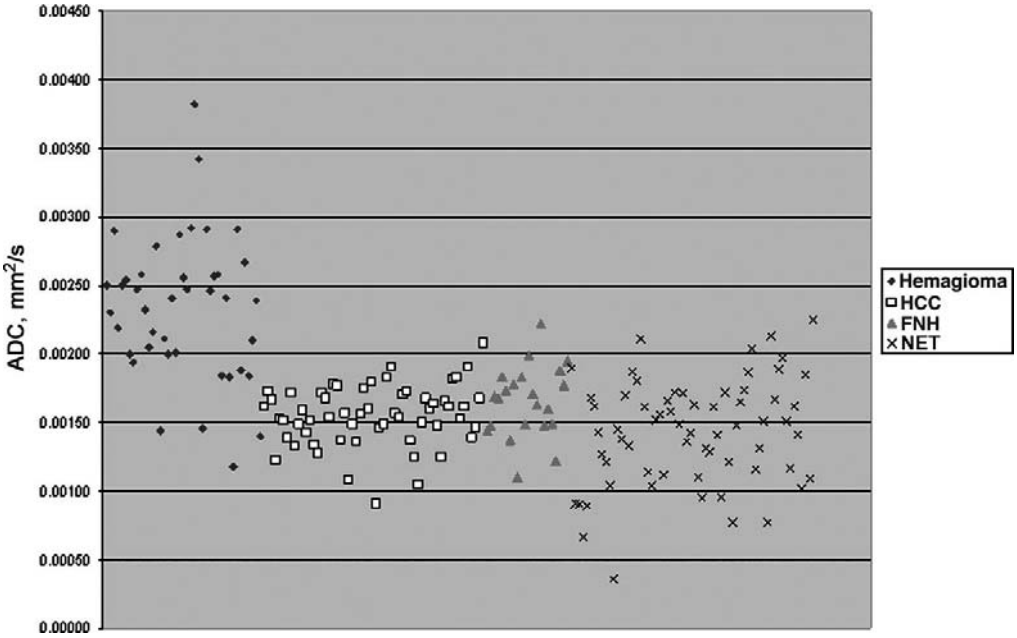

Figure 10.5 Scatterplot of the ADC values of malignant and benign focal hepatic lesions obtained with DW MR imaging.

REFERENCES

1) Le Bihan D, Breton E, Lallemand D, et al. MR imaging of intravoxel incoherent motions: application to diffusion and perfusion in neurologic disorders. Radiology. 1986;161:401-407.
2) Le Bihan D, Breton E, Lallemand D, et al. Separation of diffusion and perfusion in intravoxel incoherent motion MR imaging. Radiology. 1988;168:497-505.
3) Moffat BA, Chenevert TL, Lawrence TS, et al. Functional diffusion map: a noninvasive MRI biomarker for early stratification of clinical brain tumor response. Proc Natl Acad Sci U S A. 2005;102:5524-5529.
4) Moffat BA, Chenevert TL, Meyer CR, et al. The functional diffusion map: an imaging biomarker for the early prediction of cancer treatment outcome. Neoplasia. 2006;8:259-267.
5) Toshikuni N, Takagi S, Morii K, et al. Education and imaging. Hepatobiliary and pancreatic: calcified cavernous hemangiomas in the liver. J Gastroenterol Hepatol. 2006;21:1626.
6) Taouli B, Vilgrain V, Dumont E, et al. Evaluation of liver diffusion isotropy and characterization of focal hepatic lesions with two single-shot echo-planar MR imaging sequences: prospective study in 66 patients. Radiology. 2003;226:71-78.
7) Kamel IR, Bluemke DA, Eng J, et al. The role of functional MR imaging in the assessment of tumor response after chemoembolization in patients with hepatocellular carcinoma. J Vasc Interv Radiol. 2006;17:505-512.
8) Moteki T, Horikoshi H. Evaluation of hepatic lesions and hepatic parenchyma using diffusion-weighted echo-planar MR with three values of gradient b-factor. J Magn Reson Imaging. 2006;24:637-645.
9) Nasu K, Kuroki Y, Nawano S, et al. Hepatic metastases: diffusion-weighted sensitivity-encoding versus SPIO-enhanced MR imaging. Radiology. 2006;239:122-130.
10) Quan XY, Sun XJ, Yu ZJ, et al. Evaluation of diffusion weighted imaging of magnetic resonance imaging in small focal hepatic lesions: a quantitative study in 56 cases. Hepatobiliary Pancreat Dis Int. 2005;4:406-409.
11) Karhunen PJ. Benign hepatic tumours and tumour like conditions in men. J Clin Pathol. 1986;39:183-188.
12) Semelka RC, Sofka CM. Hepatic hemangiomas. Magn Reson Imaging Clin N Am. 1997;5:241-253.

13) Nelson RC, Chezmar JL. Diagnostic approach to hepatic hemangiomas. Radiology. 1990;176:11-13.
14) Quinn SF, Benjamin GG. Hepatic cavernous hemangiomas: simple diagnostic sign with dynamic bolus CT. Radiology. 1992;182:545-548.
15) Semelka RC, Brown ED, Ascher SM, et al. Hepatic hemangiomas: a multi-institutional study of appearance on T_2-weighted and serial gadolinium-enhanced gradient-echo MR images. Radiology. 1994;192:401-406.
16) Soyer P, Dufresne AC, Somveille E, et al. Hepatic cavernous hemangioma: appearance on T_2-weighted fast spin-echo MR imaging with and without fat suppression. AJR Am J Roentgenol. 1997;168:461-465.
17) Moody AR, Wilson SR. Atypical hepatic hemangioma: a suggestive sonographic morphology. Radiology. 1993;188:413-417.
18) Yamashita Y, Hatanaka Y, Yamamoto H, et al. Differential diagnosis of focal liver lesions: role of spin-echo and contrast-enhanced dynamic MR imaging. Radiology. 1994;193:59-65.
19) Mitsudo K, Watanabe Y, Saga T, et al. Nonenhanced hepatic cavernous hemangioma with multiple calcifications: CT and pathologic correlation. Abdom Imaging. 1995;20:459-461.
20) Jang HJ, Kim TK, Lim HK, et al. Hepatic hemangioma: atypical appearances on CT, MR imaging, and sonography. AJR Am J Roentgenol. 2003;180:135-141.
21) Albrecht T, Hohmann J, Oldenburg A, et al. Detection and characterisation of liver metastases. Eur Radiol. 2004;14(suppl 8): P25-P33.
22) Braga L, Semelka RC, Danet IM, et al. Liver metastases from unknown primary site: demonstration on MR images. Magn Reson Imaging. 2003;21:871-877.
23) Chung JJ, Kim MJ, Kim KW. Mangafodipir trisodium-enhanced MRI for the detection and characterization of focal hepatic lesions: is delayed imaging useful? J Magn Reson Imaging. 2006;23:706-711.
24) Elsayes KM, Narra VR, Yin Y, et al. Focal hepatic lesions: diagnostic value of enhancement pattern approach with contrast-enhanced 3D gradient-echo MR imaging. Radiographics. 2005;25:1299-1320.
25) Namasivayam S, Martin DR, Saini S. Imaging of liver metastases: MRI. Cancer Imaging. 2007;7:2-9.
26) Namasivayam S, Salman K, Mittal PK, et al. Hypervascular hepatic focal lesions: spectrum of imaging features. Curr Probl Diagn Radiol. 2007;36:107-123.
27) Sahani DV, Kalva SP. Imaging the liver. Oncologist. 2004;9:385-397.

28) Hosch WP, Schmidt SM, Plaza S, et al. Comparison of CT during arterial portography and MR during arterial portography in the detection of liver metastases. AJR Am J Roentgenol. 2006;186:1502-1511.
29) Seltzer SE, Getty DJ, Pickett RM, et al. Multimodality diagnosis of liver tumors: feature analysis with CT, liver-specific and contrast-enhanced MR, and a computer model. Acad Radiol. 2002;9:256-269.
30) Tomemori T, Yamakado K, Nakatsuka A, et al. Fast 3D dynamic MR imaging of the liver with MR SmartPrep: comparison with helical CT in detecting hypervascular hepatocellular carcinoma. Clin Imaging. 2001;25:355-361.
31) Ito K, Mitchell DG, Outwater EK, et al. Hepatic lesions: discrimination of nonsolid, benign lesions from solid, malignant lesions with heavily T_2-weighted fast spin-echo MR imaging. Radiology. 1997;204:729-737.
32) Baker LL, Kucharczyk J, Sevick RJ, et al. Recent advances in MR imaging/spectroscopy of cerebral ischemia. AJR Am J Roentgenol. 1991;156:1133-1143.
33) Schaefer PW, Grant PE, Gonzalez RG. Diffusion-weighted MR imaging of the brain. Radiology. 2000;217:331-345.
34) Tsuruda JS, Chew WM, Moseley ME, et al. Diffusion-weighted MR imaging of extraaxial tumors. Magn Reson Med. 1991;19:316-320.
35) Muller MF, Prasad P, Siewert B, et al. Abdominal diffusion mapping with use of a whole-body echo-planar system. Radiology. 1994;190:475-478.
36) Kim T, Murakami T, Takahashi S, et al. Diffusion-weighted single-shot echoplanar MR imaging for liver disease. AJR Am J Roentgenol. 1999;173:393-398.
37) Catasca JV, Mirowitz SA. T_2-weighted MR imaging of the abdomen: fast spin-echo vs conventional spin-echo sequences. AJR Am J Roentgenol. 1994;162:61-67.
38) Choi BI, Han MC, Kim CW. Small hepatocellular carcinoma versus small cavernous hemangioma: differentiation with MR imaging at 2.0 T. Radiology. 1990;176:103-106.
39) Mitchell DG. Fast MR imaging techniques: impact in the abdomen. J Magn Reson Imaging. 1996;6:812-821.
40) Saini S, Reimer P, Hahn PF, et al. Echoplanar MR imaging of the liver in patients with focal hepatic lesions: quantitative analysis of images made with various pulse sequences. AJR Am J Roentgenol. 1994;163: 1389-1393.
41) Yu JS, Kim KW, Park MS, et al. Hepatic cavernous hemangioma in cirrhotic liver: imaging findings. Korean J Radiol. 2000;1:185-190.

42) Asbach P, Klessen C, Koch M, et al. Magnetic resonance imaging findings of atypical focal nodular hyperplasia of the liver. Clin Imaging. 2007;31:244-252.
43) Parkin DM, Bray F, Ferlay J, et al. Global cancer statistics, 2002. CA Cancer J Clin. 2005;55:74-108.
44) Kamel IR, Bluemke DA. MR imaging of liver tumors. Radiol Clin North Am. 2003;41:51-65.
45) Brancatelli G, Federle MP, Grazioli L, et al. Hepatocellular carcinoma in noncirrhotic liver: CT, clinical, and pathologic findings in 39 U.S. residents. Radiology. 2002;222:89-94.
46) Winston CB, Schwartz LH, Fong Y, et al. Hepatocellular carcinoma: MR imaging findings in cirrhotic livers and noncirrhotic livers. Radiology. 1999;210:75-79.
47) Sun XJ, Quan XY, Huang FH, et al. Quantitative evaluation of diffusion-weighted magnetic resonance imaging of focal hepatic lesions. World J Gastroenterol. 2005;11:6535-6537.
48) Chan JH, Tsui EY, Luk SH, et al. Diffusion-weighted MR imaging of the liver: distinguishing hepatic abscess from cystic or necrotic tumor. Abdom Imaging. 2001;26:161-165.
49) Ichikawa T, Haradome H, Hachiya J, et al. Diffusion-weighted MR imaging with a single-shot echoplanar sequence: detection and characterization of focal hepatic lesions. AJR Am J Roentgenol. 1998;170:397-402.
50) Namimoto T, Yamashita Y, Sumi S, et al. Focal liver masses: characterization with diffusion-weighted echo-planar MR imaging. Radiology. 1997;204:739-744.
51) Brancatelli G, Federle MP, Vullierme MP, et al. CT and MR imaging evaluation of hepatic adenoma. J Comput Assist Tomogr. 2006;30:745-750.

CHAPTER 11

DIFFUSION-WEIGHTED AND GD-EOB-DTPA CONTRAST-ENHANCED MR IMAGING FOR CHARACTERIZATION OF TUMOR NECROSIS IN AN ANIMAL MODEL

Vossen JA, Buijs M, Geschwind JF, Ventura VP, Lee KH, Bluemke DA, Kamel IR

J Comput Assist Tomogr, In Press.

ABSTRACT

PURPOSE:
To evaluate the role of diffusion-weighted magnetic resonance (MRI) in determining tumor necrosis and contrast-enhanced MRI using gadoxetic acid disodium (Gd-EOB-DTPA) in determining maximum tumor size measurement and tumor delineation compared with criterion-standard histologic measurements in the rabbit VX2 liver tumor model.

MATERIALS AND METHODS:
VX2 tumors were implanted in the liver of 13 rabbits. Magnetic resonance imaging was performed using a 1.5-T MRI scanner and extremity coil. The imaging protocol included T2-weighted fast spin-echo images, 3-dimensional T1-weighted spoiled gradient-echo images with and without fat suppression after administration of Gd-EOB-DTPA, and diffusion-weighted echo planar images. Rabbits were sacrificed, and the tumor was harvested and sliced at 4-mm intervals in the axial plane. The MRI parameters evaluated were tumor size, tumor delineation and tumor apparent diffusion coefficient (ADC) values. Histologic sections were evaluated to quantify tumor necrosis.

RESULTS:
On contrast-enhanced MRI (obtained from 11 rabbits), the mean tumor sizes were 20, 19 and 20 mm in the arterial, portal venous and delayed phases, respectively. Tumor delineation was most distinguishable in the delayed phase. On diffusion-weighted MRI (acquired in 1 rabbits), the mean tumor ADC value was 1.84 x 10^{-3} mm^2/sec. Mean tumor size at pathology was 16 mm. The mean percent necrosis of the tumor at pathology was 36%. The correlation between ADC value and percent necrosis showed an R value of 0.68.

CONCLUSION:
Contrast-enhanced MRI using Gd-EOB-DTPA may provide additional information about tumor outline in the liver. Moreover, we showed a remarkable correlation between ADC values and tumor necrosis. Thus, diffusion-weighted imaging may be useful to assess tumor necrosis; nevertheless, the search for new modalities remains important.

INTRODUCTION

Evaluation of tumor response by imaging after locoregional therapy is generally based on tumor size and tumor enhancement on contrast-enhanced computed tomography or magnetic resonance imaging (MRI) (1). Unfortunately, these imaging techniques may be limited in providing clinically satisfactory information about the extent of tumor necrosis, which is the main indicator of tumor cell death. Therefore, improvements of current imaging techniques play a critical role in finding the optimal strategy to determine treatment success and guide future therapy.

A recent imaging technique for assessment of tumor response is diffusion-weighted MRI. This imaging technique is used to detect the thermally induced random movement of water molecules in biologic tissues, known as Brownian motion (2). Diffusion may be affected by the biophysical properties of tissues such as cell organization and density, microstructure, and microcirculation. Viable tumor cells restrict the mobility of water, whereas necrotic tumor cells allow increased diffusion of water molecules caused by decreased cellularity and compromised cell membrane integrity, displayed as areas of high signal intensity (3). The primary application of diffusion-weighted MRI has been in brain imaging, mainly in the evaluation of acute cerebral infarcts (4). In the liver diffusion-weighted imaging has been used to characterize focal hepatic lesions and to assess tumor response after locoregional therapy (5-8).

Another approach to tumor evaluation is the use of tissue-specific contrast media. Normally, dynamic contrast-enhanced MRI is performed with the traditional extracellular gadolinium-based contrast agents. Gadolinium-ethoxybenzyl-diethylenetriamine- pentaacetic-acid (gadoxetic acid disodium or Gd-EOB-DTPA) is a third generation gadolinium-based MRI contrast agent with the unique ability to combine MR perfusion imaging with hepatocyte specific uptake (9, 10). Therefore, information about lesion vascularity is obtained during the dynamic phase, and information about tumor delineation is obtained during the delayed phase of imaging because to lack of uptake in the tumor.

Gadoxetic acid disodium has been useful in the evaluation of liver function and dysfunctional states such as hepatitis, and in the detection of liver metastasis and hepatocellular carcinoma (HCC) (11-13). After intravenous injection, the contrast between the lesion and surrounding

parenchyma is increased because of positive enhancement of the normal liver tissue on T1-weighted MR images.

The aim of our animal study was to evaluate the role of diffusion-weighted MRI in determining tumor necrosis and the role of contrast-enhanced MRI using Gd-EOB-DTPA in determining maximum tumor size measurement and tumor delineation compared with criterion-standard histologic measurements in the rabbit VX2 liver tumor model.

MATERIALS AND METHODS

Study Design

This study was approved by the Animal Care Committee at our facility, and was performed in accordance with our institutional guidelines. A total of 13 New Zealand White rabbits were included. Each animal received tumor implantation in the left lobe of the liver. Diffusion-weighted and contrast-enhanced MRIs were performed 2 weeks after implantation in 8 animals and 3 weeks after implantation in 5 animals to reach various degrees of necrosis within the tumors. All animals were sacrificed immediately after MRI, and their livers were explanted and submitted to a pathologist for analysis.

Tumor Implantation

Adult New Zealand white rabbits (Myrtle's Rabbitry, Thompson's Station, TN) weighing 8-9 lbs were anesthetized with a mixture of acepromazine (2.5 mg/kg; Phoenix, St Joseph, MO) and ketamine hydrochloride (44 mg/kg; Phoenix) administered intramuscularly. The VX2 tumor cell suspension was first injected into the hind legs of 2 carrier rabbits and grown for 2 weeks. Resultant tumors were harvested from each carrier, and a tumor suspension was prepared from each harvested tumor by dissection of viable tumor tissue and aseptic mincing. For the rabbits that were going to receive the VX2 tumor implanted in the liver, intravenous access was gained via a marginal ear vein, and 0.1 to 0.2 ml (2.5 to 5 mg) of sodium pentobarbital (Abbott Laboratories, Abbott Park, IL) was given periodically to maintain anesthesia. The abdomen of each recipient rabbit was shaved and disinfected with ethanol and povidine iodine. The liver of the rabbit was exposed by a midline incision, and then an aliquot of the tumor cell suspension (0.2 ml) was injected directly using a 21-gauge

angiocatheter into the left lobe of the liver to develop a solitary lesion with adequate surrounding liver parenchyma. The abdomen was closed in 2 layers. The tumor was allowed to grow in the rabbit livers for 14 to 21 days. Because of the fast growing and aggressive nature of the VX2 tumors, various degrees of necrosis are obtained at different time points after implantation.

MRI Technique

All 13 rabbits underwent MRI immediately before they were sacrificed. Diffusion-weighted and contrast-enhanced MRIs were performed 2 weeks after implantation in 8 animals and 3 weeks after implantation in 5 animals. MRI was performed by using a 1.5-T MRI scanner (CV/i; GE Healthcare, Milwaukee, WI) and dedicated phased-array body coils. Precontrast axial acquisitions included T2-weighted fast spin-echo images with fat suppression, breath-hold diffusion-weighted echoplanar images (matrix, 128 × 128; slice thickness, 8 mm; interslice gap, 2 mm; b values, 0 and 500 mm^2/sec; TR/TE, 5000-6500/110 msec; receiver bandwidth, 64 kHz) and T1-weighted three-dimensional fat-suppressed spoiled gradient-echo images with and without fat suppression. All animals received 0.025 mmol/kg of body weight dose of a 0.25 mol/L of Gd-EOB-DTPA (Schering AG, Berlin, Germany) intravenously at a speed of 2 mL/sec. The line was flushed with 5 mL of 0.9% saline. Dynamic imaging was performed in the arterial (2-5 sec after injection) and portal venous phase (20 sec after injection) using the T1-weighted three-dimensional fat-suppressed spoiled gradient-echo sequence with and without fat suppression. In addition, delayed T1-weighted three-dimensional fat-suppressed spoiled gradient-echo with fat suppression were performed 10 minutes after contrast administration.

Image Analysis

Magnetic resonance image processing and apparent diffusion coefficient (ADC) maps were generated using a commercially available Advantage Windows workstation (GE Healthcare, Milwaukee, WI). Images were interpreted by consensus of two experienced MR radiologists. Apparent diffusion coefficient maps were generated from the diffusion-weighted images, and the values were recorded by placing a region of interest (ROI) over the entire lesion, as seen on the image with the largest lesion size. Separate ADC maps were generated by placing the ROI on the viable region and necrotic regions of each tumor. Histologic slides were

used to determine the position of the necrotic and viable regions. Other parameters evaluated were tumor size and delineation in arterial, portal venous phase, and 10 min post injection. Tumor size was measured in all 3 phases of contrast enhancement, using electronic calipers. Tumor delineation was scored using the following 5-grade scale; grade 1 indicates no distinguishable outline of the tumor, grade 2 is defined as tumor outline seen in 90 degrees along the tumor border, grade 3 is defined as outline seen in 180 degrees along the tumor border, grade 4 is defined as outline seen in 270 degrees along the tumor border, and grade 5 indicates a definite distinguishable tumor seen all along the tumor border (360 degrees).

Histologic Analysis

All animals were euthanized under deep anesthesia by slow injection of a lethal dose (100 mg/5 ml) of sodium pentobarbital intravenously after the completion of MRI. Immediately after euthanasia, the liver of the rabbits was carefully removed and subsequently placed in 10% formaldehyde for fixation. After fixation, the liver was examined, and the liver tumor was dissected out of the nontumorous liver tissue. Tumors were sliced at 3- to 4-mm intervals in the axial plane to correspond to the plane of the MR images and placed in standard cassettes. To maintain proper orientation, the dorsal and medial sides of each slice were stained with different colors. All sections were submitted to a pathologist for histologic preparation. The tissue slices were embedded in paraffin, and 2 sections of each paraffin block were stained with hematoxylin-eosin. A Nikon SMZ800 microscope was coupled with a Nikon digital sight DS-U1 camera (resolution, 1376 x 1032). The images of the tumors were captured at a magnification of ×10. Digital images were first converted to jpeg format and then imported into ImageJ. The ImageJ 1.37v software (National Institutes of Health, Bethesda, MD) was used to estimate the percentage of necrosis within the tumor. For each liver tumor, the 3 axial slides representing the most central part of the tumor were selected. For each slide, an ROI was delineated around the entire tumor, and another ROI was delineated around the necrotic part of the tumor. The mean ratio of necrotic part to the total tumor was calculated for each liver tumor. To assess tumor size, the axial slide representing the center of the tumor was selected. The tumor size was recorded as the maximum diameter in millimeter along the same plane and axis used on MRI.

Statistical Analysis

The collected data were entered into a Microsoft Excel spreadsheet (Microsoft, Redmond, WA). Tumor size, tumor enhancement during contrast-enhanced MRI, and ADC values were correlated with pathologic findings using Pearson product moment correlation coefficient (r). The estimates of fractions of viable cells obtained with MRI and histopathology were compared using Student t-test. P-values < 0.05 were considered to indicate significant difference at 95% confidence interval.

RESULTS

All implantations were successful, and in all 13 rabbits, a tumor developed. All rabbits underwent MRI. Two rabbits died after diffusion-weighted imaging but before injection of contrast medium.

The results of experiments are presented in Table 11.1. The mean duration between implantation and MRI was 16 (+/- 3.3) days. All tumors appeared heterogeneous on T2-weighted images (Fig 11.1A). On contrast-enhanced MRI (n = 11), the mean tumor sizes were 20 mm (range, 12-36 mm), 19 mm (range, 12-33 mm), and 20 mm (range, 13-36 mm) in the arterial, portal venous, and delayed phase, respectively. Tumor delineation as scored on the 5-grade scale was most distinguishable in the delayed phase for all tumors, with scores from 3 to 5. The portal venous phase was equal or superior to the arterial phase for the distinction of tumor outline in 82% of the lesions.

On diffusion-weighted MRI, all 13 lesions were markedly hyperintense compared with the surrounding liver parenchyma. The mean ADC value was 1.84×10^{-3} mm^2/sec (Fig 11.1B). All tumors were sliced in the axial plane to correspond to the plane of the MR images and placed in standard cassettes. Proper orientation was maintained by staining the dorsal and medial sides of each slice with different colors (Fig 11.2). At pathologic analysis, all tumors were undifferentiated and consisted of necrotic and viable cells (Fig 11.1C). The mean tumor size at pathology was 16 mm (range, 8-27 mm). The mean percent necrosis at the tumor's pathologic condition was 36% (range, 11-80%). The correlation between ADC value and percent necrosis showed an R value of 0.68 (Fig 11.3). In addition, the tumor size measured at pathology and percent necrosis showed a strong correlation, with an R value of 0.91. Compared with peripheral viable areas,

the central necrotic areas of the tumor showed a significantly higher ADC value of 2.25 x 10^{-3} mm^2/sec compared with 1.39 x 10^{-3} mm^2/sec ($p = 0.02$).

The tumor size on all phases of contrast-enhanced MRI showed a strong correlation with the tumor size on pathology (Fig 11.4), with the strongest correlation in the portal venous phase. The mean tumor size of all 3 obtained phases on contrast-enhanced MRI was 28% (0-62%) larger than the pathologic tumor size for 10 lesions. One lesion was slightly (4%) smaller on contrast-enhanced MRI than on its actual pathologic appearance. The remaining 2 lesions were not measured because contrast was not administered owing to the animal's death after the diffusion-weighted images were acquired. This difference in tumor size showed no correlation with tumor size ($R = 0.12$) or tumor necrosis ($R = 0.014$).

DISCUSSION

In the clinical setting, it is of crucial importance to determine tumor delineation and accurately differentiate between viable tumor and necrotic tumor, especially in treatment planning and the evaluation of treatment success. The aim of our animal study was to evaluate the role of diffusion-weighted MRI in determining tumor necrosis and contrast-enhanced MRI using Gd-EOB-DTPA in determining maximum tumor size measurement and tumor delineation using pathologic correlation. Our results indicate that diffusion-weighted MRI may be useful in quantifying tumor necrosis. Gadoxetic acid disodium, however, did not provide additional information on tumor necrosis but was valuable in determining tumor outline.

Necrosis is the most common morphologic alteration found in tumors and surrounding tissue after radiotherapy and chemotherapy. In view of the emergence of new anticancer therapies, which are based on stabilizing disease rather than causing tumor disappearance, tumor necrosis has become the most important indicator of successful therapy (14, 15). Moreover, the degree of therapy-induced necrosis has been shown to be associated with long-term prognosis in some tumors (16). Thus, although reduction in tumor size is the conventional method to assess tumor response, the percentage of tumor necrosis after therapy may be more informative (17).

Gadoxetic acid disodium is a more specific and sensitive cellular marker for hepatocyte function than are current techniques such as gadolinium MRI and biphasic computed tomographic imaging (18). The uptake and accumulation of Gd-EOB-DTPA is caused by a lipophilic ethyl-

oxybenzyl group resulting in selective enhancement of the normally functioning liver. Gadoxetic acid disodium enters into the hepatocytes through the organic anion-transporting polypeptide 1, which is involved in the hepatocellular uptake of bilirubin. Hereby, the possibility to detect tumors within the liver is increased because undifferentiated neoplastic cells, which lack anion transport and phagocytic functions, cannot extract Gd-EOB-DTPA from the blood. Thus, the healthy liver parenchyma is enhanced, whereas the tumors do not possess normally functioning hepatocytes and therefore lack accumulation, appearing as hypointense lesions (19). Our results confirmed the specific uptake of Gd-EOB-DTPA by healthy liver tissue in the delayed phase. However, parts of the tumor that were viable on pathologic analysis showed similar absence of the uptake of contrast compared with parts of the tumor that were necrotic on pathology. Therefore, Gd-EOB-DTPA did not provide valuable information on tumor necrosis but was useful in determining tumor outline.

Diffusion-weighted MRI and ADC values represent the cellular integrity and motion of water molecules in biologic tissues and are thereby able to provide insight into tumor microstructure (20). The motion includes not only molecular diffusion of water but also microcirculation of blood (microperfusion). In the liver, diffusion-weighted imaging has been used to characterize focal hepatic lesions and to assess tumor response (21, 22). Viable tumors are high in cellularity. These cells have an intact cell membrane that restricts the mobility of water molecules and causes a relatively low ADC value. Conversely, cellular necrosis causes increased membranous permeability, which allows water molecules to move freely and thus causes a relative increase in the ADC value. In our animal study we demonstrated that ADC values are strongly correlated to the percentage of tumor necrosis on pathologic analysis ($R = 0.68$). These results reinforce the notion that diffusion-weighted MRI is useful in assessing tumor necrosis. Moreover, because pathologic correlation in the clinical setting is rarely possible, for obvious ethical reasons, these results add evidence to the use of diffusion-weighted MRI in evaluating tumor necrosis.

Although tumor sizes measured on contrast-enhanced MRI and on their actual pathologic appearance were strongly correlated, we found a significant difference between radiologic and pathologic tumor sizes. This difference had poor positive correlation with tumor necrosis ($R = 0.014$), showing the same tendency in both viable and necrotic tumors. Moreover, this difference between contrast-enhanced MRI and pathologic findings was seen in both small and large tumors. One possible explanation for these

findings in large necrotic tumors is the partial shrinkage of these tumors during liver fixation. It is possible that small viable tumors decrease in size at pathology because of the cessation of blood flow. Our findings are similar to those of a previous report, concluding that there is no adequate correlation between the radiologic and histologic sizes of HCC (23).

This study has several limitations. First, our study group was relatively small, so further studies with a larger sample size are needed to confirm our conclusions. Second, the VX2 tumor used in our study is of nonhepatic origin. However, it has proven to be convenient to study liver cancer in the animal because of the similarities in blood supply, genotype, and metabolism to advanced human HCC (24). Last, because it is difficult to use breath-holding or respiratory gating techniques in rabbits, respiratory movement during abdominal MRI might degrade image quality to some extent and cause variations in measurements.

In conclusion, contrast-enhanced MRI using Gd-EOB-DTPA may provide additional information about tumor outline in the liver. Moreover, we showed a remarkable correlation between ADC values and tumor necrosis. Thus, diffusion-weighted imaging may be useful to assess tumor necrosis; nevertheless, the search for new modalities remains important.

TABLES & FIGURES

ID	Time between Implantation and MRI (days)	Tumor size (mm) Arterial	Tumor size (mm) PV	Tumor size (mm) Delayed	Tumor size (mm) Pathology	ADC-value tumor (x 10^{-3} mm^2/sec)	% Necrosis on pathology	Delineation Arterial	Delineation Portal Venous	Delineation Delayed
1	13	16.1	15.2	14.6	14.5	1.45	19	2	3	5
2	13	13.3	11.5	13.0	7.8	1.97	17	1	2	3
3	13	19.5	17.2	17.6	12	1.63	22	2	1	4
4	14	14.0	13.7	14.9	10.8	1.69	20	1	2	4
5	14	14.4	15.4	16.4	15	1.65	22	1	1	3
6	14	NA	NA	NA	11	0.80	11	NA	NA	NA
7	15	12.1	12.7	13.5	13.3	1.61	32	1	2	3
8	15	12.5	12.6	13.4	10.8	1.56	26	2	3	5
9	17	23.6	18.5	21.1	21	1.31	38	2	1	4
10	18	20.5	21.2	21.6	13.5	2.93	40	1	1	4
11	21	34.7	33.0	35.7	26	2.84	72	1	2	3
12	21	35.7	32.9	33.5	27	2.11	69	1	2	4
13	22	NA	NA	NA	20.5	2.34	80	NA	NA	NA

Table 11.1 Imaging and pathologic variables for all 13 rabbits.

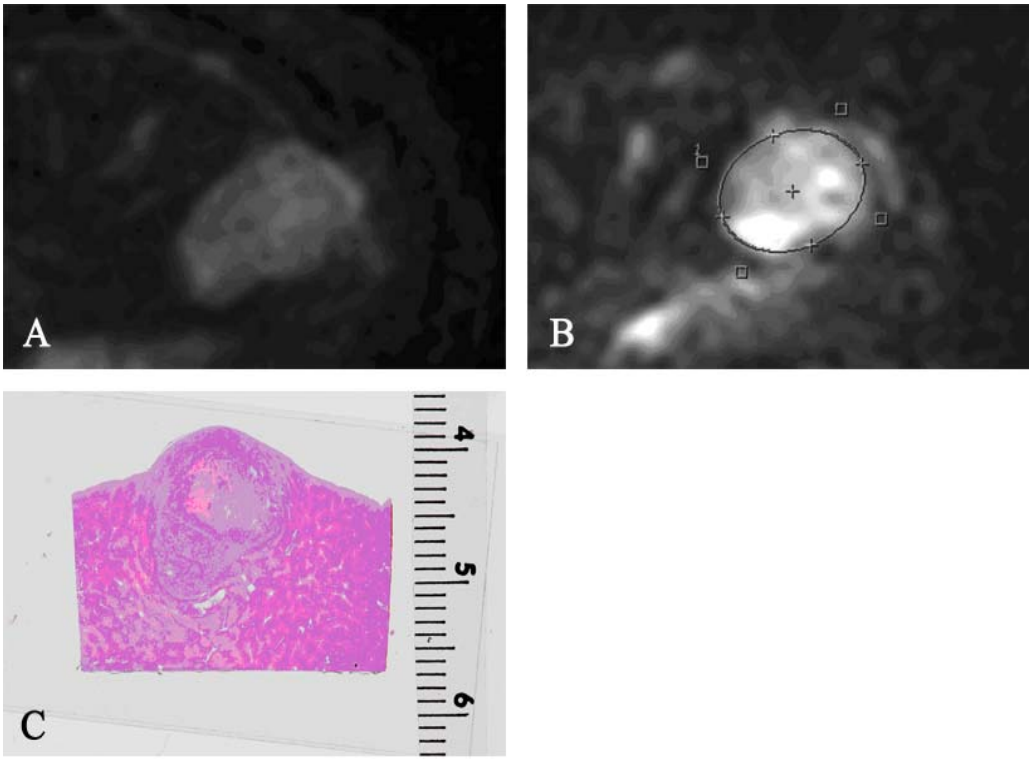

Figure 11.1 (A) shows a typical example of a rabbit VX2 tumor in the left lateral lobe of the liver appearing heterogeneously bright on T2 weighted images.
(B) shows the diffusion-weighted MR image of the same lesion. After placing a ROI on the lesion, mean ADC value was calculated to be 2.93 x 10^{-3} mm^2/sec.
(C) shows the same tumor after H&E staining consisting of necrotic (central) and viable (periphery) areas.

Figure 11.2 shows the method of staining of the pathology specimen in order to maintain proper anatomical orientation.

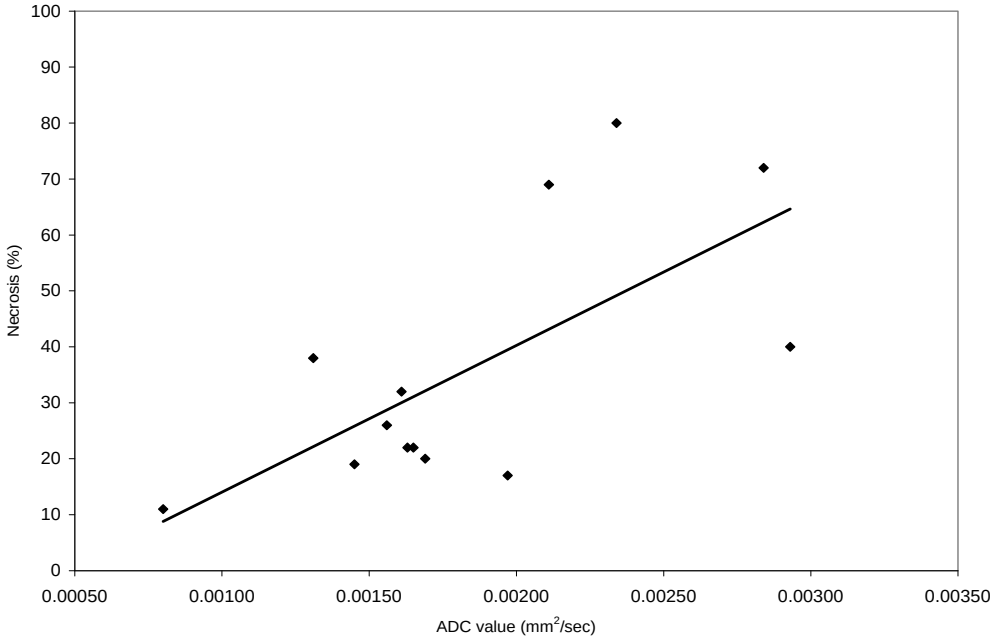

Figure 11.3 Correlation between ADC value and percent necrosis. R was 0.68

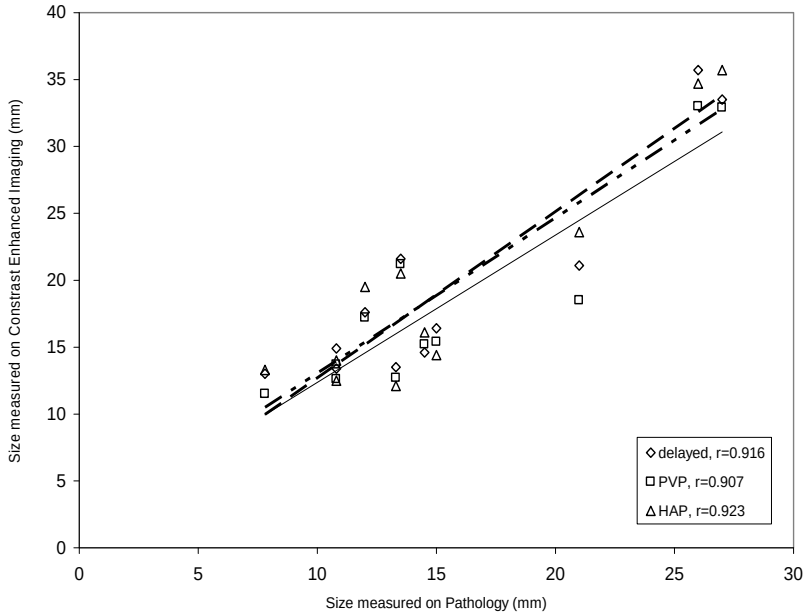

Figure 11.4 Correlation between tumor size on contrast-enhanced MR imaging and tumor size on pathology.

REFERENCES

1) Vossen JA, Buijs M, Kamel IR. Assessment of tumor response on MR imaging after locoregional therapy. Tech Vasc Interv Radiol 2006; 9:125-132.
2) Le Bihan D, Breton E, Lallemand D, Aubin ML, Vignaud J, Laval-Jeantet M. Separation of diffusion and perfusion in intravoxel incoherent motion MR imaging. Radiology 1988; 168:497-505.
3) Benveniste H, Hedlund LW, Johnson GA. Mechanism of detection of acute cerebral ischemia in rats by diffusion-weighted magnetic resonance microscopy. Stroke 1992; 23:746-754.
4) Schaefer PW, Grant PE, Gonzalez RG. Diffusion-weighted MR imaging of the brain. Radiology 2000; 217:331-345.
5) Buijs M, Kamel IR, Vossen JA, Georgiades CS, Hong K, Geschwind JF. Assessment of metastatic breast cancer response to chemoembolization with contrast agent enhanced and diffusion-weighted MR imaging. J Vasc Interv Radiol 2007; 18:957-963.
6) Taouli B, Vilgrain V, Dumont E, Daire JL, Fan B, Menu Y. Evaluation of liver diffusion isotropy and characterization of focal hepatic lesions with two singleshot echo-planar MR imaging sequences: prospective study in 66 patients. Radiology 2003; 226:71-78.
7) Deng J, Rhee TK, Sato KT, et al. In vivo diffusion-weighted imaging of liver tumor necrosis in the VX2 rabbit model at 1.5 Tesla. Invest Radiol 2006; 41:410-414.
8) Deng J, Virmani S, Young J, et al. Diffusion-weighted PROPELLER MRI for quantitative assessment of liver tumor necrotic fraction and viable tumor volume in VX2 rabbits. J Magn Reson Imaging 2008; 27:1069-1076.
9) Hamm B, Staks T, Muhler A, et al. Phase I clinical evaluation of Gd-EOB-DTPA as a hepatobiliary MR contrast agent: safety, pharmacokinetics, and MR imaging. Radiology 1995; 195:785-792.
10) Reimer P, Rummeny EJ, Shamsi K, et al. Phase II clinical evaluation of Gd-EOBDTPA: dose, safety aspects, and pulse sequence. Radiology 1996; 199:177-183.
11) Huppertz A, Balzer T, Blakeborough A, et al. Improved detection of focal liver lesions at MR imaging: multicenter comparison of gadoxetic acid-enhanced MR images with intraoperative findings. Radiology 2004; 230:266-275.
12) Tsuda N, Kato N, Murayama C, Narazaki M, Yokawa T. Potential for differential diagnosis with gadolinium-ethoxybenzyl-diethylenetriamine

pentaacetic acidenhanced magnetic resonance imaging in experimental hepatic tumors. Invest Radiol 2004; 39:80-88.

13) Zizka J, Klzo L, Ferda J, Mrklovsky M, Bukac J. Dynamic and delayed contrast enhancement in upper abdominal MRI studies: comparison of gadoxetic acid and gadobutrol. Eur J Radiol 2007; 62:186-191.
14) Livraghi T, Goldberg SN, Lazzaroni S, et al. Hepatocellular carcinoma: radiofrequency ablation of medium and large lesions. Radiology 2000; 214:761-768.
15) Llovet JM, Real MI, Montana X, et al. Arterial embolisation or chemoembolisation versus symptomatic treatment in patients with unresectable hepatocellular carcinoma: a randomised controlled trial. Lancet 2002; 359:1734- 1739.
16) Yan K, Chen MH, Yang W, et al. Radiofrequency ablation of hepatocellular carcinoma: Long-term outcome and prognostic factors. Eur J Radiol 2008; 67:336-347
17) Bruix J, Sherman M, Llovet JM, et al. Clinical management of hepatocellular carcinoma. Conclusions of the Barcelona-2000 EASL conference. European Association for the Study of the Liver. J Hepatol 2001; 35:421-430.
18) Halavaara J, Breuer J, Ayuso C, et al. Liver tumor characterization: comparison between liver-specific gadoxetic acid disodium-enhanced MRI and biphasic CT-- a multicenter trial. J Comput Assist Tomogr 2006; 30:345-354.
19) Saito K, Kotake F, Ito N, et al. Gd-EOB-DTPA enhanced MRI for hepatocellular carcinoma: quantitative evaluation of tumor enhancement in hepatobiliary phase. Magn Reson Med Sci 2005; 4:1-9.
20) Nasu K, Kuroki Y, Nawano S, et al. Hepatic metastases: diffusion-weighted sensitivity-encoding versus SPIO-enhanced MR imaging. Radiology 2006; 239:122-130.
21) Bruegel M, Holzapfel K, Gaa J, et al. Characterization of focal liver lesions by ADC measurements using a respiratory triggered diffusion-weighted single-shot echo-planar MR imaging technique. Eur Radiol 2007.
22) Kamel IR, Reyes DK, Liapi E, Bluemke DA, Geschwind JF. Functional MR imaging assessment of tumor response after 90Y microsphere treatment in patients with unresectable hepatocellular carcinoma. J Vasc Interv Radiol 2007; 18:49-56.
23) Mejia GA, Gomez MA, Serrano J, et al. Correlation between the radiologic and histologic size of hepatocellular carcinoma in patients eligible for liver transplantation. Transplant Proc 2006; 38:1394-1395.

24) Geschwind JF, Artemov D, Abraham S, et al. Chemoembolization of liver tumor in a rabbit model: assessment of tumor cell death with diffusion-weighted MR imaging and histologic analysis. J Vasc Interv Radiol 2000; 11:1245-1255.

CHAPTER 12

QUANTITATIVE PROTON MR SPECTROSCOPY AS A BIOMARKER OF TUMOR NECROSIS IN THE RABBIT VX2 LIVER TUMOR

Buijs M, Vossen JA, Geschwind JF, Salibi N, Pan L, Ventura VP, Liapi E, Lee KH, Kamel IR

Submitted for publication.

ABSTRACT

PURPOSE:
The aim of our animal study was to compare metabolic (quantification of tumor choline concentration) MR imaging findings to percent necrosis at pathology in rabbits bearing VX2 liver tumors.

MATERIALS AND METHODS:
VX2 tumors were implanted in the liver of 16 rabbits. MR imaging was performed using a 1.5-T MRI scanner and extremity coil. 1H MRS imaging protocol was used. Rabbits were sacrificed immediately after imaging and the tumor was harvested and sliced at 4 mm intervals in the axial plane. Choline concentration was calculated and was compared to percent tumor necrosis at pathology.

RESULTS:
Mean tumor size at pathology was 16 mm (Range: 12-22). Mean percentage of necrosis at pathology was 22 % (Range: 4 - 44%). Choline concentration correlated well with percentage of necrosis on pathology and showed an R value of 0.78.

CONCLUSION:
Choline concentration showed a relatively high correlation with tumor necrosis on pathology. Thus 1H MRS may be useful to assess tumor necrosis.

INTRODUCTION

Assessment of tumor response by imaging is conventionally based on tumor size and tumor enhancement on contrast-enhanced CT or MR imaging (1, 2). In addition to these traditional modalities, diffusion-weighted MR imaging has increasingly been used to assess tumor response by measuring the apparent diffusion coefficient (ADC) value (3-5). However, to date there is no reliable imaging technique for monitoring the early response to locoregional therapy.

Proton MR spectroscopy (1H MRS) is a noninvasive imaging technique that may be utilized to quantify biochemical metabolite concentrations. 1H MRS has been successfully utilized as a diagnostic tool for tumors in the brain, breast and prostate and in the evaluation of treatment response to chemotherapy in tumors of the head and neck (6-11). In the liver, 1H MRS has been used to evaluate diffuse hepatic disease such as hepatic steatosis, chronic hepatitis and cirrhosis (12-14). The role of 1H MRS in evaluating tumor response after locoregional therapy, however still has to be established.

In vivo 1H MRS can be used to differentiate between benign and malignant lesions based on the evaluation of choline levels detected in the lesion (15). Elevation of the intensity of the choline peak is believed to represent an increased biosynthesis of membrane phospholipids and therefore represents cellular proliferation. Viable tumors consist of rapidly proliferating cells, thereby causing a high choline peak, whereas necrotic tumors have decreased cellularity, thus causing the choline peak to diminish.

Quantification of the choline concentration is essential to characterize changes after locoregional therapy. Several quantification techniques have been used for in vivo 1H MRS (16). Quantification is the procedure to estimate numerical values of metabolite concentrations by comparing in vivo signals from a volume of interest to a standard signal from an internal or external reference. Several studies performed 1H MRS using an external reference (17). Unfortunately, this procedure, which requires accurate calibration, is extensive and therefore impractical in the clinical setting. For this reason, water was used as an internal reference in this study.

The aim of our animal study was to compare metabolic (quantification of tumor choline concentration) to percent tumor necrosis at pathology in rabbits bearing VX2 liver tumors.

MATERIALS AND METHODS

Animals

This study was approved by the Animal Care Committee at our facility, and was performed in accordance with our institutional guidelines. Adult New Zealand white rabbits weighing 8-9 lbs (n = 16; Myrtle's Rabbitry, Thompson's Station, TN) underwent implantation of rabbit VX2 tumor in the liver.

Study design

A total of 16 New Zealand white rabbits were included in the study. Each animal received tumor implantation in the left lobe of the liver. 1H MRS imaging was performed 2 weeks after implantation in 6 animals and 3 weeks after implantation in 10 animals to reach various degrees of necrosis within the tumors. All animals were sacrificed immediately after MR imaging and their livers were explanted and submitted to pathology for analysis.

Tumor implantation

All rabbits were anesthetized with a mixture of acepromazine (2.5 mg/kg; Phoenix, St Joseph, MO) and ketamine hydrochloride (44 mg/kg; Phoenix) administered intramuscularly. The VX2 tumor cell suspension was first injected into the hind legs of carrier rabbits and grown for 2 weeks. For the rabbits that were going to receive the VX2 tumor implanted in the liver, intravenous access was gained via a marginal ear vein, and 0.1 to 0.2 ml (2.5 to 5 mg) of sodium pentobarbital (Abbott Laboratories, Abbott Park, IL) was given periodically to maintain anesthesia. The liver of the rabbit was exposed by a midline incision, then an aliquot of the tumor cell suspension (0.2 ml) was injected directly using a 21-gauge angiocatheter into the left lobe of the liver to develop a solitary lesion with adequate surrounding liver parenchyma. The tumor was allowed to grow in the rabbit livers for 11 to 21 days to induce variable degrees of necrosis.

MRI Technique

All 16 rabbits underwent MR imaging immediately before they were sacrificed. MR imaging was performed by using clinical 1.5T MR systems scanner (CV/i; GE Healthcare, Milwaukee, WI) and dedicated phased-array body coils. Acquisitions included a T2 weighted fast spin-echo (FSE) imaging with fat suppression (TR/TE 4000/103; FOV 380).

The spectroscopic voxel was positioned within the liver tumor based on a combination of 3D-GRE T1 images and T2 sagittal images, to cover the entire lesion with minimal inclusion of surrounding tissue. Localized 1H MRS was performed with a point-resolved spectroscopy spin-echo sequence, which included a WET based water suppression scheme (18). The field homogeneity was optimized over the selected voxel of interest using an automated 3D-shim followed by optimization with manual shimming as needed. The following acquisition parameters were used: TR/TE, 1500/30 msec; averages 128; spectral width 1000 Hz; and vector size of 1024 data points.

Image Analysis

Spectra were processed by a single experienced physicist (--) with 20 years experience in spectroscopic analysis, using Spectroscopy taskcard available on a Siemens workstation running the Syngo platform (Siemens Healthcare, Erlangen, Germany). Processing included zero filling to 2048 data points, multiplication by a Gaussian filter with less than 1-Hz line broadening, Fourier transformation, and phase and baseline corrections. Automated curve fitting was performed which yielded choline peak amplitude, linewidth, and peak integral (area) value. Choline peak area and linewidth were tabulated and serial measurements were performed on separate days for each tumor. The choline concentration was calculated with the internal water reference technique using the following equation:

$$[\mathrm{Cho}] = \frac{S_{Cho}}{S_{water}} \times \frac{n_{water}}{n_{Cho} \times MW_{water}} \times \frac{f\,T1_{water}}{f\,T1_{Cho}} \times \frac{f\,T2_{water}}{f\,T2_{Cho}}$$

where [Cho] is the concentration of choline in the tumor; S_{Cho} is the integral value of choline at 3.22 ppm; S_{water} is the integral value of the unsuppressed water signal; n_{Cho} and n_{water} are the numbers of 1H nuclei contributing to the choline and water resonances respectively; MW_{water} is the molecular weight of water; f T1, or (1-exp(-TR/T1)), is the T1 correction factor for partial

saturation; f T2, or (exp(-TE/T2)), is the correction factor for signal loss from T2 relaxation. Relaxation times T1 and T2 of choline and water in tumor voxels of two rabbits were measured. T1 was measured using TE of 30 ms and eight values of TR between 500ms and 6000ms. T2 was measured using TR of 2000 ms and eight TE values between 30 and 400 ms. The resulting relaxation times are $T1_{cho}$ of (1293 ± 75) ms, $T1_{water}$ of (912 ± 200) ms, $T2_{cho}$ of (276 ± 30) ms and $T2_{water}$ of (86 ± 11) ms.

Histologic analysis

All animals were euthanized under deep anesthesia by slow injection of a lethal dose (100mg/5ml) of sodium pentobarbital intravenously after the completion of MR imaging. Immediately after euthanasia, the liver of the rabbits was carefully removed and subsequently placed in 10% formaldehyde for fixation. After fixation, the liver was examined and the liver tumor was dissected out of the nontumorous liver tissue. Tumors were sliced at 3- to 4-mm intervals in the axial plane to correspond to the plane of the MR images and placed in standard cassettes. To maintain proper orientation, the dorsal and medial sides of each slice were stained with different colors. All sections were submitted to pathology for histologic preparation. The tissue slices were embedded in paraffin and two sections of each paraffin block were stained with hematoxylin-eosin (HE). A Nikon SMZ800 microscope was coupled with a Nikon digital sight DS-U1 camera (resolution 1376 x 1032). Images of the tumors were captured at a magnification of ×10. Digital images were first converted to jpeg format and then imported into ImageJ 1.37v (NIH, Bethesda, MD). ImageJ software was used to estimate the percentage of necrosis within the tumor. For each liver tumor the axial slide representing the part of the tumor with the largest diameter was selected. For each slide a region of interest (ROI) was delineated around the entire tumor and another ROI was delineated around the necrotic part of the tumor. The mean ratio of necrotic/total tumor size was calculated for each liver tumor. Tumor size was recorded as the maximum diameter in mm.

Statistical Analysis

Regression analysis was performed using Microsoft Excel. A comparison was made between the choline concentration and the percentages of necrosis on pathology. An *r*-value > 0.7 was considered a good correlation, R = 0.4–0.7 a moderate correlation and R < 0.4 a poor correlation.

RESULTS

All implantations were successful and in all 16 rabbits a solid tumor developed. Liver spectra were acquired in all rabbits (Figure 12.1A), all of whom tolerated the imaging procedure and related deep anesthesia without complications. Results of experiments are presented in Table 12.1. Mean duration between implantation and MR imaging was 17 days (Range: 11-21).

On 1H MRS the spectroscopic voxel size ranged from 1.7-6 cm^3, depending on the size of the tumor. Although measurements in the liver are known to be susceptible to motion artifacts, a good spectral quality was consistently observed (Figure 12.1B). A choline resonance was detected at 3.22 ppm in 13 of the 16 (81%) spectra. However, in 3 animals no spectra were detected. Using equation 1, the calculated choline levels ranged from 0.21-8.96 mmol/kg.

At pathologic analysis a solid tumor was identified in all livers (Figure 12.1C). Tumors were undifferentiated and consisted of necrotic and viable cells. Mean tumor size at pathology was 16 mm (Range: 11-22). Mean percentage of necrosis at pathology was 22% (Range: 4-44). Choline concentration correlated well with percentage of necrosis at pathology and showed an R value of 0.78 (Figure 12.2).

DISCUSSION

Assessment of tumor response after locoregional therapy has become increasingly important, since these therapies have become the mainstay of treatment for the growing population of patients with unresectable hepatocellular carcinoma (HCC) (19). Response to locoregional therapy is most often characterized by an increase in tumor necrosis without immediate change in tumor size. Therefore, current imaging modalities focus on the visualization of tumor necrosis (2). The aim of our study was to perform a precise comparison between choline concentration as calculated by 1H MRS and percentage of tumor necrosis measured at pathology.

In order to obtain an accurate measurement of necrosis on pathology, we followed several steps. First, we created a range of necrosis by allowing the liver tumors to grow for various periods after implantation (11-21 days).

In our experience, an interval <10 days results in tumors that are too small to be characterized by imaging, whereas an interval >21 days may result in an unacceptable tumor burden. Next, we carefully aligned the liver anatomically after explantation, to match the images in the axial plane. Furthermore, we were able to secure the entire tumor on a slide and used advanced software to calculate the exact percentage of necrosis per slide. Last, for each liver tumor the axial slide representing the part of the tumor with the largest diameter was selected and matched with the axial MR image in order to precisely compare measurements of necrosis.

1H MRS is a powerful, noninvasive tool for biochemically characterizing normal and abnormal tissues in vivo. The clinical use of 1H MRS is well established in the brain (20). However detection of metabolites other than water and fat in the body has been challenging due to contamination from high lipid signals and due to signal distortions and signal loss from moving organs. With the availability of techniques that overcome these challenges, 1H MRS of other organs besides the brain has become possible. In the liver, 1H MRS has been used to evaluate diffuse hepatic disease, characterize hepatic lesions and assess early tumor response after locoregional therapy (3).

The elevation of choline levels in a lesion detected with 1H MRS can be used to distinguish malignant from benign lesions. Choline is one of the components of phosphatidylcholine, an essential element of phospholipids in the cell membrane. Malignant tumors usually exhibit a high proliferation of cells and thus are associated with increased metabolism of cell membrane components. This biochemical background will lead to an increased presence of choline in viable cancer cells. On the contrary, necrotic tumors have a lower cell density, which leads to a decrease of the choline concentration (15). In our animal study, a choline resonance was detected in 13 out of 16 liver tumors. In three animals we were not able to detect a choline peak which may be due to breathing and cardiac movement. In patients, however, breath-hold acquisitions can be obtained, thereby improving the identification of small amounts of choline within the tumors.

In the clinical setting, quantification of the choline concentration is of great importance. Various approaches have been utilized to calibrate MR signals based on internal or external standards (21). Internal standard methods have most often been used to calibrate liver spectra. Their utilization is based on the assumption that the concentrations of some metabolites such as tissue water are relatively constant. The use of water as

an internal reference has found widespread use in single-voxel 1H MRS (22). Acquisition of the large water signal as an internal reference requires few averages and a short scan time. Measurements with and without water suppression are acquired from the same selected volume without the need for additional shimming between measurements. In our study, we consistently observed a high intensity water peak, which was positioned at 4.7 ppm used a reference with in vivo 1H MRS.

Our study showed that the choline concentration measured with 1H MRS had a strong correlation with tumor necrosis at pathology (n = 13, R = 0.78). A high percentage of necrosis at pathology corresponded with a low choline concentration measured on 1H MRS, whereas a low percentage of necrosis corresponded with a high choline concentration. Therefore, 1H MRS may be useful in determining tumor response after locoregional therapy.

This study has several limitations. First, the VX2 tumor used in our study is of non-hepatic origin. However, it has proven to be convenient to study liver cancer in the animal because of the similarities in blood supply, genotype and metabolism to advanced human HCC (23). Second, since it is difficult to use breath-holding or respiratory gating techniques in rabbits, respiratory movement during abdominal MR imaging might degrade image quality to some extent and cause variations in measurements. Third, the use of an internal reference standard may be influenced by the variation in concentration under pathologic conditions.

In conclusion, our study demonstrated that the quantification of tumor necrosis by measuring choline concentrations in liver tumors using 1H MRS with water as an internal reference was feasible. The calculated choline levels correlated well with the percentage of tumor necrosis at pathology. Therefore, it is expected that quantitative 1H MRS measurement might be of additional value in the MR imaging of liver tumors.

TABLES & FIGURES

ID	Duration between implantation and MRI (days)	Size at pathology (mm)	Necrosis at pathology (%)	Choline concentration (mmol/kg)
1	21	20	27	4.25
2	21	13.5	33	3.01
3	21	21.5	27	1.89
4	21	21.5	30	---
5	19	12	44	0.21
6	19	13	28	2.9
7	19	17.5	15	3.26
8	20	13	31	1.26
9	20	11	11	7.26
10	20	13	20	8.95
11	11	14	18	6.62
12	11	21	7	---
13	12	12	4	---
14	12	19	19	4.14
15	12	20	16	8.96
16	12	16	13	8.71
Mean	17	16	22	4.72

Table 12.1 Imaging and pathology variables for all 16 rabbits.
In animals with ID 4, 12 and 13, the choline peak was not detected.

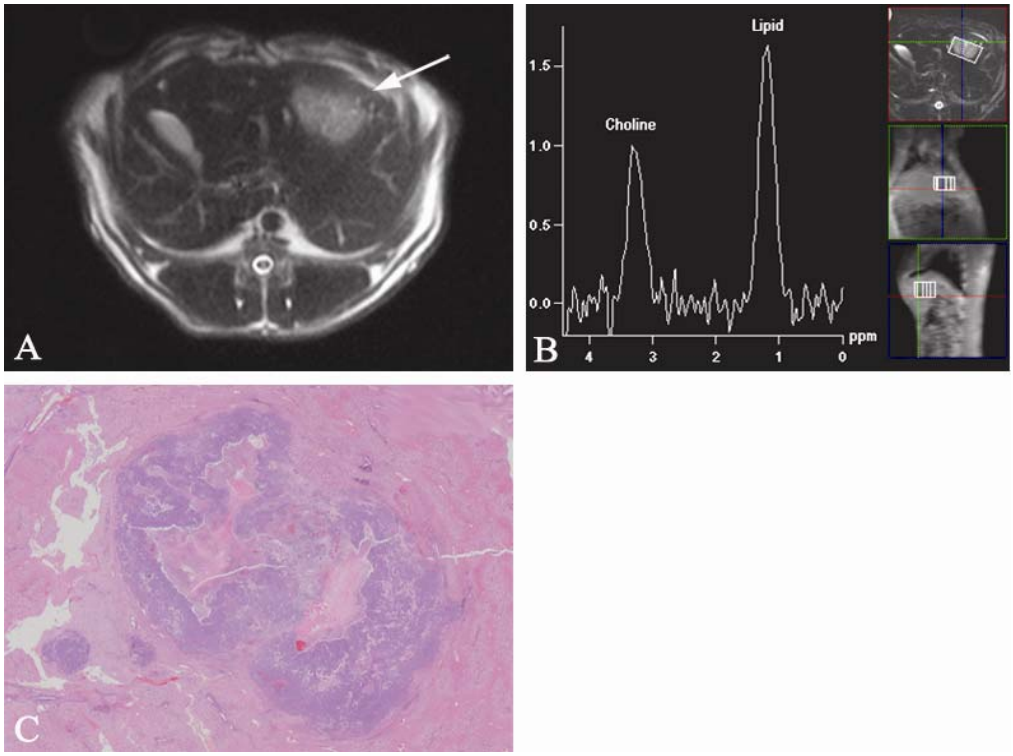

Figure 12.1 (A) shows a typical example of a rabbit VX2 tumor in the left lateral lobe of the liver two weeks after implantation. The lesion appears heterogeneously bright on T2 weighted images. The lesion size in the superior-inferior direction was approximately 15 mm. The spectroscopic voxel (size 12×20×15 mm^3) is superimposed on the hyperintense lesion on the T2 image. (B) shows the water suppressed spectrum obtained from this lesion. The images on the right indicate the voxel placement within the liver tumor. The spectrum consists of a choline (cho) resonance at 3.2 ppm and a lipid resonance at 1.3 ppm, acquired with a TR of 1500 ms, TE of 135ms, 64 averages and 1min 36s measurement time. The Gaussian model fitting of the choline peak produces a measurement of [Cho] = 8.71 ± 2.18 mmol/kg. (C) shows the same tumor after H&E staining.

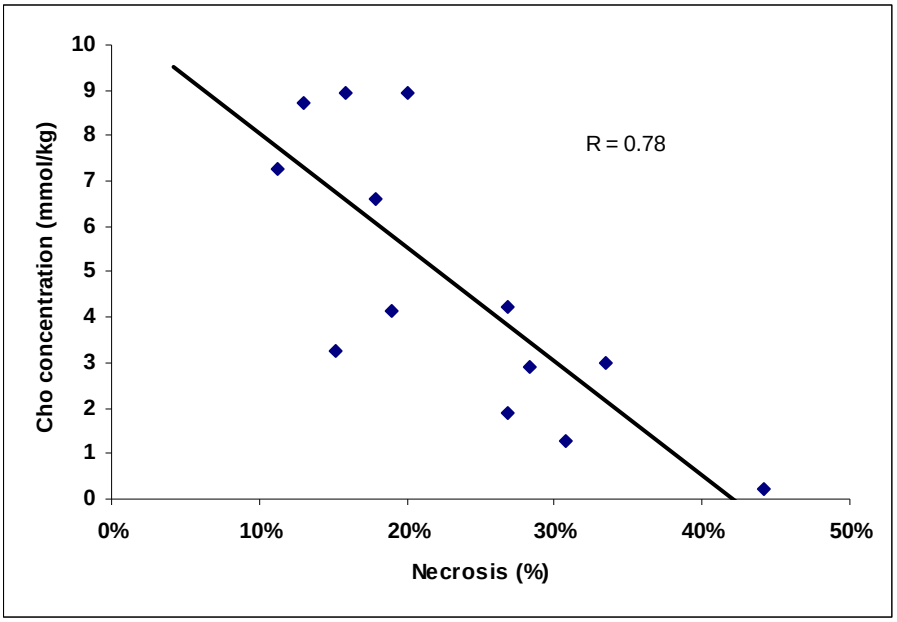

Figure 12.2 Correlation between choline concentration and percent necrosis (n = 13, R = 0.78).

REFERENCES

1) Vossen JA, Buijs M, Kamel IR. Assessment of tumor response on MR imaging after locoregional therapy. Tech Vasc Interv Radiol 2006; 9:125-132.
2) Bruix J, Sherman M, Llovet JM, et al. Clinical management of hepatocellular carcinoma. Conclusions of the Barcelona-2000 EASL conference. European Association for the Study of the Liver. J Hepatol 2001; 35:421-430.
3) Chen CY, Li CW, Kuo YT, et al. Early response of hepatocellular carcinoma to transcatheter arterial chemoembolization: choline levels and MR diffusion constants--initial experience. Radiology 2006; 239:448-456.
4) Moffat BA, Chenevert TL, Lawrence TS, et al. Functional diffusion map: a noninvasive MRI biomarker for early stratification of clinical brain tumor response. Proc Natl Acad Sci U S A 2005; 102:5524-5529.
5) Buijs M, Vossen JA, Hong K, Georgiades CS, Geschwind JF, Kamel IR. Chemoembolization of hepatic metastases from ocular melanoma: assessment of response with contrast-enhanced and diffusion-weighted MRI. AJR Am J Roentgenol 2008; 191:285-289.
6) Moller-Hartmann W, Herminghaus S, Krings T, et al. Clinical application of proton magnetic resonance spectroscopy in the diagnosis of intracranial mass lesions. Neuroradiology 2002; 44:371-381.
7) Yeung DK, Cheung HS, Tse GM. Human breast lesions: characterization with contrast-enhanced in vivo proton MR spectroscopy--initial results. Radiology 2001; 220:40-46.
8) Hollingworth W, Medina LS, Lenkinski RE, et al. A systematic literature review of magnetic resonance spectroscopy for the characterization of brain tumors. AJNR Am J Neuroradiol 2006; 27:1404-1411.
9) King AD, Yeung DK, Ahuja AT, Leung SF, Tse GM, van Hasselt AC. In vivo proton MR spectroscopy of primary and nodal nasopharyngeal carcinoma. AJNR Am J Neuroradiol 2004; 25:484-490.
10) Shah GV, Gandhi D, Mukherji SK. Magnetic resonance spectroscopy of head and neck neoplasms. Top Magn Reson Imaging 2004; 15:87-94.
11) Mueller-Lisse UG, Scherr MK. Proton MR spectroscopy of the prostate. Eur J Radiol 2007; 63:351-360.
12) Longo R, Ricci C, Masutti F, et al. Fatty infiltration of the liver. Quantification by 1H localized magnetic resonance spectroscopy and

comparison with computed tomography. Invest Radiol 1993; 28:297-302.
13) Orlacchio A, Bolacchi F, Angelico M, et al. In vivo, high-field, 3-Tesla 1H MR spectroscopic assessment of liver fibrosis in HCV-correlated chronic liver disease. Radiol Med (Torino) 2008; 113:289-299.
14) Cho SG, Kim MY, Kim HJ, et al. Chronic hepatitis: in vivo proton MR spectroscopic evaluation of the liver and correlation with histopathologic findings. Radiology 2001; 221:740-746.
15) Ruiz-Cabello J, Cohen JS. Phospholipid metabolites as indicators of cancer cell function. NMR Biomed 1992; 5:226-233.
16) Fischbach F, Bruhn H. Assessment of in vivo 1H magnetic resonance spectroscopy in the liver: a review. Liver Int 2008; 28:297-307.
17) Bakken IJ, Gribbestad IS, Singstad TE, Kvistad KA. External standard method for the in vivo quantification of choline-containing compounds in breast tumors by proton MR spectroscopy at 1.5 Tesla. Magn Reson Med 2001; 46:189-192.
18) Ogg RJ, Kingsley PB, Taylor JS. WET, a T1- and B1-insensitive water-suppression method for in vivo localized 1H NMR spectroscopy. J Magn Reson B 1994; 104:1-10.
19) Georgiades CS, Hong K, Geschwind JF. Radiofrequency ablation and chemoembolization for hepatocellular carcinoma. Cancer J 2008; 14:117-122.
20) Kwock L, Smith JK, Castillo M, et al. Clinical role of proton magnetic resonance spectroscopy in oncology: brain, breast, and prostate cancer. Lancet Oncol 2006; 7:859-868.
21) Li CW, Kuo YC, Chen CY, et al. Quantification of choline compounds in human hepatic tumors by proton MR spectroscopy at 3 T. Magn Reson Med 2005; 53:770-776.
22) Barker PB, Soher BJ, Blackband SJ, Chatham JC, Mathews VP, Bryan RN. Quantitation of proton NMR spectra of the human brain using tissue water as an internal concentration reference. NMR Biomed 1993; 6:89-94.
23) Geschwind JF, Artemov D, Abraham S, et al. Chemoembolization of liver tumor in a rabbit model: assessment of tumor cell death with diffusion-weighted MR imaging and histologic analysis. J Vasc Interv Radiol 2000; 11:1245-1255.

PART IV

SUMMARY

The aims of this thesis were, first, to investigate the toxicities associated with trans-arterial chemoembolization (TACE) of liver tumors and to evaluate the use of MR imaging in characterizing tumor response after this locoregional therapy, second, to further develop intra-arterial therapy of liver tumors with 3-bromopyruvate (3-BrPA), a novel anti-cancer agent, and finally, to assess the value of new MR imaging techniques in the characterization of liver lesions. In *Chapter 1*, the general introduction, an overview of these aims and an outline of the thesis are presented.

Toxicities associated with TACE

One of the main concerns regarding systemic chemotherapy in the treatment of liver cancer is the fact that patients who receive this form of treatment may experience side effects that include pain, nausea, vomiting, myelosuppresion, and alopecia and/or serious adverse events such as cardiac toxicity. The subjectively reported side effects of TACE are mild compared with those caused by systemic chemotherapy. Because the focus of most studies is patient survival rather than toxicities caused by TACE, precise analysis of potential TACE-induced systemic toxicities is lacking. Therefore, *in Chapter 2*, we determined the toxicity profiles of TACE at 6 months and 1 year after treatment in patients with HCC using a standardized oncology protocol (CTCAE, version 3.0) so that TACE could be compared with the use of the systemic chemotherapeutic agents most commonly used for liver cancer (ie, doxorubicin, cisplatin, and 5-fluorouracil). Grade 3 or 4 toxicity 6 and 12 months, respectively, after treatment included leukocytopenia (7% and 19%); anemia (9% and 19%); thromobocytopenia (13% and 23%); prolonged activated partial thromboplastin time (8% and 18%); elevated aspartate aminotransferase (15% and 18%), alanine aminotransferase (10% and 18%), and alkaline phosphatase (8% and 18%) levels; hypoalbuminemia (10% and 19%); hyperbilirubinemia (10% and 22%); and alopecia (18%). These toxicity rates were considerably lower than those reported after treatment with currently used systemic chemotherapeutic agents, whose dosing is limited by systemic toxicity. Our study results showed that TACE has a favorable long-term toxicity profile in

patients with HCC. These data clearly support the role of TACE in the treatment of patients with nonresectable HCC. Furthermore, these results give clinicians a good overview of the toxicities that can be expected after TACE and thereby will be helpful for optimizing treatment strategies.

MR imaging after TACE

In *Chapter 3*, we summarized the current available literature on the role of MR imaging in assessing treatment response after various locoregional therapies that are commonly used to treat patients with hepatic malignancies. Assessment of tumor response after locoregional therapies is important in determining treatment success and in guiding future therapy. Magnetic resonance imaging plays an important role in evaluating treatment response to new therapies directed toward liver cancer treatment. The traditional and accepted criteria to characterize tumor response in oncology, namely the Response Evaluation Criteria in Solid Tumors (RECIST) and the European Association for the Study of the Liver (EASL) criteria, use decrease in tumor size and lesion enhancement as an indicator of successful therapy. A more recent evaluation method is the Apparent Diffusion Coefficient (ADC) measured by diffusion-weighted MR imaging. Diffusion-weighted MR imaging and ADC values map the thermally induced motion of water molecules in tissues and thereby are able to provide insight into tumor microstructure. We described the role of tumor size and lesion enhancement as well as ADC mapping. We also discussed the magnetic resonance imaging findings after radiofrequency ablation (RFA), TACE and radioembolization.

In the subsequent chapters of Part I we assessed the value of functional MR imaging in the evaluation of early tumor response after TACE. Furthermore, we compared tumor response based on functional MR imaging versus traditional imaging assessment based on iodized oil deposition, tumor size, and tumor enhancement. According to protocol, patients received contrast medium–enhanced and diffusion MR imaging 4–6 weeks after TACE to assess tumor response. *Chapter 4* focused on breast cancer liver metastases, which are mainly hypovascular in nature. We evaluated a total number of 27 lesions, with a mean diameter of 5.5 cm. Although mean tumor size decreased by 18% after treatment, no tumors met RECIST for complete response (ie, complete disappearance of target lesions) and only 7 of 27 met RECIST for partial response (i.e., >30% decrease in target lesion size). After treatment, decrease of tumor enhancement in the arterial (32%) and portal venous (39%) phases was

statistically significant ($p < 0.0001$). Mean tumor ADC increased by 27% ($p < 0.0001$) after TACE, whereas ADC remained unchanged in non-tumorous liver, spleen, and kidney.

In *Chapter 5* we analyzed liver metastases derived from neuroendocrine primaries, which are mainly hypervascular in nature. We analyzed 66 targeted lesions in 26 patients (18 men, eight women; mean age, 57 years) with hepatic metastases of neuroendocrine tumors treated with TACE. Mean tumor size and percentage enhancement in the arterial and portal venous phases decreased significantly after treatment ($p < 0.0001$). The tumor ADC increased from 1.51×10^{-3} mm^2/sec before treatment to 1.79×10^{-3} mm^2/sec after treatment ($p < 0.0001$), but the ADCs for the liver and spleen remained unchanged. Despite the change in tumor size, no patient in this cohort achieved complete response according to World Health Organization criteria and Response Evaluation Criteria in Solid Tumors, which was in line with our findings in the breast cancer cohort described in *Chapter 4*. Partial response was achieved in only 27% and 23% of the patients according to the respective criteria.

We confirmed these data in metastatic leiomyosarcoma (*Chapter 6*) and metastatic ocular melanoma (*Chapter 7*). A total of 31 liver lesions were evaluated in 10 patients with metastatic leiomyosarcoma using MR imaging studies before and after TACE. These lesions had a mean size of 4.8 cm before treatment. Tumor size decreased only by 2% immediately after treatment. Decrease of tumor enhancement after treatment was significant ($p < 0.0001$) in the arterial phase (69%) as well as in the portal venous phase (64%). After TACE, mean tumor ADC increased by 20% ($p = 0.0015$), whereas mean non-treated liver, spleen, and muscle ADC values did not change significantly ($p = 0.44$, $p = 0.287$, and $p = 0.098$, respectively).

In *Chapter 7*, a total of 21 metastatic ocular melanoma liver lesions were evaluated in six patients. Arterial phase enhancement decreased 41% after TACE, and the decrease was statistically significant ($p = 0.0002$). Venous phase enhancement decreased 56%, also statistically significant ($p < 0.0001$). Diffusion-weighted MRI was useful in monitoring response after treatment. The mean tumor ADC increased 48% after TACE ($p = 0.0003$), whereas the ADC remained unchanged in non-tumorous liver, spleen, and muscle. Although mean tumor size decreased 16% from 4.9 to 4.1 cm after TACE, none of the lesions met the RECIST for complete response

(disappearance of all measurable disease), and only eight lesions were considered partial responders (> 30% decrease in size).

Taken together, our results showed that in patients with liver metastases treated with TACE, although changes in tumor size were small, significant early changes in the treated lesions occurred on contrast medium–enhanced and diffusion-weighted MR imaging. These changes included decrease in tumor enhancement and increase in tumor ADC value, which suggest increasing tumor necrosis and cell death and can therefore be used to assess response of targeted tumors.

Intra-arterial treatment with 3-bromopyruvate

In Part II, we focused on the development of a new therapeutic strategy for liver cancer. 3-BrPA, a synthetic brominated derivate of pyruvic acid, acts as an irreversible glycolytic inhibitor and is a highly promising candidate for intra-arterial administration in patients with liver cancer. Various studies showed that 3-BrPA is a potent inhibitor of tumor cell proliferation in vitro. Moreover, the ability of 3-BrPA to promote cancer cell death has been demonstrated during in vivo pre-clinical testing, resulting in significant survival benefit in various animal models.

In *Chapter 8*, we compared the influence of partial hepatectomy, intra-arterial treatment with 3-BrPA and TACE in the treatment of liver cancer. VX2 tumors were implanted in the left lateral lobe of the liver of 20 rabbits. Tumors were allowed to grow for 14 days. Rabbits were divided in four groups. Group 1 (n = 2) was sacrificed 14 days post implantation. Groups 2, 3 and 4 (n = 6 per group) underwent left lateral hepatectomy, a 1 h intra-arterial infusion with 3-BrPA and TACE, respectively. Animals in groups 2, 3 and 4 were further subdivided into three groups of two animals each corresponding to the time-point of sacrifice after the procedure (7, 14 and 21 days, respectively). After sacrifice, organs were harvested, fixed and analyzed. Pathologic examination showed lung metastases in all 20 rabbits. Abdominal cavity dissemination was seen in five rabbits in Group 2, two rabbits in Group 3 and all rabbits in Group 4. Kidney metastases were seen in two rabbits treated with TACE. We concluded, that intra-arterial delivery of 3-BrPA may result in a favorable metastatic profile when compared to both liver resection and TACE for the treatment of liver cancer.

The aim of *Chapter 9* was to determine the biodistribution and tumor targeting ability of ^{14}C-labeled 3-bromopyruvate ((^{14}C) 3-BrPA) after intra-

arterial and intravenous delivery in the VX2 rabbit model. In addition, we evaluated the effects of (^{14}C) 3-BrPA on tumor and healthy tissue glucose metabolism by determining ^{18}F-deoxyglucose (FDG) uptake. Last, we determined the survival benefit of intra-arterial administered 3-BrPA. In total, 60 rabbits with VX2 liver tumor received either 1.75 mM [^{14}C] 3-BrPA via intra-arterial administration, 1.75 mM [^{14}C] 3-BrPA via intravenous administration, 20 mM [^{14}C] 3-BrPA via intravenous administration, or 25 ml of phosphate-buffered saline (PBS). All rabbits (with the exception of the 20 mM intravenous group) received FDG 1 h before sacrifice. Next, we compared survival of animals treated with intra-arterial administered 1.75 mM 3-BrPA in 25 ml of PBS (n = 22) with controls (n = 10). After intra-arterial infusion, tumor uptake of [^{14}C] 3-BrPA was 1.8 ± 0.2% percentage of injected dose per gram of tissue (%ID/g), whereas other tissues showed minimal uptake. After intravenous administration (1.75 mM), tumor uptake of [^{14}C] 3-BrPA was 0.03 ± 0.01% ID/g. After intra-arterial administration of [^{14}C] 3-BrPA, tumor uptake of FDG was 26 times lower than in controls. After intravenous administration of [^{14}C] 3-BrPA, there was no significant difference in tumor FDG uptake. Survival analysis showed that rabbits treated with 1.75 mM 3-BrPA survived longer (55 days) than controls (18.6 days). We can therefore conclude that intra-arterially delivered 3-BrPA has a favorable biodistribution profile, combining a high tumor uptake resulting in blockage of FDG uptake with no effects on healthy tissue. The local control of the liver tumor by 3-BrPA resulted in a significant survival benefit.

In a subsequent study (Addendum) we evaluated the anti-glycolytic effects of 3-BrPA on rats bearing RMT mammary tumors, by determining FDG uptake after intravenous administration of the therapeutic dose. 16 rats bearing RMT tumors were treated either with 15 mM 3-BrPA in 2.5 ml of PBS or with 2.5 ml of PBS. After treatment, all rats received FDG and were sacrificed 1 h later. 3-BrPA treatment significantly decreased FDG uptake in tumors by 77% ($p < 0.002$). FDG uptake did not significantly decrease in normal tissues after treatment. Our study showed that 3-BrPA exhibits a strong anti-glycolytic effect on RMT cells implanted in rats.

Advances in imaging of liver lesions

Diagnostic imaging is crucial in determining treatment strategies in patients with liver cancer. In Part III we discussed advances in imaging of liver lesions. In *Chapter 10*, we assessed the accuracy of diffusion-weighted MR imaging in differentiating between hemangiomas and other relatively

common hypervascular liver lesions, including focal nodular hyperplasia (FNH), HCC, and hypervascular liver metastases. A retrospective review of 182 hypervascular liver lesions in 117 patients was performed. Lesions included were typical and atypical hemangioma (n = 38), HCC (n = 58), FNH (n = 22), and neuroendocrine tumor metastases (NET; n = 64) with a mean tumor size of 5.3 cm. Mean ADC value for hemangioma, HCC, FNH, and NET was 2.29×10^{-3}, 1.55×10^{-3}, 1.65×10^{-3}, and 1.43×10^{-3} mm^2/sec, respectively. There was a statistically significant difference in the ADC value of hemangioma compared with that of FNH ($p < 0.001$), HCC ($p < 0.001$), and NET ($p < 0.001$), respectively. The area under the receiver operating characteristic curve was 0.91. These data support our hypothesis that diffusion-weighted MR imaging and ADC maps can provide rapid quantifiable information to differentiate typical and atypical hemangiomas from other hypervascular liver lesions.

Another approach to tumor characterization and treatment evaluation is the use of tissue-specific contrast media. *Chapter 11* reported on the role of diffusion-weighted MR imaging in determining tumor necrosis and contrast-enhanced MR imaging using Gd-EOB-DTPA. Maximum tumor size measurement and tumor delineation were determined and compared to gold standard histologic measurements in the rabbit VX2 liver tumor model. On contrast-enhanced MR imaging (acquired in 11 rabbits), mean tumor size was 20 mm, 19 mm and 20 mm in the arterial, portal venous and delayed phase, respectively.

Tumor delineation was best distinguishable in the delayed phase. On diffusion-weighted MR imaging (acquired in 13 rabbits), mean tumor ADC value was 1.84×10^{-3} mm^2/sec. Mean tumor size at pathology was 16 mm. Mean percentage necrosis at pathology was 36%.

Correlation between ADC value and percentage necrosis showed an R value of 0.68. Contrast-enhanced MR imaging using Gd-EOB-DTPA may provide additional information about tumor outline in the liver. Moreover, we showed a remarkable correlation between ADC values and tumor necrosis. Thus, diffusion weighted imaging may be useful to assess tumor necrosis; nevertheless, the search for new modalities remains important.

Finally, Proton MR spectroscopy (^1H MRS) is an imaging technique that may be utilized to quantify biochemical metabolite concentrations. In *Chapter 12* we compare the metabolic (absolute quantification of tumor choline concentration) MR imaging findings to percent necrosis at

pathology in rabbits bearing VX2 liver tumors. VX2 tumors were implanted in the liver of 16 rabbits. Mean tumor size at pathology was 16 mm (range: 12-22). Mean percentage of necrosis at pathology was 22 % (range: 4 - 44%). Choline concentration correlated well with percentage of necrosis at pathology and showed an R value of 0.78. In conclusion, choline concentration showed a relatively high correlation with tumor necrosis at pathology. Therefore, 1H MRS may be useful to assess tumor necrosis.

SAMENVATTING

De doelstellingen van dit proefschrift waren 1. om de bijwerkingen van transarteriële chemo-embolisatie (TACE) voor lever tumoren te onderzoeken en om het gebruik van MR beeldvorming te evalueren voor het characterizeren van tumor respons na deze locoregionale therapie. 2. om intra-arteriële behandeling van lever tumoren met 3-bromopyruvate, een nieuw potentieel antikanker medicijn, verder te ontwikkelen en 3. om de waarde van nieuwe MR beeldvorming technieken te beoordelen voor de karakterisatie van lever tumoren. In *hoofdstuk 1*, de algemene introductie, wordt een overzicht gegeven van deze doelstellingen en de indeling van dit proefschrift.

Bijwerkingen van TACE

Een van de grootste bezwaren omtrent systemische chemotherapie voor de behandeling van lever kanker is het optreden van bijwerkingen zoals pijn, misselijkheid, vomitus, beenmerg suppressie, alopecia en hart toxiciteit. De subjectieve bijwerkingen van TACE zijn mild in vergelijking met die van systemische chemotherapie. Omdat de focus van de meeste studies ligt op de gemiddelde algemene overleving, in plaats van bijwerken veroorzaakt door TACE, mist er een gedetailleerde analyse van de bijwerkingen na deze locoregionale therapie. In *hoofdstuk 2* hebben we de bijwerkingen van TACE 6 maanden en 1 jaar na behandeling van patiënten met HCC geanalyseerd met behulp van een gestandaardiseerd oncologisch system (CTCAE, versie 3.0) opdat de bijwerkingen na TACE kunnen worden vergeleken met de bijwerkingen van conventionele systemische chemotherapie gebruikt in de behandeling van lever kanker (doxorubicin, cisplatin en 5- fluorouracil). Geobserveerde graad 3 of 4 bijwerkingen 6 en 12 maanden na behandeling waren respectievelijk leukocytopenie (7% en 19%); anemie (9% en 19%); verhoogde aPTT (8% en 18%); thromobocytopenie (13% en 23%); verhoogd AST (15% en 18%); verhoogd ALT (10% en 18%); verhoogd alkalisch fosfatase (8% en 18%); verlaagd albumine (10% en 19%); verhoogd bilirubine (10% en 22%) en alopecia (18%). De geobserveerde bijwerken waren aanzienlijk minder dan de mate van bijwerkingen na conventionele chemotherapie zoals deze bekend zijn in de literatuur. Onze studie toonde aan dat TACE een mild bijwerkingspatroon vertoont in patiënten met HCC. Onze data bevestigen de rol van TACE in de behandeling van niet operabel HCC. Bovendien geven onze resultaten een goed overzicht voor clinici over de te verwachten

bijwerkingen na behandeling met TACE en zullen daarom belangrijk zijn in het verbeteren van behandelingsstrategieën.

MR beeldvorming na TACE

In *hoofdstuk 3* geven we een samenvatting van de huidige literatuur over de rol van MR beeldvorming in het evalueren van tumor respons na verschillende locoregionale therapieën die op dit moment in gebruik zijn voor de behandeling van lever tumoren. Het evalueren van tumor respons na locoregionale therapieën is belangrijk in het bepalen van het success van de gekozen behandeling en het opstellen van een behandelplan. MR beeldvorming speelt een belangrijke rol in de evaluatie van tumor respons na nieuwe locoregionale therapieën gericht op de behandeling van lever kanker. De conventionele algemeen geaccepteerde criteria voor het bepalen van tumor repons in de oncologische wereld, namelijk de RECIST en EASL criteria, zijn gebaseerd op een afname van tumor grootte en het verminderd aankleuren van de tumor. Een recentere methode van evaluatie is de diffusiemap (ADC) zoals gemeten door diffusie gewogen MR beeldvorming. Diffusie gewogen MR beeldvorming en ADC waardes meten de temperatuur afhankelijke beweeglijkheid van watermoleculen in weefsels en geven daarbij inzicht in de tumor micro-omgeving. Wij beschrijven de rol van tumor grootte, het verminderd aankleuren en veranderde ADC waardes na behandeling met RFA, TACE en radio-embolisatie.

In de daaropvolgende hoofdstukken van deel I analyseren we het gebruik van functionele MR beeldvorming in het evalueren van tumor repons na TACE. Ook vergelijken we tumor respons zoals bepaald met behulp van functionele MR beeldvorming met tumor respons bepaald met behulp van traditionele beeldvorming aan de hand van lipiodol depositie, verandering van tumor grootte en verminderde oplichting. In *hoofdstuk 4* richten we ons op lever metastasen van borstkanker, die voornamelijk hypovasculaire kenmerken hebben. We hebben een total aantal van 27 laesies geëvalueerd met een gemiddelde diameter van 5.5 cm. Hoewel tumor grootte met 18% verminderde na TACE, voldeed geen enkele laesie aan de RECIST criteria voor volledige tumor response (dat wil zeggen het volledig verdwijnen van de laesie na behandeling) en slechts 7 van de 27 laesies voldeden aan de RECIST criteria voor partiële respons (dwz >30% afname in tumor grootte). Na TACE werd er een significante vermindering gezien in het aankleuren van de laesies, zowel in de arteriele fase (32%) als in de portale fase (39%) ($p < 0.0001$). De gemiddelde ADC waarde van de tumor

nam toe met 27% ($p < 0.0001$) na TACE, terwijl de ADC waarde van de gezonde lever, milt en nier onveranderd bleef.

In *hoofdstuk 5* bestuderen we lever metastasen van neuroendocrine tumoren, die voornamelijk hypervasculair zijn. We analyseerden 66 met TACE behandelde laesies in 26 patiënten (18 mannen en 8 vrouwen, met een gemiddelde leeftijd van 57 jaar) met neuroendocriene lever metastasen. De gemiddelde tumor grootte en het aankleuren in de arteriële en portale fase verminderde significant na de behandeling ($p < 0.0001$). De gemiddelde ADC waarde van de tumor nam toe van 1.51×10^{-3} mm^2/sec voorafgaande aan de behandeling tot 1.79×10^{-3} mm^2/sec na de behandeling ($p < 0.0001$), terwijl de ADC waardes van de gezonde lever en milt onveranderd bleven. Ondanks de afname van de tumor grootte na de behandeling, voldeed geen enkele patiënt in ons cohort aan de criteria van de WHO en RECIST voor tumor repons, hetgeen in overeenkomst is met de gevonden resultaten in het borstkanker cohort zoals beschreven in *hoofdstuk 4*. Partiële repons werd slechts waargenomen in 27% (WHO criteria) en 23% (RECIST) van de patiënten.

In de volgende hoofdstukken bevestigen we deze resultaten in lever metastasen van patiënten met een leiomyosarcoom (*hoofdstuk 6*) en lever metastasen van patiënten met een oog melanoom. We evalueerden 31 lever metastasen in 10 patiënten met een leiomyosarcoom met behulp van MR beeldvorming voor en na behandeling met TACE. Deze tumoren hadden een gemiddelde grootte van 4.8 cm voor de behandeling. De tumor grootte verminderde slechts met 2% direct na de behandeling. De aankleuring van de tumor verminderde significant na de behandeling, zowel in de arteriele fase (69%) als in de portaal veneuze fase (64%) ($p < 0.0001$). Na TACE nam de gemiddelde ADC waarde van de tumor toe met 20 % ($p = 0.0015$), terwijl de ADC waardes van de gezonde, onbehandelde lever, milt en spier geen significante veranderingen lieten zien ($p = 0.44$, $p = 0.287$ en $p = 0.098$, respectievelijk). De gemiddelde overleving van het cohort was 21 maanden na de eerste behandeling met TACE.

In *hoofdstuk 7* evalueren we 21 lever metastasen in 6 patiënten met een oog melanoom. Aankleuring in de arteriele fase nam af met 41% na TACE, en dit verschil was statistisch significant ($p = 0.0002$). Oplichting in de portaal veneuze fase verminderde met 56% en ook dit verschil was statistisch significant ($p < 0.0001$). Diffusie gewogen MRI was geschikt voor het evalueren van tumor respons na de behandeling met TACE. De gemiddelde ADC waarde van de tumor nam toe met 48% na TACE ($p =$

0.0003), terwijl de ADC waardes van de gezonde lever, milt en spier onveranderd bleven. Hoewel de gemiddelde tumor grootte afnam met 16% van 4.9cm tot 4.1 cm na de behandeling, geen enkele tumor voldeet aan de criteria voor algehele repons volgens RECIST en slechts 8 tumoren voldeden aan de criteria voor partiele repons.

Samengevat, ook al waren de veranderingen in tumor grootte na behandeling met TACE in patiënten met lever metastasen klein, contrast MR beeldvorming en diffusie gewogen MR beeldvorming waren in staat significante veranderingen waar te nemen kort na de behandeling met TACE. Deze veranderingen waren een afname in het aankleuren van de tumor en een toename in de ADC waarde van de tumor. Beide suggeren een toename in necrose en het afsterven van de tumor cellen en kunnen daarom gebruikt worden voor het evalueren van tumor respons in met TACE behandelde tumoren.

Intra-arteriële behandeling met 3-bromopyruvate

In deel 2 leggen we ons toe op de ontwikkeling van een nieuwe behandeling strategie voor lever kanker. 3-BrPA, een synthetisch gebromineerd derivaat van pyruvaat zuur, zorgt voor een onomkeerbare inhibitie van glycolyse en is een veelbelovende kandidaat voor de intra-arteriële behandeling van lever kanker.

In *hoofdstuk 8* vergelijken we het success van partiële lever resectie, intra-arteriële behandeling met 3-BrPA en TACE in de behandeling van lever kanker in een diermodel. VX2 tumoren werden geïmplanteerd in de linker lever kwab van 20 konijnen en groeiden 2 weken. Vervolgens werden de konijnen verdeeld in 4 groepen. Groep 1 (n = 2) werd 2 weken na tumor implantatie opgeofferd. Groep 2, 3 en 4 (n = 6 per groep) werden behandeld met respectievelijk een partiele lever resectie, intra-arteriel toegediende 3-BrPA en TACE. De dieren in deze groepen werden verder onderverdeeld in 3 groepen met elk 2 dieren, corresponderend met het tijdpunt waarop de dieren werden opgeofferd (respectievelijk 7, 14 en 21 dagen). Na sterfte werden alle organen uitgenomen, gefixeerd en geanalyseerd. Pathologische analyse liet long metastasen zien in alle dieren. Metastasen in de buikholte werden gezien in 5 dieren in groep 2, 2 dieren in groep 3 en alle dieren in groep 4. Nier metastasen werden gevonden in 2 dieren behandeld met TACE. Onze resultaten laten zien dat intra-arteriele therapie met 3-BrPA kan resulteren in gunstigere metastatische kenmerken dan na behandeling met resectie of TACE.

Het doel van *hoofdstuk 9* was om de biodistributie en tumor selectiviteit van intra-arterieel toegediend ^{14}C gelabeld 3-BrPA te vergelijken met intraveneus toegediend ^{14}C 3-BrPA door gebruik te maken van het VX2 lever kanker diermodel. Ook evalueerden we het effect van 3-BrPA op het glucose metabolisme van tumor en gezond weefsel door de opname van FDG te bepalen. Ten slotte onderzochten we de invloed van intra-arterieel toegediend 3-BrPA op overleving. 60 konijnen met VX2 lever tumoren werden behandeld met 1.75 mM [^{14}C] 3-BrPA, intra-arterieel toegediend, 1.75 mM [^{14}C] 3-BrPA, intraveneus toegediend, 20 mM [^{14}C] 3-BrPA intraveneus toegediend, of 25 ml zoutoplossing. Alle konijnen (behalve de dieren in de 20 mM groep) kregen FDG toegediend 1 uur voor sterfte. Vervolgens vergeleken we de overleving van dieren behandeld met intra-arterieel toegediend 1.75 mM 3-BrPA (n = 22) met controle dieren (n = 10). Na intra-arteriele toediening was tumor opname van [^{14}C] 3-BrPA 1.8 ± 0.2% van de toegediende dosis per gram weefsel (%TD/g), terwijl alle andere weefsels minimale opname lieten zien. Na intraveneuze toediening (1.75 mM) was tumor opname van [^{14}C] 3-BrPA 0.03 ± 0.01% TD/g. Na intra-arteriële toediening van 3-BrPA was de FDG opname in de tumor 26 maal lager dan de FDG opname in controle dieren. Na intraveneuze toediening van [^{14}C] 3-BrPA werd er geen verschil gezien in de opname van FDG door de tumor in vergelijking met controle dieren. Konijnen behandeld met intra-arterieel toegediend 1.75 mM 3-BrPA leefden significant langer (55 dagen) dan controle dieren (18.6 dagen). Daaruit concluderen we dat intra-arterieel toegediend 3-BrPA een gunstig biodistributie patroon heeft, dat resulteert in een hoge opname door de tumor terwijl gezonde weefsels gespaard blijven. De locale controle van de lever tumor door intra-arterieel toegediend 3-BrPA leidt tot een significant grotere overlevingskans.

In een vervolgstudie (Addendum) evalueren we de anti-glycolytische effecten van 3-BrPA in ratten met RMT tumoren, door de FDG opname te bepalen na intraveneuze toediening van de therapeutische dosis. Zestien ratten met RMT tumoren werden behandeld met 15 mM 3-BrPA in 2.5 ml zoutoplossing of met 2.5 ml zoutoplossing zonder 3-BrPA. Na behandeling ontvingen alle dieren FDG en werden 1 uur later opgeofferd. Behandeling met 3-BrPA resulteerde in een met 77% verminderde FDG opname in de tumoren ($p < 0.002$). Gezonde weefsels lieten geen significant verschil zien in FDG opname na de behandeling met 3-BrPA. Onze resultaten laten zien dat 3-BrPA een sterk antiglycolytisch effect heeft op RMT tumoren in ratten.

Nieuwe ontwikkelingen in de beeldvorming van lever tumoren

Diagnostische beeldvorming speelt een grote rol in het vormen van beslissingen omtrent behandelingsstrategieen voor patienten met lever kanker. In deel III behandelen we de nieuwe ontwikkelingen in de beeldvorming van lever tumoren. In *hoofdstuk 10* onderzoeken we de juistheid van diffusie gewogen MRI in het onderscheiden van hemangiomen van andere veel voorkomende hypervasculaire lever tumoren zoals focale nodulaire hyperplasie (FNH), hepatocellulair carcinoom (HCC) en hypervasculaire lever metastasen. 182 hypervasculaire lever tumoren in 117 patienten werden retrospectief geanalyseerd. De tumoren werden als volgt geclassificeerd: typisch en atypisch hemangioom (n = 38), HCC (n = 58), FNH (n = 22) en lever metastasen van neuroendocriene tumoren (n = 64) met een gemiddelde tumor grootte van 5.3 cm. De gemiddelde ADC waardes voor hemangiomen, HCC, FNH en metastasen waren respectievelijk 2.29 x 10^{-3}, 1.55 x 10^{-3}, 1.65 x 10^{-3} en 1.43 x 10^{-3}. We vonden een statistisch significant verschil in ADC waardes van hemangiomen in vergelijking met ADC waardes van FNH ($p < 0.001$), HCC ($p < 0.001$) en metastasen ($p < 0.001$). De oppervlakte onder de ROC grafiek was 0.91. Deze resultaten ondersteunen de hypothese dat diffusie gewogen MRI snelle, accurate en kwantificeerbare informatie kan geven en zo een onderscheid kan maken tussen hemangiomen en andere hypervasculaire lever tumoren.

Een andere toepassing voor het karakteriseren van lever tumoren is het gebruik van weefsel specifieke contrast vloeistoffen gedurende MR beeldvorming. In *hoofdstuk 11* rapporteren we de rol van diffusie gewogen MR beeldvorming in het bepalen van tumor necrose en de rol van contrast MR beeldvorming. Maximale tumor grootte en tumor omlijning worden bepaald in het VX2 diermodel en vergeleken met de gouden standard, gemeten gedurende histologisch onderzoek. Op contrast MR beeldvorming (n = 11), de gemiddelde tumor grootte was respectievelijk 20 mm, 19mm en 20 mm in de arteriële, portaal veneuze en laat veneuze fase. Tumor omlijning was het best waar te nemen in de vertraagde fase. Op diffusie gewogen MR beeldvorming, de gemiddelde ADC waarde was 18.4 x 10^{-3} mm^2/sec. De gemiddelde tumor grootte tijdens pathologische analyse was 16 mm. Tijdens pathologische analyse werd er gemiddeld 36% necrose gezien. Correlatie tussen ADC waardes en het necrose percentage liet een R waarde van 0.68 zien. Hieruit concluderen wij dat de contrast vloeistof Gd-EOB-DTPA van toegevoegde waarde kan zijn bij het weergeven van tumor omlijning op MR beeldvorming. Bovendien lieten we een goede correlatie

zien tussen de ADC waarde enerzijds en het necrose percentage anderzijds. Dit ondersteunt onze hypothese dat diffusie gewogen MR beeldvorming nuttig kan zijn in het evalueren van tumor necrose. Desondanks blijft de zoektocht naar nieuwe, betere modaliteiten belangrijk.

Ten slotte is proton MR spectroscopie een beeldvormende techniek die gebruikt kan worden voor het kwantificeren van biochemische concentraties van metabolieten. In *hoofdstuk 12* vergelijken we metabole (absolute kwantifikatie van de choline concentratie) MR beeldvorming met de gevonden hoeveelheid necrose tijdens pathologisch onderzoek in VX2 lever tumoren in konijnen. De gemiddelde tumor grootte tijdens pathologisch onderzoek was 16 mm (n = 16). De gemiddelde hoeveelheid necrose was 22 %. De choline concentratie in de tumor liet een sterke correlatie zien met de hoeveelheid necrose (R = 0.78). Hieruit concluderen wij dat proton MR spectroscopie nuttig kan zijn voor het bepalen van tumor necrose.

DANKWOORD

De volgende mensen zouden wij graag danken voor hun bijdrage aan de totstandkoming van dit proefschrift.

Prof. Dr. P.J. van Diest, beste Paul, wij zijn je erg dankbaar voor de mogelijkheden die je voor ons gecreeerd hebt, dit proefschrift is het resultaat van jouw inzet en vertrouwen. Je steun, goede adviezen en de vrijheid die je ons geboden hebt, hebben ons de kans gegeven om ons te ontwikkelen tot ware wetenschappers. We zijn er trots op dat we bij jou mogen promoveren

Prof. Dr. E. van der Wall, beste Elsken, dank voor je promotorschap. Je hebt ons de mogelijkheid geboden tot het omzetten van een ongelofelijk leerzame en onvergetelijke periode in dit boekje.

Prof. Dr. J.F. Geschwind, dear Jeff, thank you very much for your efforts as a mentor during the last 3 years. It has been a wonderful experience! Your continuous support and trust have given us the opportunity to grow in both clinical and basic science research. Your lab is the best learning environment an aspiring researcher could wish for, and we are very grateful you gave us a chance to become part of it.

Dr. M. Vali, dear Moose, you are a driving force behind the second part of this thesis. You helped us shape our careers, and did so with astonishing alacrity and energy. For all (research) problems you have a creative solution and most important of all, you taught us how to ask questions.

De leden van de beoordelingscommissie bestaande uit Prof. dr. D.H. Biesma, Prof. dr. W.P.T.M. Mali, Prof. dr. P.R Luijten, Prof. dr. G.J.A. Offerhaus en Prof. dr. F. Miedema danken wij voor de moeite die zij hebben genomen voor de beoordeling van het manuscript.

Dr. I.R. Kamel, dear Ihab, thank you for providing invaluable insight and feedback on how to formulate a significant research objective, collect the appropriate data, and use proper statistical methods to translate these data into a scientific manuscript.

Our dear colleagues: Christos, Kelvin, Lora, Y'ammie, Jazz, Jim, Lia, Ana, Maria, Eleni, Shanm, Labiq, Rani, Dorian, Shinichi, Pramod, Ming, Lori, Sue, thank you all! Beste Willy, dankjewel voor al je hulp!

(VERVOLG) **MANON**

It has been almost 3 years since I moved to the US to pursue a Ph.D. degree, and it has been an amazing journey. Thank you all for being there for me, in good times and in bad!

Beste Pien, collega promovendus, vriendin, oud-huisgenoot (x3), we gaan promoveren! Dat we dat samen doen heeft het zoveel makkelijker en gezelliger gemaakt! Samen hebben we de oversteek gemaakt naar de andere kant van de oceaan en samen hebben we de eerste stappen gezet in de wetenschappelijke wereld. Dit boekje is het eindresultaat van een prachtige periode, dankjewel! Ik wens je heel veel success met de Radiologie opleiding!

Mijn paranimfen, Dr. P.R.A. Buijs en Dr. A.E.C.J.M. Struijs. Pascal, lief broertje, dankjewel dat je er altijd voor me bent, ook al betekent dat soms dat je rechtstreeks vanuit de nachtdienst in het vliegtuig moet stappen. Ik hoop dat je over enige tijd ook zelf je proefschrift mag verdedigen! Marie-Chantal, lief vriendinnetje, ik ben super blij dat jij op deze dag naast me staat. Of we elkaar nou dagelijks zien (zoals tijdens dat fantastische chirurgie co-schap) of 1x per jaar omdat we ons allebei op een ander continent bevinden (maar in ieder geval minimaal 1x per jaar, waar dan ook!), onze vriendschap werkt! Nog even doorzetten en dan heb je zelf je boekje af!

Christianne, lief vriendinnetje, dankjewel voor onze heerlijke gesprekken, je steun, vertrouwen en gezelligheid. Zodra we elkaar zien na een lange periode, pakken we de draad weer op en voelt het als vanouds! Het lijkt wel alsof je nog steeds om de hoek woont!

Lieve papa en mama, bedankt voor jullie onvoorwaardelijke liefde, steun en vertrouwen in mij! Dankzij jullie ben ik waar ik nu ben. Altijd hebben jullie me vrij gelaten zelf te kiezen en me gesteund in mijn keuzes. Het is goed om te weten dat jullie achter me staan!!

My dear husband, thank you for being you, for bringing out the best in me, for creating a home away from home. You are my partner in crime. Your love and support mean the world to me. You and me! I love ya!

(VERVOLG) **PIEN**

And now this amazing adventure is finished! Fortunately, I was never alone. There were people with whom I worked, people who believed in me, supported me and helped me. All those people I would like to thank.

Lieve Manon, collega promovendus, het was een lange weg en ik blij dat we dit project samen hebben afgesloten. Het was fijn om samen hard te werken, volledig op één lijn te zitten en recht op ons doel af te gaan. Dank je.

Mijn paranimfen: Lieve Marielle, ik ben trots dat jij op deze dag naast me staat en we samen onze sterretjes kunnen tellen. Lieve Jaap, grote/kleine broer, ik ben blij dat je er bent.

Beste Maarten, bedankt voor het ontwerpen van de prachtige kaft.

Lieve papa, mama, en Jaap ondanks de afstand zijn jullie altijd dichtbij. Bedankt voor jullie vertrouwen, liefde en onvoorwaardelijke steun. Zonder jullie was dit niet gelukt.

Dear Teo, thank you for being there, sharing my life and showing me, day after day that life is good.

CURRICULUM VITAE

Manon Buijs was born on November 15th, 1982, in Brunssum, the Netherlands. In 2000, after graduating from high school at the Katholiek Gymnasium Rolduc in Kerkrade, she attended Medical School at the University of Maastricht, graduating in September 2006. During her last year of Medical School, she did a research elective at the Johns Hopkins University School of Medicine, Department of Surgery and Interventional Radiology (supervisors: Prof. Dr. JFH Geschwind and Prof. Dr. MA Choti), eventually leading to the present thesis. Since November 2006 she is working as a Postdoctoral Research Fellow in the department of Interventional Radiology of the Johns Hopkins University School of Medicine (supervisors: Prof. Dr. JFH Geschwind and Dr. M Vali).

Josephina Anna (Pien) Vossen was born on December 28th, 1981, in ‘s-Hertogenbosch, the Netherlands. In 2000, after graduating from high school at the Dr-Knippenberg College in Helmond, she attended Medical School at the University of Maastricht, graduating in September 2006. During her last year of Medical School, she did a research elective at the Johns Hopkins University School of Medicine, Department of Surgery and Interventional Radiology (supervisors: Prof. Dr. JFH Geschwind and Prof. Dr. MA Choti), eventually leading to the present thesis. Since November 2006 she is working as a Postdoctoral Research Fellow in the department of Interventional Radiology of the Johns Hopkins University School of Medicine (supervisors: Prof. Dr. JFH Geschwind and Dr. M Vali).